

**ENGINEERING STUDIES IN ADVANCED PLA MATERIALS –
STEREOCHEMISTRY, STEREOCOMPLEXATION, AND THERMAL RECYCLING
OF PLA**

By

Mohammed A Alhaj

A DISSERTATION

**Submitted to
Michigan State University
in partial fulfillment of the requirements
for the degree of**

Materials Science and Engineering – Doctor of Philosophy

2022

ABSTRACT

ENGINEERING STUDIES IN ADVANCED PLA MATERIALS – STEREOCHEMISTRY, STEREOCOMPLEXATION, AND THERMAL RECYCLING OF PLA

By

Mohammed A Alhaj

Poly lactide (PLA) polymers are the world's foremost 100% biobased resin with both composting and recycling end-of-life options in harmony with Ellen MacArthur Foundation "Circularity Model." It is commercially manufactured by converting lactic acid to lactide, which is then polymerized to PLA. These molecules present unique and intriguing stereochemistry that dictate manufacturing, performance properties, and processability. However, it is seldom discussed and not well understood in the role stereochemistry can play and impact product performance and use. In the current work, we critically review and discuss the stereochemical implications for PLA through studies on different PLA compositions.

To-date, it is unclear the origin of D-content present in commercial grade PLA, although it is assumed to originate from D-lactide. In this work, we validate that manufacture of lactide monomer from (L)- lactic acid predominantly results in a mixture of L and meso (DL), not L- and D- lactide. Optical rotation and ^1H NMR studies are used to elucidate this stereochemistry. Copolymers of L-lactide and meso-lactide and copolymers of L-lactide and D-lactide are synthesized via bulk polymerization at various compositions. The optical rotation, tacticity, crystallinity, and thermal properties of synthesized copolymers are characterized. The optical rotation of poly(meso-lactide) has also been reported for the first time in this text. Differential scanning calorimetry (DSC) and ^1H NMR studies confirm that PLA transitions from a predominantly isotactic, semi-crystalline polymer to a predominantly atactic, amorphous polymer when one copolymerizes greater than 10% meso-lactide with L-lactide. The stereochemical

composition, mechanical and rheological properties of commercial grade PLA are measured to elucidate the effect of stereochemistry on the tensile and rheological behavior of PLA. We conclude this section with studies on PLA stereochemistry and its influence on immune cellular response. Hydrolytic degradation of semi-crystalline and amorphous PLA is analyzed via molecular weight characterization and lactic acid abundance. Semi-crystalline and amorphous PLA are then studied as potential carriers for glycolytic inhibitors.

The stereochemistry of PLA and its implication on performance properties are further explored in studies on stereocomplex PLA. A pilot-scale continuous manufacturing process of stereocomplex PLA is developed and optimized by melt-blending a 1:1 blend of high molecular weight poly(L-lactide) (PLLA) and high molecular weight poly(D-lactide) (PDLA) in a co-rotating twin screw extruder. Stereocomplexation is first characterized via DSC at different temperatures and times. The optimal reaction temperature and reaction time are found and used to process >95% stereocomplex PLA conversion (melting peak temperature $T_{pm} = 240^{\circ}\text{C}$). Stereocomplex PLA is used as an additive to produce 70% PLLA/30% stereocomplex PLA composites. The crystallinity, thermal properties, and tensile properties of composites are then characterized. A study on stereocomplex PLA and its effect on the crystallization kinetics of PLLA is conducted. 5% stereocomplex PLA is blended with 95% PLLA to analyze its use as a nucleating agent.

The final section discusses a pilot-scale end-of-life method for PLA via thermal recycling. This study continues previous studies on PLA thermodepolymerization by scaling up the reversible reaction in a pilot-scale batch reactor. PLA is run at various temperatures and times to elucidate the processing conditions that yield the highest lactide conversion. The chemical purity, optical purity, lactide yield and stereoisomeric composition of the final lactide product are characterized by DSC, optical rotation, mass balance, and ^1H NMR, respectively.

Copyright by
MOHAMMED A ALHAJ
2022

ACKNOWLEDGEMENTS

This dissertation would not have been possible without the wealth of support I was provided during my PhD. First and foremost, I would like to sincerely thank Dr. Ramani Narayan in his guidance and support throughout my graduate program. He instilled in me a passion to target sustainability issues in the field of materials science by providing me the freedom to explore the field of bioplastics. I would also like to thank my committee members for their support: Dr. Andre Lee, Dr. Shiwang Cheng, Dr. Patrick S Walton, and Dr. Mojgan Nejad. A special thanks goes to Dr. Bin Tan for his advice and guidance during the early years of my PhD. His valuable guidance provided me a more comprehensive understanding of my work in biobased, biodegradable polymers. A special thanks goes to the previous and current members of the Biobased Materials Research Group (BMRG) for their encouragements, guidance, and motivation. I would like to particularly thank my lab mate Dr. Apoorva Kulkarni for helping me in so many ways throughout my PhD.

I am thankful for the financial support provided by the Michigan State University (MSU) Department of Chemical Engineering and Materials Science (first and fifth years) and by the NSF-GRFP fellowship (second, third, and fourth years). A special thanks goes to Dr. Katy Colbry for her valuable guidance and assistance in my NSF-GRFP fellowship application. I may have not been honored with this valuable fellowship if it was not for her help. I am thankful for MSU Composite Materials and Structures Center and Michigan Biotechnology Institute for providing laboratory space and equipment for my studies. A special thanks goes to Dr. Ed Drown for his guidance in injection molding of plastics, and his patience in our training. I am thankful for Dr.

Daniel Holmes and Dr. Babak Borhan of MSU Department of Chemistry for providing equipment on NMR and optical rotation studies (polarimeter), respectively.

I am grateful for the bulk PLA polymer samples donated to our group by Derek Atkinson of Total Corbion, Shilpa Manjure and Sayli Bote of Northern Technology International Corporation (NTIC), and our colleagues at NatureWorks. I would have not been able to complete my studies if it was not for their kind donation. Dr. Jean-Marie Raquez and Dr. Jeremy Odent of University of Mons are kindly acknowledged for hosting me in Belgium to learn more about PLA polymer synthesis and reactive extrusion. The skills I attained during my stay at Mons have helped me immensely throughout my PhD program. A special mention goes to my friend and colleague Dr. Chima Maduka, MD, PhD who invited me to an opportunity to apply my research to an innovative medical device project. My collaboration with him and Dr. Christopher Contag is one of the most inspirational and memorable projects that I will forever be grateful for. I will always be thankful for the encouragement and motivation Chima provided during my PhD. My deepest thanks also go to the undergraduate research assistants who helped me carry out my experiments and data analysis. Specifically, Nicole Mancina, Melissa Joslyn, Jakob Emrich, and Tytus Sewell have been valuable assets to our lab group who I will forever be grateful to; their work ethic and determination cannot be matched.

Finally, I wish to express my gratitude towards my parents and siblings for their emotional support and love during my five years away from them. I would not be where I am today if it was not for my family. Thank you for helping me be the man I am today.

TABLE OF CONTENTS

LIST OF TABLES	x
LIST OF FIGURES	xii
KEY TO SYMBOLS OR ABBREVIATIONS	xvii
1. INTRODUCTION & BACKGROUND	1
1.1. The Impact of Fossil-Based Plastics	1
1.2. The Promise of Bioplastics.....	3
1.3. Polylactide	6
1.3.1 PLA Stereochemistry	8
1.3.2 PLA End-of-Life Scenarios.....	10
1.4. Summary of Work	13
2. THE STEREOCHEMISTRY OF PLA AND ITS IMPLICATION ON PERFORMANCE PROPERTIES.....	15
2.1. Introduction	15
2.2. Experimental.....	18
2.2.1 Materials and Reagents	18
2.2.2 Synthesis of PLA	19
2.2.3 Characterization and Analysis	20
2.2.4 The Role of PLA Stereochemistry in Immune Cellular Response	23
2.2.4.1 Materials & Reagents.....	23
2.2.4.2 PLA Breakdown and Extraction.....	24
2.2.4.3 Glycolytic Inhibition of PLA.....	24
2.3. Results and Discussion	26
2.3.1 Chemical Structure.....	26
2.3.2 Optical Rotation.....	26
2.3.3 Effect of Meso-Lactide and D-Lactide on Optical Rotation of PLA	28
2.3.4 Effect of Meso-Lactide and D-Lactide on Specific Rotation of PLA	30
2.3.5 Identification and Quantification of Stereoisomers in Commercial Grade PLA.....	31
2.3.6 Validation of Stereoisomers in Commercial Grade PLA	32
2.3.7 Tacticity.....	33
2.3.7 Crystallinity.....	36
2.3.8 Thermal Stability	38
2.3.9 Tensile Properties.....	39
2.3.10 Rheological Properties	42
2.3.11 The Role of PLA Stereochemistry in Immune Cellular Response	43
2.3.11.1 PLA Breakdown and Extraction.....	43
2.3.11.2 Glycolytic Inhibition of PLA.....	47
2.4. Conclusion and Next Steps	53

3. REACTIVE EXTRUSION OF HIGH MOLECULAR WEIGHT STEREOCOMPLEX PLA FOR ADDITIVES APPLICATION DEVELOPMENT	55
3.1. Introduction	55
3.2. Experimental	58
3.2.1 Pilot-Scale Manufacturing of Stereocomplex PLA via Reactive Extrusion	58
3.2.1.1 Materials	58
3.2.1.2 Characteristics of Stereocomplex Formation	58
3.2.1.3 Reactive Extrusion of Stereocomplex PLA	60
3.2.1.4 Characterization & Analysis	62
3.2.2 Development of Molecular Composites using Stereocomplex PLA Particles in a Thermoplastic PLA Matrix	64
3.2.2.1 Materials	64
3.2.2.2 Reactive Extrusion of PLA/Stereocomplex PLA Composites	65
3.2.2.3 Characterization & Analysis	66
3.3. Results & Discussion	69
3.3.1 Pilot-Scale Manufacturing of Stereocomplex PLA via Reactive Extrusion	69
3.3.1.1 Characteristics of Stereocomplex Formation	71
3.3.1.2 Confirmation of Stereocomplex Formation via FTIR	73
3.3.1.3 Crystal Structure Characterization via WAXD	75
3.3.1.4 Thermal Characterization via DSC	76
3.3.1.5 Thermal Degradation of Stereocomplex PLA	78
3.3.2 Development of Molecular Composites using Stereocomplex PLA Particles in a Thermoplastic PLA Matrix	79
3.3.2.1 Thermal Characterization of PLA/Stereocomplex PLA Composites	79
3.3.2.2 WAXD of PLA/Stereocomplex PLA Composites	85
3.3.2.3 Tensile Properties of PLA/Stereocomplex PLA Composites	86
3.3.2.4 Effect of Stereocomplex PLA on the Isothermal Crystallization Kinetics of PLA	92
3.4. Conclusion & Next Steps	96
4. THERMAL RECYCLING OF PLA VIA THERMO-DEPOLYMERIZATION	98
4.1. Introduction	98
4.2. Experimental	100
4.2.1 Lab-Scale Thermal Recycling of PLA in a Reaction Vessel	100
4.2.1.1 Materials & Reagents	100
4.2.1.2 Thermodepolymerization of PLA	100
4.2.1.3 Characterization & Analysis	102
4.2.2 Pilot-Scale Thermal Recycling of PLA in a Batch Reactor	104
4.2.2.1 Materials & Reagents	104
4.2.2.2 Thermodepolymerization of PLA	104
4.2.3 Life Cycle Assessment of PLA – Composting vs Thermal Recycling	105
4.2.3.1 Introduction	105
4.2.3.2 Product & Process Description	106
4.2.3.3 Goal and Scope	108
4.3. Results and Discussion	110
4.3.1 Lab-Scale Thermal Recycling of PLA in a Reaction Vessel	110

4.3.1.1	Purity Determination and Stereoisomeric Composition.....	110
4.3.1.2	Thermodepolymerization Kinetics.....	112
4.3.2	Pilot-Scale Thermal Recycling of PLA in a Batch Reactor	115
4.3.2.1	Purity and Yield of Lactide	115
4.3.3	Life Cycle Inventory	116
4.3.3.1	Carbon Efficiency of Systems	116
4.3.3.2	PLA Composting (System 1) LCI.....	116
4.3.3.3	PLA Recycling (System 2) LCI.....	122
4.3.4	Life Cycle Impact Assessment	129
4.3.4.1	Global Warming Impact Category	129
4.3.4.2	Land Use Impact Category	131
4.3.4.3	Water Use Impact Category	132
4.3.4.4	Resource Depletion	134
4.3.5	Sensitivity Analysis	135
4.3.5.1	Corn Production.....	135
4.3.5.2	Percentage of PLA Recycled.....	136
4.3.5.3	Sensitivity Analysis for Land Usage.....	136
4.3.5.4	Sensitivity Analysis for Water Usage	137
4.3.5.5	Sensitivity Analysis for Resource Depletion.....	138
4.3.5.6	Sensitivity Analysis for Global Warming Potential.....	139
4.4.	Conclusion & Next Steps	140
5.	SUMMARY AND FUTURE WORK	143
	BIBLIOGRAPHY	147

LIST OF TABLES

Table 2-1. Optical rotation of pure lactide samples	27
Table 2-2. Optical rotation of pure PLA samples	28
Table 2-3. Calculated % D-content based on optical rotation	32
Table 2-4. Measured optical rotation versus calculated optical rotation as a	33
Table 2-5. DSC data on PLLA, poly(meso-lactide), and poly(L-co-meso-lactide).....	38
Table 2-6. Mechanical properties of Ingeo PLA standard grades.....	42
Table 2-7. Molecular weights of commercial grade PLA before and after extraction in Milli-Q water (H ₂) and HG media	44
Table 2-8. Molecular weight reduction and corresponding D-content for commercial grade PLA	44
Table 2-9. Oligomers of L- and D-lactic acid detectable in PLA extracts from Milli-Q water....	46
Table 3-1. Material properties of Total Corbion standard grades of PLA.....	58
Table 3-2. Material properties of NatureWorks Ingeo standard grades of PLA.....	65
Table 3-3. Recent studies on stereocomplex PLA	70
Table 3-4. DSC results on the thermal properties and crystallinity of stereocomplex PLA at various collection times	78
Table 3-5. Mechanical properties of extruded neat PLA vs their composite counterparts	91
Table 3-6. Tensile properties (upper/lower bounds) of stereocomplex PLA based on ROM	92
Table 3-7. Crystallization half times and Avrami constants for neat PLA and PLA composite samples at different temperatures	96
Table 4-1. Wiedema method used to evaluate LCA data	109
Table 4-2. Summary of purity and isomeric composition results of lactide products from PLA depolymerization at various temperatures.....	112

Table 4-3. Equilibrium monomer concentration and corresponding rate constants at various temperatures.....	114
Table 4-4. Summary of purity and isomeric composition results of lactide products from PLA depolymerization at various temperatures.....	115
Table 4-5. Carbon efficiency for primary and secondary scenario	116
Table 4-6. Corn Cultivation Material and Energy Inputs and Outputs	117
Table 4-7. Corn Wet Milling Material and Energy Inputs and Outputs.....	118
Table 4-8. Dextrose Production Material and Energy Inputs and Outputs.....	119
Table 4-9. Lactic Acid Production Material and Energy Inputs and Outputs	120
Table 4-10. Lactide Production Material and Energy Inputs and Outputs.....	120
Table 4-11. PLA Polymerization Material and Energy Inputs and Outputs.....	121
Table 4-12. PLA Composting Material and Energy Inputs and Outputs	122
Table 4-13. Corn Cultivation Material and Energy Inputs and Outputs	123
Table 4-14. Corn Wet Milling Material and Energy Inputs and Outputs.....	124
Table 4-15. Dextrose Production Material and Energy Inputs and Outputs.....	125
Table 4-16. Lactic Acid Production Material and Energy Inputs and Outputs	126
Table 4-17. Lactide Production Material and Energy Inputs and Outputs.....	126
Table 4-18. PLA Polymerization Material and Energy Inputs and Outputs.....	127
Table 4-19. PLA Recycling Material and Energy Inputs and Outputs.....	128
Table 4-20. PLA Composting Material and Energy Inputs and Outputs	128
Table 4-21. Contribution analysis of global warming potential	130
Table 4-22. Contribution analysis for land use	131
Table 4-23. Contribution analysis for water use	133
Table 4-24. Contribution analysis for resource depletion	134

LIST OF FIGURES

Figure 1-1. Biodegradability of plastics and other raw materials in marine environment [4]	1
Figure 1-2. Diagram defining sources and degradability of commercial plastics	3
Figure 1-3. Test method to measure biodegradation rate (left) for validation of complete biodegradation (right) [38]	6
Figure 1-4. Life cycle of PLA.....	7
Figure 1-5. One platform C6 sugars biorefinery to produce PLA from corn starch.....	8
Figure 1-6. (a) 99% optically pure PLLA structure (b) 99% optically pure PDLA structure (c) poly(DL-Lactide) w/ 10% D-content (d) poly(L-co-meso-lactide) w/ 10% D-content.....	10
Figure 1-7. PLA formation and possible end-of-life scenarios	11
Figure 2-1. (a) Direct polycondensation route of PLA vs (b) Ring-opening polymerization route of PLA	15
Figure 2-2. Lactic acid and lactide stereoisomers, and their respective polymer structures	17
Figure 2-3. ROP of lactide to form PLA via coordination insertion with tin (II) ethylhexanoate	20
Figure 2-4. Polystyrene calibration curve for size exclusion chromatography analysis; MW range from 35000 to 900000.....	21
Figure 2-5. (a) FTIR spectra of poly(meso-lactide) (b) Confirmation of PLA polymerization characterized by the absorption band at $\sim 1725\text{ cm}^{-1}$	26
Figure 2-6. Optical rotation of poly(L-co-D-lactide) at different compositions of D-lactide (2-20wt%) and poly(L-co-meso-lactide) at different compositions of meso-lactide (2-20wt%). The experimentally observed values are represented as symbols, whereas the theoretical calculations are represented as lines.....	29
Figure 2-7. Specific rotation of poly(L-co-meso-lactide) and poly(L-co-D-lactide) at different compositions of meso, D, and poly-meso content (0-20wt%)	31
Figure 2-8. NMR spectrum displaying the isisi and iiiss resonances for D-lactide and meso-lactide, respectively in (a) 3052D and (b) 4060D	32
Figure 2-9. NMR spectra of (a) poly(L-lactide) and (b) poly(meso-lactide).....	34

Figure 2-10. Ring-opening polymerization of meso-lactide via coordination insertion; atactic PLA is produced as while the integrity of the stereocenter is preserved, the meso-lactide can insert from both the R or S side, making it random insertion	34
Figure 2-11. NMR spectra of poly(L-co-meso-lactide) at (a) 2% meso content (b) 4% meso content (c) 10% meso content (d) 20% meso content.....	35
Figure 2-12. DSC data on the second heating cycle for poly(L-lactide) and poly(meso-lactide)	36
Figure 2-13. DSC data on the second heating scan for poly(L-co-meso-lactide) at 2% meso content, 4% meso content, 10% meso content, and 20% meso content.....	37
Figure 2-14. Thermal degradation of (a) PLLA and (b) poly(meso-lactide)	38
Figure 2-15. Stress-strain curves of Ingeo standard grades of PLA	39
Figure 2-16. Complex viscosity of NatureWorks PLA standard grades at various meso-lactide content; 3100HP – 1%, 3052D – 9%, 4060D- 22 wt%.....	43
Figure 2-17. NMR spectrum displaying the isisi and iiiss resonances for D-lactide and meso-lactide, respectively in LX930.....	45
Figure 2-18. ESI-MS data displaying water-soluble degradation products (i.e.: lactic acid) for PLA samples after hydrolysis in water at 37°C for 12 days; the legend shows the lactic acid oligomers (mono-, di-, tri-, etc.) that appear for each sample after hydrolysis	46
Figure 2-19. Thermal degradation behavior of glycolytic inhibitors: (a) 2DG (b) 3PO (c) a.a. (d) DIDS (e) CHC (f) Metformin	49
Figure 2-20. Isothermal degradation kinetics of glycolytic inhibitors: (a) 2DG (b) 3PO (c) a.a. (d) DIDS (e) CHC (f) Metformin; weight loss at 0 minutes for 2DG, 3PO, and a.a. are due to DSC temperature equilibration	50
Figure 2-21. SEM images and EDX elemental map of 3100HP and glycolytic inhibitors- (a) SEM S image of 3100HP + a.a. (b) EDX S map of chlorine in 3100HP + a.a. (c) SEM CS image of 3100HP + a.a. (d) EDX CS map of chlorine in 3100HP + a.a. (e) SEM S image of 3100HP + DIDS (f) EDX S map of sulfur in 3100HP + DIDS (g) SEM CS image of 3100HP + DIDS (h) EDX CS map of sulfur in 3100HP + DIDS	52
Figure 3-1. PLA materials of various configurations and tacticities, in order of increasing melting point and crystallinity.....	56
Figure 3-2. First DSC thermogram of pellets comprising 50% stereocomplex crystallites/50% PLA homocrystallites based on melting enthalpy calculations	59

Figure 3-3. Processing conditions for first trial run of stereocomplex PLA in a co-rotating twin-screw extruder type ZSE 27 HP–PH from Leistritz.....	60
Figure 3-4. DSC thermograms on stereocomplex PLA (a) First heating scan - stereocomplex crystallite formation (b) Second heating scan – thermal dissociation of stereocomplex crystallites to homocrystallites	61
Figure 3-5. Processing conditions for new trial run of stereocomplex PLA in a co-rotating twin-screw extruder type ZSE 27 HP–PH from Leistritz.....	62
Figure 3-6. Processing conditions for composites manufacturing of PLA/Stereocomplex PLA composites in a co-rotating twin-screw extruder type ZSE 27 HP–PH from Leistritz.....	66
Figure 3-7. Schematic representation depicting the competitive formation of stereocomplex crystallites during extrusion of PLLA and PDLA	70
Figure 3-8. DSC thermograms displaying stereocomplex formation after sample is held isothermally for 1-3 minutes at temperatures of (a) 180°C (b) 190°C (c) 200°C (d) 210°C (e) 220°C (f) 230°C	72
Figure 3-9. (a) Isothermal stereocomplexation (b) Effect of temperature on stereocomplex formation	73
Figure 3-10. (a) FTIR spectra of PLLA (black line) and stereocomplex PLA (red line) (b) FTIR spectra displaying characteristic absorption bands. Spectra displayed involves stereocomplex PLA collection time at 20 minutes.....	74
Figure 3-11. WAXD profiles of (a) pure PLLA and (b) Stereocomplex PLA (50/50 L/D)	75
Figure 3-12. Crystal structure of stereocomplex PLA [143]	76
Figure 3-13. DSC thermograms of stereocomplex PLA at sample collection times of (a) 5 minutes (b) 10 minutes (c) 20 minutes (d) 40 minutes	77
Figure 3-14. Thermal degradation of (a) stereocomplex PLA and (b) PLLA (L175).....	79
Figure 3-15. DSC thermograms of 70% 3100HP/30% stereocomplex PLA at sample collection times of (a) 5 minutes (b) 10 minutes (c) 20 minutes (d) 40 minutes	82
Figure 3-16. DSC thermograms of 70% 4060D/30% stereocomplex PLA at sample collection times of (a) 5 minutes (b) 10 minutes (c) 20 minutes (d) 40 minutes	84
Figure 3-17. DSC thermograms of 95% 3100HP/5% stereocomplex PLA	84
Figure 3-18. WAXD profiles of (a) 70% 3100HP/30% Stereocomplex PLA (b) 70% 4060D/30% Stereocomplex PLA (c) 95% 3100HP/5% Stereocomplex PLA.....	85

Figure 3-19. Tensile stress strain curves of reprocessed neat PLA vs PLA/Stereocomplex PLA composites (a) Extruded 3100HP, 70% 3100HP/30% Stereocomplex PLA, 95% 3100HP/5% Stereocomplex PLA (b) Extruded 4060D, 70% 4060D/30% Stereocomplex PLA	87
Figure 3-20. DSC thermograms displaying the isothermal melt crystallization times at different temperatures for (a) Neat PLA (3100HP) and (b) PLA (3100HP) + 5% Stereocomplex	93
Figure 3-21. Fractional crystallinity vs time of (a) Neat PLA (3100HP) and (b) PLA (3100HP) + 5% Stereocomplex at different temperatures.....	93
Figure 3-22. Avrami double log plots for the crystallization of (a) Neat PLA (3100HP) and (b) PLA (3100HP) + 5% Stereocomplex at different temperatures	94
Figure 3-23. Half time to crystallization vs isothermal crystallization temperatures for neat PLA (3100HP) and PLA (3100HP) + 5% Stereocomplex at different temperatures	95
Figure 4-1. Reversible reaction of PLA	99
Figure 4-2. Experimental setup (a) The reaction vessel containing PLA with 0.6 wt% Sn[Oct] ₂ is heated in the oil bath and connected to a (b) condenser that is wrapped with heating tape to ensure lactide vapor passage to the (c) lactide collectors. The lactide collectors are connected to a (d) vapor trap via a tube, and the vapor trap connects to the vacuum pump (not shown).....	101
Figure 4-3. Proposed two-step depolymerization mechanism of PLA in presence of Sn[Oct] ₂ catalyst [73]	102
Figure 4-4. Schematic diagram of PLA thermodepolymerization in a (a) batch reactor. The PLA sample (reactant 1) and catalyst Sn[Oct] ₂ (reactant 2) are added to the reactor. Over a period of time, the lactide sample is vacuum pumped to the (b) lactide collector. Any residual lactide is captured by the (c) vapor trap to vacuum.....	105
Figure 4-5. Primary scenario of PLA production from corn cultivation to composting	107
Figure 4-6. Primary scenario of PLA production from corn cultivation to recycling.....	107
Figure 4-7. DSC purity determination of PLA samples for (a) PLLA at 200°C (b) RePLA at 200°C (c) PLLA at 220°C (d) RePLA at 220°C (e) PLLA at 240°C (f) RePLA at 240°C	110
Figure 4-8. Racemization mechanism of PLA depolymerization based on Sn (II) reaction on asymmetrical methine carbon	111
Figure 4-9. Lactide yield of PLA depolymerization at different temperatures	114
Figure 4-10. Arrhenius model on temperature dependence of the depolymerization rate constant of L-lactide with stannous octoate catalyst	115

Figure 4-11. Global warming potential of PLA recycling vs composting	130
Figure 4-12. Land usage of PLA recycling vs composting	132
Figure 4-13. Water usage of PLA recycling vs composting.....	133
Figure 4-14. Resource depletion for PLA recycling vs composting	135
Figure 4-15. Effect of variation in corn production and recycling on land usage	137
Figure 4-16. Effect of variation in recycling on water usage	138
Figure 4-17. Effect of variation in recycling on water usage	139
Figure 4-18. Effect of variation in recycling on global warming potential.....	140
Figure 4-19. Two-step PLA recycling process via thermodepolymerization in a batch reactor, followed by polymerization in a co-rotating twin screw extruder. Diagram includes the temperature profile and screw configuration required to produce high molecular weight PLA from lactide.	142

KEY TO SYMBOLS OR ABBREVIATIONS

PLA	Poly lactide
PLLA	Poly(L-lactide)
PDLA	Poly(D-lactide)
PMLA	Poly(meso-lactide)
PLMLA	Poly(L-co-meso-lactide)
PDLLA	Poly(DL-lactide)
PLA-Stx	Stereocomplex poly lactide
REX	Reactive extrusion
TGA	Thermogravimetric analysis
DSC	Differential scanning calorimetry
GPC	Gel permeation chromatography
GC	Gas chromatography
NMR	Nuclear magnetic resonance
SEM	Scanning electron microscopy
FTIR	Fourier transform infrared spectroscopy
DCM	dichloromethane
o.p.	optical purity
α_{obs}^{25}	observed optical rotation
$[\alpha]^{25}$	specific rotation

1. INTRODUCTION & BACKGROUND

1.1. The Impact of Fossil-Based Plastics

Plastics make up about 10% of household waste, with the majority disposed in landfill [1], [2]. An estimated 60-80% of waste are plastics found in the ocean or on beaches. One report estimates 2.3 billion pieces of plastics recovered from Southern California beaches over a span of 72 hours, weighing about 30,500 kg. The majority of this plastic waste were polystyrene foams (71%) , miscellaneous fragments (14%), pre-production pellets (10%), and whole items (1%); 81% of all plastics ranged between 1 and 4.75mm in size [3]. As seen in **Figure 1-1**, the estimated time for plastics to biodegrade in the ocean can take up to 600 years- 50 years for styrofoam cups and 450 years for plastic bottles [4].

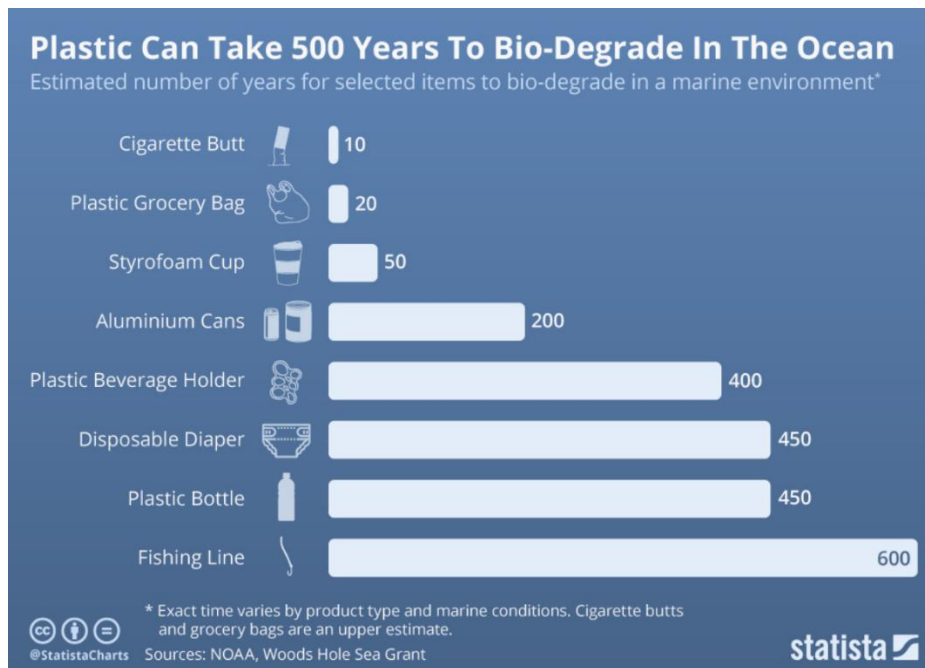


Figure 1-1. Biodegradability of plastics and other raw materials in marine environment [4]

The Central Pollution Control Board (CPCB) reports the plastic consumption in India to be 8 million tons per annum, while about 5.7 million tons of plastic is converted into waste annually [5]. In 2007, over 250 million tons of plastic waste were produced [6]. The lack of biodegradability,

compostability and low density of plastics make them unfit for landfill disposal [7]. In 2009, an estimated 230 million tons of plastic were produced, where 25% of these plastics were used in the European Union (EU) [8]. Thermoplastics have been a focus, as they have caused several issues in India, including choked sewers, animal death and clogged soils [6]. As a result, researchers must target sustainable environment and sustainable health issues, as plastics are having a detrimental cause to not only the environment, but the health of the people.

One report by the Center for International Environmental LAW (CIEL) states that annual emissions could grow to more than 2.75 billion metric tons of CO₂e from plastic production and incineration by 2050. Their total greenhouse gas (GHG) emissions are predicted to be over 56 gigatons CO₂e by 2050, or between 10–13 percent of the total carbon budget [9]. The United Nations Development Program (UNDP) has also stressed the importance of working towards a sustainable economy, with efficient use of natural resources, and the minimization of waste/pollution [10]. The global plastics production reached up to 370 mega tons in 2019 [11]. As of 2015, 79% of all plastic produced had been accumulating in landfills and the environment [12]. The UN Environment Programme (UNEP) reports that only 9% of all plastic ever produced has been recycled, whereas 12% has been incinerated and the rest accumulates in landfills [13]. Plastic debris in the natural environment is extremely persistent, with degradation in seawater estimated to range from hundreds to thousands of years [14], [15]. The challenges of targeting these sustainability issues involve the production of plastics, misuse, and pollution, ranging from single dose product packaging, mixed plastic packages, and littering, to microplastics, high-carbon footprints, and lack of appropriate labeling.

1.2. The Promise of Bioplastics

In order to reduce the environmental impact of petroleum-based plastics, bioplastics are currently being studied as a potential substitute for commercial application. The term biobased and biodegradable are not interchangeable. Biobased polymers define materials derived from renewable resources (i.e.: corn starch, potato starch, cassava starch, etc.), whereas biodegradable polymers are consumed by microorganisms under specific environmental conditions [16]–[18] (See **Figure 1-2**). Examples of biobased, biodegradable polymers include polylactide (PLA), polyhydroxyalkanoates (PHAs) and bio-based polybutylene succinate (bio-PBS), as well as starch-based thermoplastics (TPS) [19]–[22]. Examples of biobased polymers are biobased polyamides (bio-PA), polyethylene (bio-PE), polyethylene terephthalate (bio-PET) [23], [24]. Lastly, biodegradable polymers that are based on fossil resources include polybutylene succinate (PBS), polycaprolactone (PCL), polyvinyl alcohol (PVA), and polybutylene adipate terephthalate (PBAT) [25]–[28]. Furthermore, polymers such as bio-PE, which are bio-based and chemically identical to their fossil-based counterparts, are typically referred to as drop-in polymers.

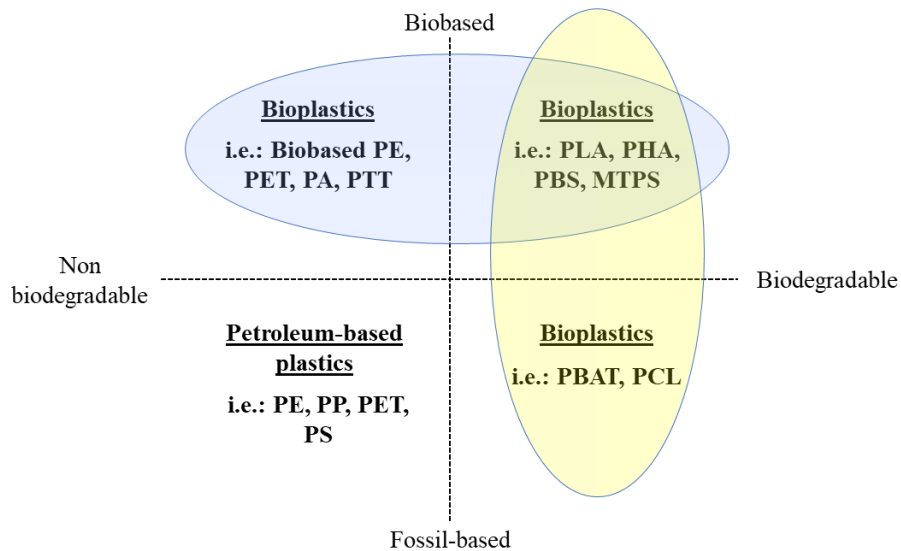


Figure 1-2. Diagram defining sources and degradability of commercial plastics

The current bioplastics market is relatively small in comparison to the petroleum-based plastics industry. According to a report by European Bioplastics, the global production of bioplastics in 2018 was around 2 mega tons, whereas the global production for petroleum-based plastics was estimated to be around 360 mega tons. Statistics show that the bioplastics market will gradually grow for the next five years, increasing in volume by around 40% [29].

As previously discussed, biobased polymers are either completely or partly derived from some type of natural source, which may include plants, microorganisms, algae, and food waste. There are several biobased polymers that are obtained from polymers that form directly within microorganisms and plants. For example, cellulose—the most naturally abundant organic compound and the main ingredient in plant fibers—has been commercially available since the 19th century. There are three routes to produce bio-based plastics: (1) polymerization of bio-based monomers; (2) modification of naturally occurring polymers; (3) extraction of polymers from microorganisms [30]. American Society for Testing and Materials (ASTM) developed a standard test method, ASTM D6866, to determine bio-based content. Originally developed for the US Department of Agriculture (USDA) Bio-Preferred program, this test method uses radio-labelling of carbon to quantify the bio-based content of materials [31]. This has been widely used by industries and universities alike to incorporate biobased content into commercial plastics, such as polyethylene terephthalate (PET).

While the infrastructure of recycling will remain for many years to come, another end-of-life process must be introduced to dispose of raw materials. Development of biodegradable or industrially compostable polymers is a solution researchers have been studying to replace non-degradable plastics. As explained previously, biodegradable polymers are susceptible to be broken down into smaller molecules due to the action of microorganisms. Microorganisms utilize the

carbon content to extract energy for their processes. Specifically, the material is first broken down into smaller molecules by enzyme secretion or disintegration. The molecules are then transported into the organisms' cell, then they are oxidized to carbon dioxide and water. Biodegradable polymers have the potential to improve soil fertility, reduce petroleum-based plastic disposal, and reduce the cost of generated waste. However, there are several challenges that must be overcome before scaling up biodegradable polymers as alternatives to petroleum-based polymers [32], [33]:

1. The biodegradation rate is often dictated by the type and composition of the substances in bioplastic.
2. Certain environmental conditions (temperature, humidity, etc.) are required for biodegradation within a reasonable timeframe (4-6 weeks)
3. Biodegradable polymers have inferior material properties compared to conventional plastics. They require additional additives to improve the properties.

There are several standards in place to determine biodegradability and compostability under specific environmental conditions. In order to market a commercial plastic as biodegradable or compostable, the main standards to follow are the European EN 13432 or EN 14995, the international ISO 17088 or the ASTM D6400 [34]–[37]. Several factors must be considered to conform to the standards, including a simulated environment, the biodegradability indicator, the inoculum, test duration, number of replicates required, and the percent biodegradation to pass the test [38]. It can be noticed that the biodegradability evaluation is carried out by different experimental methodologies, such as release of carbon dioxide and oxygen demand measurements. The fundamental requirements of these worldwide standards for complete biodegradation based on composting are: (1) Conversion to carbon dioxide, water, and biomass via microbial action (2) At least 90% conversion of the carbon in the test material to carbon dioxide (3) Rate of

biodegradation must match natural resources (i.e.: leaves, grass) (4) Time for complete biodegradation must be less than or equal to 6 months. These conditions are further described in **Figure 1-3** [38].

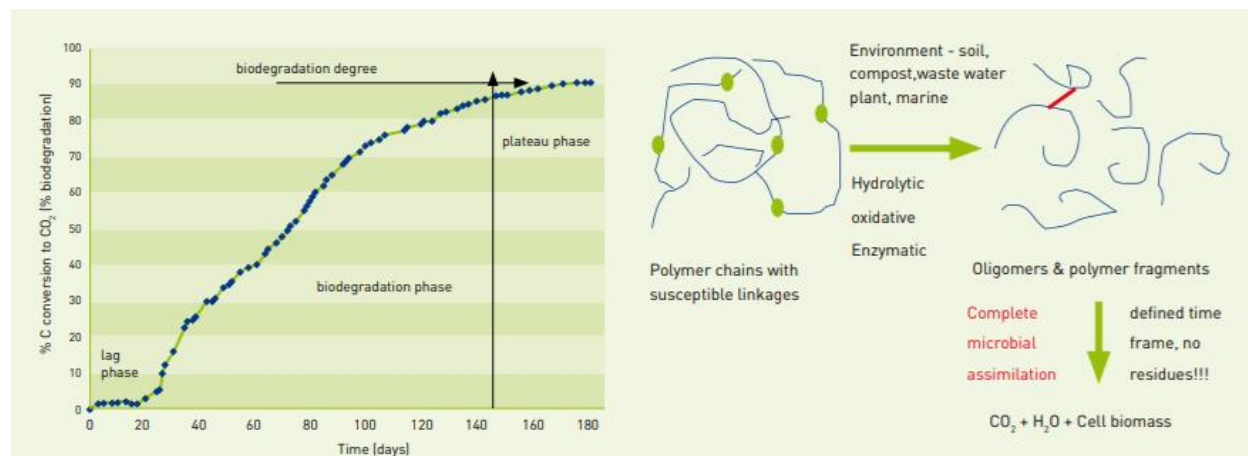


Figure 1-3. Test method to measure biodegradation rate (left) for validation of complete biodegradation (right) [38]

Certain biobased polymers, such as PLA, also happen to be biodegradable under controlled conditions (i.e.: temperature, humidity), which offers the added value of having a viable end-of-life option [39]. These conditions are controlled by the material properties (i.e.: glass transition temperature), which can in turn be modified solely based on the stereochemistry of the PLA polymer. Thus, PLA is one of the few bioplastics that holds the most promise when to addressing the plastics waste problem by closing the loop around the production and use cycle.

1.3. Polylactide

Poly lactide (PLA) is a material that is both biobased and industrially compostable, and a highly versatile thermoplastic. Poly lactide (PLA) has been a promising candidate in medical applications (i.e.: drug delivery) and environmentally friendly applications (i.e.: packaging) due to its biocompatibility and biodegradable behavior. Synthesis of high molecular weight polymer is usually done via the melt polymerization method without solvent, at high temperatures (130-220°

C). Tin (II) ethylhexanoate ($\text{Sn}[\text{Oct}]_2$) is the preferred candidate for catalyzing the reaction due to its rapid polymerization rate, low degree of racemization at higher temperatures, and low toxicity [40].

Figure 1-4 displays the chemistry behind PLA's cradle-to-grave system, starting from corn starch and ending at CO_2 and H_2O from biodegradation. In order to produce high molecular weight PLA, dextrose must be obtained via enzyme hydrolysis from starch; starch is refined from crops such as sugarcane, corn, and even cassava. Lactic acid can then be fermented from dextrose, and then dimerized to lactide via a two-step polymerization-depolymerization reaction. After further purification, high molecular weight PLA can be produced by ring-opening polymerization of lactide in the melt form [41], [42].

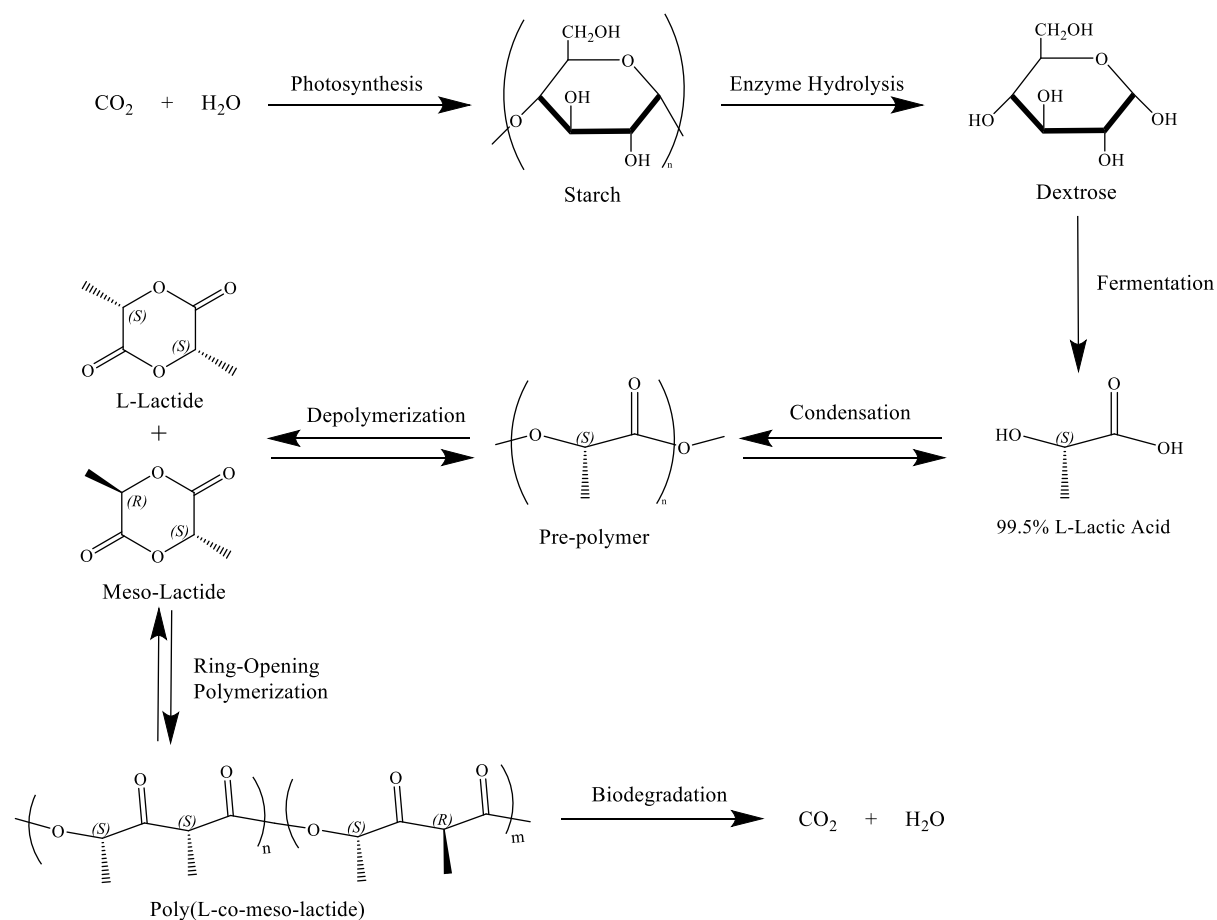


Figure 1-4. Life cycle of PLA

The common classification of a bio-refinery approach is based on four main features (1) Platform (2) Feedstock (3) Products and (4) Processes [43]. The classification diagram for PLA bio-refinery is shown in **Figure 1-5**. It is a one platform (C6 sugars), one feedstock (corn kernel) bio-refinery, for producing polylactide via melt polymerization of lactide.

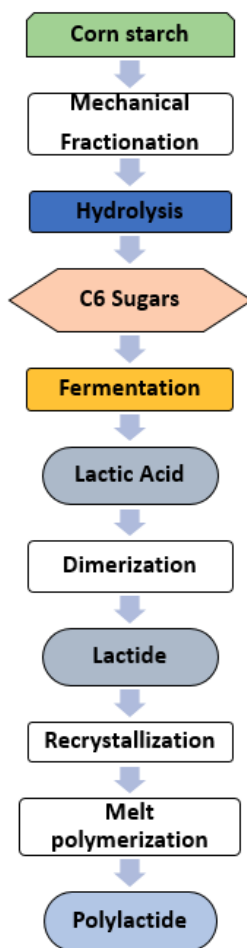


Figure 1-5. One platform C6 sugars biorefinery to produce PLA from corn starch

1.3.1 PLA Stereochemistry

Poly lactide's (PLA) versatility is due to its unique stereochemical structure, in that the composition of its respective lactide isomers directly determines the material properties of the resulting polymer; this, in turn, determines the final application of the PLA product. As a chiral molecule, PLA's cyclic monomer lactide possesses three different stereoisomers: L-lactide, D-lactide, and

meso-lactide. The meso compound possesses considerably different properties (mechanical, thermal, etc.) compared to lactide's enantiomers, and it produces a completely amorphous polymer due to the atactic structure of the resulting polymer [44]. The lactide ratio formed follows closely to the statistical distribution of *R* and *S* lactic acids, with the two pure enantiomers being D (*RR*) and L (*SS*), as well as the meso compound (*RS*). Statistically, if the lactic acid is 98% L and 2% D, then the *SS* lactide is 96.04%, the *RR* lactide 0.04%, and *RS* lactide 3.92%. One study developed a technique to analyze the D-lactide content in a lactide stereoisomeric mixture using a combination of gas-chromatography-polarimetry. The method can be used to distinguish between the stereoisomers and impurities (lactic acid, oligomers) [45]. By adding D-isomer or meso-isomer into an L-isomer based PLA system, the polymer chains widen and cannot be packed into an ordered manner compared to enantiopure PLLA (**Figure 1-6a**). The resulting material, poly(DL-lactide) (PDLLA) (**Figure 1-6c**) or poly(L-co-meso-lactide) (PLMLA) (**Figure 1-6d**), is characterized by its material properties which may be modulated based on the different L/D or L/meso compositions.

By controlling the crystallinity of the material using the stereoisomers, one can modify the performance of the polymer [46]–[49]. Primary suppliers of PLA, such as NatureWorks and Total Corbion, have optimized this method at controlling the crystallinity and molecular weights of PLA at industrial scale via reactive extrusion [50]. Understanding how the stereochemistry of PLA plays a role in the polymer's material behavior is key to optimizing the production process to obtain desired properties of the product. Exploring the fundamental stereochemistry of PLA and its effect on material properties forms the primary focal point of this thesis.

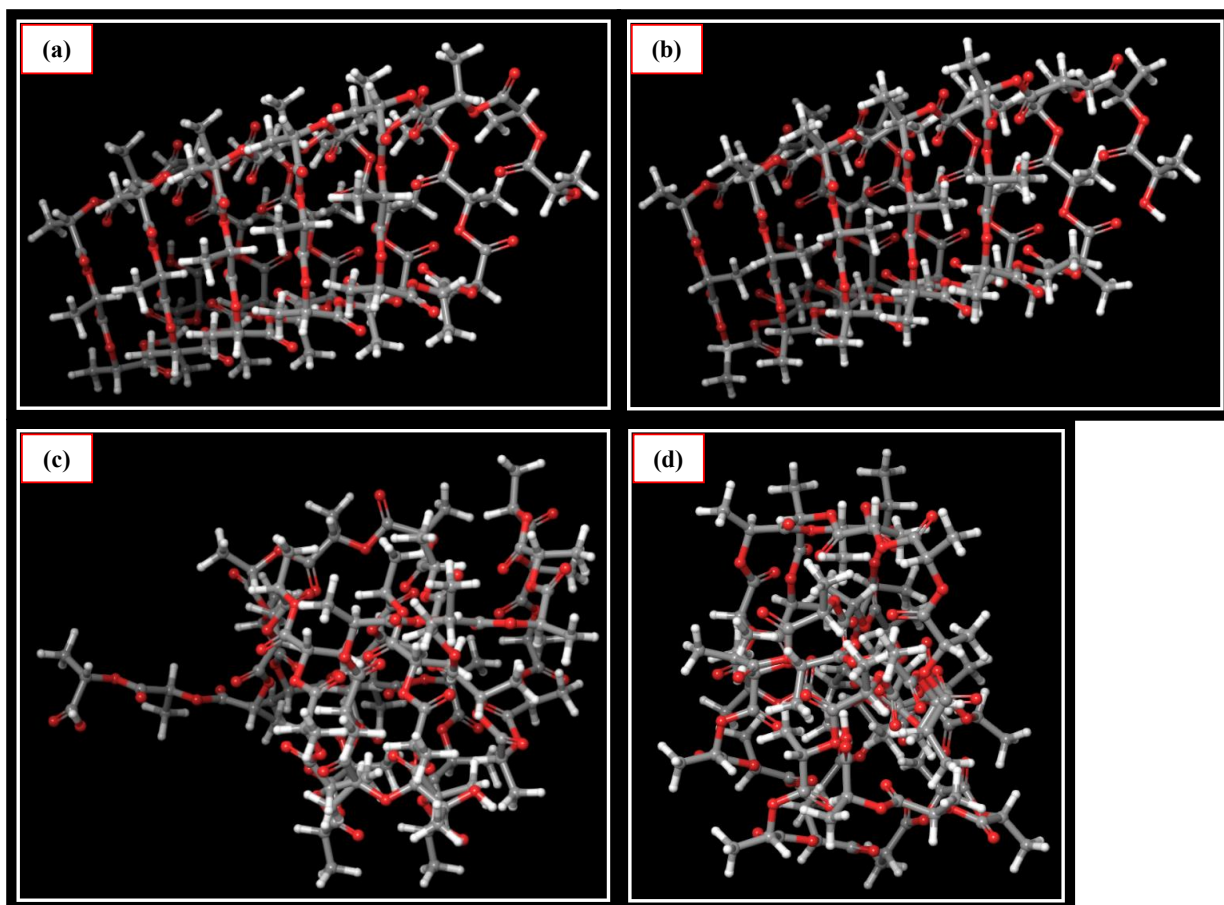


Figure 1-6. (a) 99% optically pure PLLA structure (b) 99% optically pure PDLA structure (c) poly(DL-Lactide) w/ 10% D-content (d) poly(L-co-meso-lactide) w/ 10% D-content

1.3.2 PLA End-of-Life Scenarios

Despite the advantageous properties of being biobased and biodegradable, the mismanagement of PLA's end-of-life still contributes to plastic pollution. It is often misunderstood in the scientific community that PLA readily degrades in the natural environment. This misunderstanding is complicated further by the various studies testing PLA biodegradability under variable conditions and environments [51]. Several studies have reported that PLA does not degrade or slowly degrades in soil/compost temperatures under 50°C [52]–[54]. Since soil temperature is below 35°C, it would take a year or more to fully degrade PLA. However, studies have shown that PLA will readily degrade in compost temperatures up to PLA glass transition (50-60°C) based on carbon

dioxide release [55], [56]. In an anaerobic environment, PLA degradation widely varies depending on mesophilic or thermophilic temperatures, the inoculum used to increase the rate and extent of biodegradation, and the optimization of solid content [57]. Several studies on PLA anaerobic digestion have been outlined and shown to be effective in a lab-scale environment [58]. More recently, the effectiveness of anaerobic digestion of PLA in pilot scale was studied. PLA samples were degraded at 55°C for five weeks in a pilot scale reactor, and biogas production ($\text{CH}_4 + \text{CO}_2$) was analyzed. Results showed that there was less than 50% degradation for PLA in that timeframe, suggesting that anaerobic digestion is not feasible for PLA at industrial biogas plants [59].

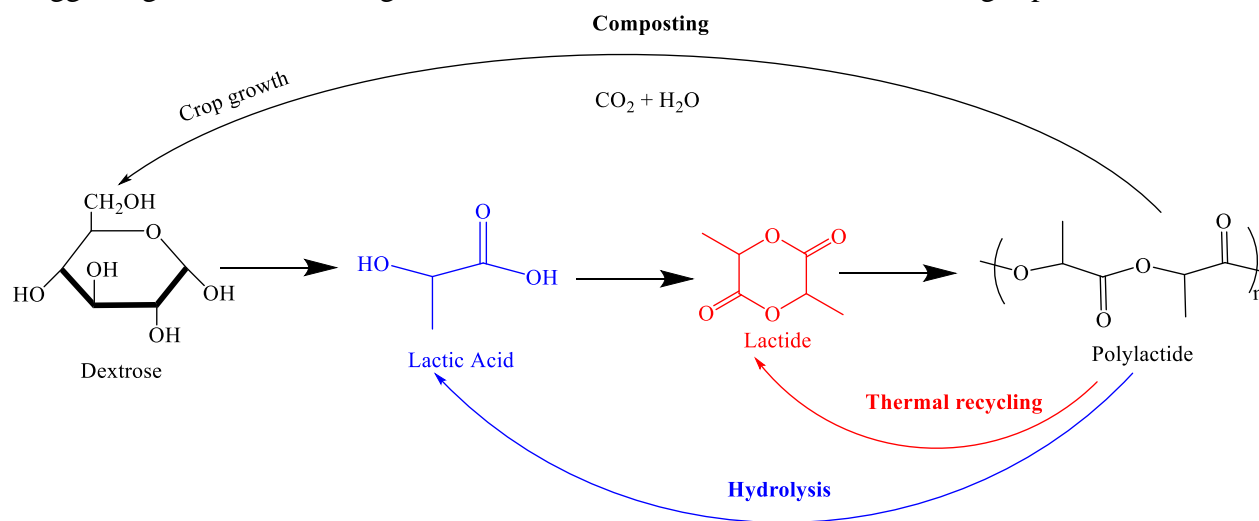


Figure 1-7. PLA formation and possible end-of-life scenarios

PLA degradation in marine environments has also been a challenging obstacle for researchers due to a wide range of variables and conditions that need to be considered. Studies have shown that no PLA degradation occurred within a year at room temperature in a seawater and freshwater environment [60], [61].

While industrial composting is currently the novel method for PLA end-of-life, the product is lost as CO_2 and water, with no recovery gained compared to recyclable plastics (i.e.: polyethylene, polypropylene). As a result, researchers have looked into chemical recycling options due to the

benefit of recovering valuable materials (i.e.: lactic acid, oligomers, etc) from PLA as well as the method's tolerance to contamination with other plastics; this, in turn, reduces the need for costly separation [62], [63]. Ironically, the effectiveness of the recycling option depends on the stereochemistry of the polymer in that it must be maintained throughout the process, such as in PLA hydrolysis.

Due to PLA's poor solubility in aqueous media, PLA must be hydrolyzed at high temperatures or strong acidic/basic conditions to produce lactic acid. The mechanism behind the heterogeneous hydrolysis of PLA depends on a number of factors, such as hydrolysis rate and rate of water diffusion into the particle, which depends on molecular weight, pH, temperature, and the shape of the polymer. In the case of bulk degradation, where water diffusivity is faster than hydrolysis, the polymer maintains its shape but loses volume and molecular weight homogeneously across the whole sample; otherwise, surface erosion occurs in which mass loss occurs only on the surface while bulk remains intact [64], [65]. There have been several recent studies reporting the hydrolytic degradation of PLA [66]–[68]. Hydrolytic degradation involves water diffusion into the bulk of the material, which begins in the amorphous regions then crystalline domains. One group detected a faster degradation rate when PLA was submerged in 50% ethanol compared to water, which was due to the rapid ethanol diffusion rate [67]. Other studies have tested the use of nanoclays and surfactant on PLA biodegradation, but further studies were needed to conclude the effectiveness on hydrolytic degradation [69].

Along with hydrolysis, pyrolysis is another chemical recycling route that is being currently explored as a possible PLA end-of-life process. One study explored the lactide formation from PLA thermodepolymerization as a function of time, temperature, and catalyst concentration using thermogravimetric analysis (TGA), studying the reversible rate kinetics. A full weight loss was

observed at 210°C after 30 minutes using a 0.6wt% catalyst concentration of Sn[Oct]₂ [70]. A study on the pyrolysis mechanism of PLA to lactide using tin catalyst has also been reported based on four different end-groups and molecular weights of PLA. Researchers concluded that thermodepolymerization of PLA yields lactide through the unzipping and intramolecular transesterification reactions; this includes the backbiting reaction caused by the Sn-carboxylate and Sn-alkoxide chain ends, which are formed from the carboxyl/hydroxyl end-groups of PLA [71]. Both hydrolysis and pyrolysis highly depend on maintaining the stereochemistry of the product in order to avoid further purification. It is in this area that we discuss how PLA's versatility affects its possible end-of-life scenarios.

1.4. Summary of Work

This thesis is broken down into three sections focused on polylactide (PLA) stereochemistry. The first section focuses on understanding the fundamental stereochemistry of PLA and its implication on material performance. Synthesized copolymers of L-lactide and D-lactide as well as synthesized copolymers of L-lactide and meso-lactide are developed. Optical rotation analysis is used to analyze the effect of D-lactide and meso-lactide on the stereochemistry of PLA. Based on this analysis, the stereoisomeric composition of commercial grade PLA is identified and quantified using optical rotation and ¹H NMR. The effect of the stereoisomeric composition on the tacticity and thus crystallinity of synthesized poly(L-co-meso-lactide) is then analyzed to understand the role of stereochemistry in polymer chain packing and thermal properties. The role of stereochemistry in the tensile and rheological behavior in commercial PLA is also reported in this thesis. We conclude this section with characterizing the effect of PLA stereochemistry in immune cellular response, particularly PLA breakdown and extraction due to hydrolytic degradation.

The next section continues studies in PLA stereochemistry by focusing on PLA stereocomplexation; it consists of two parts. Part I focuses on developing a pilot-scale continuous manufacturing setup to produce stereocomplex PLA via reactive extrusion of high molecular weight poly(L-lactide) (PLLA) and high molecular weight poly(D-lactide) (PDLA). The characteristics of stereocomplexation are analyzed to understand the effect of temperature and time and thus optimize the processing conditions. Stereocomplex PLA is first confirmed via Fourier transform infrared spectroscopy (FTIR). The crystal structure, crystallinity, and stereocomplex formation are then characterized using wide angle X-ray diffraction (WAXD). These results are further supplemented with differential scanning calorimetry (DSC), in addition to characterizing the thermal properties of stereocomplex PLA.

The value and application of stereocomplex PLA are then studied in Part II. Particularly, stereocomplex PLA is studied for potential application as a reinforcing fiber/filler and as a nucleating agent for PLA homopolymers. Molecular composites comprising stereocomplex PLA particles in a thermoplastic PLA matrix are developed via twin-screw extrusion. The crystallinity and dispersity of the filler are characterized at different collection times via DSC and WAXD. The tensile properties of the composites are then characterized and compared with reprocessed neat PLA (the matrix). Finally, the isothermal crystallization kinetics are studied using Avrami analysis to analyze the effect of stereocomplex PLA as a nucleating agent on PLA.

The final part discusses an end-of-life method to recycle PLA via thermo-depolymerization. The depolymerization kinetics, lactide yield, lactide purity, and stereoisomeric composition of the final product are analyzed via mass balance, DSC, and gas chromatography-polarimetry, respectively. A life-cycle assessment is finally carried out to look into the environmental impact of end-of-life recycling versus composting PLA.

2. THE STEREOCHEMISTRY OF PLA AND ITS IMPLICATION ON PERFORMANCE PROPERTIES

2.1. Introduction

Poly lactide (PLA) is extensively used in medical applications (drug delivery, scaffolds, bone growth and tissue regeneration) and recently in industrial products such as packaging and 3D-printing [19], [72]–[79]. PLA can be manufactured by direct polycondensation (**Figure 2-1a**) or ring-opening polymerization (ROP; **Figure 2-1b**). In ROP, the lactic acid is first dimerized to lactide via a two-step polymerization-depolymerization reaction. The ROP route to PLA is the commercially preferred method by industries (NatureWorks (150kton plant in USA) and Total Corbion (75kton plant in Thailand, and 100kton plant in France)) [41], [42]. Emerging PLA companies in China also follow the lactide ROP technology.

PLA's cyclic monomer lactide possesses three different stereoisomers: L-lactide, D-lactide, and meso-lactide. L-lactide and D-lactide stereoisomers possess identical physical and chemical properties, except in their ability to rotate plane of polarized light, and they produce semi-crystalline polymers; meso-lactide is optically inactive [45], [80]–[84]. The meso compound possesses different physical/chemical properties and will result in an amorphous polymer [77].

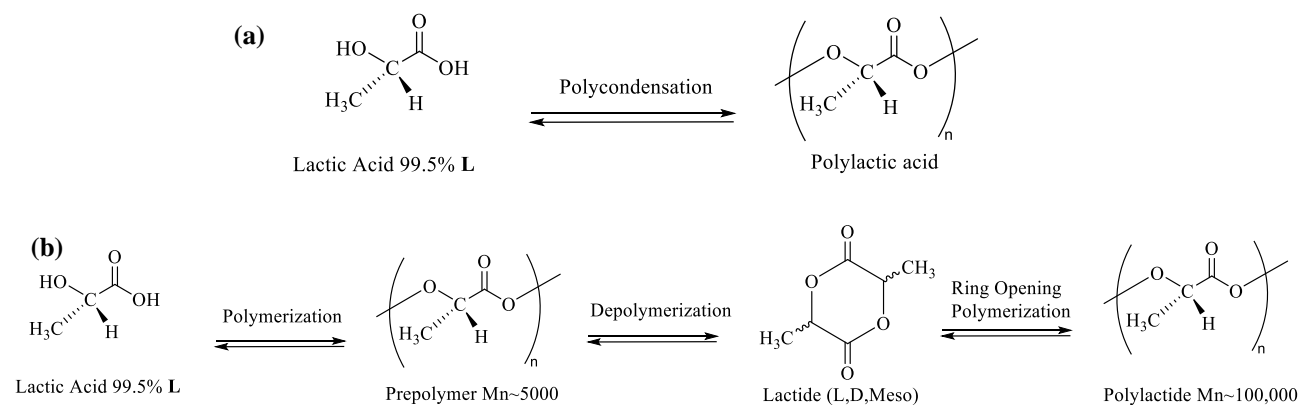


Figure 2-1. (a) Direct polycondensation route of PLA vs (b) Ring-opening polymerization route of PLA

By controlling the crystallinity of the material using the stereoisomers, the performance of the polymer may be modified [46], [49], [85], [86]. More importantly, the composition of lactide isomers (L, D, meso) influences the material properties of the resulting polymer, which in turn determines the end application of PLA. Most literature reports identify the stereochemistry to comprise L-lactide and D-lactide [50], [87]–[92]. This is erroneous and needs to be corrected.

The lactide ratio formed follows closely to the statistical distribution of D- (*R*) and L- (*S*) lactic acids, with the two pure enantiomers being D (*RR*) and L (*SS*); meso compounds are *RS*. Statistically, if the lactic acid is 98% L and 2% D, then the L (*SS*) lactide will be 96.04%, the meso (*RS*) lactide 3.92%, and the D- (*RR*) lactide only 0.04%. Therefore, manufacture of lactide monomer from (L)- lactic acid predominantly results in a mixture of **L- and meso-lactide**, not L- and D- lactide (See **Figure 2-2**). Theoretically, ring-opening polymerization of L-lactide should yield isotactic poly(L-lactide), D-lactide would yield isotactic poly(D-lactide), and meso-lactide would yield syndiotactic poly(meso-lactide); we will prove that poly(meso-lactide) is in fact **atactic**, not syndiotactic.

The objective of this paper is to clarify these statements and document that commercial PLA is predominantly composed of L-lactide and meso-lactide, and that poly(meso-lactide) is an atactic polymer. Copolymers of L- and meso-lactide (0-20wt%, 100wt%) as well as copolymers of L- and D-lactide (0-20wt%) are synthesized for optical rotation and ¹H NMR studies. Optical rotation and ¹H NMR studies are used to validate this stereochemistry and determine the meso-lactide content in standard commercial grade samples of PLA. The tacticity, crystallinity, and material properties (thermal, mechanical, and rheological) of poly(L-co-meso-lactide) are also reported.

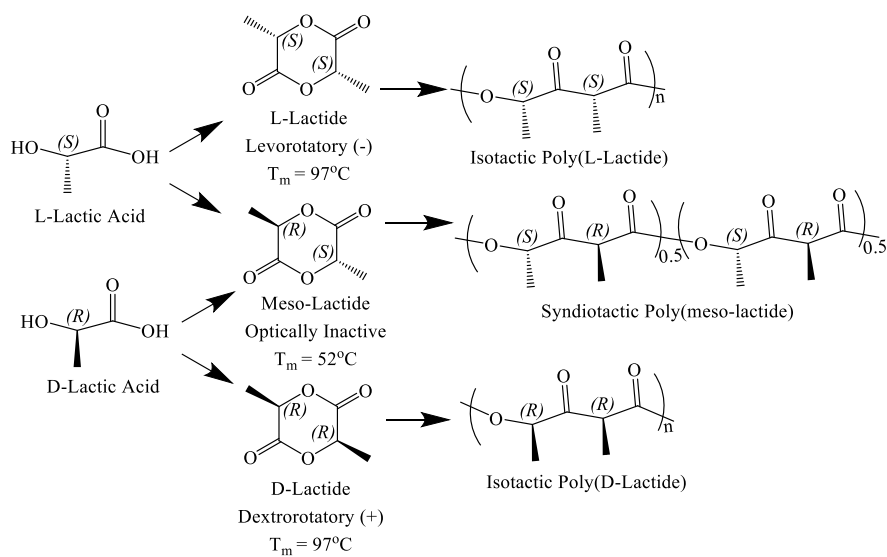


Figure 2-2. Lactic acid and lactide stereoisomers, and their respective polymer structures

We conclude this chapter by discussing the role of PLA stereochemistry in metabolic reprogramming, particularly in the materials science aspect. Recent studies have shown that PLA can mechanistically remodel metabolism in cells leading to a reactive immune microenvironment characterized by increases in proinflammatory cytokines. As a result, a biocompatibility paradigm can be developed by identifying metabolism as a target for immunomodulation to increase tolerance to biomaterials. This ensures safe clinical application of PLA-based implants for soft- and hard-tissue regeneration, as well as advancing nanomedicine and drug delivery.

PLA grades of varying stereoisomer content were selected for their high molecular weights and represent a range of physicochemical properties (stereochemistry, crystallinity, degradation period), which constitute important considerations in selecting PLA for hard and soft tissue engineering. Hydrolytic degradation of PLA has been characterized in high glucose (HG) media – 30 mM- and Milli-Q Type 1 ultrapure water via molecular weight analysis. Degradation products of PLA, including oligomers and monomers of lactic acid, were characterized via electrospray ionization-mass spectrometry (ESI-MS) to confirm that PLA degradation drives adverse host immune responses such as long-term inflammation and excessive fibrosis. In order to reduce

inflammation and excessive fibrosis, a melt-blending technique via micro-extrusion has been developed to load glycolytic inhibitors onto PLA materials of varying stereochemical composition. This will potentially allow for large PLA-based implants to be safely applied in joint reconstruction, fracture repair, sports medicine, bone and soft tissue (tendon, cartilage, ligament) engineering.

2.2. Experimental

2.2.1 Materials and Reagents

L-lactide and D-lactide were obtained from Total Corbion, whereas meso-lactide was provided by NatureWorks. All monomers were recrystallized twice using ethyl acetate, and once using anhydrous toluene. They were then vacuum dried at 35°C for 48 hours, then stored in an Argon atmosphere at -20 °C. Using GC, 99.3% monomer purity was determined for L-lactide and D-lactide, and 99.7% monomer purity was determined for meso-lactide. 99% optically pure poly(L-lactide) (L175) and poly(D-lactide) (D120) as well as amorphous grades of PLA were provided by Total Corbion as samples for polarimetry. Semi-crystalline (3100HP & 3052D) and amorphous (4060D) grades of PLA were provided by NatureWorks. The degree of crystallinity was 50% (3100HP), 0.6% (3052D), and 0% (4060D) based on the second differential scanning calorimetry (DSC) heating scan; the melting enthalpy for 100% crystalline PLA used in the calculations was 93 J/g [93]. Sn[Oct]₂ was the catalyst used for polymerization of lactide and was purchased from Millipore Sigma. Deuterated chloroform (CDCl₃), HPLC grade chloroform (CHCl₃), HPLC grade tetrahydrofuran (THF), and anhydrous toluene were purchased from Millipore Sigma. HPLC grade dichloromethane (DCM) and ethyl acetate were both obtained from VWR. These reagents were used as is and were not purified any further.

2.2.2 Synthesis of PLA

Meso-lactide from NatureWorks' M700 standard grade was recrystallized three times from anhydrous toluene, then polymerized to poly(meso-lactide). The reaction vessel and other glassware components were dried in an oven at 120 °C for 24 hours. The vessel was then flame-dried and purged with Argon before adding the monomer. The monomer and vessel were vacuum dried at 40°C for 48 hours. The polymerization reaction was carried out for 8 hours under rigorous mixing at 260 RPM, at a constant melting temperature of 180 °C. Sn[Oct]₂ (monomer to catalyst ratio - M/C=5000) was the catalyst used in the reaction. The reaction is based on a coordination insertion mechanism, where a hydroxyl compound is required as an initiator. The alcohol first reacts with the catalyst to form a tin alkoxide bond by ligand exchange. Afterwards, Sn[Oct]₂'s tin atom coordinates with an exocyclic carbonyl oxygen from lactide in the alkoxide form; this coordination enhances the lactide carbonyl group's electrophilicity and initiator's alkoxide group nucleophilicity. The acyl-oxygen bond of the lactide breaks, "opening" the lactide chain to allow insertion into the alkoxide of the catalyst. This is followed by polymer propagation as the lactide molecules are added to the tin-oxygen bond, forming the polymer [94], [95]. The stereochemistry was preserved as per the reported coordination insertion mechanism. For transfer purposes, a 4wt% catalyst solution was prepared in anhydrous toluene. A similar procedure (reaction temperature $T_{rxn} = 150^{\circ}C$, reaction time $t_{rxn} = 1.5$ hours) was followed to synthesize pure PLLA, copolymers of meso and L-lactide at different compositions of meso (2, 4, 10, and 20 wt%), as well as copolymers of D and L-lactide at varying D compositions (2, 4, 10, 20, and 50 wt%).

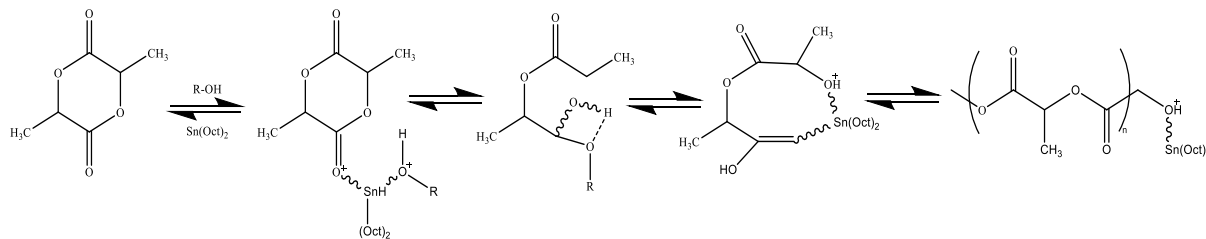


Figure 2-3. ROP of lactide to form PLA via coordination insertion with tin (II) ethylhexanoate

2.2.3 Characterization and Analysis

Using a Shimadzu IRAffinity-1, the chemical structure of PLA was verified by FTIR spectra from 500 to 4600 cm^{-1} . The tacticity was also confirmed by procuring the ^1H NMR spectrum for the polymer, using an Agilent DDR2 500 MHz NMR spectrometer equipped with 7600AS 96 sample autosamplers running VnmrJ 3.2A. The spectrum was acquired from $\sim 0.2\%$ solutions in CDCl_3 , with the methyl protons decoupled from the methine protons during the acquisition time. The monomer conversion was analysed by obtaining the ^1H NMR spectrum for the polymer, using an Agilent DDR2 500 MHz NMR spectrometer equipped with 7600AS 96 sample autosamplers running VnmrJ 3.2A. The spectrum was acquired from $\sim 0.2\%$ solutions in CDCl_3 , with the methyl protons decoupled from the methine protons during the acquisition time. For analysis, the methine protons have different chemical shifts in the monomer (5.04 ppm) from the polymer (5.13–5.25 ppm). Integrating the area under each peak directly provides the percent monomer conversion [96]. $>98\%$ monomer conversion was confirmed for all PLA samples.

The purity was analysed using gas chromatography (GC). GC was done on a Shimadzu GC-2010 with a flame ionization detector (FID) and a Stabilwax fused silica column (30 m x 0.25 mm i.d.; film thickness- 0.25 μm); helium was used as the carrier gas. The operating conditions were as follows. The temperatures of the injector and FID were 200 and 270 $^\circ\text{C}$, respectively. The initial temperature of the column oven was 50 $^\circ\text{C}$, and then ramped up to 260 $^\circ\text{C}$ at a rate of 25 $^\circ\text{C}/\text{min}$;

the temperature was then held for 30 minutes. The flow rate of the carrier gas was 1.9 $\mu\text{L}/\text{min}$, and the split ratio was 20:1. 0.20 μL of 500 ppm lactide in dichloromethane was injected into the GC. Gel permeation chromatography (GPC) was conducted to characterize the polymer molecular weights (MW) using a Waters 600 controller equipped with Optilab T-rEX refractive index (RI) and TREOS II multi-angle light scattering (MALS) detectors (Wyatt Technology Corporation), and a PLgel 5 μm MIXED-C column (Agilent Technologies) with chloroform eluent (1 mL/min). Polystyrene standards (Alfa Aesar) with M_n ranging from 35000 to 900000 Da were used for calibration. The calibration curve is shown below (**Figure 2-4**).

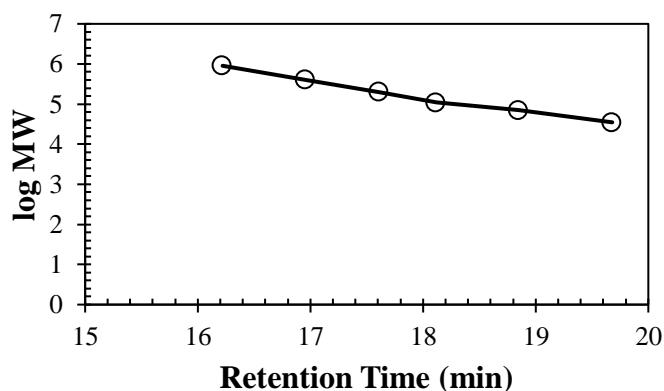


Figure 2-4. Polystyrene calibration curve for size exclusion chromatography analysis; MW range from 35000 to 900000

Identification and quantification of the stereoisomers (L and meso or L and D) in PLA samples was conducted using optical rotation and ^1H NMR. For ^1H NMR, Thakur's technique is used [46]. Optical rotation is used to determine D-content in PLA. Using ^1H NMR, the *is**is* and *ii**ss* hexad resonances at 5.232 and 5.208 ppm are analysed to identify for D-lactide and meso-lactide, respectively.

Polarimetry was used to analyze the optical rotation of lactide and its respective PLA polymer with a JASCO P2000 polarimeter. The optical rotation is defined as the rotation of the orientation of the plane of polarization about the optical axis of linearly polarized light as it travels through a

material [97]. The optical rotation was measured in chloroform for the polymers and dichloromethane for the monomers, at a concentration of 1 g/mL. Conditions were set at 25 °C and 589 nm wavelength. Three measurements were averaged for the optical rotation of each sample. Sucrose was used as a standard reference material, and its specific optical rotation was reported at ~67°. The optical purity (o.p) was also calculated using:

$$\boxed{o.p. = \frac{\alpha_{obs}^{25}}{[\alpha]^{25}}} \quad \text{Equation 1}$$

Where α_{obs}^{25} is the observed optical rotation of the sample and $[\alpha]^{25}$ is the specific rotation of the pure enantiomer at room temperature ($[\alpha]^{25} = \pm 270^\circ$ for 100% optically pure L-lactide and D-lactide and $[\alpha]^{25} = \pm 156^\circ$ for 100% optically pure poly(L-lactide) and poly(D-lactide)).

Differential scanning calorimetry (DSC) was done with a TA DSC Q20 to analyse the thermal properties of PLA, for poly(meso-lactide), pure PLLA, and poly(L-co-meso-lactide). The procedure was as follows. Temperature was equilibrated to -20 °C, then ramped up to 200 °C at a heating rate of 10 °C/min; temperature was then held isothermally for 5 minutes. Afterwards, it was cooled back to -20 °C at a rate of 10 °C/min, then held isothermally for 2 minutes. Finally, the material was heated back to 200 °C at 10 °C/min. The glass transition temperature (T_g) and melting peak temperature (T_{pm}) were identified using ASTM D3418 and ISO 11357-3 [98], [99]. The crystallinity was calculated using TA Instruments' procedure, taking the melting enthalpy for a single crystal of PLA to be ~ 93 J/g according to Fischer [100], [101].

The thermal decomposition temperature and percent weight loss of synthesized poly(L-lactide) and poly(meso-lactide) were quantified using a thermogravimetric analyser (TGA) – TA TGA Q50. About 10 mg of sample was heated from 25 to 550 °C at 20 °C/min.

The tensile properties of NatureWorks standard grades of PLA have been analyzed. Mechanical testing samples were first injection molded at 190°C and 75 RPM using a DSM 15CC mini-

extruder & 3.5CC mini-injection molder. Samples were then annealed in an oven at 100 °C for 2 hours. Tensile testing was performed in an Instron model 5565-P6021 as per ASTM D882 [102]. A TA Advanced Rheometer Discovery HR was used to characterize the linear viscoelastic behavior of NatureWorks PLA; a dynamic frequency sweep test was run at 180°C and 5% strain.

2.2.4 The Role of PLA Stereochemistry in Immune Cellular Response

2.2.4.1 Materials & Reagents

L175 (99.99% optically pure PLLA), D120 (99.99% optically pure PDLA), and LX930 (amorphous grade PLA) were provided by Total Corbion. 3100HP (semi-crystalline PLLA) and 4060D (amorphous grade PLA) were provided by NatureWorks. Stereocomplex PLA was manufactured by melt blending L175 and D120 at a 50/50 ratio via reactive extrusion (See *Section 3.2.1.3*). PLA samples were sterilized by exposure to ultraviolet radiation for 30 minutes [103]. Samples were then dried in an oven at 45°C for 24 hours.

Deionized water was purified using a Milli-Q® Reference Water Purification System (Millipore Sigma). High glucose (HG) medium comprised of DMEM medium, 10% heat-inactivated Fetal Bovine Serum and 100 U/mL penicillin-streptomycin (all from ThermoFischer Scientific). Glucose levels in complete medium were evaluated by a hand-held GM-100 glucose meter (BioReactor Sciences) according to manufacturer's instruction. 3-(3-pyridinyl)-1-(4-pyridinyl)-2-propen-1-one (3PO) (MilliporeSigma), 2-deoxyglucose (2DG) (MilliporeSigma), aminooxyacetic acid (a.a.) (Sigma-Aldrich), metformin (Sigma-Aldrich), 2-Cyano-3-(4-hydroxyphenyl)-2-propenoic acid (CHC), and 4,4'-Diisothiocyano-2,2'-stilbenedisulfonic acid (DIDS) (Sigma Aldrich) were used for glycolytic inhibition of PLA in cell culture medium. HPLC grade chloroform (CHCl₃) purchased from Millipore Sigma. These reagents were used as is and were not purified any further.

2.2.4.2 *PLA Breakdown and Extraction*

PLA extraction was performed for 12 days in a shaker (37 °C) at 250 rpm, after which extracts were decanted. Breakdown products (extracts) [104] of PLA, were obtained by suspending 4 g of PLA pellets in 25 mL of Milli-Q water, as well as 4 g of PLA in 25 mL of HG medium.

Gel permeation chromatography (GPC) was conducted to characterize the polymer molecular weight degradation after extraction in Milli-Q water and HG media using a Waters 600 controller equipped with Optilab T-rEX refractive index (RI) and TREOS II multi-angle light scattering (MALS) detectors (Wyatt Technology Corporation), and a PLgel 5 μ m MIXED-C column (Agilent Technologies) with chloroform eluent (1 mL/min). Polystyrene standards (Alfa Aesar) with M_n ranging from 35000 to 900000 Da were used for calibration.

Breakdown products of PLA extracts in Milli-Q water were characterized via D- and L-lactic acid assay kits (Sigma-Aldrich) and electrospray ionization-mass spectrometry (ESI-MS) [105]. Blank Milli-Q water was first injected in the mass spectrometer. 5 μ L of sample were then injected in the mass spectrometer while flowing water/acetonitrile (50:50). Ionization was done using negative ion mode electrospray on a Xevo G2-XS QToF system (Waters).

2.2.4.3 *Glycolytic Inhibition of PLA*

The objective of this study is to: Successfully load glycolytic inhibitors onto amorphous PLA (4060D) and semi-crystalline PLA (3100HP) scaffolds via melt-blending for potential glycolytic inhibition on inflammation and fibrosis in both a femoral defect and a subcutaneous model. A solventless technique via micro-extrusion has been developed to load glycolytic inhibitors (3PO, 2DG, a.a., CHC, DIDS, metformin) onto PLA. This method avoids using organic solvents which may chemically react with glycolytic inhibitors, and organic solvents have been reported to be cytotoxic [106]. We performed a thermogravimetric analysis (TGA) using a TA TGAQ50 to

determine the thermal stability of our inhibitors during processing. Performing TGA allowed us to assess and compensate for thermal degradation of glycolytic inhibitors. First, about 10 mg of sample was heated from 25 to 550 °C at 20 °C/min to assess the thermal decomposition temperature. Next, samples were run at the determined processing temperature (190°C) for melt blending with PLA. Inhibitors were held isothermally at 190°C for 15 minutes to determine ideal processing time and inhibitor loading efficiency.

PLA (3100HP & 4060D) and glycolytic inhibitors were then loaded and melt-blended in a DSM 15CC mini-extruder at 190°C and 75 RPM for 5 minutes. 90 mg of inhibitors were pre-mixed with PLA (pellets and powder for dispersion), totaling a sample weight of ~10 g. Samples were then pelletized and sealed. Next, to ensure uniform distribution of the inhibitors in PLA after melt-mixing, we performed scanning electron microscopy - energy-dispersive X-ray spectroscopy (SEM-EDX) [107]. Samples were run in a JEOL 6610LV SEM with an energy dispersive X-ray spectroscopy attachment. The samples analyzed were ~3mm in length and were coated in Iridium for analysis. Samples were analyzed at x250 magnification and an accelerating voltage of 10kV to prevent damage/melting of the PLA matrix. Spot size was set to 60 for high resolution, and images were focused and contrasted to provide the highest image quality.

Uniformity of the drugs within the PLA matrix was confirmed using EDX by analyzing the distinguishing elements between the drugs and PLA. a.a. distribution and composition were analyzed based on its elemental concentration of chlorine and DIDS's uniformity was analyzed based on its elemental concentration of sulfur. Surface and cross-sectional elemental mapping images were taken to confirm the distribution and concentration of inhibitors throughout the surface and bulk of PLA.

2.3. Results and Discussion

2.3.1 Chemical Structure

Synthesis of poly(meso-lactide) ($M_n = 5053$ g/mol) was confirmed in the below FTIR spectra (Figure 2-5). The spectrum showed peaks corresponding to asymmetric (3035 cm^{-1}) and symmetric -CH stretching (2910 cm^{-1}). The peak at 1757 cm^{-1} confirms PLA polymerization, as lactide's peak is generally at $\sim 1725\text{ cm}^{-1}$ [108].

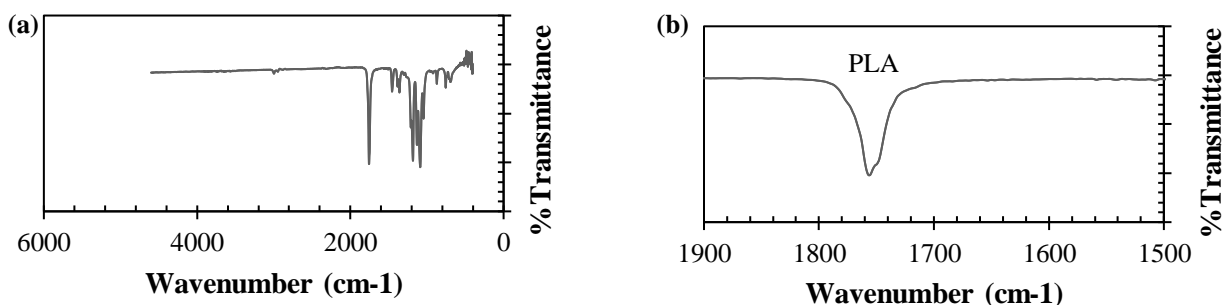


Figure 2-5. (a) FTIR spectra of poly(meso-lactide) (b) Confirmation of PLA polymerization characterized by the absorption band at $\sim 1725\text{ cm}^{-1}$

2.3.2 Optical Rotation

Table 1 compares experimental results of commercial grade lactide versus literature data, and we found that neat L-lactide and D-lactide were $>99\%$ optically pure, indicating enantiomerically pure monomer. Meso-lactide was optically inactive. From a stereochemical perspective, this agrees with theoretical values, as meso-lactide's *RS* stereoconfiguration cancels out optical activity. The slight optical activity detected in meso-lactide is most likely from L-lactide contamination, which could not be removed via recrystallization. Racemic lactide (50/50 D/L) was also determined to be optically inactive. Compared to meso-lactide, racemic lactide's optical inactivity is due to a 50/50 mixture of two enantiomers – L-lactide and D-lactide. There are equal amounts of lactide units comprising an *RR* configuration (D-lactide) and units comprising an *SS* configuration (L-lactide).

Table 2-1. Optical rotation of pure lactide samples

Sample	α_{obs}^{25} (°)	o.p. (%)
Pure Meso/M700* (NatureWorks)	-1.48 ± 0.03	N/A
Pure Meso/M3002* (NatureWorks)	-20.7 ± 0.16	N/A
Racemic D-/L-Lactide (BMRG)	0	N/A
Lumilact L (Total Corbion)	-268.5	99.44
Lumilact D (Total Corbion)	+269.1 ± 1.53	99.67
Purasorb L (Total Corbion)	-269.8 ± 0.99	99.92
Purasorb D (Total Corbion)	+269.6 ± 0.14	99.85
Pure L-Lactide [45]	-266.3	98.63
Pure D-Lactide [45]	+266.3	98.63
Pure L-Lactide [83]	-270	100
Pure D-Lactide [83]	+270	100

*Meso-lactide's optical rotation is not zero due to residual L-lactide contamination

In PLA's case, the reported optical rotations of enantiomerically pure PLLA and PDLA typically lie between $\pm 140^\circ$ and $\pm 156^\circ$ [109]. The chemical composition of these polymers was expressed by the mole fraction of the D-unit:

$$X_D = \frac{D\text{-lactate unit}}{D\text{-lactate unit} + L\text{-lactate unit}} \quad \text{Equation 2}$$

$$X_D = \frac{\alpha_{obs}^{25} - (-156)}{156 - (-156)} \quad \text{Equation 3}$$

Using this expression, the average isotactic sequence length of the polymers was calculated:

$$L(\text{lactate}) = \frac{2}{X_D} \quad \text{Equation 4}$$

The factor of 2 was used for the calculation of the L-lactate unit to consider both enantiomers.

Optical rotation data for synthesized PLLA and PDLA correlates well with literature results (**Table 2-2**). >99% optical purity was obtained for both PLLA and PDLA. The optical rotation of poly(meso-lactide) was -1.39° , confirming that the polymer is optically inactive. In poly(L-co-D-lactide)'s case, a racemic mixture of 50% L-lactide/50%D-lactide is pre-mixed before polymerization. Polarimetry confirms that *rac*-poly(L-co-D-lactide) is also optically inactive.

Table 2-2. Optical rotation of pure PLA samples

Sample	α_{obs}^{25} (°)	o.p. (%)	X_D	L
Pure PLLA (BMRG)	-156 ± 0.01	99.99	0	∞
Pure PDLA (BMRG)	+156 ± 0.01	99.99	1	2
Pure poly(meso-lactide) (BMRG)	-1.39 ± 0.24	N/A	N/A	N/A
rac-poly(L-co-D-lactide) (BMRG)	0	N/A	N/A	N/A
Pure PLLA [80]	-150	96.15	0.019	105.26
Pure PDLA [80]	+150	96.15	0.98	2.04
Pure PLLA [84]	-156	100	0	∞
Pure PDLA [84]	+156	100	1	2

*Michigan State University Biobased Materials Research Group (BMRG) samples were synthesized using Total Corbion's Lumilact L/D grade of lactide and NatureWorks' M700 grade of meso-lactide

2.3.3 Effect of Meso-Lactide and D-Lactide on Optical Rotation of PLA

Polarimetry was used to analyse the effect of lactide stereoisomers on PLA's optical activity. Each sample's experimentally observed optical rotation was measured in a polarimeter and graphed. Theoretical calculations were also done to understand the effect of stereoisomer concentration on the observed optical rotations. Four mixed compositions (2, 4, 10, 20 wt% D) of poly(L-co-D-lactide) (**Figure 2-6**) were formulated in chloroform at a concentration of 1 g/mL. In the case of poly(L-co-D-lactide), the observed optical rotation was theoretically calculated using the equation below:

$$\alpha_{obs}^{25} = -156c_L + 156c_D \quad \text{Equation 5}$$

Where c_L is the concentration of PLLA ($[\alpha]_{25} = -156^\circ$) and c_D is the concentration of PDLA ($[\alpha]_{25} = +156^\circ$). The observed optical rotation of poly(L-co-D-lactide) increases linearly by 6° for every 2% D-lactide copolymerized with L-lactide (See **Figure 2-6** Δ ; $R^2 = 0.9997$). This agrees with our theoretical calculations, as D-lactide contributes to the optical activity.

Similarly, four mixed compositions (2, 4, 10, 20 wt% meso) of poly(L-co-meso-lactide) were analysed. In the case of poly(L-co-meso-lactide), the observed optical rotation was theoretically calculated using the equation below:

$$\alpha_{obs}^{25} = -156c_L + 0c_{meso} \quad \text{Equation 6}$$

Where c_L is the concentration of PLLA ($[\alpha]_{25} = -156^\circ$) and c_{meso} is the concentration of poly(meso-lactide) ($[\alpha]_{25} = 0^\circ$). Meso-lactide is optically inactive and does not contribute to the optical rotation.

The optical rotation of poly(L-co-meso-lactide) increases linearly by 3° for every 2% meso-lactide copolymerized with L-lactide (See **Figure 2-6** ○; $R^2 = 0.9997$). This is also in agreement with our theoretical calculations, as meso-lactide does not contribute to the optical activity.

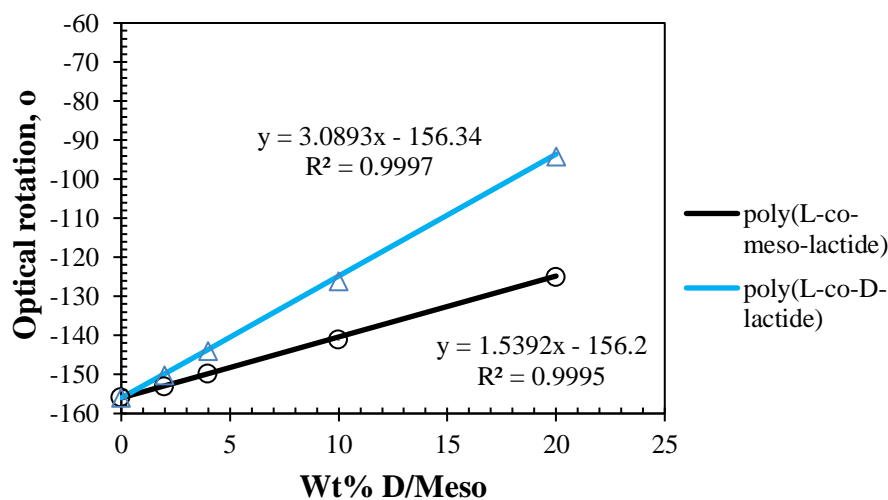


Figure 2-6. Optical rotation of poly(L-co-D-lactide) at different compositions of D-lactide (2-20wt%) and poly(L-co-meso-lactide) at different compositions of meso-lactide (2-20wt%). The experimentally observed values are represented as symbols, whereas the theoretical calculations are represented as lines

It is clear that the optical rotation of a PLA composition containing D-lactide is different than a PLA composition containing meso-lactide. This is due to the influence of *R* stereoconfiguration in both copolymers originating from D-lactide and meso-lactide. D-lactide's contribution to the

optical rotation of poly(L-co-D-lactide) is double the contribution that meso-lactide has on poly(L-co-meso-lactide)'s optical rotation. This effect is logical from a stereochemical perspective, as meso-lactide's two stereocarbons are of the *RS* configuration, whereas D-lactide's stereocarbons are of the *RR* configuration. The plane of polarization will rotate further in the clockwise direction (+) as additional *R* configurational sequences are introduced in the PLA copolymer. Therefore, optical rotation analysis can be used to establish whether PLA is a mixture of L-lactide and D-lactide or meso-lactide.

2.3.4 Effect of Meso-Lactide and D-Lactide on Specific Rotation of PLA

The specific rotation was taken for poly(L-co-D-lactide) and poly(L-co-meso-lactide) (**Figure 2-7**). The specific rotation was calculated per concentration of L-lactide (100%, 98%, 96%, 90%, 80%) in the copolymer samples using the following equation:

$$[\alpha]_{sp}^{25} = \frac{\alpha_{obs}^{25}}{c_L * l} \quad \text{Equation 7}$$

Where α_{obs}^{25} is the observed optical rotation, c_L is the concentration of L-lactide, and l is the path length.

Figure 2-7 shows that the specific rotation for poly(L-co-D-lactide) increases linearly as D-lactide increases. This is because D-lactide is optically active and will rotate the plane of polarized light. In the case of poly(L-co-meso-lactide), the specific rotation does not change as the meso-lactide content increases, maintaining an optical rotation of $\sim -156^\circ$ - the optical rotation for enantiomerically pure PLLA. This is because meso-lactide is optically inactive and poly(L-co-meso-lactide) maintains its L- optical activity. Therefore, using specific rotation, we can establish whether PLA contains D-lactide or meso-lactide. Such a relationship will enable us to validate the stereoisomeric composition of PLA commercial grades.

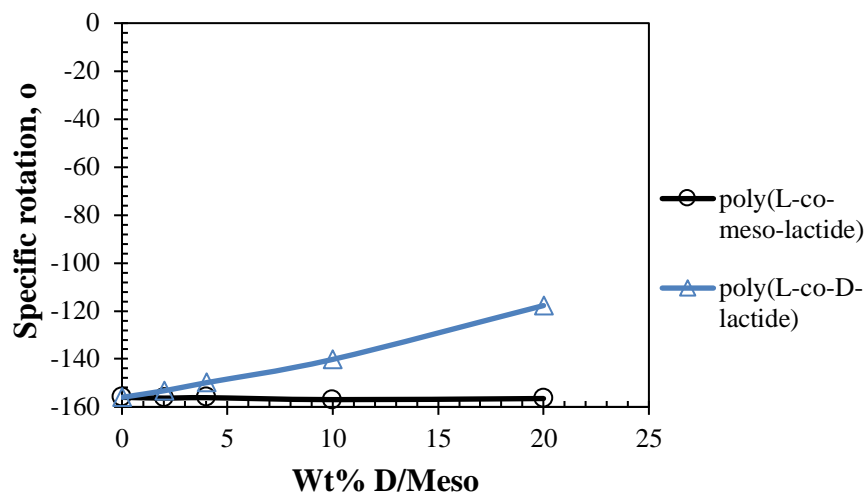


Figure 2-7. Specific rotation of poly(L-co-meso-lactide) and poly(L-co-D-lactide) at different compositions of meso, D, and poly-meso content (0-20wt%)

2.3.5 Identification and Quantification of Stereoisomers in Commercial Grade PLA

Three standard grades of PLA were analysed using Thakur's method of stereoisomer identification to establish the stereoisomer content: 3100HP, 3052D, 4060D [46]. The percent D-content ($R\%$) was first measured using optical rotation. The optical purity is also considered to be the enantiomeric excess for an enantiomeric mixture,

$$o.p. = \frac{\alpha_{obs}^{25}}{[\alpha]^{25}} = \boxed{S(\%) - R(\%)} \quad \text{Equation 8}$$

The total molar composition will always equal 100% for any enantiomeric mixture:

$$100\% = S(\%) + R(\%) \quad \text{Equation 9}$$

Summing Equation 8 and Equation 9, we can calculate the percent L-content ($S\%$) to be:

$$2S = 100\% + o.p.(\%) \rightarrow \boxed{S = \frac{100\% + o.p.(\%)}{2}} \quad \text{Equation 10}$$

Subtracting the above equation by 100% will give the percent D-content, which was measured to be ~0.5% for 3100HP, ~4% for 3052D, and ~11% for 4060D (**Table 2-3**).

Table 2-3. Calculated % D-content based on optical rotation

Sample	α_{obs}^{25} (°)	o.p. (%)	D-content (%)
3100HP	-154.5 ± 0.50	99.04	0.5
3052D	-143.4 ± 0.05	91.92	4
4060D	-122.7 ± 0.02	78.65	11

^1H NMR was then used to identify the major stereoisomer (D-lactide or meso-lactide) that contributes to the D-content. Using ^1H NMR, *iiiss* hexad resonances were observed at ~ 5.212 ppm for 3052D (**Figure 2-8a**) and 4060D (**Figure 2-8b**), with a small fraction of *isisi* resonances at ~ 5.237 ppm. 3100HP's NMR spectrum did not show resonances for either meso-lactide or D-lactide. Results show that the major stereoisomers in 3052D and 4060D are L-lactide and meso-lactide, with $<1\%$ D-lactide. The percent meso-lactide was estimated to be $\sim 1\%$ for 3100HP, $\sim 9\%$ for 3052D and $\sim 22\%$ for 4060D.

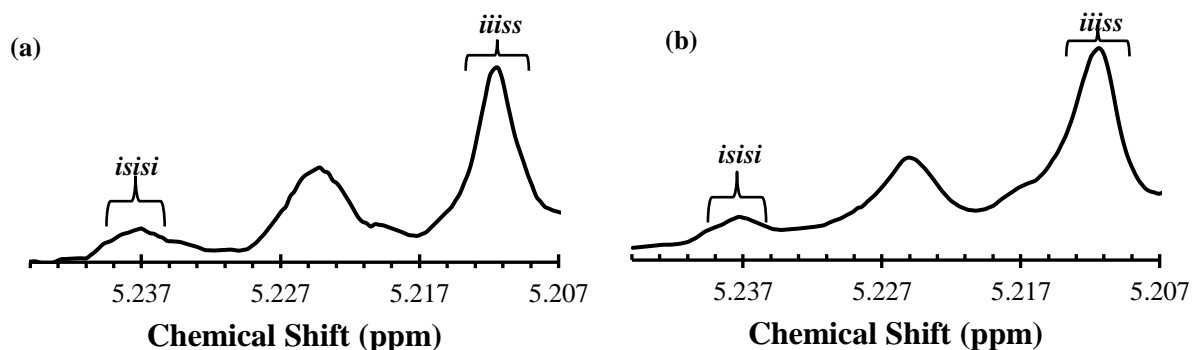


Figure 2-8. NMR spectrum displaying the *isisi* and *iiiss* resonances for D-lactide and meso-lactide, respectively in (a) 3052D and (b) 4060D

2.3.6 Validation of Stereoisomers in Commercial Grade PLA

Optical rotation analysis was used to validate the stereoisomers in commercial grade PLA. The observed optical rotation was first measured for all three commercial grade PLA samples: 3100HP, 3052D, and 4060D. The percent meso-lactide (estimated in section 3.4) was then input in the equation generated for poly(L-co-meso-lactide) in **Figure 2-6**:

$$\alpha_{L-meso}^{25} = 1.5392M_{wt\%} - 156.2 \quad \text{Equation 11}$$

where α_{L-meso}^{25} is the calculated optical rotation of a poly(L-co-meso-lactide) mixture of L and meso-lactide isomers and $M_{wt\%}$ is the % meso-lactide content in the mixture.

The experimentally observed optical rotation α_{obs}^{25} and calculated optical rotation α_{L-meso}^{25} were compared to verify the stereoisomer content in PLA. **Table 2-4** displays the data.

Table 2-4. Measured optical rotation versus calculated optical rotation as a function of meso-lactide content

<u>Sample</u>	α_{obs}^{25} (°)	α_{L-meso}^{25} (°)	$M_{wt\%}$ (%)
3100HP	-154.5 ± 0.50	-154.7	1
3052D	-143.4 ± 0.05	-142.3	9
4060D	-122.7 ± 0.02	-122.3	22

As seen in **Table 2-4**, the calculated optical rotation matches closely with the measured optical rotation. This data confirms that **meso-lactide**, not D-lactide, is the major stereoisomer that contributes to the D-content in commercial grade PLA.

2.3.7 Tacticity

The transition from isotactic to atactic PLA, based on the percentage of meso content added, is of interest, for fine control of the polymer's crystallinity. The tacticity and residual lactide of synthesized poly(meso-lactide), poly(L-lactide), as well as copolymers of both stereoisomers were analysed and compared using ¹H NMR.

As expected, poly(L-lactide)'s spectrum represents an isotactic structure (**Figure 2-9a**), as represented by the iii tetrad sequences (5.14-5.20 ppm), with ~90% monomer conversion. This indicates that the existing (S) asymmetric centers are completely retained during the polymerization. In contrast, poly(meso-lactide)'s spectrum represents a predominantly atactic structure (**Figure 2-9b**), with >99% monomer conversion. This is characterized by the sis tetrad peaks between 5.2 to 5.3 ppm. In addition, the originally iii tetrad sequences from PLLA's

spectrum transition to *isi*, *iss*, *ssi*, and *sss* tetrad configurational sequences. Pentad configurational sequences were assigned for the peaks based on Kaperczyk's analysis using HETCOR NMR, indicating a random statistical distribution of tetrad tacticities [110].

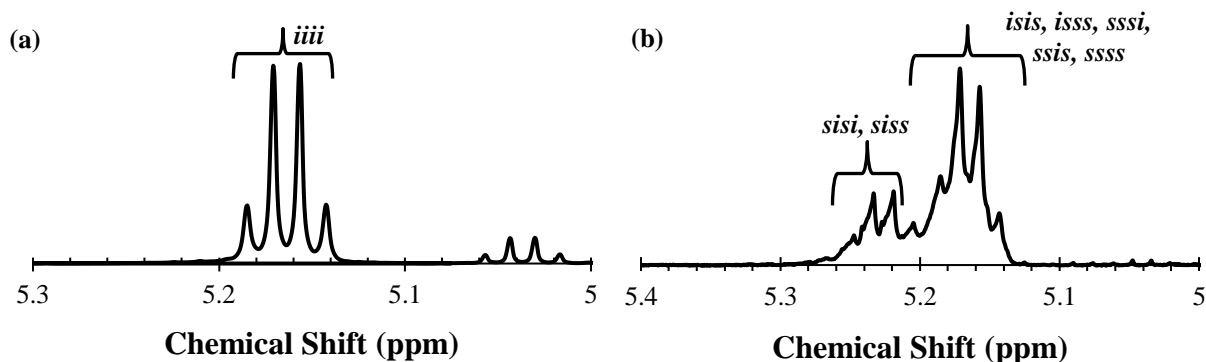


Figure 2-9. NMR spectra of (a) poly(L-lactide) and (b) poly(meso-lactide)

These results disprove the theory that poly(meso-lactide) is syndiotactic. This is due to meso-lactide's behavior during ring-opening polymerization via coordination insertion with stannous octoate catalyst (**Figure 2-10**). While the integrity of the *RS* stereocenters of meso-lactide are preserved, the meso-lactide chain can insert from either the *R* or *S* side, representing random insertion of the lactide chain.

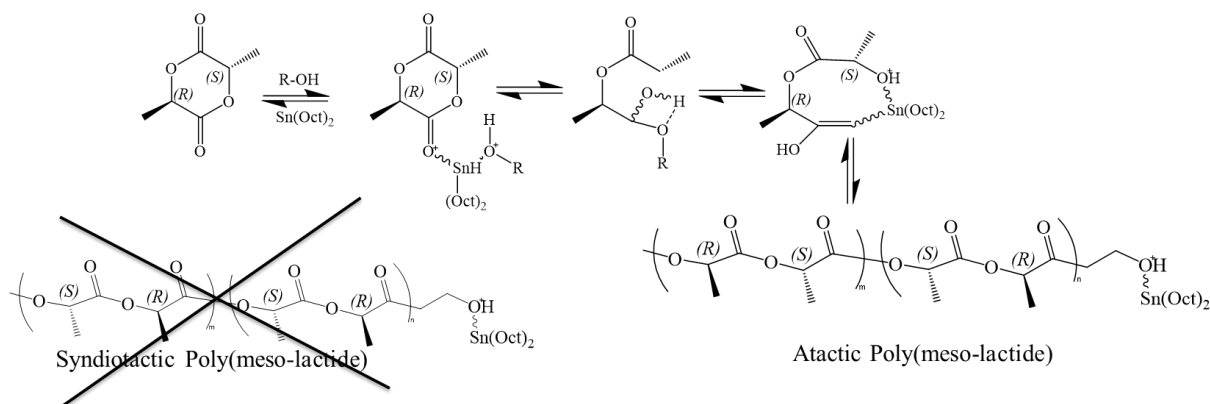


Figure 2-10. Ring-opening polymerization of meso-lactide via coordination insertion; atactic PLA is produced as while the integrity of the stereocenter is preserved, the meso-lactide can insert from both the *R* or *S* side, making it random insertion

As seen in **Figures 2-11a** and **2-11b**, adding ~2% meso content or ~4% meso content results in minimal change in the spectrum aside from slight noise between 5.20-5.25 ppm. However, adding 10% meso content leads to the formation of peaks in this range. **Figure 2-11c** represents a predominantly isotactic structure of PLA, with the formation of sis tetrads between 5.2 to 5.25 ppm, as explained by Ovitt and Coates [111].

At 20% meso content (**Figure 2-11d**), a predominantly atactic structure of PLA is observed. The signals representing sis tetrad sequences are more emphasized, whereas the originally iii tetrad sequences (5.14-5.20 ppm) transition to isi, iss, ssi, and sss tetrad configurational sequences. Based on this data, we can conclude that PLA transitions from a predominantly isotactic structure to a predominantly atactic structure between 10-20% meso content.

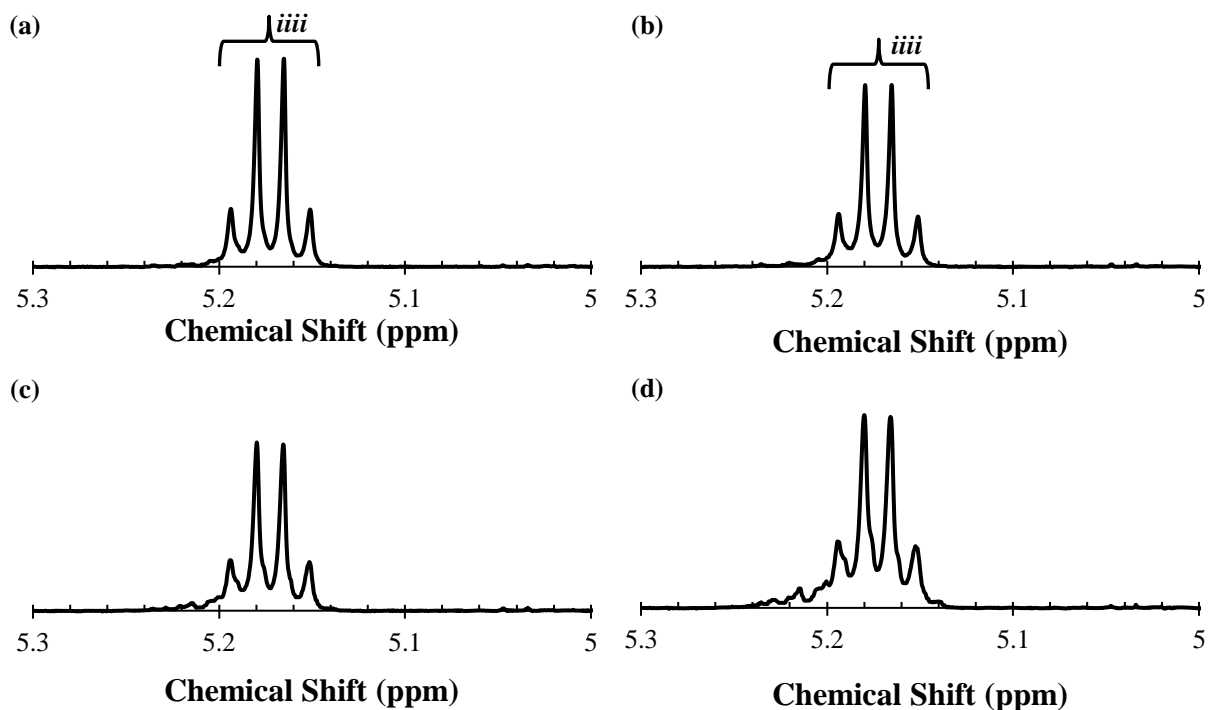


Figure 2-11. NMR spectra of poly(L-co-meso-lactide) at (a) 2% meso content (b) 4% meso content (c) 10% meso content (d) 20% meso content

2.3.7 Crystallinity

DSC was used to confirm the crystallinity of poly(L-co-meso-lactide) in relation to its isomer content. It has already been well-established by the scientific community that PLA transitions from a semi-crystalline structure to an amorphous grade structure at >12% D-lactide [112], [113]. Theoretically, PLLA and PDLA are semi-crystalline due to their isotactic structure. However, a polymer with a certain amount of meso content should also be amorphous due to its *RS* stereoconfiguration. The *SS* sequences of PLLA will transition from an ordered chain to a random chain as you add more meso-lactide (*RS*) to the polymer. Feng et. al have run thermal analysis studies on PLA of varying stereoisomer content [113]. DSC data on poly(L-co-meso-lactide) was analysed at different compositions of meso (0-20wt%). **Figure 2-12** displays the DSC graph for PLLA, indicating a semi-crystalline (32% crystallinity) structure with a melting peak temperature at ~172 °C. For the case of poly(meso-lactide), no melting peak was observed, validating its amorphous structure.

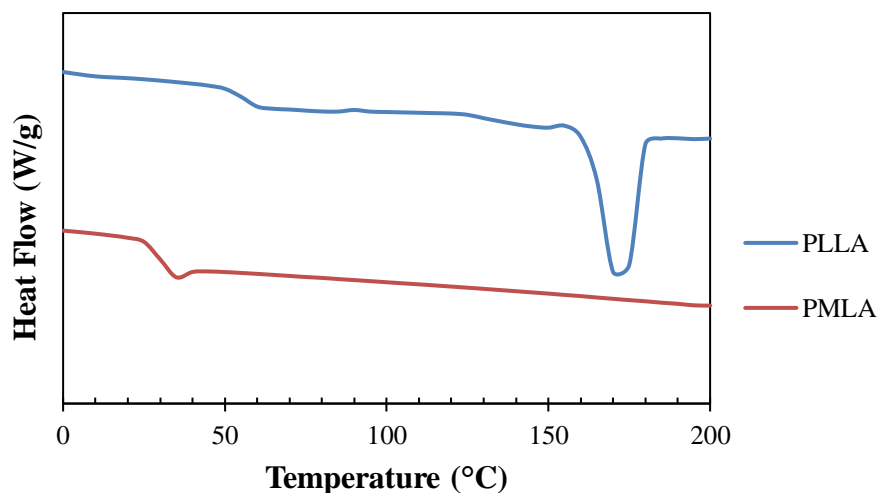


Figure 2-12. DSC data on the second heating cycle for poly(L-lactide) and poly(meso-lactide)

The transition from semi-crystalline to amorphous grade PLA can be seen in **Figure 2-13**. Using this method, we were able to confirm that PLA transitions to an amorphous polymer when one copolymerizes greater than 10% meso-lactide with L-lactide. A melting peak, albeit small, is still seen for PLA containing 10% meso-lactide, but it is completely gone at 20%, indicating a completely amorphous polymer.

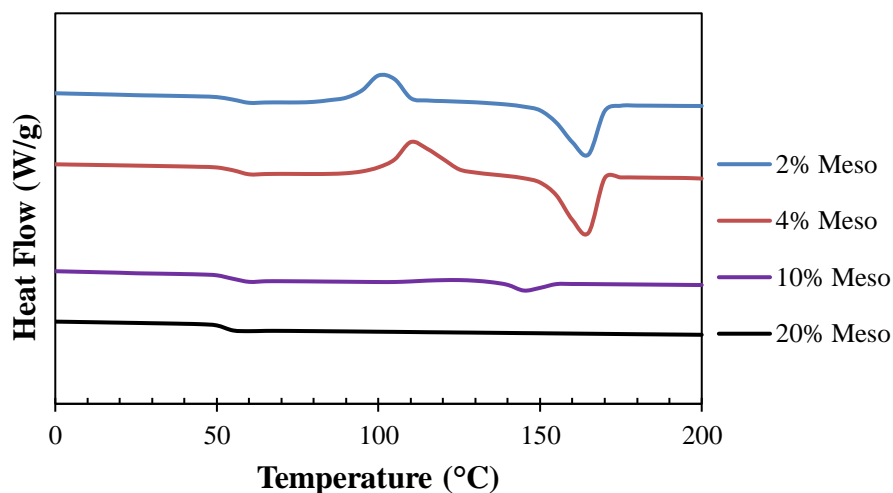


Figure 2-13. DSC data on the second heating scan for poly(L-co-meso-lactide) at 2% meso content, 4% meso content, 10% meso content, and 20% meso content

Table 2-5 provides a side-by-side comparison on the glass transition temperature, melting point, and percent crystallinity of PLLA, poly(meso-lactide), and copolymers of both L-lactide and meso-lactide. We can see that there is no noticeable difference in the glass transition temperature of poly(L-lactide) and poly(L-co-meso-lactide). However, in poly(meso-lactide)'s case, the glass transition temperature greatly reduced to slightly above room temperature. This is due to the low molecular weight of the product (~5000 Da), as Sn[Oct]₂ is not a reliable catalyst to produce high molecular weight poly(meso-lactide).

In conclusion, a noticeable decrease in the melting peak temperature is seen with increasing meso content, until there is no melting point at 20% meso, indicating an amorphous polymer. Similarly,

the percent crystallinity decreases as L-lactide is copolymerized with meso-lactide. Based on the trend, we have estimated the % meso content to be >10% required to transition PLA from a semi-crystalline to amorphous structure.

Table 2-5. DSC data on PLLA, poly(meso-lactide), and poly(L-co-meso-lactide)

<u>Sample</u>	<u>T_g (°C)</u>	<u>T_{pm} (°C)</u>	<u>X_c (%)</u>
Poly(L-lactide)	55.19	172.53	21.50
Poly(98%-L-co-2%-meso-lactide)	56.42	166.1	19.35
Poly(96%-L-co-4%-meso-lactide)	56.42	164.33	16.02
Poly(90%-L-co-10%-meso-lactide)	55.65	144.13	9.03
Poly(80%-L-co-20%-meso-lactide)	54.27	N/A	0
Poly(meso-lactide)	31.17	N/A	0

2.3.8 Thermal Stability

Using TGA analysis, the thermal decomposition temperature of poly(meso-lactide) was determined and compared to synthesized poly(L-lactide). From **Figure 2-14a**, the decomposition temperature was analyzed to be ~324°C, with a percent weight loss of ~96%. This is lower than our synthesized PLLA (**Figure 2-14b**), whose decomposition temperature was determined to be ~361°C with similar loss. This may be due to the significantly lower molecular weight of poly(meso-lactide) ($M_n = 5053$ Da) compared to PLLA ($M_n = 123010$ Da).

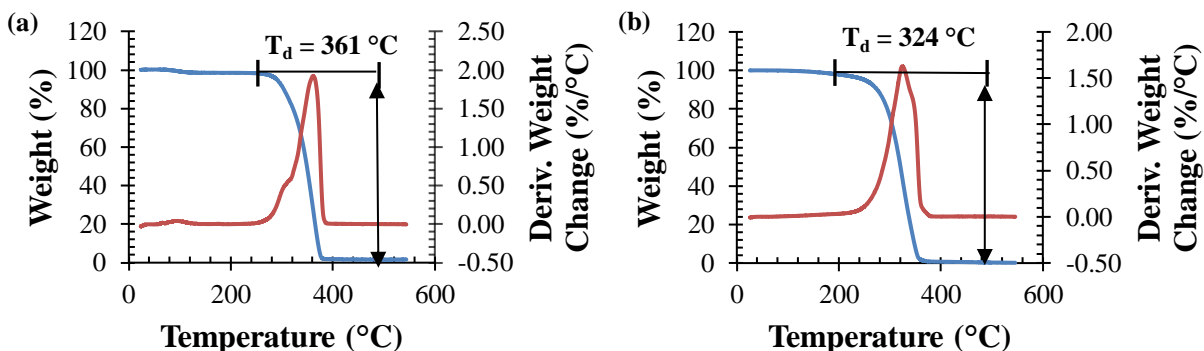


Figure 2-14. Thermal degradation of (a) PLLA and (b) poly(meso-lactide)

2.3.9 Tensile Properties

Tensile testing was conducted on NatureWorks Ingeo standard grades of PLA 3100HP (50% crystalline), 3052D (0.6% crystalline), and 4060D (amorphous) to analyze the effect of meso-lactide on PLA's mechanical properties. It has already been established that the tensile strength and elongation at break will decrease as more D-lactide is copolymerized with L-lactide [114]. Theoretically, a similar mechanical behavior should be seen as meso-lactide is copolymerized with L-lactide. This is confirmed in **Figure 2-15** which displays the stress-strain curves for 3100HP, 3052D, and 4060D.

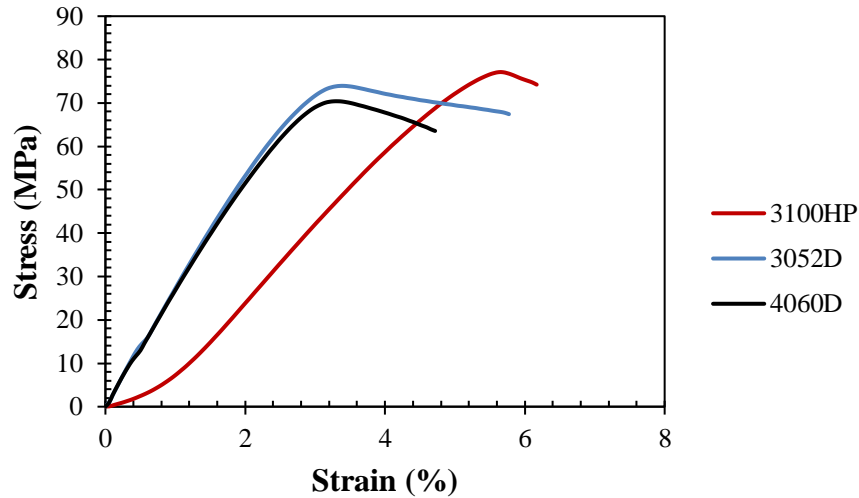


Figure 2-15. Stress-strain curves of Ingeo standard grades of PLA

Data was taken for 5 samples of each PLA standard grade. **Figure 2-15** displays the samples closest to the average data on the mechanical properties. For 3100HP, the average tensile stress at break (σ_{break}) was found to be about 72.8 ± 2.6 MPa, with a corresponding tensile strain at break (ϵ_{break}) of $5.7 \pm 0.50\%$. 3052D experienced a tensile stress at break at about 67.2 ± 2.4 MPa, with a corresponding tensile strain at break of about $5.8 \pm 0.56\%$. For 4060D, the average tensile stress at break was found to be about 65.8 ± 2.8 MPa, with a corresponding tensile strain at break of $4.4 \pm 0.6\%$. The yield strength (σ_y) was measured at 0.2% offset, which is defined as the amount of

stress that will result in a plastic strain of 0.2%. This is the yield strength that is commonly quoted by raw material suppliers and process engineers [115]. Using this method, the yield strength was estimated to be $\sigma_y = 70.2 \pm 2.3$ MPa for 3100HP, $\sigma_y = 68.4 \pm 2.1$ MPa for 3052D, and $\sigma_y = 65.0 \pm 1.8$ MPa for 4060D. The ultimate tensile strength (σ_{ult}) was estimated to be the maximum stress applied to each PLA sample. As a result, the ultimate tensile strength was measured to be $\sigma_{ult} = 73.7 \pm 2.9$ MPa for 3100HP, $\sigma_{ult} = 72.4 \pm 2.3$ MPa for 3052D, and $\sigma_{ult} = 71.4 \pm 2.4$ MPa for 4060D. The elastic modulus ($E_{elastic}$) was calculated as the slope of the linear portion of the stress strain curves for each sample. The elastic modulus was averaged out to be about $E_{elastic} = 1.7 \pm 0.052$ GPa for 3100HP, $E_{elastic} = 2.7 \pm 0.085$ GPa for 3052D, and $E_{elastic} = 2.8 \pm 0.097$ GPa for 4060D. Up to the elastic limit, the strain in the material is elastic and will be recovered when the load is removed so that the material returns to its original length. If the material is loaded beyond the elastic limit, permanent deformation occurs within the material, which is also referred to as plastic strain. The ductility herein is defined as the plastic strain to failure (ϵ_p) and is calculated by the following formula:

$$\epsilon_p = \epsilon_T - \epsilon_e$$

Where ϵ_T is the total strain and ϵ_e is the elastic strain [116].

Thus, the plastic strain to failure was calculated to be $\epsilon_p = 1.33\%$ for 3100HP, $\epsilon_p = 2.75\%$ for 3052D, and $\epsilon_p = 2.68\%$ for 4060D.

In order to find how much energy a material can absorb and plastically deform without fracturing, the toughness (U_T) was calculated using the composite Simpson's rule to integrate the area under the stress strain curves. The interval of integration (a,b) is first broken up into a number of small sub-intervals n , then Simpson's rule is applied to each sub-interval; the results are then summed

up to produce an approximation for the integral over the entire interval. Simpson's rule is given by:

$$\int_a^b f(x)dx = \frac{h}{3} [f(x_0) + 2 \sum_{j=1}^{n/2-1} f(x_{2j}) + 4 \sum_{j=1}^{n/2} f(x_{2j-1}) + f(x_n)]$$

Where $x_j = a + j \cdot h$ for $j = 0-n$, and $h = (b-a)/n$; $x_0 = a$ and $x_n = b$ [117].

Using this technique, the toughness was calculated to be $U_T = 2872.77 \text{ J/m}^3$ for 3100HP, $U_T = 2958.78 \text{ J/m}^3$ for 3052D, and 2292.34 J/m^3 for 4060D. 3052D clearly has a higher toughness compared to the other two PLA grades. There does not seem to be a trend in percent meso-lactide content or crystallinity vs toughness. We hypothesize that 3052D absorbs the most energy to plastically deform without fracturing due to its small percentage of crystallinity. It is not completely amorphous like 4060D, but it also does not possess a high level of crystallinity like 3100HP. It may be that the small presence of these crystalline regions provides the material the resilience to absorb such a high amount of energy during plastic deformation.

Contrary to the toughness, the modulus of resilience (U_R) was calculated to measure the amount of strain energy per unit volume that a material can absorb without permanent deformation. The modulus of resilience is typically calculated as the area under the stress-strain curve up to the elastic strain. However, since the elastic limit and the yield point are typically very close, U_R can be approximated as the area under the stress-strain curve up to the yield strength [118]. This is represented by the following formula:

$$U_R = \frac{\sigma_y^2}{2E_{elastic}}$$

The modulus of resilience was estimated to be $U_R = 1.45 \text{ MPa}$ for 3100HP, $U_R = 0.87 \text{ MPa}$ for 3052D, and $U_R = 0.75 \text{ MPa}$ for 4060D. This decrease in resilience is most likely due to a decrease in crystallinity, causing the material to absorb less strain energy per unit volume.

These results are represented in **Table 2-6** below. It is clearly shown that yield strength, ultimate tensile strength, and resilience will decrease as more meso-lactide is copolymerized with L-lactide. This may be due to the increase in amorphous regions as meso-lactide content increases. The disorder in PLA polymer chains leads to brittleness in the structure, which explains the increase in stiffness and ductility as more meso-lactide content increases.

Table 2-6. Mechanical properties of Ingeo PLA standard grades

Sample	σ_{break} (MPa)	ϵ_{break} (%)	σ_y (MPa)	σ_{ult} (MPa)	$E_{elastic}$ (GPa)	ϵ_p (%)	U_T (J/m ³)	U_R (MPa)
3100HP	72.8 ± 2.6	5.7 ± 0.5	70.2 ± 2.3	73.7 ± 2.9	1.7 ± 0.052	1.33	2872.77	1.45
3052D	67.2 ± 2.4	5.1 ± 0.56	68.4 ± 2.1	72.4 ± 2.3	2.7 ± 0.085	2.75	2958.78	0.87
4060D	65.8 ± 2.8	4.4 ± 0.6	65.0 ± 1.8	71.4 ± 2.4	2.8 ± 0.097	2.68	2292.34	0.75

2.3.10 Rheological Properties

Although meso-lactide content mainly influences the crystallinity of PLLA, the melt rheological properties may also illustrate differences between PLA of various stereoisomeric compositions. This is because the affinity of molecules in the melt state may affect the polymer's viscoelastic properties [119]. The rheological behavior of NatureWorks PLA standard grades at various meso-lactide content (3100HP – 1%, 3052D – 9%, 4060D- 22 wt%) has been characterized. **Figure 2-16** shows that at 180°C, 4060D possessed the highest viscosity, which may be due to the higher molecular weight. On the other hand, 3100HP with a lower molecular weight depicts a higher viscosity than 3052D, which may be due to its crystallization behavior at processing temperatures above PLA's melting temperature.

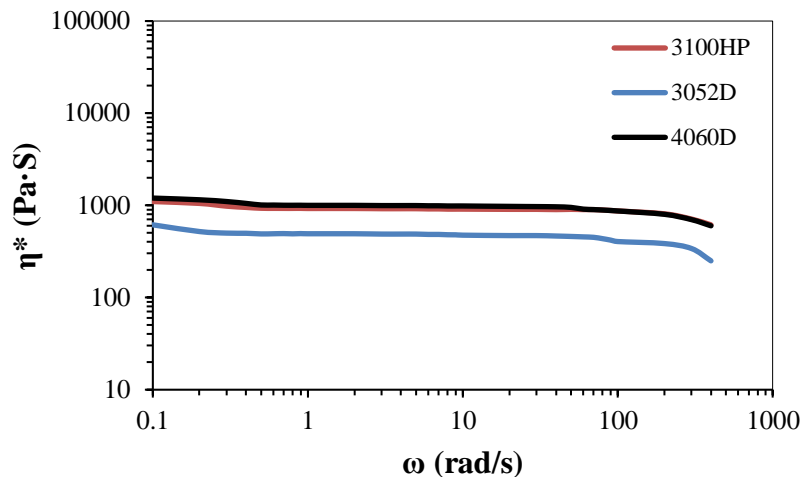


Figure 2-16. Complex viscosity of NatureWorks PLA standard grades at various meso-lactide content; 3100HP – 1%, 3052D – 9%, 4060D- 22 wt%

2.3.11 The Role of PLA Stereochemistry in Immune Cellular Response

2.3.11.1 PLA Breakdown and Extraction

The molecular weight of various PLA samples (L175, D120, LX930, 3100HP, 4060D) was characterized before and after extraction. **Table 2-7** below details the molecular weights of pure PLA samples as well as samples after extraction in Milli-Q water and HG medium. **Table 2-8** details the percent D-content (characterized based on **Section 2.3.5** and **2.3.6**) and percent degradation in number-average (M_n) and weight-average (M_w) molecular weights after extraction. The highest amount of degradation occurs in amorphous grade PLA LX930 after extraction in Milli-Q water, with a 23% reduction in number-average molecular weight and a 16% reduction in weight-average molecular weight. Strangely enough, the second highest amount of degradation occurs in semi-crystalline PLLA L175 and semi-crystalline PLA 3100HP after extraction in HG media, both with a 14% reduction in number-average molecular weight. It was initially assumed that amorphous grade PLA 4060D would show similar bulk degradation behavior to LX930, but its molecular weight reduction is in fact on the lower end, with only about 8-9% reduction in molecular weights.

Table 2-7. Molecular weights of commercial grade PLA before and after extraction in Milli-Q water (H₂) and HG media

Sample Code	Corresponding PLA	M _n (Da)	M _w (Da)	PDI
PLA-1	L175/PLLA	102697 ± 3250	171675 ± 4320	1.672
PLA-1 (HG)	L175/PLLA	88422 ± 2100	143515 ± 2560	1.623
PLA-1 (H ₂ O)	L175/PLLA	94173 ± 2030	160516 ± 3140	1.811
PLA-2	D120/PDLA	91760 ± 3180	150515 ± 4250	1.640
PLA-2 (HG)	D120/PDLA	82951 ± 1890	148230 ± 3230	1.787
PLA-2 (H ₂ O)	D120/PDLA	90384 ± 3200	146945 ± 2890	1.626
PLA-4	LX930/amorphous	109098 ± 5340	191250 ± 6540	1.793
PLA-4 (HG)	LX930/amorphous	98079 ± 4380	169555 ± 4570	1.729
PLA-4 (H ₂ O)	LX930/amorphous	83787 ± 1920	160365 ± 3570	1.914
SC	3100HP/semi-crystalline	87390 ± 2840	157060 ± 3640	1.797
SC (HG)	3100HP/semi-crystalline	75155 ± 1340	140540 ± 2390	1.870
SC (H ₂ O)	3100HP/semi-crystalline	81010 ± 2640	147335 ± 2670	1.819
A	4060D/amorphous	113270 ± 1880	200200 ± 2150	1.767
A (HG)	4060D/amorphous	100923 ± 3380	185365 ± 3900	1.837
A (H ₂ O)	4060D/amorphous	103302 ± 2180	185250 ± 3560	1.793

Table 2-8. Molecular weight reduction and corresponding D-content for commercial grade PLA

Sample Code	D-content (%)	M _n Reduction (%)	M _w Reduction (%)
PLA-1 (HG)	<0.1	13.9	16.4
PLA-1 (H ₂ O)	<0.1	8.3	6.5
PLA-2 (HG)	>99.9	9.6	1.5
PLA-2 (H ₂ O)	>99.9	1.5	2.4
PLA-4 (HG)	8	10.1	11.3
PLA-4 (H ₂ O)	8	23.2	16.1
SC (HG)	0.5	14.0	10.5
SC (H ₂ O)	0.5	7.3	6.2
A (HG)	11	10.9	7.4
A (H ₂ O)	11	8.8	7.5

The reason for LX930's behavior may be described by its stereochemical composition. LX930's D-content (8% D) may be less than 4060D (11% D), but its ¹H NMR spectrum (**Figure 2-17**) indicates that only 54% D-content comes from meso-lactide; 46% is D-lactide. This composition is distinguishable from NatureWorks 4060D, whose D-content mainly consists of meso-lactide

with <0.1% D-lactide. The presence of D-lactide chains mixed with meso-lactide chains may cause even more amorphous domains to be created, thus causing such high bulk degradation.

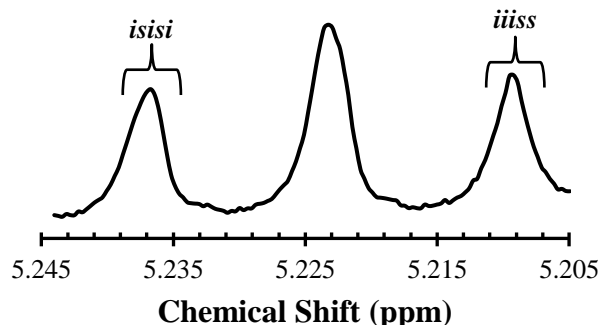


Figure 2-17. NMR spectrum displaying the *isisi* and *iiiss* resonances for D-lactide and meso-lactide, respectively in LX930

3100HP and L175's behavior in HG media suggest that that degradation can be detected over a short period for semi-crystalline PLLA with glucose priming. This is due to a supplementation of carbon in the medium, which suggests that hydrolytic degradation of PLA is constitutive when targeting other nutrient and carbon sources in the environment [120]. While not as high, noticeable degradation is seen for the other PLA samples in HG media - ~10% reduction in M_n . This explains that hydrolytic degradation depends on the primary carbon source in the media.

As seen in **Table 2-9**, lactic acid oligomers were detected in PLA extracts after 12 days based on the lactic acid assay. Although using the standard D/L-lactic acid enzyme-based determination assays could not effectively measure levels in HG media, a 7.8- and 5.2-fold increase in L-lactic acid was observed in amorphous (4060D) and semi-crystalline (3100HP) PLA extracts, respectively, in Milli-Q water. Similarly, we observed a 2.7- and 2.8-fold increase in D-lactic acid in amorphous and crystalline PLA extracts, respectively. This data suggests that hydrolytic degradation is taking place in PLA at temperatures below glass transition (~50-60°C). However, the lactic acid release, and thus degradation, cannot be quantified with this method.

Table 2-9. Oligomers of L- and D-lactic acid detectable in PLA extracts from Milli-Q water

Sample	L-lactic acid	D-lactic acid
3100HP Extract	0.0034 ± 0.0025	0.0021 ± 0.0010
4060D Extract	0.0051 ± 0.0004	0.0023 ± 0.0002

Hydrolytic degradation of PLA was further confirmed based on ESI-MS results (**Figure 2-18**). The water fractions after 12 days at 37°C were analyzed to identify the water-soluble degradation products and to follow the degradation process. Similar behavior in the product patterns was observed between L175 and 3100HP, but there was a significant difference compared to D120, 4060D, and stereocomplex PLA. The most noticeable peaks in the spectra for both materials were sodium adducts of lactic acid oligomers appearing at $m/z = 18 + 23 + 72 \times n$, where 72 is the molar mass of the repeat unit and 18 is the molar mass of the end groups.

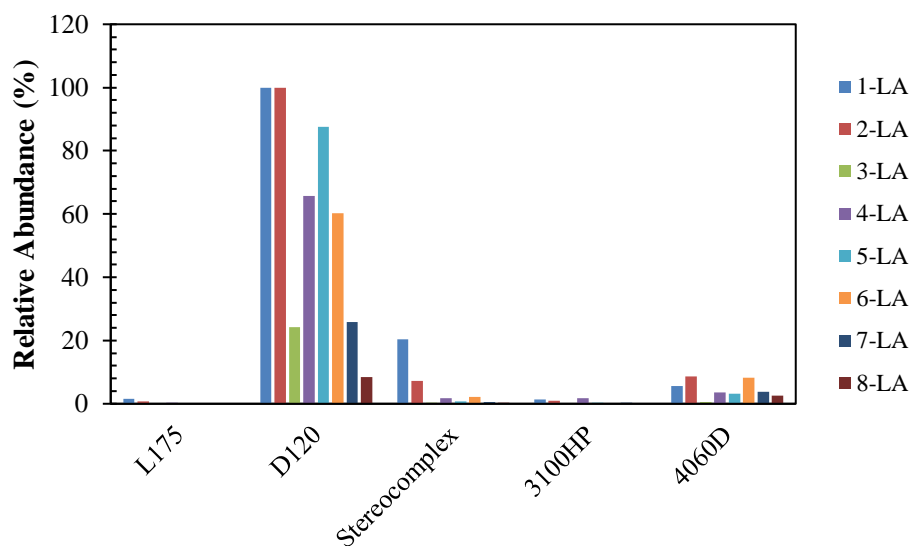


Figure 2-18. ESI-MS data displaying water-soluble degradation products (i.e.: lactic acid) for PLA samples after hydrolysis in water at 37°C for 12 days; the legend shows the lactic acid oligomers (mono-, di-, tri-, etc.) that appear for each sample after hydrolysis

For 3100HP and L175, a small amount of mono and di-lactic acid (m/z 89.023 and 161.044) was observed in the PLLA samples. D120 released the largest abundance of degradation products, displaying a multiple series of lactic acid oligomers (at least 3). One series is the $89.023 + 72.021n$

set of peaks, which is from unmodified lactic acid. The other major series is offset by 39.992 Da ($201.0363 + 72.021n$). 4060D displayed mono-, di- and a small amount of tri-lactic acid masses as well as some masses consistent with higher oligomers (521.15, 593.17, 665.19, 737.21, 809.23, 881.23). This higher fraction of lactic acid release may be related to the *R* configuration in PDLA and amorphous grade PLA. When hydrolysis occurs, the amorphous domains of a polymer are usually broken down first. We hypothesize that the *R* configurational sequences in PLA chains are broken down first and much more quickly than the *S* configurational sequences. PDLA and amorphous grade PLA samples are broken down into D-lactic acid oligomers at a high rate compared to the degradation of PLLA into L-lactic acid oligomers. Finally, mono- and di-lactic acid peaks were observed at m/z 89.023 and 161.044 as well as the m/z 201.036 and 273.057 peaks which were in the PDLA sample. This is consistent with the spectra for PLLA and PDLA, as stereocomplex PLA is a blend of both materials. We conclude that hydrolytic degradation takes place at a low rate for most PLA samples, with the exception of PDLA. Stereochemistry plays an important role in commercial application, particularly in the medical device area. One must consider the stereochemical composition depending on the degradation required for medical implants.

2.3.11.2 Glycolytic Inhibition of PLA

The thermal decomposition temperature of glycolytic inhibitors was first characterized to analyze for possible degradation during processing with PLA. **Figure 2-19** displays the temperature at which the glycolytic inhibitor, or substances within the inhibitor, completely degrades. 2DG's graph (**Figure 2-19a**) displays two decomposition temperatures at $\sim 164^{\circ}\text{C}$ and $\sim 254^{\circ}\text{C}$, with a 91.5% weight loss, indicating 2+ major substances in the inhibitor's composition; the drug begins to decompose at $\sim 140^{\circ}\text{C}$. As PLA's processing temperature is $\sim 190^{\circ}\text{C}$, thermal degradation of

2DG will occur during processing, and one must compensate for the drug's weight loss during processing. **Figure 2-19b** shows the maximum thermal decomposition temperature for 3PO's complete weight loss at $\sim 273^{\circ}\text{C}$, indicating one major ingredient within the inhibitor's composition. While this degradation temperature is above PLA's processing temperature, 3PO starts to decompose at $\sim 172^{\circ}\text{C}$; moderate thermal degradation of the inhibitor will still occur during PLA processing. a.a. (**Figure 2-19c**) displays two major peaks at $\sim 176^{\circ}\text{C}$ and $\sim 211^{\circ}\text{C}$, with an 86.3% weight loss overall; a.a. starts to decompose at $\sim 142^{\circ}\text{C}$. Results indicate there are 2+ major ingredients comprising the glycolytic inhibitor, and that major degradation will most likely occur over processing with PLA.

Compared to the previous three inhibitors discussed, DIDS's thermal behavior (**Figure 2-19d**) shows that only 47% weight loss occurs at a decomposition temperature of $\sim 433^{\circ}\text{C}$, and that it starts to degrade at temperatures as high as $\sim 376^{\circ}\text{C}$. This indicates that $>50\%$ of DIDS's composition maintains its composition at temperatures up to $\sim 550^{\circ}\text{C}$. The robust thermal degradation behavior may be due to the strong (aryl) $\text{C}-\text{SO}_3^-$ bond in the sulfonic acid group of the inhibitor. It is concluded that little to no thermal degradation may occur for DIDS during processing with PLA. CHC's thermal decomposition graph (**Figure 2-19e**) displays similarly robust behavior against thermal degradation, starting to decompose at $\sim 217^{\circ}\text{C}$ with a 77% weight loss at $\sim 277^{\circ}\text{C}$. Data indicates that minimal degradation should occur while melt blending CHC with PLA. Metformin's thermal degradation graph (**Figure 2-19f**) displays two major peaks at $\sim 301^{\circ}\text{C}$ and $\sim 505^{\circ}\text{C}$, with possible overlapping peaks at temperatures between 200 and 375°C ; this indicates multiple substances with varying thermal decomposition temperatures. Metformin only starts to degrade at $\sim 222^{\circ}\text{C}$. Metformin's degradation behavior can be most likely explained by the multiple amino groups in the chemical structure.

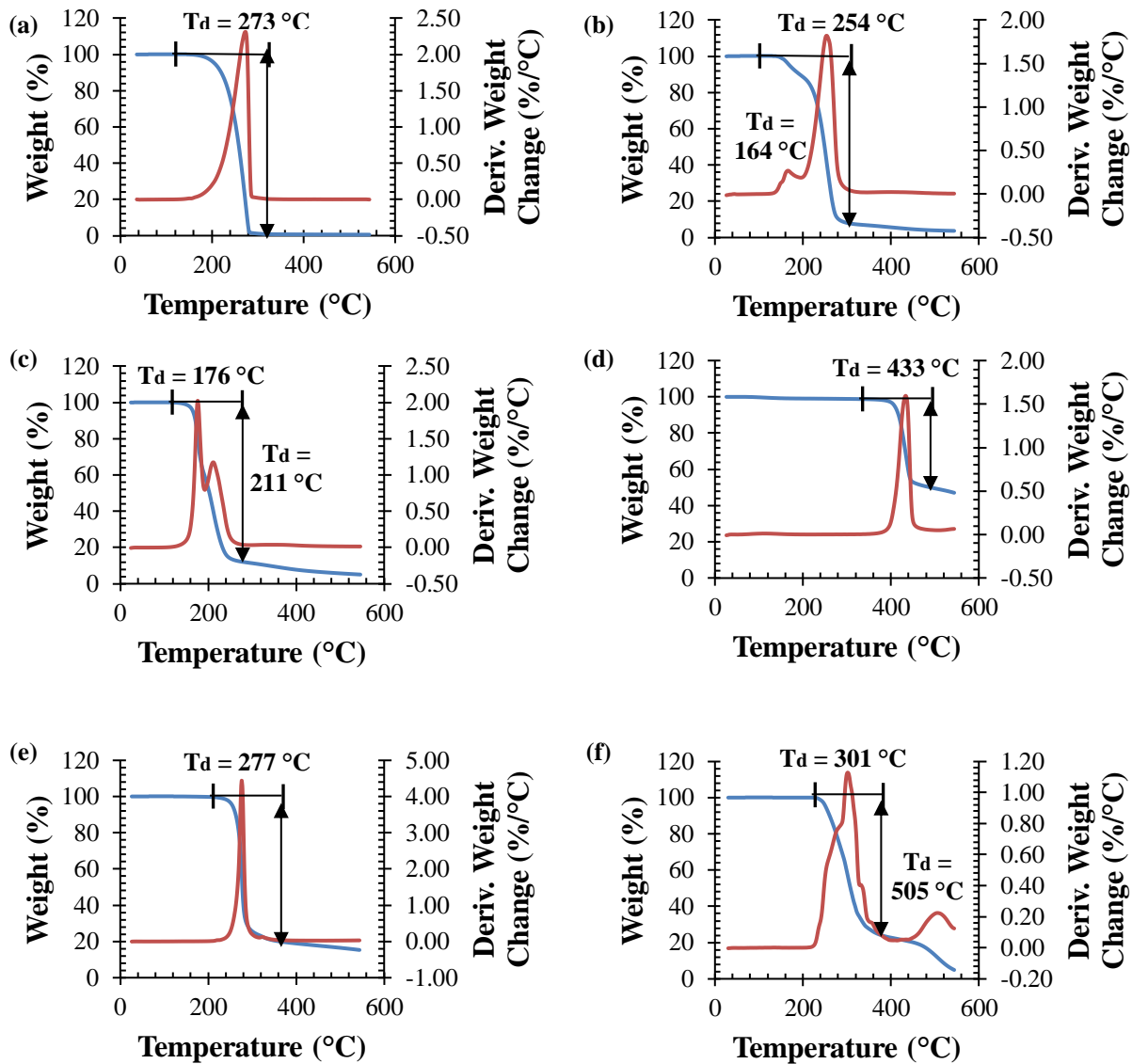


Figure 2-19. Thermal degradation behavior of glycolytic inhibitors: (a) 2DG (b) 3PO (c) a.a. (d) DIDS (e) CHC (f) Metformin

TGA results indicated that 2DG, 3PO, and a.a. will most likely experience moderate to extreme thermal degradation, while DIDS, CHC, and metformin may experience minimal degradation at PLA processing temperature (190°C). An isothermal degradation kinetics experiment was also run on the glycolytic inhibitors to analyze the weight loss over time at 190°C. These results would provide more precise data on how much degradation will occur in each sample when processing the material with PLA at 190°C and 5 minutes. Results are shown in **Figure 2-20**.

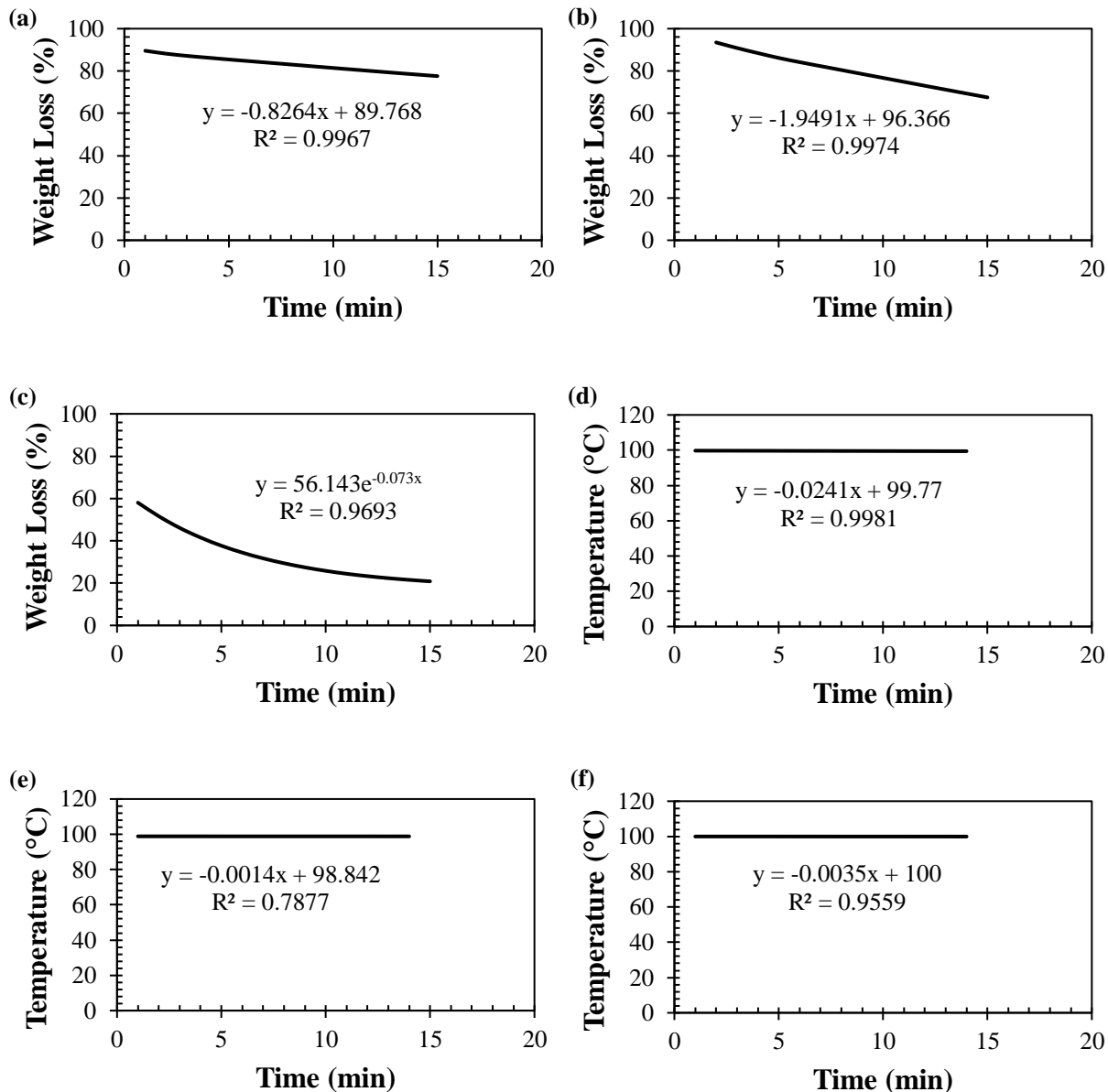


Figure 2-20. Isothermal degradation kinetics of glycolytic inhibitors: **(a)** 2DG **(b)** 3PO **(c)** a.a. **(d)** DIDS **(e)** CHC **(f)** Metformin; weight loss at 0 minutes for 2DG, 3PO, and a.a. are due to DSC temperature equilibration

As seen in **Figure 2-20a**, 2DG decomposes at ~12.5% of its weight over a period of about 15 minutes. Data suggests that ~4% thermal degradation will occur for 2DG during processing with PLA at 190°C. The starting weight (~90%) of the sample is due to degradation from DSC temperature equilibration. 3PO (**Figure 2-20b**) experiences more accelerated degradation

compared to 2DG, with ~29% weight loss in 15 minutes. Results show that ~10% thermal degradation will occur in 2DG in 5 minutes of processing with PLA. 2DG and 3PO's thermal degradation behavior represent zero-order rate kinetics, with rate constants of 0.83 and 1.95, respectively.

Figure 2-20c displays a.a.'s thermal decomposition graph, representing an exponential decrease in weight loss over time at a constant temperature of 190°C. This represents a first-order rate kinetics behavior as opposed to 2DG and 3PO's zero-order degradation kinetics. Plotting a logarithmic graph of this behavior results in a rate constant of 0.073. This corresponds to the 39% weight loss that occurs over 15 minutes of heating at 190°C. ~12% weight loss will occur in a.a. while processing with PLA over a 5 minute run time.

Compared to the previous three inhibitors discussed, CHC, DIDS, and metformin undergo little to no thermal degradation at PLA processing temperatures. This correlates well with results in **Figure 2-19**, suggesting that there are no substances within these glycolytic inhibitors that will thermally degrade over time at 190°C. We conclude that we must compensate for the weight loss of 2DG, 3PO, and a.a. for targeting our drug concentration within PLA.

After melt blending the glycolytic inhibitors with semi-crystalline grade PLA 3100HP and amorphous grade PLA 4060D, uniformity and dispersity of the inhibitor within PLA were analyzed via SEM-EDX. a.a. and DIDS were chosen for analysis due to their high concentration of elements distinguishable from PLA. Chlorine distribution was analyzed for a.a., whereas sulfur was analyzed for DIDS. Cross-sectional (CS) and surface (S) SEM images for each semi-crystalline PLA sample and their respective elemental maps are shown in **Figure 2-21**. Similar results were seen for all other PLA + inhibitor blends, including the amorphous PLA matrix.

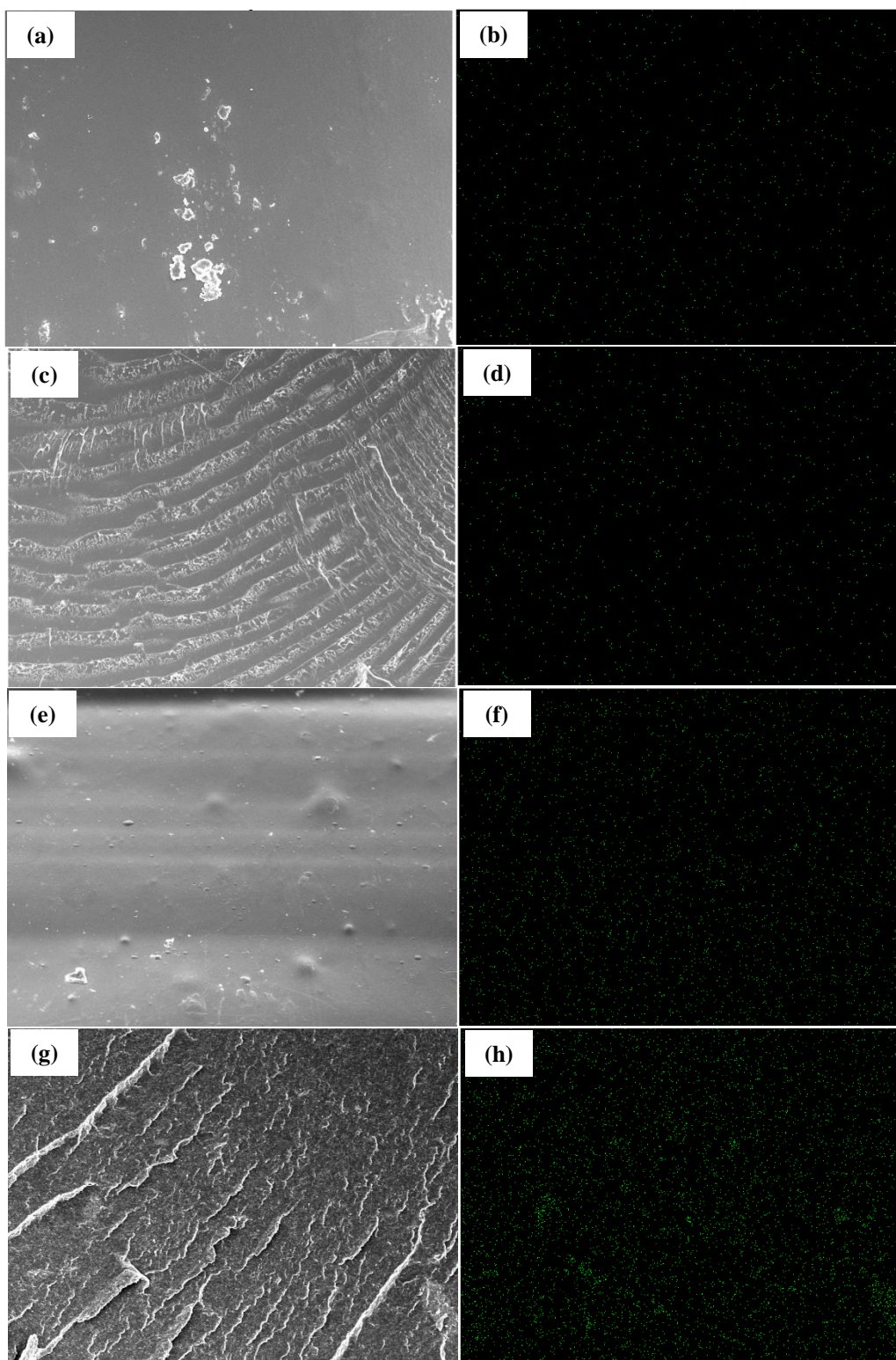


Figure 2-21. SEM images and EDX elemental map of 3100HP and glycolytic inhibitors- **(a)** SEM S image of 3100HP + a.a. **(b)** EDX S map of chlorine in 3100HP + a.a. **(c)** SEM CS image of 3100HP + a.a. **(d)** EDX CS map of chlorine in 3100HP + a.a. **(e)** SEM S image of 3100HP + DIDS **(f)** EDX S map of sulfur in 3100HP + DIDS **(g)** SEM CS image of 3100HP + DIDS **(h)** EDX CS map of sulfur in 3100HP + DIDS

As seen in **Figure 2-21**, the SEM images are clear of any pores or particles, indicating a smooth surface and clear bulk for the PLA + inhibitor blends. Based on **Figures 2-21b** and **d**, ~0.2wt% concentration of chlorine was detected throughout the surface and bulk of PLA; this corresponds to the theoretical target concentration of a.a. required in the PLA samples, based on atomic mass calculations. Chlorine is also uniformly distributed throughout the PLA surface and bulk, indicating uniform distribution of a.a. within the PLA matrix. **Figures 2-21f** and **h** also display uniform distribution of DIDS within PLA, resulting in ~2.0wt% of sulfur in the surface and bulk of PLA (~2.2wt% was our target concentration of sulfur). These results show that the glycolytic inhibitors are distributed evenly, regardless of the bulk or surface location, and that micro-extrusion can be used to mix PLA and drugs for bone growth or tissue regeneration applications.

2.4. Conclusion and Next Steps

It has been shown that optical rotation and ^1H NMR can be used to identify the stereochemical isomers within a PLA sample, and whether the D-content originates from meso-lactide or pure D-lactide. We have confirmed that commercial grade PLA samples are mainly composed of L-lactide and meso-lactide, with <1% D-lactide.

Synthesized poly(meso-lactide) was determined to be optically inactive and comprises a predominantly atactic, amorphous structure; there is no change in the optical rotation if meso-lactide is polymerized. A similar behavior is seen when copolymerizing meso-lactide with L-lactide. When considering the specific rotation per concentration of L-lactide in poly(L-co-meso-lactide), we conclude that the copolymer maintains its L (*SS*) stereoconfiguration no matter how much meso-lactide is added. This is confirmed via optical rotation analysis, where we have estimated the specific rotation to be $\sim -156^\circ$ regardless of the meso content in poly(L-co-meso-lactide).

It has also been observed that PLA transitions from a predominantly isotactic, semi-crystalline polymer to a predominantly atactic, amorphous polymer as more meso-lactide- at >10% meso- is copolymerized with L-lactide. The reason for this structure change is most likely due to random insertion of meso-lactide to the *R* and *S* stereocenters. This random structure results in the polymer unable to pack into an ordered manner, which leads to an amorphous polymer.

Tensile testing results show that PLA's mechanical properties such as the yield strength, ultimate tensile strength, and modulus of resilience all decrease as the percent meso-lactide content increases. This may be due to a reduction in crystallinity due to increase in amorphous regions; adding more meso (*RS*)-lactide chains causes disorder within the originally ordered L (*SS*)-lactide chains. This reduction in crystallinity increases the polymer's brittleness, which means an increase in the stiffness but a decrease in the tensile strength and resilience.

Finally, results on the melt rheological behavior of NatureWorks PLA standard grades at various meso-lactide content lead us to conclude that the stereochemical composition is not the primary factor in PLA's complex viscosity. There are other factors one must consider, such as the molecular weight of the polymer, as well as its tendency to crystallize at processing temperatures above melt temperature.

PLA's stereochemistry plays an important role in determining the material properties of the final product. Future work recommendations include analyzing the stereochemistry of PLA when copolymerizing all three stereoisomers (L, D, meso) at various compositions. Tacticity, optical rotation, crystallinity, and other material properties should be analyzed to further explore the effect of stereochemistry on the material product. Future work will also follow the immune response to stereochemistry based on PLA metabolic reprogramming. Applications include bone growth and tissue regeneration applications using PLA implants.

3. REACTIVE EXTRUSION OF HIGH MOLECULAR WEIGHT STEREOCOMPLEX PLA FOR ADDITIVES APPLICATION DEVELOPMENT

3.1. Introduction

From the previous chapter, studies showed how the stereochemistry can play a role in the material properties of polylactide (PLA). Increasing D-lactide content or meso-lactide content when copolymerizing with L-lactide would lead to a reduction in the polymer's melting point and crystallinity. However, the same behavior cannot be said when physically mixing PLLA and PDLA as opposed to copolymerizing L-lactide and D-lactide. When the interaction between polymers of varying configurations and/or tacticities dominates over the one between polymers with similar configurations and/or tacticities, a stereoselective interaction between the polymers takes place. Such association is defined as stereocomplex formation aka stereocomplexation [121]. Stereocomplexation of PLA may occur in solution, in the melt state, or during polymerization. Based on several studies, researchers have deduced that the ratio of stereocomplex crystallites to homocrystallites is mainly affected by the molecular weights of the homopolymers, the optical purities of the homopolymers, and the mixing ratio [82], [121]–[124]. By blending PLLA and PDLA at a 1:1 ratio above their melting point, one can form a stereocomplex that has a melting point that is 50°C higher than the PLA homopolymers. The mechanism behind the observed increase in melting temperature is related to the packing of the stereocomplex helices, which are stabilized by strong van der Waals interactions and hydrogen bonding [125], [126]. **Figure 3-1** displays PLA materials of varying tacticities and configurations, in order of increasing melting temperature and crystallinity, with stereocomplex PLA ranking the highest in material performance.

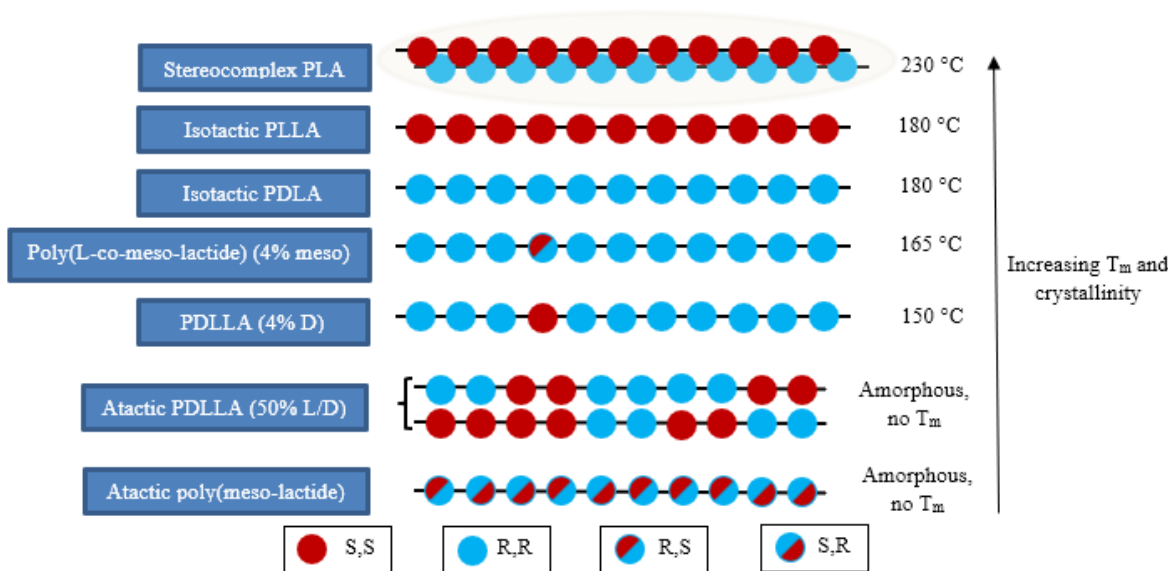


Figure 3-1. PLA materials of various configurations and tacticities, in order of increasing melting point and crystallinity

In order to improve thermal/mechanical performance as well as hydrolysis resistance of PLA, researchers have conducted many studies on PLA stereocomplexation [127]–[131]. Li et. al processed a 1:1 blend of PLLA and PDLA of various molecular weights in a rheometer with a rotating speed of 50 rpm at a processing temperature of 220°C for 5 min. Blends of PLAs with the lowest molecular weights ($M_v = 30\text{--}40$ kDa) possessed the highest stereocomplex crystallite formation ($f_{sc} = 81.0\%$), the highest total crystallinity ($X_c = 30.6\%$), and the second highest stereocomplex melting peak temperature ($T_{pm} = 224.4^\circ\text{C}$). Strangely enough, the blends of PLAs with the highest molecular weights ($M_v = 86\text{--}96$ kDa) possessed the second highest stereocomplex crystallite formation ($f_{sc} = 76.1\%$), the second highest total crystallinity ($X_c = 30.5\%$), and the highest stereocomplex melting peak temperature ($T_{pm} = 228.7^\circ\text{C}$) [132].

These results lead to the conclusion that PLA homopolymers of high melting temperatures and crystallinities are favorable for stereocomplex crystallite formation. Moreover, when the

crystallinities of the stereocomplex PLA of two different MW blends (low/high) are similar, the blend with higher molecular weight facilitates a higher stereocomplex melting peak temperature. To avoid thermal degradation of PLA chains and suppress the growth of PLA homocrystallites due to high temperature processing, Gao et. al presents an alternative route to rapidly prepare exclusive PLA stereocomplex induced by shear stress at low temperature (190 °C) extrusion. Using poly(butylene adipate-co-terephthalate) (PBAT), PLA crystallization was accelerated and processability of the PLA stereocomplex at low temperature was improved due to the decrease in the melt flow's activation energy. PLLA ($M_w = 210$ kDa) and PDLA ($M_w = 68$ kDa) were melt-blended in a 1:1 ratio with PBAT content ranging from 0-50% based on the total weight of PBAT to PLLA/PDLA blends. Compared to Li's conditions, melt blending took place in a rheometer with a rotating speed of 50 rpm at a processing temperature of 190°C for 5 min. At 10% PBAT content, torque was estimated to be ~39 N m. Full stereocomplexation occurred, and crystallinity and stereocomplex melting peak temperature both increased to 56.7% and 228°C, respectively [133]. These results justify that PBAT can be used as a possible additive to continuously produce exclusive stereocomplex PLA at low processing temperatures.

Despite the abundant research on stereocomplex PLA, there have been no publications defining an efficient solventless, industrial scale method to produce exclusive stereocomplex PLA using high molecular weight (MW) PLA. Herein, we describe a pilot-scale continuous manufacturing method via reactive extrusion to produce exclusive stereocomplex PLA from 1:1 blending of high molecular weight PLLA and PDLA homopolymer. The characteristics of stereocomplex formation are first characterized to optimize the processing parameters for achieving the highest stereocomplex formation and optimal thermal properties (crystallinity, melt temperature, etc.). Stereocomplex PLA is then continuously produced as pellets in a co-rotating twin screw extruder

(L/D = 40 and screw diameter = 27 mm). The final product is then used as an additive to develop molecular composites. Stereocomplex PLA particles are used as a filler for PLLA matrix to potentially improve the mechanical properties and crystallization kinetics of the PLLA sample. We conclude this chapter with improvements and suggestions for production and application of stereocomplex PLA.

3.2. Experimental

3.2.1 Pilot-Scale Manufacturing of Stereocomplex PLA via Reactive Extrusion

3.2.1.1 Materials

99.99% neat PLLA (L175) and PDLA (D120) were obtained from Total Corbion (The Netherlands) in the form of pellets, and they were dried for 24 hours at 45°C. **Table 3-1** summarizes their material properties. Optical purity was confirmed via polarimetry. <0.1% meso-lactide content was reported based on ¹H NMR and polarimetry. PLLA and PDLA were pre-mixed at a 50/50 ratio then further dried for another 24 hours. No reagents were used.

Table 3-1. Material properties of Total Corbion standard grades of PLA

Sample	α_{obs}^{25} (°)	o.p. (%)	D-content (%)	$M_{wt\%}$ (%)	T_g (°C)	T_{pm} (°C)	X_c (%)	M_n (kDa)	M_w (kDa)	PDI
L175	-155.5	99.68	0.16	0.075	63.13	175.10	47.52	103	172	1.67
D120	+155.7	99.81	0.095	0.047	62.21	177.52	51.40	92	150	1.64

3.2.1.2 Characteristics of Stereocomplex Formation

The optimal processing conditions for stereocomplexation were determined via DSC. A pellet comprising 50% stereocomplex PLA/50% PLA homopolymer was first developed and characterized via DSC as shown below in **Figure 3-2**. The fractional stereocomplex crystallites f_{sc} and homocrystallites f_{hc} were calculated based on melting enthalpy integration:

$$f_{sc} = \frac{X_{sc}}{X_{sc} + X_{hc}}$$

$$f_{hc} = \frac{X_{hc}}{X_{sc} + X_{hc}} = 1 - f_{sc}$$

Where X_{sc} and X_{hc} are the experimental crystallinities of the stereocomplex crystallites and homocrystallites, respectively [134].

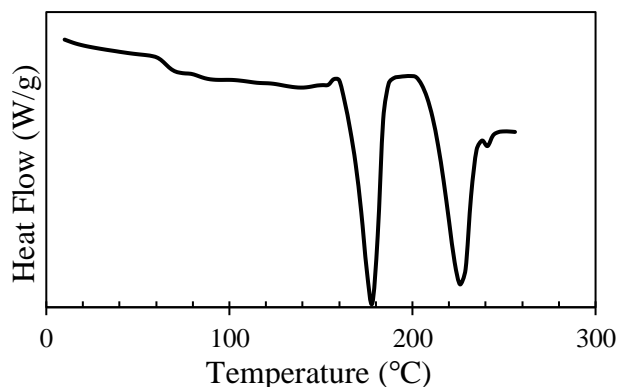


Figure 3-2. First DSC thermogram of pellets comprising 50% stereocomplex crystallites/50% PLA homocrystallites based on melting enthalpy calculations

50% stereocomplex PLA and 50% PLA homocrystals were confirmed based on the melting peaks at 225°C and 178°C, respectively. It is assumed that the PLA homocrystals are an unreacted blend of PLLA and PDLA. The conversion of this unreacted blend of PLA homocrystallites to stereocomplex crystallites was characterized based on time and temperature. The temperature was first equilibrated to 180/190/200/210/220/230°C; these temperatures were chosen as they are at or above the melting peak temperature of PLA (~180°C). It is required to process PLLA and PDLA in the liquid state to form stereocomplex PLA in order to allow for freedom of motion in the molecules [121]. The temperature was then held constant at 1/2/3 minutes, as processing time in the extruder is no more than 3 minutes. Samples were then cooled to 0°C at 10°C/min, then held isothermally for 2 minutes. A heating scan was finally run at 10°C/min to 250°C. This heating scan was then analyzed to calculate the fractional stereocomplex crystallites based on melting enthalpy integration. The stereocomplex formation was plotted at different times and temperatures to model the kinetics.

3.2.1.3 Reactive Extrusion of Stereocomplex PLA

The procedure thereof involves a pilot-scale technique to continuously produce stereocomplex PLA in a co-rotating twin screw extruder (L/D = 40 and screw diameter = 27 mm). High molecular weight PLLA ($M_n = 150$ kDa) and PDLA ($M_n = 142$ kDa) were blended in a 1:1 ratio with no additives into the feeding zone of a co-rotating twin-screw extruder type ZSE 27 HP-PH from Leistritz (Nürnberg, Germany).

The heating system was divided into 10 heating zones. The temperature profile was carefully chosen according to previous studies on the thermal behavior of stereocomplex PLA during processing. As seen in **Figure 3-3**, it was discovered that processing a 1:1 blend of PLLA and PDLA at temperatures lower (~190-200°C) than the melting peak temperature of stereocomplex PLA (~230-240°C) would lead to solidification of the product within the extruder. This is especially true when setting such temperatures in the first few heating zones of the extruder. The reason for this behavior is due to the formation of stereocomplex PLA within the extruder, in that the heating zones' temperatures are not high enough to flow the product through the extruder.

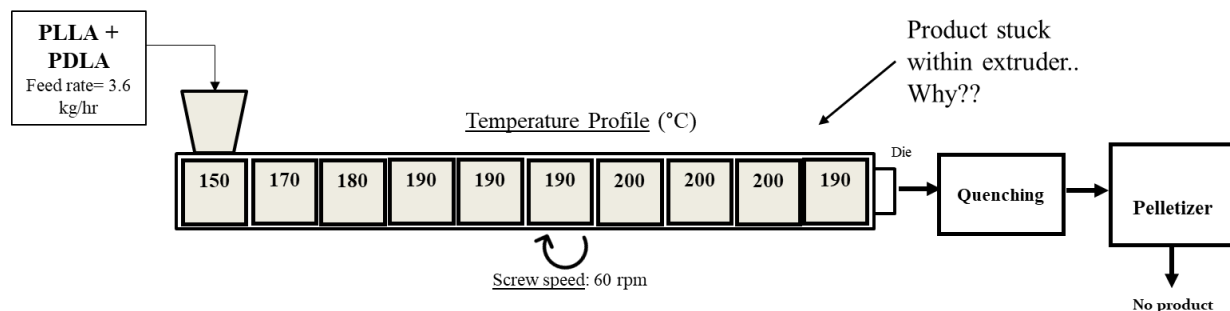


Figure 3-3. Processing conditions for first trial run of stereocomplex PLA in a co-rotating twin-screw extruder type ZSE 27 HP-PH from Leistritz

Differential scanning calorimetry (DSC) studies (**Figure 3-4**) also show that processing the PLLA/PDLA blend at temperatures at or above the melting point of stereocomplex PLA leads to thermal dissociation of the stereocomplex. This means that the stereocomplex PLA product reverts

to its respective PLLA and PDLA homopolymers. The reason behind this behavior is most likely due to chain slipping and breakage of the stereocomplex crystallites due to melting. The product stems from a physical blend, not a chemical reaction, of two polymers. This results in thermal instability at or above its melting peak temperature; it is an entropy driven process. In the melt state, the PLLA and PDLA units that once formed a stereocomplex are now free to move about in any order compared to the solid state; there is an increase in the molecular motion of the system, and thus, an increase in entropy. This increased freedom of motion results in a higher variation in possible locations for the molecules.

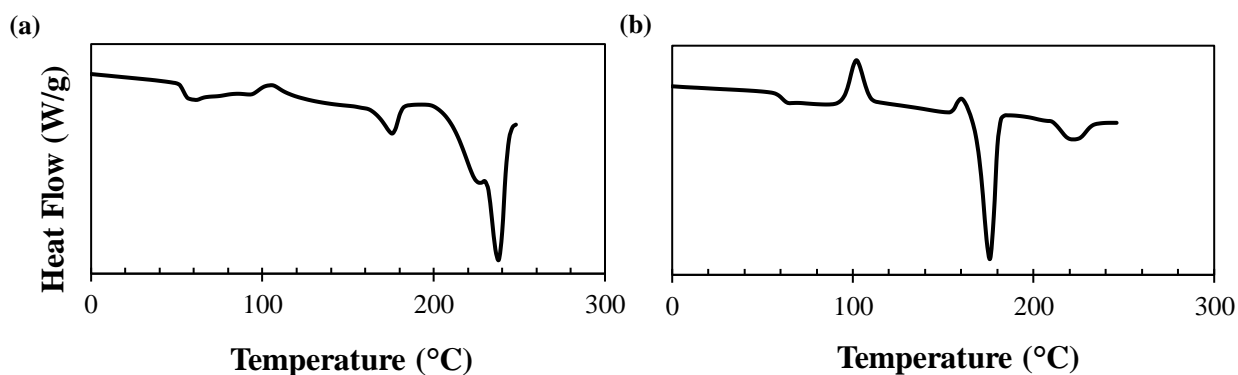


Figure 3-4. DSC thermograms on stereocomplex PLA (a) First heating scan - stereocomplex crystallite formation (b) Second heating scan – thermal dissociation of stereocomplex crystallites to homocrystallites

Taking these factors into consideration, one must carefully consider the temperature conditions to process stereocomplex PLA. A temperature profile of 160/170/180/180/180/210/220/220/220/230 (Heating Zone 1 to Die Temperature) was chosen based on DSC results on stereocomplexation kinetics (See *Section 3.3.1.1*). This profile focuses on heating the beginning of the extruder barrel at temperatures high enough (up to 180°C) to flow the PLLA/PDLA blend but low enough to prevent excess stereocomplex formation too early. The end of the barrel is then heated at higher temperatures (~210-220°C) to accelerate stereocomplexation within the last minute of the process.

This method prevents solidification and thermal dissociation of the final product, allowing for continuous manufacturing of stereocomplex PLA.

Figure 3-5 displays the final processing conditions chosen to extrude stereocomplex PLA. A feed rate of 3 kg/hour and screw speed of 50 rpm was chosen. The screw configuration was constructed to allow for optimal mixing and transport of the PLLA and PDLA homopolymers. Kneading elements were placed in the first and second half of the barrel in between the conveying elements. This was to allow for mixing in the first and last minute of processing, while enabling material transport throughout the extruder. Residence time was 2.5 minutes until the product was extruded out of a 5 mm diameter strand die, then quenched in a cold-water bath and pelletized. Samples were collected at different time intervals (5, 10, 20, 40 minutes) to analyze the dispersity of the stereocomplex. Samples were then dried in an oven at 55°C for 24 hours.

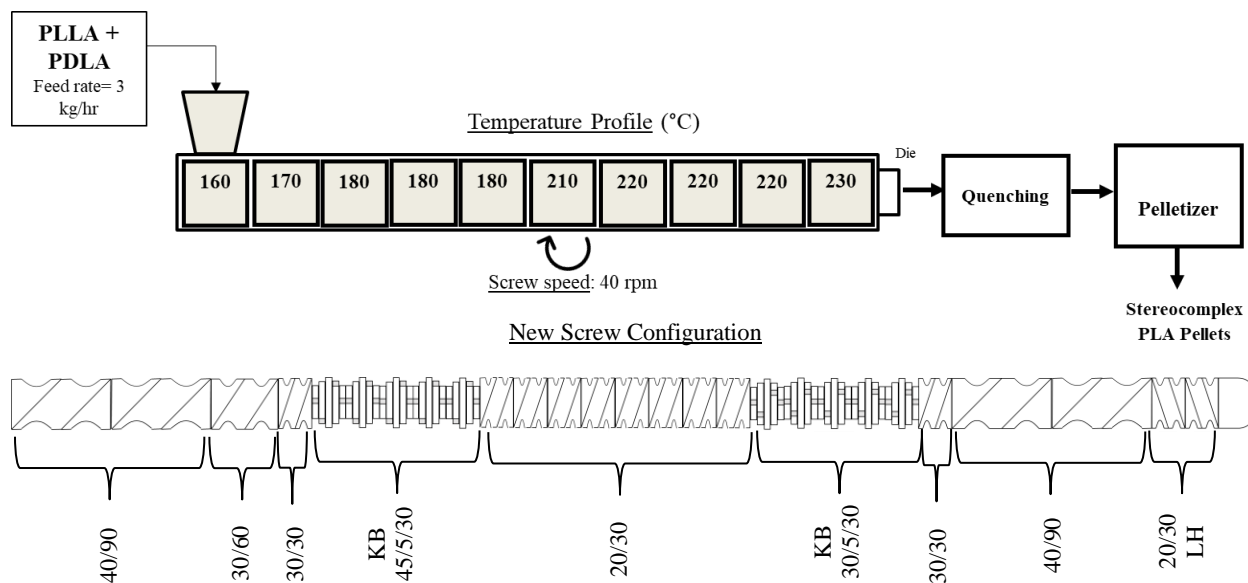


Figure 3-5. Processing conditions for new trial run of stereocomplex PLA in a co-rotating twin-screw extruder type ZSE 27 HP-PH from Leistritz

3.2.1.4 Characterization & Analysis

PLA stereocomplexation was confirmed using a Shimadzu IRAffinity-1. The changes in the conformation of PLA chains can be observed using attenuated total reflectance-Fourier transform

infrared spectroscopy (ATR-FTIR). The α helix (wavenumber 921 cm^{-1}), which is characteristic to PLLA and PDLA, is transformed into a more compact β helix (wavenumber 908 cm^{-1}) [135]. Stereocomplex PLA's spectrum was analyzed and compared to neat PLLA (L175).

The crystal structure of the samples was determined by wide angle X-ray diffraction (WAXD). The spectra were recorded with a Rigaku Smartlab X-ray Diffractometer at room temperature using $\text{CuK}\alpha$ radiation at 40 kV and 44 mA. The specimens were scanned in the scanning range of 5°-30° at a scan speed of 3°/min. Spectra were analyzed using GSAS-II [136]. f_{hc} and f_{sc} are the fractional amounts of homocrystallites and stereocomplex crystallites, respectively, developed during processing under non-isothermal conditions; they can be calculated using the following equations:

$$f_{sc} = \frac{A_{sc}}{A_{sc} + A_{hc}}$$

$$f_{hc} = 1 - f_{sc} = \frac{A_{hc}}{A_{sc} + A_{hc}}$$

Where A_{sc} and A_{hc} are the integrated area under the respective curves for stereocomplex crystallites and homocrystallites, respectively. The total crystallinity was also calculated using the following equation:

$$X_c = \frac{A_{sc} + A_{hc}}{A_{sc} + A_{hc} + A_{amph}}$$

Where A_{amph} is the integrated area under the curve for the amorphous phase.

These calculations were supplemented via DSC using a TA Instruments DSC Q20. The thermal properties were also characterized. The temperature was first equilibrated to 0 °C, then the temperature was ramped up to 260 °C at a heating rate of 10 °C/ min. A second heating scan was not run because, above its melting peak temperature (~240 °C), stereocomplex PLA thermally

dissociates into its constituent homopolymers. f_{sc} and f_{hc} can be calculated using the following equations:

$$f_{sc} = \frac{X_{sc}}{X_{sc} + X_{hc}}$$

$$f_{hc} = \frac{X_{hc}}{X_{sc} + X_{hc}} = 1 - f_{sc}$$

Where X_{sc} and X_{hc} are the crystallinities of the stereocomplex crystallites and homocrystallites, respectively [134]. The total crystallinity can then be calculated via the following formula:

$$X_c = \frac{\Delta H_{m,sc} + \Delta H_{m,hc}}{f_{sc} * \Delta H_{m,sc}^0 + f_{hc} * \Delta H_{m,hc}^0}$$

Where $\Delta H_{m,sc}$ and $\Delta H_{m,hc}$ are the experimental melting enthalpies for stereocomplex and PLA, and $\Delta H_{m,sc}^0$ and $\Delta H_{m,hc}^0$ are the theoretical enthalpy values for a single crystal of β -form stereocomplex (142 J/g) and a single crystal of α -form homocrystallite (93 J/g) [93], [137].

The thermal decomposition temperature and percent weight loss were quantified via thermogravimetric analysis (TGA), specifically the TGA Q50. About 10 mg of sample was heated from 25 to 550°C at 20 °C/min.

3.2.2 Development of Molecular Composites using Stereocomplex PLA Particles in a Thermoplastic PLA Matrix

3.2.2.1 Materials

3100HP and 4060D– semi-crystalline and amorphous grades of PLA by NatureWorks, respectively – were used as the polymer matrices for composites manufacturing. The material properties of both PLA grades are listed below in **Table 3-2**. Stereocomplex PLA, manufactured based on *Section 3.2.1.3*, was used as the filler (5% and 30%) for composites manufacturing. PLA

and stereocomplex PLA were pre-mixed at a 70/30 and 95/5 ratio in an aluminum tray then further dried for another 24 hours at 45°C.

Table 3-2. Material properties of NatureWorks Ingeo standard grades of PLA

Sample	α_{obs}^{25} (°)	o.p. (%)	D-content (%)	$M_{wt\%}$ (%)	T_g (°C)	T_{pm} (°C)	X_c (%)	M_n (kDa)	M_w (kDa)	PDI
3100HP	-154.5	99.04	0.5	1	63.29	176.59	50.14	87	157	1.80
4060D	-122.7	78.65	11	22	59.05	N/A	0	113	200	1.77

3.2.2.2 Reactive Extrusion of PLA/Stereocomplex PLA Composites

PLA/stereocomplex PLA composites were continuously manufactured in a pilot-scale co-rotating twin screw extruder (L/D = 40 and screw diameter = 27 mm). Three different compositions were blended into the feeding zone of a co-rotating twin-screw extruder type ZSE 27 HP–PH from Leistritz (Nürnberg, Germany): (1) 70% 3100HP/30% stereocomplex PLA (2) 70% 4060D/30% stereocomplex PLA and (3) 95% 3100HP/5% stereocomplex PLA. The 70/30 composition was developed to analyze the effect of stereocomplex PLA on the mechanical properties of PLA homopolymer. The 95/5 composition was produced to characterize the role of stereocomplex PLA as a potential nucleating agent for semi-crystalline PLA homopolymer.

PLA homopolymer matrix, in the form of pellets, was first pre-mixed with stereocomplex PLA filler, also in the form of pellets. Mixtures were then dried for 48 hours at 50°C.

The extruder processing conditions are listed below in **Figure 3-6**. The temperature profile used on the extruder from the feed section to the die was as follows: 160/170/180/190/190/190/195/195/195/190. This temperature profile was chosen to allow for viscous flow of the PLA matrix (melting peak temperature $T_{pm} = 180^\circ\text{C}$ for 3100HP, softening temperature $T_{soft} = 150^\circ\text{C}$ for 4060D) while allowing for dispersion of the stereocomplex PLA filler without melting. This is also to prevent thermal dissociation of the stereocomplex PLA filler.

A feed rate of 3.6 kg/hour and screw speed of 40 rpm was chosen. The screw configuration was constructed to allow for optimal mixing and transport of the PLA homopolymer matrix and stereocomplex PLA filler. Kneading elements were placed in the first and second half of the barrel in between the conveying elements. This was to allow for mixing in the first and last minute of processing, while enabling material transport throughout the extruder. Residence time was 2.5 minutes until the product was extruded out of a 5 mm diameter strand die, then quenched in a cold-water bath and pelletized. Samples were collected at different time intervals (5, 10, 20 minutes) to account for the dispersity of the filler in the matrix. Samples were then dried in an oven at 55°C for 24 hours, then characterized.

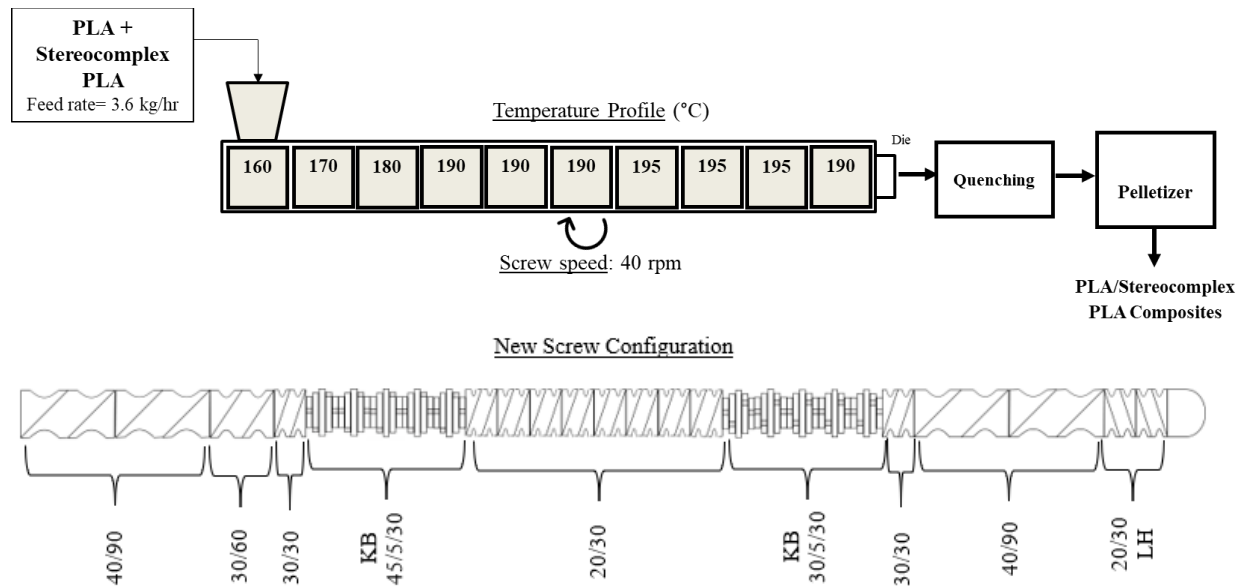


Figure 3-6. Processing conditions for composites manufacturing of PLA/Stereocomplex PLA composites in a co-rotating twin-screw extruder type ZSE 27 HP–PH from Leistritz

3.2.2.3 Characterization & Analysis

DSC was conducted using a TA Instruments DSC Q20 to characterize the dispersity of stereocomplex PLA filler in PLA homopolymer matrix at different time intervals. The temperature

was first equilibrated to 0 °C, then the temperature was ramped up to 260 °C at a heating rate of 10 °C/ min. A second heating scan was not run because, above its melting peak temperature (~240 °C), stereocomplex PLA thermally dissociates into its constituent homopolymers. f_{sc} and f_{hc} were calculated using the following equations:

$$f_{sc} = \frac{X_{sc}}{X_{sc} + X_{hc}}$$

$$f_{hc} = \frac{X_{hc}}{X_{sc} + X_{hc}} = 1 - f_{sc}$$

The total crystallinity was also calculated via the following formula:

$$X_c = \frac{\Delta H_{m,sc} + \Delta H_{m,hc}}{f_{sc} * \Delta H_{m,sc}^0 + f_{hc} * \Delta H_{m,hc}^0}$$

The crystallinity and filler content of the composites were further characterized via wide angle X-ray diffraction (WAXD). The spectra were recorded with a Rigaku Smartlab X-ray Diffractometer at room temperature using CuK α radiation at 40 kV and 44 mA. The specimens were scanned in the scanning range of 5°-30° at a scan speed of 3°/min. Spectra were analyzed using GSAS-II [136]. f_{hc} and f_{sc} are the fractional amounts of homocrystallites and stereocomplex crystallites, respectively, developed during processing under non-isothermal conditions; they were calculated using the following equations:

$$f_{sc} = \frac{A_{sc}}{A_{sc} + A_{hc}}$$

$$f_{hc} = 1 - f_{sc} = \frac{A_{hc}}{A_{sc} + A_{hc}}$$

Where A_{sc} and A_{hc} are the integrated area under the respective curves for stereocomplex crystallites and homocrystallites, respectively. The total crystallinity was also calculated using the following equation:

$$X_c = \frac{A_{sc} + A_{hc}}{A_{sc} + A_{hc} + A_{amph}}$$

Where A_{amph} is the integrated area under the curve for the amorphous phase.

The thermal decomposition temperature and percent weight loss were quantified via thermogravimetric analysis (TGA), using a TA Instruments TGA Q50. About 10 mg of sample was heated from 25 to 550°C at 20 °C/min.

The tensile properties of PLA/stereocomplex PLA composites have been analyzed and compared with reprocessed neat PLA. Neat PLA (3100HP, 4060D) was first processed in a Leistritz co-rotating twin-screw extruder type ZSE 27 HP-PH (L/D = 40 and screw diameter = 27 mm) under the same conditions as the composites (See **Figure 3-6**). This was to account for material degradation during processing. Samples were then dried in an oven at 50°C for 48 hours.

Mechanical testing samples were injection molded at 190°C and 75 RPM using a DSM 15CC mini-extruder & 3.5CC mini-injection molder. This temperature was chosen to flow the matrix through the DSM while preventing thermal dissociation of the stereocomplex filler. Samples were then annealed in an oven at 100 °C for 2 hours. Tensile testing was performed using an Instron model 5565-P6021 as per ASTM D882.

The isothermal crystallization kinetics of the samples were evaluated using a TA Instruments DSC Q20. The crystallization kinetics of 95% 3100HP/5% stereocomplex PLA were compared to neat 3100HP to analyze the effect of stereocomplex PLA as a potential nucleating agent for semi-crystalline PLA. The isothermal crystallization behavior was studied using the following procedure. Samples (~10 mg) were first equilibrated at 0°C, then heated to 190°C at 10°C/min. Temperature was then held constant at 190°C for 5 minutes to remove any thermal and stress history. The samples were then cooled down at four different temperatures (95, 100, 105, 110°C) at a cooling rate of 20°C/min. They were finally set to equilibrate at each of those temperatures

for 50 minutes in order to allow for a sufficient amount of time for the crystallization process to reach completion.

3.3. Results & Discussion

3.3.1 Pilot-Scale Manufacturing of Stereocomplex PLA via Reactive Extrusion

Researchers have conducted many studies on producing stereocomplex PLA using a variety of additives, nucleating agents, rheometers, and/or solvent-based techniques [129], [138]–[141].

Table 3-3 summarizes the results in comparison to our technique. Xie et. al uses a solution casting technique with N,N',N''-tricyclohexyl-1,3,5-benzenetricarboxylamide (BTCA) nucleator for enhanced crystallization kinetics of stereocomplex crystallites; only 60% stereocomplex PLA is achieved, with a melting peak temperature of $\sim 220^{\circ}\text{C}$ [138]. Gupta et. al conducted a similar solution casting method at different compositions (1-3wt%) of modified chitosan (MCH). While $>99.99\%$ stereocomplexation was achieved, it was at the highest additive concentration (3% MCH), the melting peak temperature was very low for stereocomplex - $\sim 206^{\circ}\text{C}$, and the crystallinity was also low - $\sim 35\%$ according to DSC [141]. Su et. al presents a solventless technique, with no additives, via micro-extrusion in a rheometer to produce stereocomplex PLA from high molecular weight PLLA and PDLA; $>99.99\%$ stereocomplexation occurred, with a melting peak temperature of $\sim 230^{\circ}\text{C}$ and a crystallinity of $\sim 44\%$ [129]. Korber et. al tries to scale up this process in a pilot-scale co-rotating twin screw extruder. Without additives/nucleators, only $\sim 25\%$ stereocomplex formation occurred, with a stereocomplex melting peak temperature of $\sim 220^{\circ}\text{C}$. Only the use of two additives (aluminum complex with phosphoric ester NA-21 and NA-21 + talc) resulted in $>99.99\%$ stereocomplex formation, but the melting peak temperature was still $\sim 220^{\circ}\text{C}$ and crystallinity $\sim 40\%$ [140]. It is clear that no scalable, solventless, additive-free technique to produce exclusive stereocomplex PLA has been reported in journal articles.

Table 3-3. Recent studies on stereocomplex PLA

Group	Method	f_{sc} (%)	$T_{pm,sc}$ (°C)	X_{sc} (%)
Xie [138]	Solution casting with BTCA	60	220	23
Gupta [141]	Solution casting with MCH	100	206	35
Su [129]	Rheometer (190-220°C)	100	230	44
Korber [140]	Co-rotating twin screw extrusion (180-240°C)	25	220	10
BMRG	Co-rotating twin screw extrusion (180-220°C)	95	240	58

* f_{sc} represents the fraction of stereocomplex PLA crystallites, $T_{m,sc}$ is the melting temperature of the stereocomplex, and X_{sc} is the crystallinity of the stereocomplex.

The Biobased Materials Research Group (BMRG) has developed a pilot-scale continuous manufacturing process via twin-screw extrusion to produce >95% stereocomplex PLA with a melting temperature of ~240°C, the highest ever reported; no additives, nucleators or reagents are used, aside from high molecular weight neat PLLA and PDLA. At the proper temperature window, high stereocomplex formation can be achieved as the twin-screw extruder allows for alignment of the chains; this is due to stretching of the polymer chains in the extruder. **Figure 3-7** depicts the formation of stereocomplex PLA in an extruder using a structural sketch of the polymer chains. In the next sections, we will delve further into the results of this process.

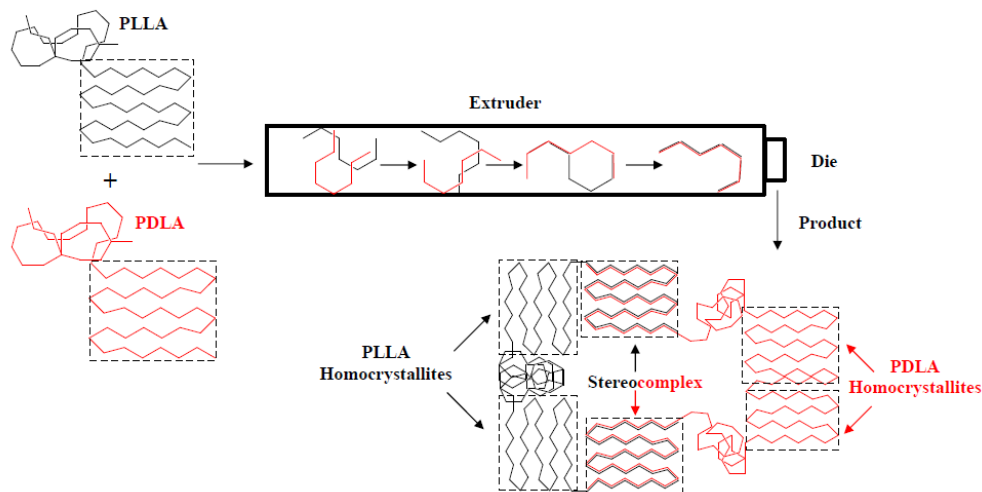


Figure 3-7. Schematic representation depicting the competitive formation of stereocomplex crystallites during extrusion of PLLA and PDLA

3.3.1.1 Characteristics of Stereocomplex Formation

In order to optimize processing conditions for stereocomplexation, DSC was run at different times and temperatures for samples comprising 50% stereocomplex PLA crystallites/50% PLA homocrystallites. Heat flow vs temperature graphs were plotted at different times; each graph represents the isothermal processing temperature the sample is held at during the run. Results are shown in **Figure 3-8**.

At 180°C (**Figure 3-8a**), ~60% stereocomplex PLA results regardless of the processing time. This is equivalent to the melting temperature of PLA homopolymer. Considering the original sample comprises 50% stereocomplex crystallites, data shows that 10% stereocomplexation will occur at PLA's melting temperature.

When the sample is held isothermally at 190°C (**Figure 3-8b**), ~70% stereocomplex PLA is calculated, resulting in 20% stereocomplex formation compared to the original sample. Processing time did not make any significant changes in this condition either.

Figure 3-8c displays the isothermal processing temperature at 200°C. Compared to the previous two runs at 180 and 190°C, the fractional stereocomplex crystallites herein was calculated to be ~90%. This is equivalent to 40% stereocomplexation occurring at this processing temperature, which is 2x the amount formed at 190°C and 4x the amount formed at 180°C.

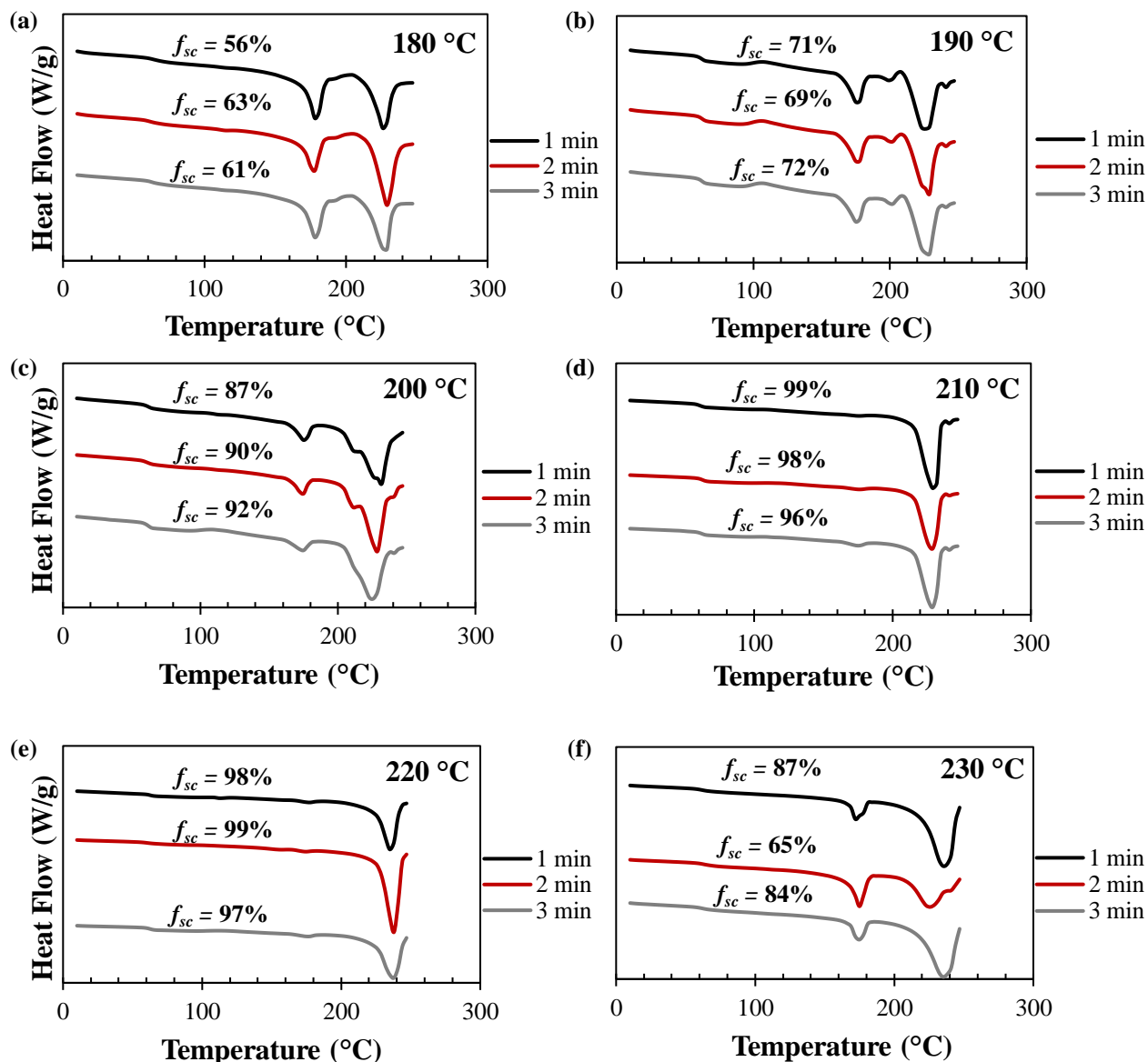


Figure 3-8. DSC thermograms displaying stereocomplex formation after sample is held isothermally for 1-3 minutes at temperatures of (a) 180°C (b) 190°C (c) 200°C (d) 210°C (e) 220°C (f) 230°C

Figures 3-8d and **e** represent 210 and 220°C isothermal processing temperatures, respectively. It is concluded that once the sample is heated to 210°C, almost 100% stereocomplex PLA is formed. However, increasing the temperature further to 230°C (**Figure 3-8f**) results in a decrease in stereocomplex crystallites compared to **Figures 3-8d** and **e**. This phenomenon is due to thermal dissociation, in which the freedom of motion in the PLLA and PDLA chains of stereocomplex

PLA increases. At 230°C, the stereocomplex PLA sample is in the melt state, resulting in an increase in molecular motion of the polymer chains, and thus an increase in entropy.

We conclude that stereocomplexation is a temperature driven process, and that time has minimal impact on the process. The phenomenon is almost instantaneous at temperatures above PLA's melting point. **Figure 3-9a** summarizes the isothermal stereocomplexation kinetics of the samples discussed. Results further confirm that stereocomplex PLA strongly depends on the processing temperature of PLLA/PDLA pre-mixtures, and that time does not play a role.

Figure 3-9b displays the effect of temperature on stereocomplex formation at 2 minutes; similar results were seen at 1 and 3 minutes. There is a linear relationship between temperature and stereocomplex formation until 210°C, where the curve flattens since ~99% stereocomplexation occurs. This leads us to further conclude that processing temperatures at 210-220°C will lead to the highest conversion of stereocomplex PLA, while preventing thermal dissociation of the sample.

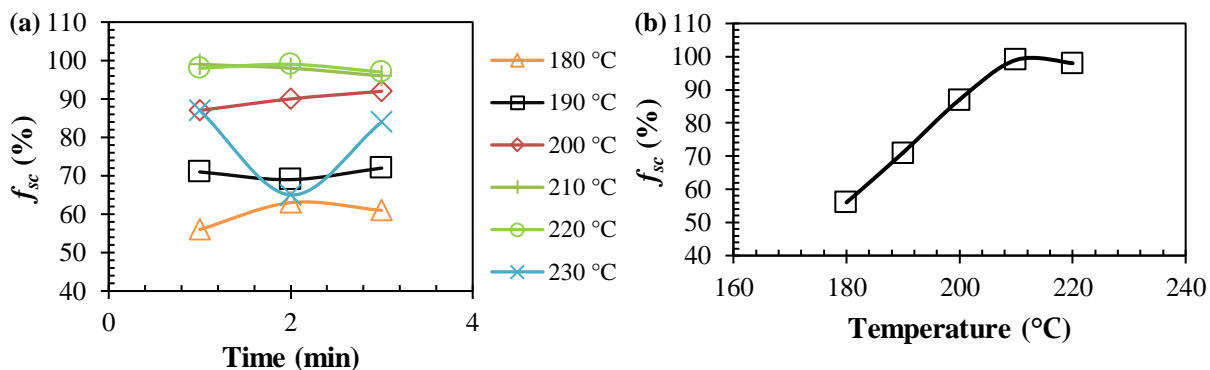


Figure 3-9. (a) Isothermal stereocomplexation (b) Effect of temperature on stereocomplex formation

3.3.1.2 Confirmation of Stereocomplex Formation via FTIR

Stereocomplexation was confirmed via ATR-FTIR in comparison to neat PLLA. **Figure 3-10a** shows the ATR-FTIR spectrum of the PLA stereocomplex compared with the spectrum of the

PLLA enantiomer. Regions of wavelength which involved characteristic changes were observed at $970\text{--}850\text{ cm}^{-1}$. These changes in conformational PLA chains represent skeletal stretching vibration of α and β helices. **Figure 3-10b** clearly depicts the α helix of the PLLA chain transformed to a more compact β helix in the stereocomplex PLA. Specifically, the absorption band at 908 cm^{-1} represents the presence of stereocomplexation. The formation of stereocomplex crystallites was the ultimate result of the stereoselective interaction between opposite enantiomeric PLA chains. It has been suggested that van der Waals forces between the carbonyl oxygen and the methyl hydrogen occur during stereocomplexation [125]. However, the establishment of hydrogen bonding between the carbonyl oxygen of one PLA compound and the methyl hydrogen of its respective enantiomeric PLA compound is responsible for the stereocomplex formation, due to presence of opposite helical structure in PLLA and PDLA. Moreover, the structural adjustment of the CH_3 group occurs prior to that of the $\text{C}\text{--}\text{O}\text{--}\text{C}$ backbone during the stereocomplexation process [126], [142]. The FTIR spectra were the same regardless of sample collection time (5, 10, 20, 40 minutes).

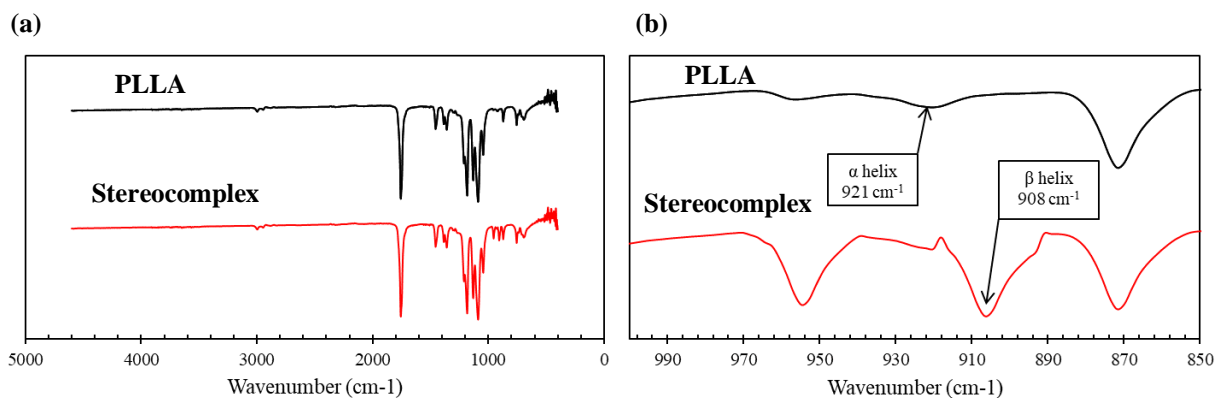


Figure 3-10. (a) FTIR spectra of PLLA (black line) and stereocomplex PLA (red line) (b) FTIR spectra displaying characteristic absorption bands. Spectra displayed involves stereocomplex PLA collection time at 20 minutes

3.3.1.3 Crystal Structure Characterization via WAXD

The crystal structure, total crystallinity and stereocomplex formation were analyzed and compared between neat PLLA and the produced stereocomplex PLA sample using wide angle X-ray diffraction (WAXD). **Figure 3-11a** displays peaks at 2θ values of 15, 17, and 19°, which represent the α form of PLLA crystallized in a pseudo-orthorhombic unit cell with dimensions: $a = 1.07$ nm, $b = 0.595$ nm, and $c = 2.78$ nm; the cell is composed of two 10_3 polymeric helices [143]–[146]. The crystallinity for the PLLA sample was estimated to be ~45%. For stereocomplex PLA (**Figure 3-10b**), the peaks observed occur at 2θ values of 12, 21, and 24°.

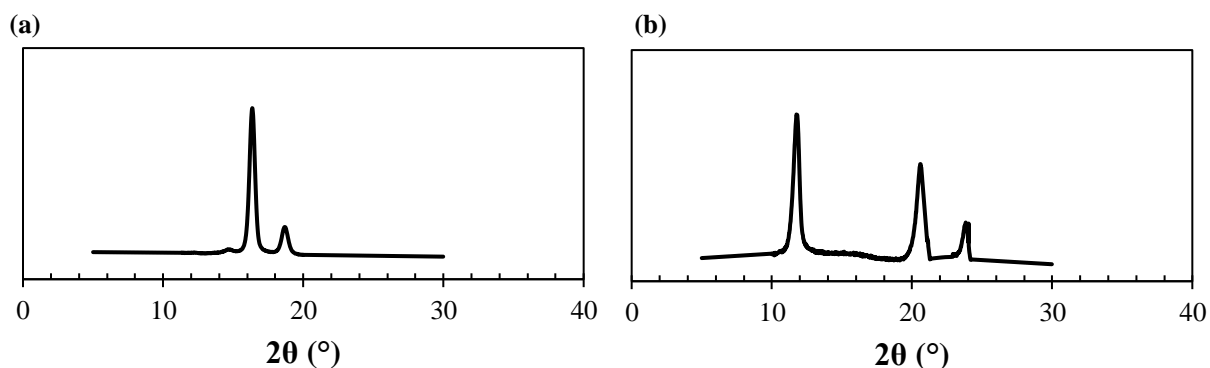


Figure 3-11. WAXD profiles of (a) pure PLLA and (b) Stereocomplex PLA (50/50 L/D)

Similar to previous reports, the spectrum represents stereocomplex PLA crystallized in a triclinic unit cell with dimensions: $a = 0.915$ nm, $b = 0.915$ nm, and $c = 0.868$ nm, $\alpha = 109^\circ$, $\beta = 109^\circ$, and $\gamma = 110^\circ$. Okihara et. al proposed that the PLLA and PDLA chains are packed regularly in a 3_1 helical conformation. As seen in **Figure 3-12**, the lattice comprising PLLA and PDLA chains with a 3_1 helical conformation has the shape of an equilateral triangle, which was proposed by Okihara to form equilateral-triangle-shaped single crystals of the stereocomplex [147], [148].

Compared to the PLLA sample analyzed, the total crystallinity was measured to be ~61%, which is higher than the crystallinity (<50%) of the PLLA and PDLA blended to produce stereocomplex PLA. These results indicate that an increase in crystallinity occurs, possibly due to the parallel

packing of the PLLA and PDLA chains that occurs during stereocomplexation. The regular packing of the enantiomeric PLA chains possessing 3_1 conformational helices represents ordered packing of the chains, which can translate to an increase in crystallinity.

Since the only peaks observed for stereocomplex PLA's WAXD profile were at 2θ values of 12, 21, and 24° , it was concluded that $>99\%$ stereocomplex formation occurred during processing of the PLLA/PDLA blends. This confirms the optimal processing conditions during extrusion required for high conversion of stereocomplex PLA.

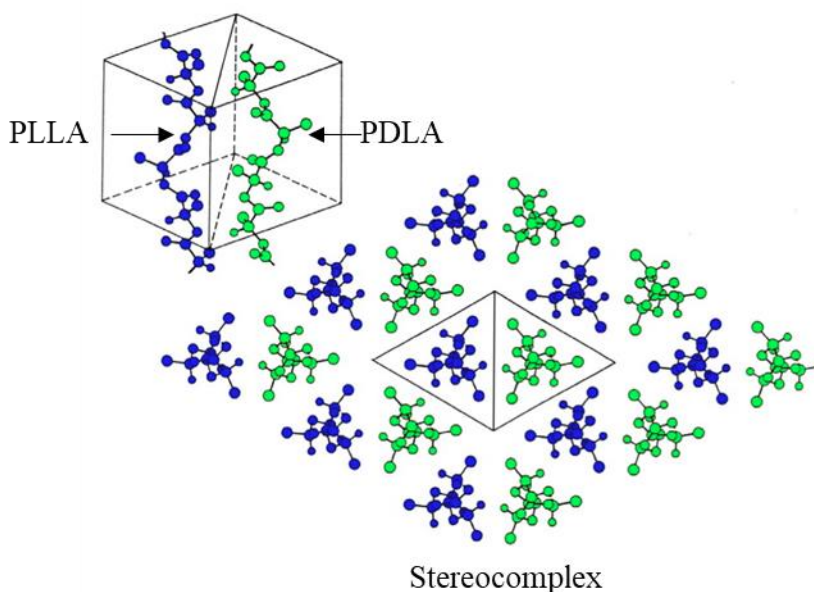


Figure 3-12. Crystal structure of stereocomplex PLA [143]

3.3.1.4 Thermal Characterization via DSC

The total crystallinity and stereocomplex formation of extruded samples were quantified using DSC at various sample collection times. **Figure 3-13** depicts the first DSC thermograms at 5-, 10-, 20-, and 40-minute collection times. No additional PLLA, PDLA, or other materials were fed to the extruder during these collection times; they were based on one batch of PLLA/PDLA pre-mixtures.

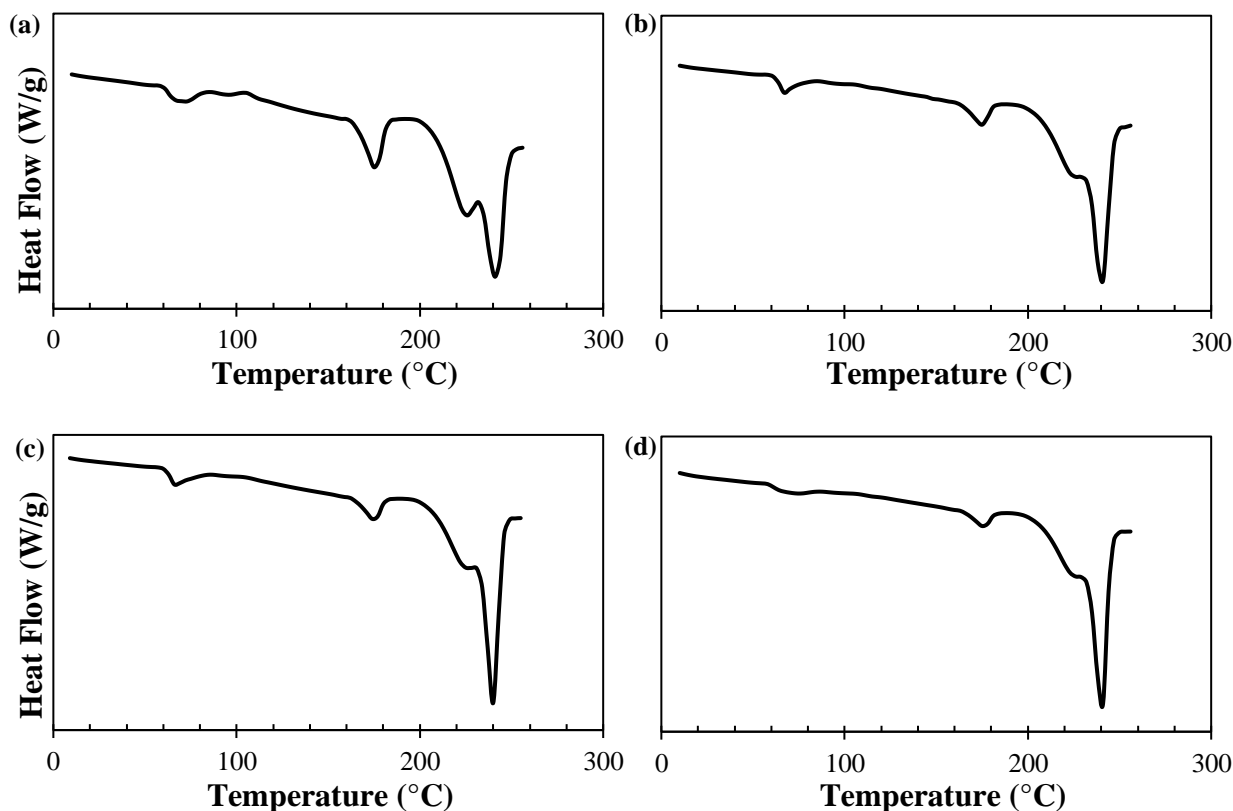


Figure 3-13. DSC thermograms of stereocomplex PLA at sample collection times of (a) 5 minutes (b) 10 minutes (c) 20 minutes (d) 40 minutes

At 5 minutes (**Figure 3-13a**), ~85% PLA stereocomplex crystallites formed, with the remaining 15% composed of PLA homocrystallites. The melting peak temperature of the stereocomplex was found to be ~241°C, while the PLA homopolymer melted at 178°C. Total crystallinity was calculated to be ~64%. A glass transition temperature was also depicted at ~63°C, most likely from the residual PLA homopolymer.

At 10 minutes (**Figure 3-13b**), ~92% PLA stereocomplex crystallites formed, with the remaining 8% composed of PLA homocrystallites. The melting peak temperature of the stereocomplex was found to be ~240°C, while the PLA homopolymer melted at 175°C. Total crystallinity was calculated to be ~61%. A glass transition temperature was also depicted at ~64°C.

20-minute collection time (**Figure 3-13c**) depicts ~93% stereocomplexation, with 7% residual homocrystallites. The melting peak temperature of the stereocomplex was found to be ~240°C,

while the PLA homopolymer melted at 175°C. Total crystallinity was calculated to be ~62%. A glass transition temperature was also depicted at ~65°C.

At 40 minutes (**Figure 3-13d**), ~95% PLA stereocomplex crystallites formed, while 5% were PLA homocrystallites. The melting peak temperature of the stereocomplex was found to be ~240°C, while the PLA homopolymer melted at 175°C. Total crystallinity was calculated to be ~56%. A glass transition temperature was also depicted at ~61°C.

Table 3-4 summarizes the DSC results discussed on stereocomplex PLA. Results show that stereocomplexation was at its lowest at 5-minute collection. This was most likely because there was not enough time for the PLLA/PDLA blend to be dispersed uniformly and stabilize. Over time, however, the blend stabilizes and up to 95% stereocomplex PLA is continuously produced through the extruder. From 10 minutes to 50 minutes, there are no significant differences in the thermal properties and stereocomplex conversion. We confirm that time to reach steady-state and uniform dispersity of stereocomplex PLA via reactive extrusion is at >5-minute collection time.

Table 3-4. DSC results on the thermal properties and crystallinity of stereocomplex PLA at various collection times

Collection Time (min)	f _{sc} (%)	X _c (%)	T _{pm,sc} (°C)	T _{pm,hc} (°C)	T _g (°C)
5	85	64	241	178	63
10	92	61	240	175	64
20	93	62	240	175	65
40	95	56	240	175	61

3.3.1.5 Thermal Degradation of Stereocomplex PLA

The thermal decomposition temperature of stereocomplex PLA was determined and compared to commercial grade poly(L-lactide) – L175. From **Figure 3-14a**, stereocomplex PLA starts to decompose at ~297°C, with a maximum thermal decomposition temperature of T_d ~376°C; a percent weight loss of ~98% is depicted. No significant difference is seen compared to commercial

PLLA, which starts to decompose at $\sim 293^{\circ}\text{C}$ and has a maximum thermal decomposition temperature of $T_d \sim 373^{\circ}\text{C}$; a percent weight loss of $\sim 99\%$ is depicted. This leads us to conclude that while stereocomplexation attributes to an increase in melting temperature, it does not necessarily attribute to improved resistance against thermal decomposition. The main factor affecting thermal degradation is most likely the molecular weight of the polymer. Since the PLLA (L175) analyzed here is the same PLLA polymer used in the production of stereocomplex PLA, the similarities in thermal degradation are understandable, as their molecular weights are assumed to be similar. It is hypothesized herein that the molecular weight of stereocomplex PLA is in fact a 50/50 ratio of the molecular weights of the PLLA and PDLA blended for stereocomplex PLA processing. To date, this has not been confirmed, as no suitable solvent has been found to dissolve stereocomplex PLA for molecular weight characterization (i.e.: GPC); this is attributed to its high crystallinity thickness [121].

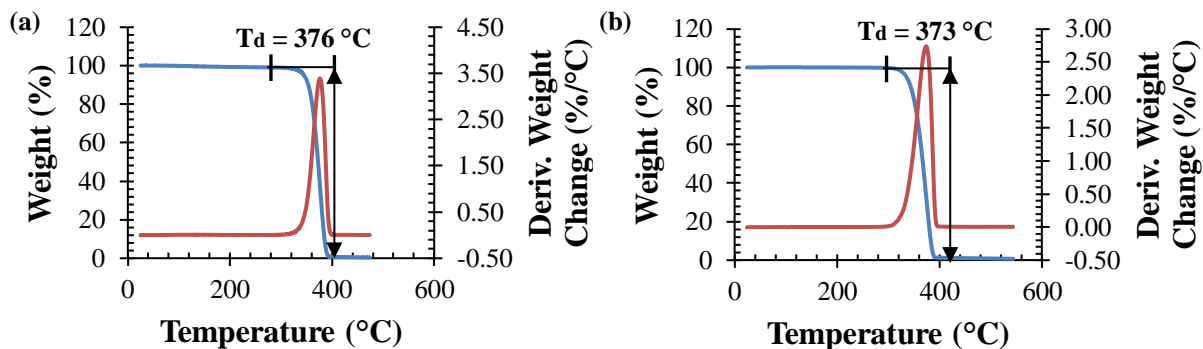


Figure 3-14. Thermal degradation of (a) stereocomplex PLA and (b) PLLA (L175)

3.3.2 Development of Molecular Composites using Stereocomplex PLA Particles in a Thermoplastic PLA Matrix

3.3.2.1 Thermal Characterization of PLA/Stereocomplex PLA Composites

DSC was used to characterize the thermal properties confirm dispersity of the PLA/stereocomplex PLA composites. For all collection times, two melting peaks representing stereocomplex PLA, at

~224°C and ~240°C, were depicted. As a result, accurate calculations of the filler dispersity in the matrix required the summation of two separate integrals for stereocomplex PLA. The formation of two melting peaks is hypothesized to be from blending of unreacted PLLA and PDLA, as there was up to 5% unreacted PLA homopolymer in the stereocomplex PLA filler. There is a chance that the PLA matrix, 3100HP or 4060D, may also blend with unreacted PDLA to form a stereocomplex. During a DSC heating scan, one must consider that the technique involves heating up the material above the melting temperature of stereocomplex PLA. This heating process may contribute to further stereocomplexation, as temperature is the driving factor behind the process, as confirmed in *Section 3.3.1.1*.

Figure 3-15 depicts the DSC thermograms of 70% 3100HP/30% stereocomplex PLA at different sample collection times (5, 10, 20, 40 minutes). At 5 minutes (**Figure 3-15a**), the composite is composed of ~74% semi-crystalline PLA matrix/26% stereocomplex PLA filler. While not significant, the filler composition is lower than the targeted composition (30%). It is assumed that the filler requires additional time to stabilize and disperse uniformly throughout the matrix, and that 5 minutes is too short of processing time to begin sample collection. Three melting peaks are depicted, one at ~179°C – the melting peak temperature of 3100HP – and two at ~224 and 239°C – melting peak temperatures representative of stereocomplex PLA. The total crystallinity was estimated to be ~46%.

At 10-minute collection time (**Figure 3-15b**), composites of ~72% semi-crystalline PLA matrix/28% stereocomplex PLA filler were produced. While these were not the exact targeted compositions, the difference was not significant enough to be of noticeable issue. Three melting peaks are depicted, one at ~178°C – the melting peak temperature of 3100HP – and two at ~224

and 238°C – melting peak temperatures representative of stereocomplex PLA. The total crystallinity was estimated to be ~49%.

20-minute collection time (**Figure 3-15c**) resulted in composites of ~70% semi-crystalline PLA matrix/30% stereocomplex PLA filler – the targeted compositions. Three melting peaks are depicted, one at ~177°C – the melting peak temperature of 3100HP – and two at ~225 and 239°C – melting peak temperatures representative of stereocomplex PLA. The total crystallinity was estimated to be ~48%.

At 40-minute collection time (**Figure 3-15d**), composites of ~70% semi-crystalline PLA matrix/30% stereocomplex PLA filler were produced – the targeted compositions. Three melting peaks are depicted, one at ~178°C – the melting peak temperature of 3100HP – and two at ~224 and 238°C – melting peak temperatures representative of stereocomplex PLA. The total crystallinity was estimated to be ~52%.

No significant differences between the melting peak temperatures of the composites were seen between collection times. However, a steady increase in the filler composition was seen, as time increased from 5 minutes to 40 minutes, until the filler composition leveled off at 30% during 20-minute collection time. This leads us to conclude that steady state processing times >10 minutes result in the stabilized processing and uniform dispersion of the composites. This gradual increase also correlates with the increase in crystallinity, from 46% to 52%, as time increased from 5 to 40 minutes. This increase may be attributed to the additional time allowed for the matrix and filler to blend and stabilize, as well as more time to cool. This increases crystallization of the PLA homopolymer chains. We confirm uniform dispersity of the 70% 3100HP/30% stereocomplex PLA composites via extrusion in a co-rotating twin screw extruder.

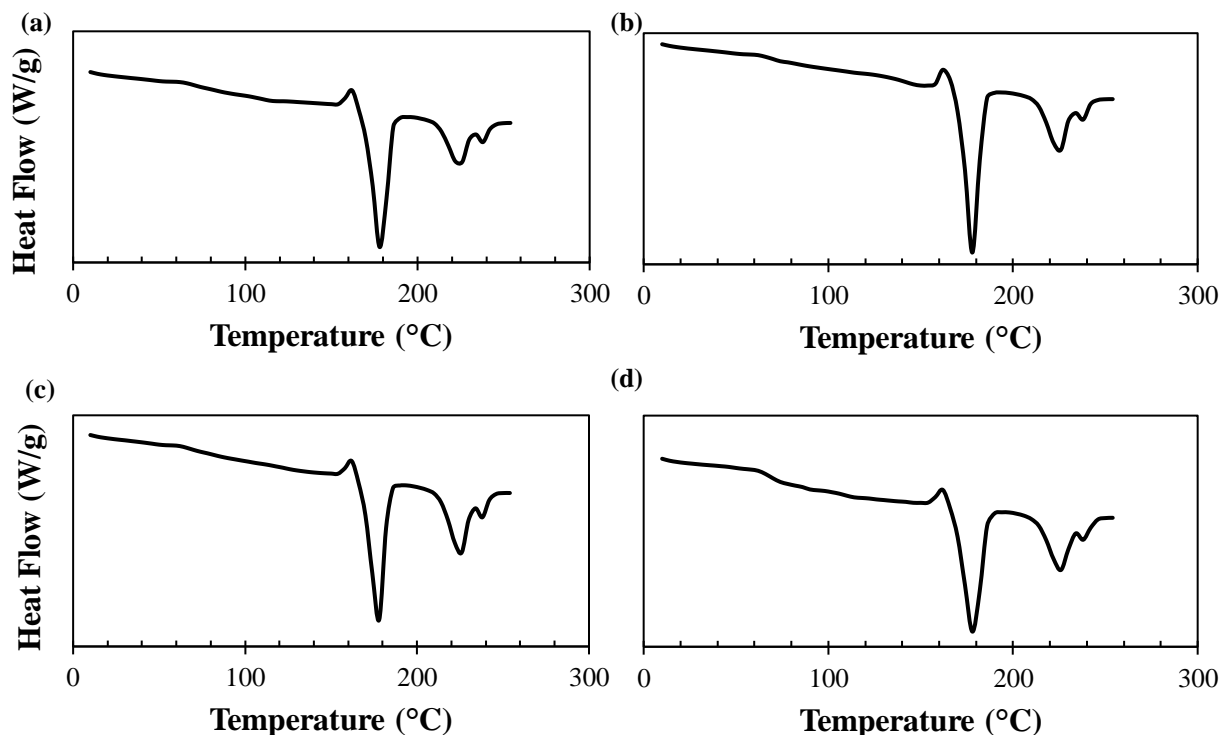


Figure 3-15. DSC thermograms of 70% 3100HP/30% stereocomplex PLA at sample collection times of (a) 5 minutes (b) 10 minutes (c) 20 minutes (d) 40 minutes

In the case of 70% 4060D/30% stereocomplex PLA composites, exact calculations of the filler and matrix compositions cannot be made, as 4060D is an amorphous polymer and does not depict a melting point. However, one can analyze dispersity by comparing the original crystallinity of the stereocomplex PLA (~56%) to the crystallinity of the filler, which should be ~30% of the original crystallinity - ~17%. One may assume that if the melting enthalpy of the stereocomplex PLA filler is ~17%, the composition should be about 70% matrix and 30% filler. **Figure 3-16** depicts the DSC thermograms of 70% 4060D/30% stereocomplex PLA at different sample collection times (5, 10, 20, 40 minutes). At 5 minutes (**Figure 3-16a**), a glass transition temperature is depicted at ~60°C. The total melting enthalpy of the stereocomplex PLA filler is ~22 J/g, which is below average compared to the filler content in the composites analyzed in **Figure 3-15**. This corresponds to ~16% crystallinity. If we compare the behavior of this sample to **Figure 3-15a**, we conclude

that the low filler content corresponds to the processing time required for the filler to stabilize and disperse uniformly throughout the matrix; 5 minutes is too short of processing time to begin sample collection.

10-minute collection time (**Figure 3-16b**) shows a glass transition temperature at $\sim 60^{\circ}\text{C}$. The total melting enthalpy of the stereocomplex PLA filler is ~ 24 J/g, which falls in the accepted range for $\sim 30\%$ filler content. This also corresponds to $\sim 17\%$ crystallinity from the stereocomplex crystallites.

20-minute collection time (**Figure 3-16c**) resulted in a glass transition temperature at $\sim 60^{\circ}\text{C}$ and a melting enthalpy of ~ 28 J/g for the stereocomplex PLA filler. This also falls in the acceptable range for $\sim 30\%$ filler content. $\sim 20\%$ crystallinity was calculated in this case.

40-minute collection time (**Figure 3-16d**) resulted in a glass transition temperature at $\sim 60^{\circ}\text{C}$ and a melting enthalpy of ~ 26 J/g for the stereocomplex PLA filler. This also falls in the acceptable range for $\sim 30\%$ filler content. $\sim 18\%$ crystallinity was calculated in this case.

Based on these results, we confirm that time to reach steady state is >5 minutes for uniform dispersity of stereocomplex filler content in amorphous grade PLA matrix. There does not seem to be a correlation between crystallinity or glass transition and sample collection time, which suggests stable processing and blending occurring throughout the extrusion process. There is a chance that a minor amount of unreacted PDLA from the stereocomplex PLA filler may have blended with the PLA matrix, which could affect material properties. However, the effect is most likely minimal, as there is a very small amount of unreacted PLLA/PDLA ($\sim 5\%$) in the stereocomplex PLA filler, which is only 30% in mass in the composites. This means that only $\sim 1.5\%$ unreacted PLLA/PDLA blend is in the composites, resulting in minimal discrepancy in the material properties.

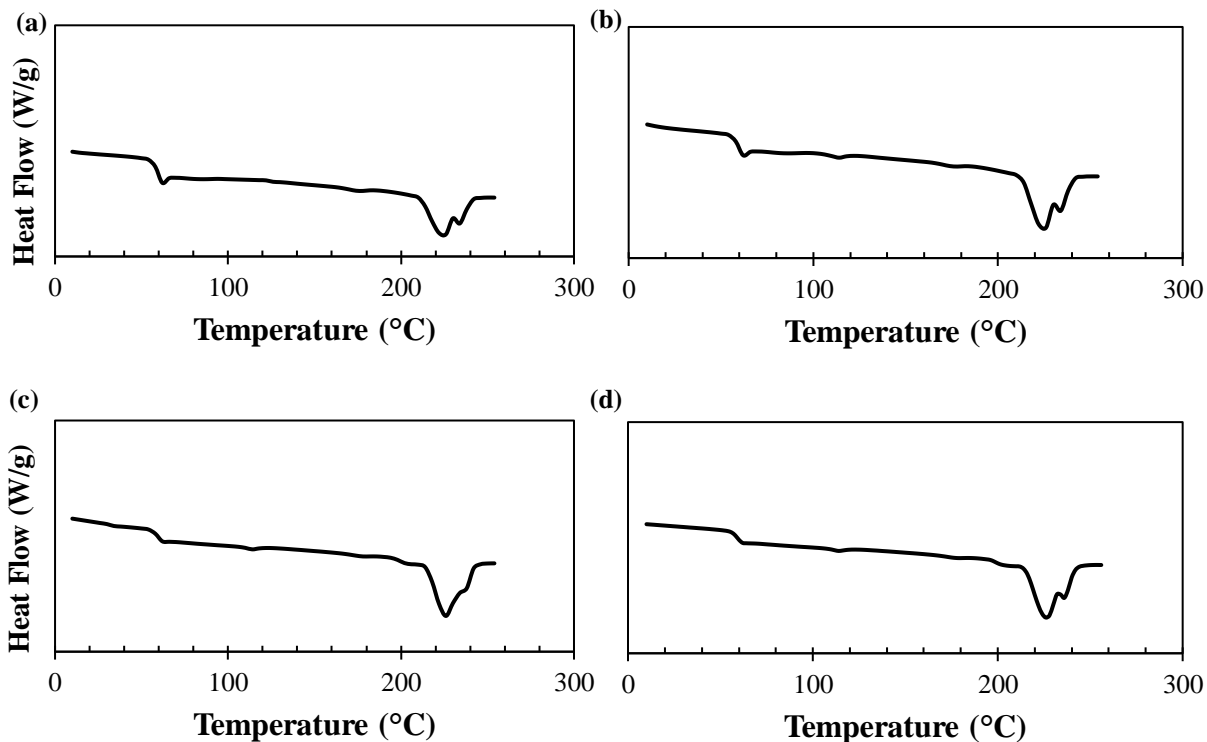


Figure 3-16. DSC thermograms of 70% 4060D/30% stereocomplex PLA at sample collection times of **(a)** 5 minutes **(b)** 10 minutes **(c)** 20 minutes **(d)** 40 minutes

In the case of the 95% 3100HP/5% stereocomplex PLA composites, DSC was not a reliable technique to detect the concentrations of filler in the polymer matrix. As seen in **Figure 3-17**, only a melting peak at 179°C, corresponding to 62% semi-crystalline PLA (3100HP) is seen. 5% is under the detectable limit for enthalpy calculations. As a result, WAXD was used as an alternative.

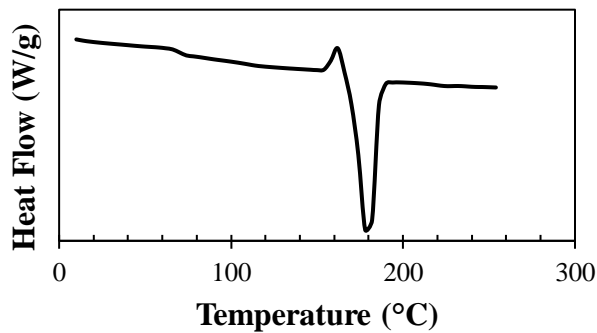


Figure 3-17. DSC thermogram of 95% 3100HP/5% stereocomplex PLA

3.3.2.2 WAXD of PLA/Stereocomplex PLA Composites

WAXD was used to further characterize the crystallinity and filler content of the PLA/Stereocomplex PLA composites. PLA homocrystallites were depicted based on the intensity peaks at 2θ values of 15, 17, and 19°, whereas stereocomplex PLA crystallites were represented based on the intensity peaks at 2θ values of 12, 21, and 24°. **Figure 3-18** displays the WAXD profiles of the three composites produced: **(a)** 70% 3100HP/30% stereocomplex PLA **(b)** 70% 4060D/30% stereocomplex PLA **(c)** 95% 3100HP/5% Stereocomplex PLA.

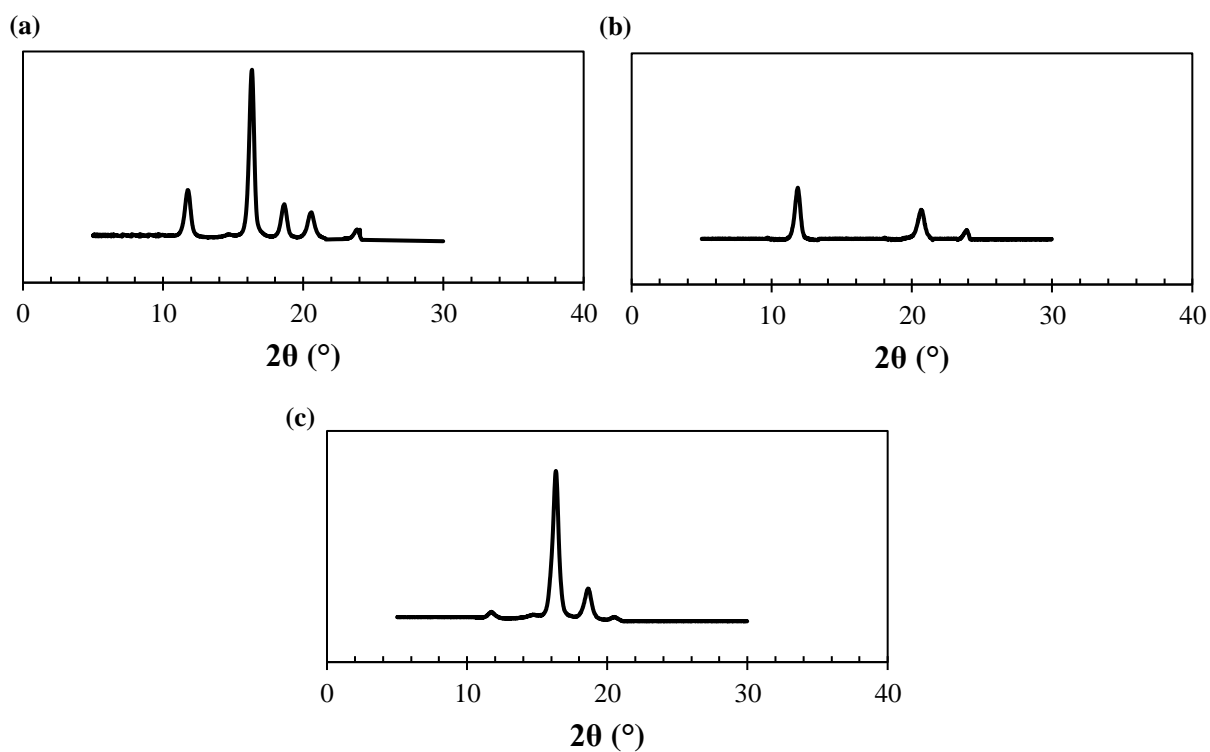


Figure 3-18. WAXD profiles of **(a)** 70% 3100HP/30% Stereocomplex PLA **(b)** 70% 4060D/30% Stereocomplex PLA **(c)** 95% 3100HP/5% Stereocomplex PLA

As seen in **Figure 3-18a**, there are peaks at 2θ values of 15, 17, and 19°, representing PLA homopolymer matrix, as well as peaks at 2θ values of 12, 21, and 24°, representing stereocomplex PLA filler. Integrating the area under the curves results in a total crystallinity of ~50% and ~31% stereocomplex PLA filler content, similar to the DSC results in **Figure 3-15**.

In **Figure 3-18b**, only peaks at 2θ values of 12, 21, and 24° depicting stereocomplex PLA are shown. This is because the PLA matrix, 4060D, is completely amorphous with 0% crystallinity. The peak intensities of stereocomplex PLA, however, do match with **Figure 3-18a**, confirming ~10% crystallinity and 30% stereocomplex PLA content in the composite.

Figure 3-18c depicts intensity peaks at 2θ values of 17 and 19° with a minor peak at 15° , representing 3100HP. Intensity peaks at 2θ values of 12 and 21° are also shown depicting stereocomplex PLA crystallites. There is no peak at 24° , most likely due to the low filler content (~5%) in the composite. Integrating the area under the curves results in a total crystallinity of ~48% and ~6% stereocomplex PLA filler.

For all samples, similar results were seen at different collection times, verifying dispersity of the filler in the matrix. WAXD further confirms the stereocomplex PLA filler content and dispersity in PLA homopolymer matrix.

3.3.2.3 Tensile Properties of PLA/Stereocomplex PLA Composites

Tensile testing was conducted on the PLA/Stereocomplex PLA composites to analyze the effect of stereocomplex PLA filler on the mechanical properties of the PLA homopolymer matrix. Previous studies have reported an improvement in the tensile properties, particularly the elastic modulus and ultimate tensile strength, of stereocomplex PLA compared to its PLA homopolymer counterpart [129], [140], [149]. Theoretically, there should be an increase in the mechanical properties of PLA homopolymer matrix if the stereocomplex PLA is used as a filler. As seen in **Figure 3-19**, three grades of composites were tested: (1) 70% 3100HP/30% Stereocomplex PLA (2) 70% 4060D/30% Stereocomplex PLA (3) 95% 3100HP/5% Stereocomplex PLA. Results were analyzed and compared with neat PLA reprocessed under the same conditions as the composites.

Data was taken for 5 samples of each composite and neat polymer. **Figure 3-19** displays the samples closest to the average data on the mechanical properties.

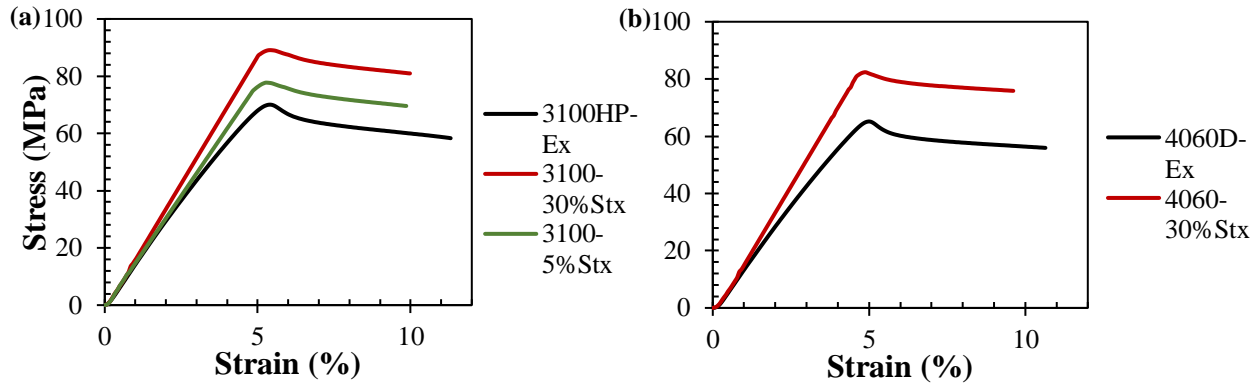


Figure 3-19. Tensile stress strain curves of reprocessed neat PLA vs PLA/Stereocomplex PLA composites (a) Extruded 3100HP, 70% 3100HP/30% Stereocomplex PLA, 95% 3100HP/5% Stereocomplex PLA (b) Extruded 4060D, 70% 4060D/30% Stereocomplex PLA

Figure 3-19a displays the stress strain curves for reprocessed neat 3100HP (3100HP-Ex) against its composite counterparts - 70% 3100HP/30% Stereocomplex PLA (3100-30%Stx) and 95% 3100HP/5% Stereocomplex PLA (3100-5%Stx). **Figure 3-19b** depicts the stress strain curves for reprocessed neat 4060D (4060D-Ex) against 70% 3100HP/30% Stereocomplex PLA (3100-30%Stx). For 3100HP-Ex, the average tensile stress at break (σ_{break}) was found to be about 58.3 ± 2.3 MPa, with a corresponding tensile strain at break (ϵ_{break}) of $11.3 \pm 0.72\%$. 3100-30%Stx experienced a tensile stress at break at about 81.0 ± 2.2 MPa, with a corresponding tensile strain at break of about $10.0 \pm 0.52\%$. For 3100-5%Stx, the average tensile stress at break was found to be about 69.6 ± 1.8 MPa, with a corresponding tensile strain at break of $9.8 \pm 0.41\%$. A noticeable increase ($\sim 38\%$) in the tensile stress at break is observed when adding 30% stereocomplex filler compared to neat 3100HP, whereas a 19% increase is seen when adding 5% stereocomplex filler. A slight decrease in tensile strain at break was observed for both composites. 4060D-Ex depicts a tensile stress at break at about 55.9 ± 1.9 MPa, with a corresponding tensile strain at break of about $10.6 \pm 0.78\%$. In comparison, 4060-30%Stx's tensile stress at break was about 35% higher (75.8

± 2.6 MPa) than its neat PLA counterpart, but its tensile strain at break was slightly lower – $9.6 \pm 0.43\%$.

The yield strength (σ_y) was measured at 0.2% offset, which is defined as the amount of stress that will result in a plastic strain of 0.2%. This is the yield strength that is commonly quoted by raw material suppliers and process engineers [115]. Using this method, the yield strength was estimated to be $\sigma_y = 68.3 \pm 2.3$ MPa for 3100HP-Ex, $\sigma_y = 77.0 \pm 3.1$ MPa for 3100-5%Stx, $\sigma_y = 88.3 \pm 2.0$ MPa for 3100-30%Stx, $\sigma_y = 60.7 \pm 2.6$ MPa for 4060D-Ex, and $\sigma_y = 81.5 \pm 1.7$ MPa for 4060-30%Stx. The ultimate tensile strength (σ_{ult}) was estimated to be the maximum stress applied to each PLA sample. As a result, the ultimate tensile strength was measured to be $\sigma_{ult} = 70.0 \pm 1.7$ MPa for 3100HP-Ex, $\sigma_{ult} = 77.7 \pm 2.8$ MPa for 3100-5%Stx, $\sigma_{ult} = 89.1 \pm 3.3$ MPa for 3100-30%Stx, $\sigma_{ult} = 65.7 \pm 2.2$ MPa for 4060D-Ex, and $\sigma_{ult} = 82.3 \pm 2.7$ MPa for 4060-30%Stx. A noticeable increase in the yield strength and the ultimate tensile strength is observed in the composites compared to their neat PLA counterparts.

The elastic modulus ($E_{elastic}$) was calculated as the slope of the linear portion of the stress strain curves for each sample. The elastic modulus was averaged out to be about $E_{elastic} = 1.4 \pm 0.063$ GPa for 3100HP-Ex, $E_{elastic} = 1.6 \pm 0.071$ GPa for 3100-5%Stx, $E_{elastic} = 1.8 \pm 0.084$ GPa for 3100-30%Stx, $E_{elastic} = 1.4 \pm 0.095$ GPa for 4060D-Ex, and $E_{elastic} = 1.8 \pm 0.085$ GPa for 4060-30%Stx. A similar trend is seen between semi-crystalline (3100HP) and amorphous grade (4060D) PLA, in that the moduli increase by about 28% when adding stereocomplex PLA filler. This means that the PLA composites are stiffer compared to their neat PLA counterparts.

Up to the elastic limit, the strain in the material is elastic and will be recovered when the load is removed so that the material returns to its original length. If the material is loaded beyond the elastic limit, permanent deformation occurs within the material, which is also referred to as plastic

strain. The ductility herein is defined as the plastic strain to failure (ϵ_p) and is calculated by the following formula:

$$\epsilon_p = \epsilon_T - \epsilon_e$$

Where ϵ_T is the total strain and ϵ_e is the elastic strain [116].

Thus, the plastic strain to failure was calculated to be $\epsilon_p = 7.18\%$ for 3100HP-Ex, $\epsilon_p = 5.41\%$ for 3100-5%Stx, $\epsilon_p = 5.40\%$ for 3100-30%Stx, $\epsilon_p = 6.74\%$ for 4060D-Ex, and $\epsilon_p = 5.44\%$ for 4060-30%Stx. Similar to the tensile strain at break, there is a slight decrease in the ductility observed in the composites compared to the neat PLA samples.

In order to find how much energy a material can absorb and plastically deform without fracturing, the toughness (U_T) was calculated using the composite Simpson's rule to integrate the area under the stress strain curves. The interval of integration (a,b) is first broken up into a number of small sub-intervals n , then Simpson's rule is applied to each sub-interval; the results are then summed up to produce an approximation for the integral over the entire interval. Simpson's rule is given by:

$$\int_a^b f(x)dx = \frac{h}{3} [f(x_0) + 2 \sum_{j=1}^{n/2-1} f(x_{2j}) + 4 \sum_{j=1}^{n/2} f(x_{2j-1}) + f(x_n)]$$

Where $x_j = a + j \cdot h$ for $j = 0-n$, and $h = (b-a)/n$; $x_0 = a$ and $x_n = b$ [117].

Using this technique, the toughness was calculated to be $U_T = 5924.36 \text{ J/m}^3$ for 3100HP-Ex, $U_T = 5505.11 \text{ J/m}^3$ for 3100-5%Stx, $U_T = 6387.22 \text{ J/m}^3$ for 3100-30%Stx, $U_T = 5228.42 \text{ J/m}^3$ for 4060D-Ex, and $U_T = 5761.15 \text{ J/m}^3$ for 4060-30%Stx. 3052D clearly has a higher toughness compared to the other two PLA grades. While there is about a 7% decrease in toughness when adding 5% filler in 3100HP, about an 8% increase in toughness is observed when adding 30% filler. A 10% increase in toughness is observed for amorphous grade PLA 4060D after addition of 30% stereocomplex

PLA filler. The highest amount of toughness is expected in 3100-30%Stx, as this material possesses the highest level of crystallinity compared to the other materials.

Contrary to the toughness, the modulus of resilience (U_R) was calculated to measure the amount of strain energy per unit volume that a material can absorb without permanent deformation. The modulus of resilience is typically calculated as the area under the stress-strain curve up to the elastic strain. However, since the elastic limit and the yield point are typically very close, U_R can be approximated as the area under the stress-strain curve up to the yield strength [118]. This is represented by the following formula:

$$U_R = \frac{\sigma_y^2}{2E_{elastic}}$$

The modulus of resilience was estimated to be $U_R = 33$ MPa for 3100HP-Ex, $U_R = 3.71$ MPa for 3100-5%Stx, $U_R = 4.33$ MPa for 3100-30%Stx, $U_R = 2.63$ MPa for 4060D-Ex, and $U_R = 3.69$ MPa for 4060D. There is a gradual increase in the resilience as more stereocomplex PLA is added to the 3100HP PLA matrix. A drastic increase in resilience is also seen when adding 30% stereocomplex PLA filler in amorphous grade 4060D PLA matrix.

The mechanical properties discussed are summarized in **Table 3-5** below. It is clearly shown that stereocomplex PLA reinforces the tensile properties of PLA, particularly the yield strength, ultimate tensile strength, elastic modulus, and resilience. This may be due to the increase in crystallinity from stereocomplex PLA, which possesses strong hydrogen bonds that result in superior mechanical properties in comparison to its PLA homopolymers [129]. This increase in order in the polymer chains leads to an increase in stiffness and other tensile properties, reinforcing the matrix polymer due to rule of mixtures.

Table 3-5. Mechanical properties of extruded neat PLA vs their composite counterparts

Sample	σ_{break} (MPa)	ϵ_{break} (%)	σ_y (MPa)	σ_{ult} (MPa)	$E_{elastic}$ (GPa)	ϵ_p (%)	U_T (J/m³)	U_R (MPa)
3100HP-Ex	58.3 ± 2.3	11.3 ± 0.7	68.3 ± 2.3	70.0 ± 1.7	1.4 ± 0.063	7.18	5924.36	3.33
3100-5%Stx	69.6 ± 1.8	9.8 ± 0.4	77.0 ± 3.1	77.7 ± 2.8	1.6 ± 0.071	5.41	5505.11	3.71
3100-30%Stx	81.0 ± 2.2	10.0 ± 0.5	88.3 ± 2.0	89.1 ± 3.3	1.8 ± 0.084	5.40	6387.22	4.33
4060D-Ex	55.9 ± 1.9	10.6 ± 0.8	60.7 ± 2.6	65.7 ± 2.2	1.4 ± 0.095	6.74	5228.42	2.63
4060-30%Stx	75.8 ± 2.6	10.6 ± 0.4	81.5 ± 1.7	82.3 ± 2.7	1.8 ± 0.085	5.44	5761.15	3.69

Mechanical testing could not be conducted on stereocomplex PLA, as thermal dissociation occurs during processing (i.e.: injection molding) for tensile bar samples; this would lead to discrepancies in results. Using the rule of mixtures (ROM), we can theoretically predict the mechanical properties of the stereocomplex PLA filler. Since this is a particle reinforced composite, tensile properties such as the elastic modulus fall between upper and lower values as per the volume fraction. In the case of the discussed molecular composites, the stereocomplex PLA particles are assumed to be evenly distributed throughout the PLA homopolymer matrix. In order to theoretically predict the upper bound-elastic modulus for stereocomplex PLA, this can be represented by the following equation,

$$E_{c,upper} = f_{sc}E_{sc} + (1 - f_{sc})E_{PLA}$$

where $E_{c,upper}$ is the elastic modulus of the composite, f_{sc} is the fraction of stereocomplex PLA filler, E_{sc} is the elastic modulus of the stereocomplex PLA filler, and E_{PLA} is the elastic modulus of the PLA homopolymer [150]. To calculate the lower bound of the elastic modulus, the following equation is used:

$$E_{c,lower} = \frac{E_{sc}E_{PLA}}{f_{sc}E_{sc} + (1 - f_{sc})E_{PLA}}$$

Although the prediction of the composite's elastic modulus in the axial direction is accurate, there is a discrepancy between experimental and theoretical (ROM) results when determining ultimate tensile strength. This is because the spread of the particles can be non-homogeneous [151]. We apply the same equations for the elastic modulus to calculate the upper and lower bounds of the ultimate tensile strength of stereocomplex PLA. **Table 3-6** lists the elastic modulus and ultimate tensile strength of stereocomplex PLA predicted via ROM.

Table 3-6. Tensile properties (upper/lower bounds) of stereocomplex PLA based on ROM

<u>Sample</u>	$\sigma_{ult,lower}$ (MPa)	$\sigma_{ult,upper}$ (MPa)	E_{lower} (GPa)	E_{upper} (GPa)
Stereocomplex	133.67	100.83	2.05	2.73

3.3.2.4 Effect of Stereocomplex PLA on the Isothermal Crystallization Kinetics of PLA

A hypothesis has been proposed in that the stereocomplex PLA particles act as nucleating sites for PLA homopolymer matrix, resulting in a much faster crystallization rate and potentially cause the growth of spherulites. These spherulites would act as stress concentrators in the PLA matrix and may account for improved mechanical properties in the bulk material. This hypothesis was tested by monitoring the isothermal crystallization kinetics of the neat PLA and its respective composite (PLA+5% Stx) via Avrami analysis. An Avrami exponent (n) value of ~3 would typically imply spherulitic growth [152], [153]. The isothermal crystallization isotherms of 3100HP (neat PLA) and PLA+5% Stx were obtained by cooling the molten polymer to the various crystallization temperatures (T_c) (**Figure 3-20**). The time for full crystallization was found to be lowest at 105°C and 100°C for neat PLA and its composite, respectively. Fractional crystallinity X_t versus time t defines the ratio of the area of the endotherm until t divided by the total area of the endotherm:

$$X_t = \frac{X_c(t)}{X_c(t_\infty)} = \frac{\int_0^t \frac{dH_c(t)}{dt} dt}{\int_0^\infty \frac{dH_c(t)}{dt} dt}$$

Where H_c is the heat flow at time t , and t_∞ is the end time for complete crystallization.

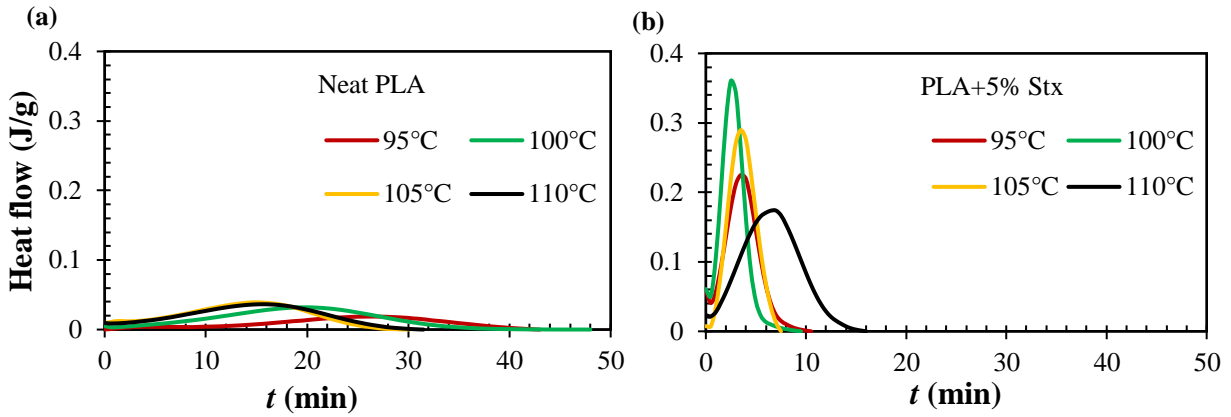


Figure 3-20. DSC thermograms displaying the isothermal melt crystallization times at different temperatures for (a) Neat PLA (3100HP) and (b) PLA (3100HP) + 5% Stereocomplex

Figure 3-21 displays the crystallization isotherms of neat PLA and the composite as a function of fractional crystallinity X_t versus time. It was observed that the rate of crystallization drastically increased due to addition of stereocomplex PLA filler. The lowest crystallization time achieved for neat PLA was about 29 minutes at 105°C, whereas the composite fully crystallized in 2 minutes at 100°C. This suggests that the stereocomplex PLA particles are acting as nucleating sites for the PLA homopolymer matrix.

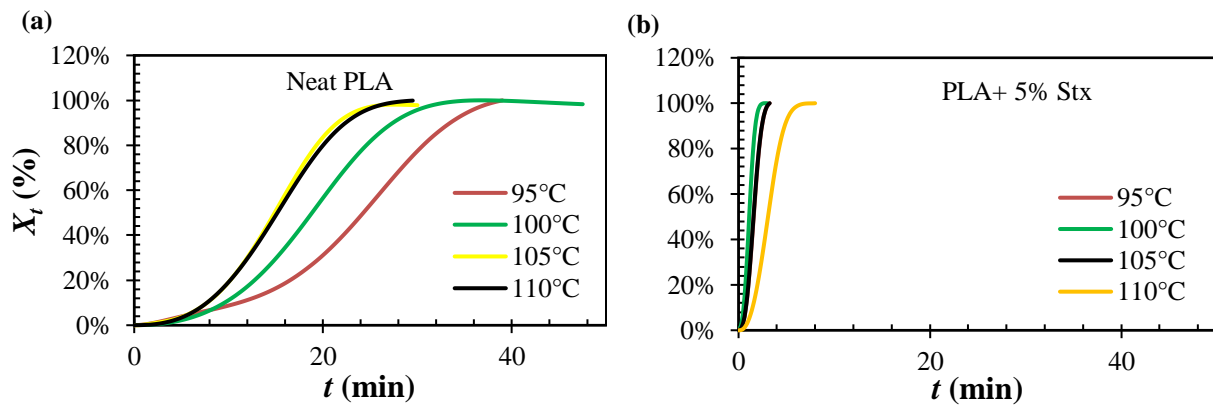


Figure 3-21. Fractional crystallinity vs time of (a) Neat PLA (3100HP) and (b) PLA (3100HP) + 5% Stereocomplex at different temperatures

The Avrami equation was used for studying the isothermal crystallization behavior of PLA and its composite comprising 5% stereocomplex PLA particles [154]. As shown below, it is often written in logarithmic form for analysis:

$$X(t) = 1 - \exp(-kt^n)$$

$$\ln[-\ln(1 - X(t))] = n \ln t + \ln k$$

where $X(t)$ is the fractional crystallinity over time t , k is the overall kinetic rate constant for nucleation and growth, and n is the Avrami exponent indicating the mechanism of nucleation and growth of the crystallites. Avrami plots of $\ln[-\ln(1 - X(t))]$ versus $\ln(t)$ were plotted to obtain the values of k and n via linear fitting as shown in **Figure 3-22**. The crystallization rates were much higher for the PLA composite comprising 5% stereocomplex PLA than the neat PLA; this was the case for all crystallization temperatures (95, 100, 105, and 110°C).

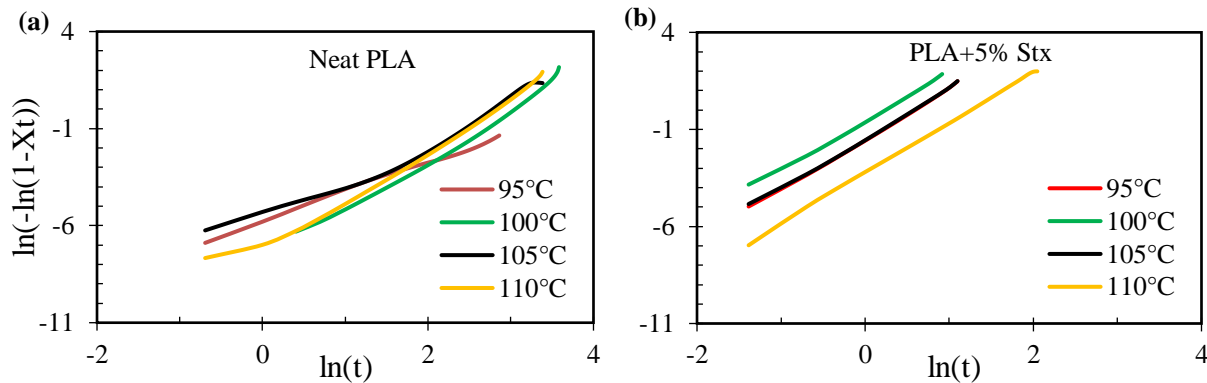


Figure 3-22. Avrami double log plots for the crystallization of (a) Neat PLA (3100HP) and (b) PLA (3100HP) + 5% Stereocomplex at different temperatures

From **Figure 3-22**, the Avrami parameters were obtained and used to calculate the half-time to crystallization, which is defined as the time to reach 50% of the total crystallinity of the polymer:

$$t_{1/2} = \ln\left(\frac{2}{k}\right)^{\frac{1}{n}}$$

The half-time to crystallization $t_{1/2}$ for neat PLA and the PLA composite are compared in **Figure 3-23** at various crystallization temperatures.

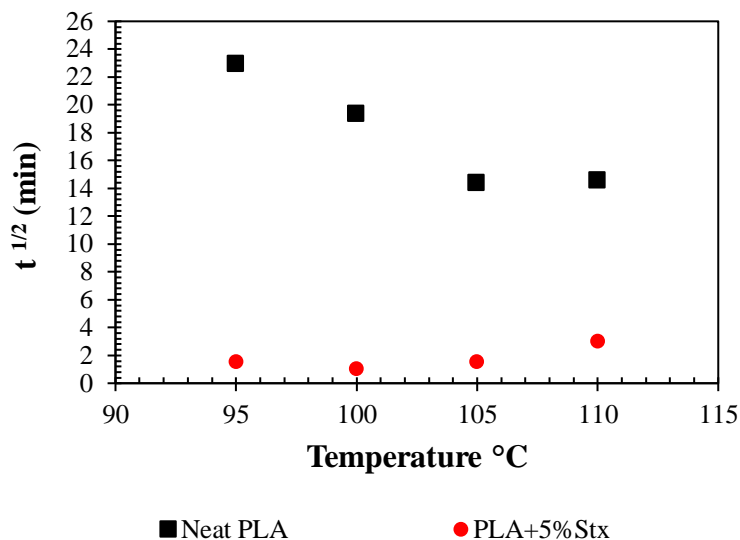


Figure 3-23. Half time to crystallization vs isothermal crystallization temperatures for neat PLA (3100HP) and PLA (3100HP) + 5% Stereocomplex at different temperatures

Figure 3-23 shows that the lowest $t_{1/2}$ for neat PLA occurs at 105°C at 14.40 minutes, whereas PLA+5% Stx's lowest $t_{1/2}$ is 1.06 minutes at 100°C. There is about a 93% reduction in the half time to crystallization when adding 5% stereocomplex PLA filler to semi-crystalline PLA. These results suggest that stereocomplex PLA acts as a nucleating agent for PLA homocrystallites to form rapidly. This hypothesis is further confirmed from Avrami analysis results in **Table 3-7**. Two-dimensional crystal growth was observed, as the Avrami exponent was estimated to be range between $2 < n < 3$, regardless of filler [154]. This data implies that no spherulitic crystal growth is taking place due to the addition of stereocomplex PLA.

It is well known in the scientific community that talc is one of the most effective nucleating agents for PLA. 1-2% of talc is blended with PLA to decrease its crystallization half time to less than a minute [155]. Although not as effective as talc, stereocomplex PLA has the potential to be a biobased, biodegradable organic nucleating agent as opposed to talc, an inorganic compound. We conclude that stereocomplex PLA acts as a nucleating agent to improve the isothermal crystallization kinetics of PLA homopolymer.

Table 3-7. Crystallization half times and Avrami constants for neat PLA and PLA composite samples at different temperatures

Sample	Temperature (°C)	$t_{1/2}$ (min)	n	$\ln k$	k
Neat PLA	95	22.95	1.929	-6.411	1.64E-03
	100	19.33	2.429	-7.560	5.21E-04
	105	14.40	2.544	-7.153	7.83E-04
	110	14.58	2.591	-7.309	6.69E-04
PLA + 5% Stx	95	1.56	2.676	-1.556	2.11E-01
	100	1.06	2.572	-0.520	5.95E-01
	105	1.54	2.564	-1.468	2.30E-01
	110	3.03	2.602	-3.254	3.86E-02

3.4. Conclusion & Next Steps

We have developed an efficient, solventless method for continuous manufacturing of stereocomplex PLA via reactive extrusion of high molecular weight PLLA and PDLA. No additives or reagents were used in the process. The effect of temperature and time on stereocomplex formation was first considered, and it was concluded that the process is temperature driven. Time did not play a role in the formation of stereocomplex PLA, as the process was almost instantaneous. The temperature was carefully considered to account for solidification and thermal dissociation of the stereocomplex PLA. The processing conditions (temperature profile, screw configuration, etc.) were thus optimized based on these results, and 95% conversion of stereocomplex PLA was achieved according to DSC results. WAXD results indicate full stereocomplexation representing a triclinic unit cell, as opposed to PLLA and PDLA's pseudo-orthorhombic crystal structure. Up to 56% total crystallinity was achieved for pure stereocomplex

PLA, and a melting peak temperature of 240°C was reported – the highest melting peak temperature reported for stereocomplex PLA to date.

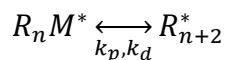
Stereocomplex PLA was tested as a potential additive for semi-crystalline and amorphous grade PLA to improve their crystallinity, mechanical properties, and crystallization kinetics. Composites of PLA homopolymer matrix and stereocomplex PLA filler were manufactured via twin-screw extrusion, and their material properties were characterized. The dispersity of the filler was verified at various collection times, and an increase in crystallinity was observed according to WAXD and DSC. The mechanical properties were characterized via tensile testing. A drastic increase in the yield strength, ultimate tensile strength, toughness, and moduli was observed in all the composites, leading us to conclude that stereocomplex PLA reinforces the material properties of PLA. Lastly, stereocomplex PLA was tested as a potential organic nucleating agent for semi-crystalline PLLA. It was concluded that one can achieve a crystallization half-time as low as one minute when adding 5% stereocomplex PLA filler in PLLA.

These results lead us to propose stereocomplex PLA as a potential organic additive that can reinforce the crystallinity, thermal properties, and mechanical properties of neat PLA. This can be used in melt-spun fibers for textiles. Next steps should focus on manufacturing PLA/stereocomplex PLA composites at various compositions aside from 5% and 30%, in order to further analyze its effect on PLA material properties. The crystallization kinetics should be analyzed at other compositions and compared with talc under the same processing conditions. Finally, one may consider other processing techniques, such as grafting of the stereocomplex PLA onto other materials to observe its effect on the material properties as opposed to physical blending. Stereocomplex PLA has commercial application as a value-added product for PLA and other polymers.

4. THERMAL RECYCLING OF PLA VIA THERMO-DEPOLYMERIZATION

4.1. Introduction

Poly lactide (PLA) is a bio-based, biodegradable polymer that has been used in widespread commercial and industrial applications. The most common end-of-life processes for PLA are composting and recycling via hydrolysis. Known for its biodegradable behavior, PLA is composted in a two-step process, disintegration and biodegradation, where the polymer chains are split apart into lactic acid; natural organisms then metabolize the lactic acid to produce carbon dioxide and water [156]. Alternatively, PLA can be collected and recycled via hydrolysis to its monomer lactic acid. As opposed to polyolefins, PLA's ester groups easily undergo hydrolytic degradation to yield low molecular weight oligomers and lactic acid monomer. This recycling process involves fully hydrolyzing the polymer to lactic acid using boiling water or steam [157]. The issue with composting is that there are limited facilities due to the specific conditions required within the process. Studies have shown that PLA will only readily degrade in a moist environment with compost temperatures up to PLA glass transition (50-60°C) based on carbon dioxide release [55], [56]. Hydrolysis is an inefficient recycling method for PLA, and it is a high energy-yielding process. This is due to the fact that the lactic acid obtained from hydrolysis must once again undergo several processes (polymerization to pre-polymer, depolymerization to lactide, lactide purification, ring-opening polymerization) to obtain high molecular weight pure PLA. Researchers have studied the unique chemical behavior behind PLA in that it undergoes a reversible reaction (**Figure 4-1**). Thermo-depolymerization of PLA occurs at temperatures above melting in order to convert the polymer back to lactide. A general reversible rate form assuming fast initiation was proposed by Witzke,



where lactide, M , is polymerized as lactic dimers on initiated polymer chains, R^* . k_p and k_d are the propagation rate constant and rate of decomposition, respectively [40].

Researchers have suggested this property might be leveraged to enable feedstock recycling of PLA [49], [158]. However, the chance of racemization may impact the optical purity and thus the material properties of the PLA product. In addition, temperature control is very important, as PLA degrades at temperatures greater than 200°C, resulting in the formation of CO, CO₂, acetaldehyde and methylketene [159].

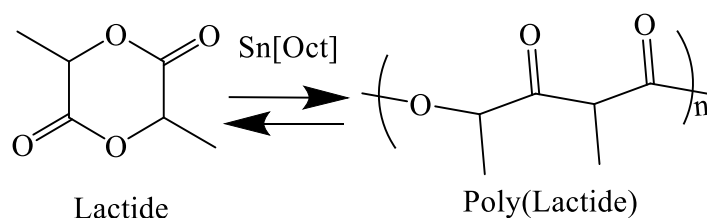


Figure 4-1. Reversible reaction of PLA

The Biobased Materials Research Group (BMRG) has developed a method to recover lactide from PLA waste via thermodepolymerization. A lab-scale technique is first proposed to test the feasibility of PLA depolymerization in a reaction vessel. The reaction is then scaled up in a batch reactor to test the scalability of the recycling process. Verification of pure lactide was obtained via differential scanning calorimetry (DSC) and gas chromatography (GC), whereas optical purity and optical rotation were analyzed via polarimetry. Lactide yield and stereoisomeric composition of the final lactide were characterized via mass balance and ¹H NMR-polarimetry. Finally, a two-step process is proposed to thermally recycle PLA via depolymerization in a batch reactor, followed by polymerization in a batch reactor. A life cycle analysis of PLA thermal recycling are studied and compared with PLA end-of-life composting.

4.2. Experimental

4.2.1 Lab-Scale Thermal Recycling of PLA in a Reaction Vessel

4.2.1.1 Materials & Reagents

Neat PLLA (L175) was obtained from Total Corbion. Polarimetry confirmed >99.9% optical purity for PLLA. Commercial biodegradable utensils (RePLA) comprising 90% PLA and 10% PBAT were purchased from Repurpose Compostables. The utensils were divided into smaller pieces (about 0.5 x 1 cm) for insertion within the reaction vessel. All materials were vacuum dried at 45°C for 48 hours to remove any residual moisture that may affect the reaction. Sn[Oct]₂ was the catalyst used for thermodepolymerization of PLLA, and was purchased from Millipore Sigma. Reported purity was 95%, with 4.6% ethylhexanoic acid, 0.3-0.5% water, and less than 0.05% tert-butylcatechol (stabilizer). HPLC grade dichloromethane (DCM) was obtained directly from VWR, with reported purity >99.8%. These reagents were used as is and not purified any further.

4.2.1.2 Thermodepolymerization of PLA

As seen in **Figure 4-2**, the experimental set-up used to investigate the thermal depolymerization of PLA materials consisted of a reaction vessel (100 mL), a hot plate, a silicone oil bath that can withstand temperatures above 200°C, an air condenser and glass connector to flow the lactide vapor, a lactide collector consisting of two glass flasks (100 ml) in series, a vapor trap, and a vacuum pump (Robinair 15500 VacuMaster). Heating tape connected to a temperature controller was used to ensure that the condenser and glass connector were heated above lactide's melting peak temperature (~96° C) so lactide would condense as a liquid and flow into the lactide collector. In order to protect the vacuum pump from clogging up due to lactide vapors, a vapor trap in an ice bath was installed in the vacuum line connecting the vacuum pump to the lactide collector. This protects the vacuum pump from lactide by solidifying the residual lactide in the vapor trap.

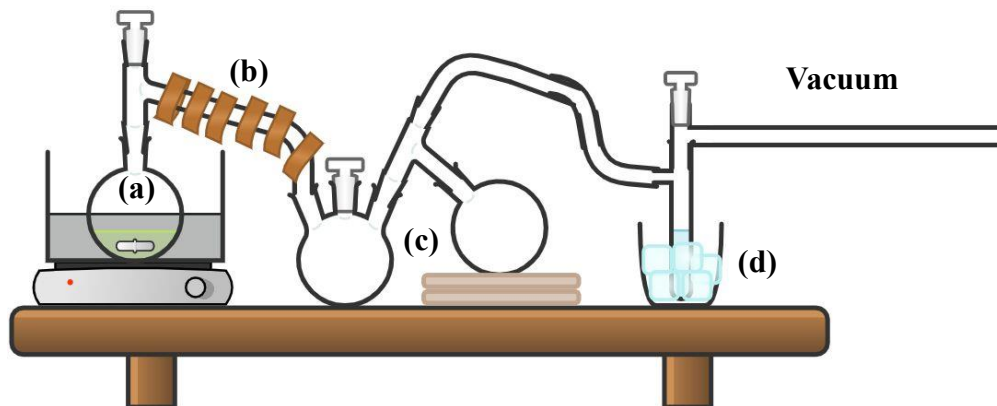


Figure 4-2. Experimental setup (a) The reaction vessel containing PLA with 0.6 wt% Sn[Oct]₂ is heated in the oil bath and connected to a (b) condenser that is wrapped with heating tape to ensure lactide vapor passage to the (c) lactide collectors. The lactide collectors are connected to a (d) vapor trap via a tube, and the vapor trap connects to the vacuum pump (not shown).

Test material (10 g) consisting of either PLLA or RePLA was weighed, transferred to the depolymerization reactor, and mixed with the catalyst Sn[Oct]₂ before heating the reaction vessel. It has previously been reported that the catalyst concentration C does not affect the equilibrium monomer concentration M_e [70]. A catalyst concentration of 0.6wt% was thus chosen. The reactions were held at five different temperatures: 200°C, 225°C, 250°C, 275°C, and 300°C. Lactide was collected at five different time intervals: 5 minutes, 10 minutes, 20 minutes, 40 minutes, and 60 minutes. A two-step mechanism (**Figure 4-3**) was initially proposed by our group for the non-equilibrium depolymerization reaction [70]. The initiation step involves the reaction of the catalyst with an ester linkage to form an activation complex. The formation of this intermediate complex can occur among any areas of the polymer chain and is not limited to the end groups. The second step involves chain scission of the intermediate complex, which leads to lactide formation. This reaction follows an unzipping depolymerization mechanism where the activated chain end back bites a neighboring ester linkage, leading to lactide formation. The depolymerization reaction has been reported to be zero-order.

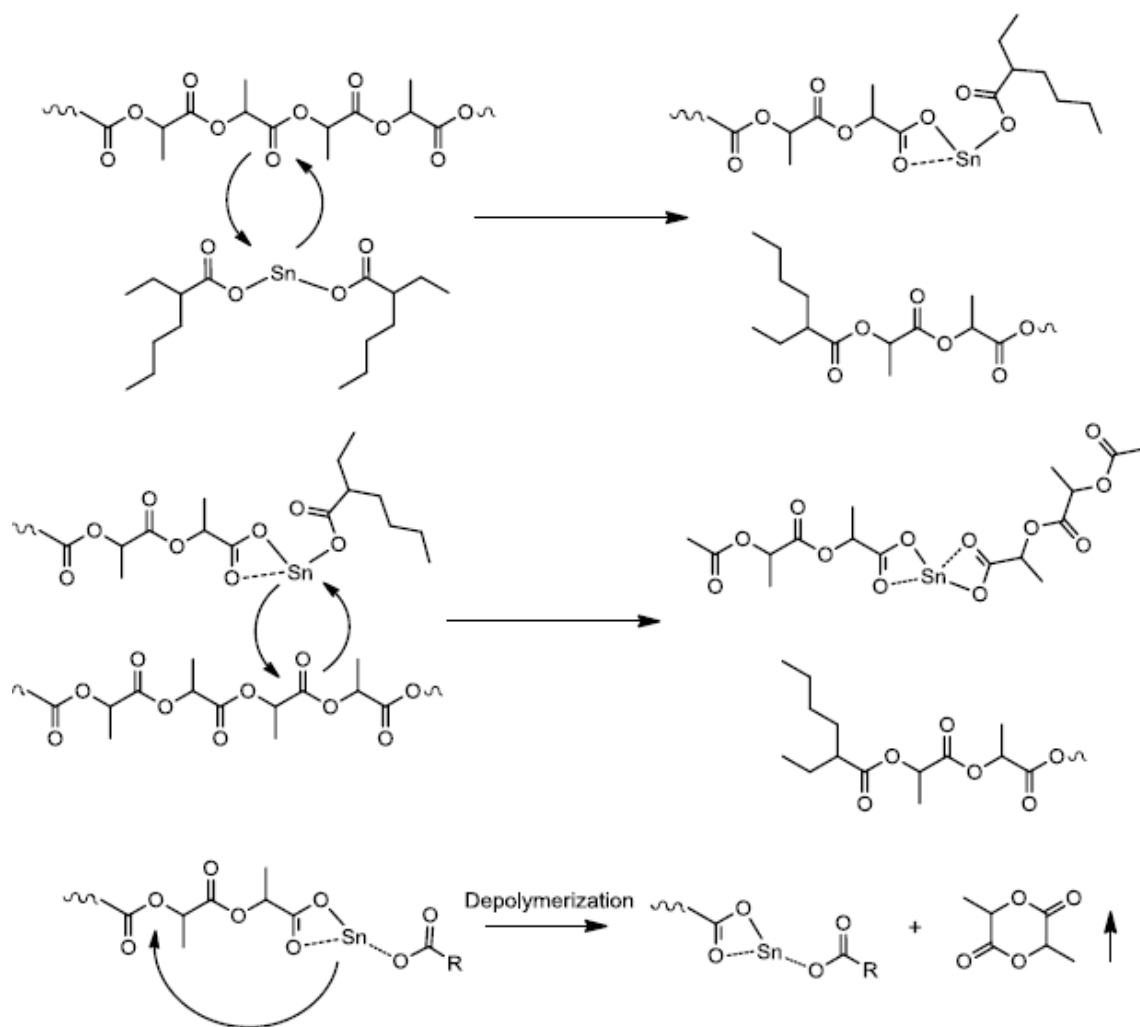


Figure 4-3. Proposed two-step depolymerization mechanism of PLA in presence of $\text{Sn}[\text{Oct}]_2$ catalyst [70]

4.2.1.3 Characterization & Analysis

The chemical purity, optical purity, stereoisomeric composition and yield of the lactide collected were characterized. Differential scanning calorimetry (DSC) was performed with a DSC Q20 to verify neat lactide and its chemical purity. Temperature was first equilibrated to 70 °C, then ramped up to 120 °C at a heating rate of 1 °C/min. The melting of a pure material takes place over a narrow temperature range, resulting in a sharp melting peak on a DSC trace at the material's characteristic melting point. For a material that only has a small amount (5-10%) of impurity, the melting peak

is depressed, resulting in broadening of the melting range [160]. This is the theory behind DSC purity determination based on melting point depression.

Polarimetry was performed with a JASCO P2000 polarimeter. The observed optical rotation, α_{obs}^{25} , was measured dichloromethane for the lactide monomers, at a concentration of 1 g/mL. Conditions were set at 25 °C and 589 nm wavelength. Three measurements were averaged for the optical rotation of each sample. Sucrose was used as a standard reference material, and its specific optical rotation was reported at $\sim 67^\circ$. The optical purity (o.p) was then calculated using the equation:

$$o.p. = \frac{\alpha_{obs}^{25}}{[\alpha]^{25}}$$

where $[\alpha]^{25}$ is the specific rotation of the pure enantiomer at room temperature ($[\alpha]^{25} = \pm 270^\circ$ for 100% optically pure L-lactide).

The optical purity is also considered to be the enantiomeric excess for an enantiomeric mixture,

$$o.p. = \frac{\alpha_{obs}^{25}}{[\alpha]^{25}} = \boxed{S(\%) - R(\%)}$$

The total molar composition will always equal 100% for any enantiomeric mixture:

$$100\% = S(\%) + R(\%)$$

Summing the above two equations, we can calculate the percent L-content ($S\%$) to be:

$$2S = 100\% + o.p.(\%) \rightarrow \boxed{S = \frac{100\% + o.p.(\%)}{2}}$$

Subtracting the above equation by 100% will give the percent D-content ($R\%$).

Gas chromatography (GC) was conducted on a Shimadzu GC-2010 with a flame ionization detector (FID) and a Stabilwax fused silica column (30 m x 0.25 mm i.d.; film thickness- 0.25 μm); helium was used as the carrier gas. The operating conditions were as follows. The temperatures of the injector and FID were 200 and 270 °C, respectively. The initial temperature of the column oven was 50 °C, and then ramped up to 260 °C at a rate of 25 °C/min; the

temperature was then held for 30 minutes. The flow rate of the carrier gas was 1.9 $\mu\text{L}/\text{min}$, and the split ratio was 20:1. 0.20 μL of 500 ppm lactide in chloroform was injected into the GC. This method determines the percent meso-lactide and percent D-/L-lactide. Combining this method with optical rotation analysis can provide results for the stereoisomeric composition of the lactide collected.

The yield of lactide was finally measured at different time intervals (5, 10, 20, 40, and 60 minutes) by weighing the amount of lactide collected versus the amount of PLA before starting the reaction.

4.2.2 Pilot-Scale Thermal Recycling of PLA in a Batch Reactor

4.2.2.1 Materials & Reagents

Neat PLLA (L175) was obtained from Total Corbion. Polarimetry confirmed >99.9% optical purity for PLLA. All materials were vacuum dried at 45°C for 48 hours to remove any residual moisture that may affect the reaction. $\text{Sn}[\text{Oct}]_2$ was the catalyst used for thermodepolymerization of PLLA, and was purchased from Millipore Sigma. Reported purity was 95%, with 4.6% ethylhexanoic acid, 0.3-0.5% water, and less than 0.05% tert-butylcatechol (stabilizer). HPLC grade dichloromethane (DCM) was obtained directly from VWR, with reported purity >99.8% . These reagents were used as is and not purified any further.

4.2.2.2 Thermodepolymerization of PLA

Test material (200 g) consisting of PLLA was weighed and mixed with the catalyst $\text{Sn}[\text{Oct}]_2$ (0.6wt%) before transferring to the batch reactor. The reactions were stirred at 100 RPM and held at five different temperatures: 200°C, 225°C, 250°C, 275°C, and 300°C. The experimental set-up (**Figure 4-4**) involved a Series 4530 2L floor stand reactor (PARR) equipped with a 4848 reactor controller (PARR). The reactor connects to a vessel for lactide collection via copper tubing

wrapped with heating tape. The lactide collector is then connected to a vapor trap in an ice bath, which is connected to the vacuum pump (Robinair 15500 VacuMaster). The reaction was run for 60 minutes, then the collected lactide was analyzed according to *Section 4.2.1.3*. The difference was that the lactide sample was not collected at several time intervals, but only at 60 minutes.

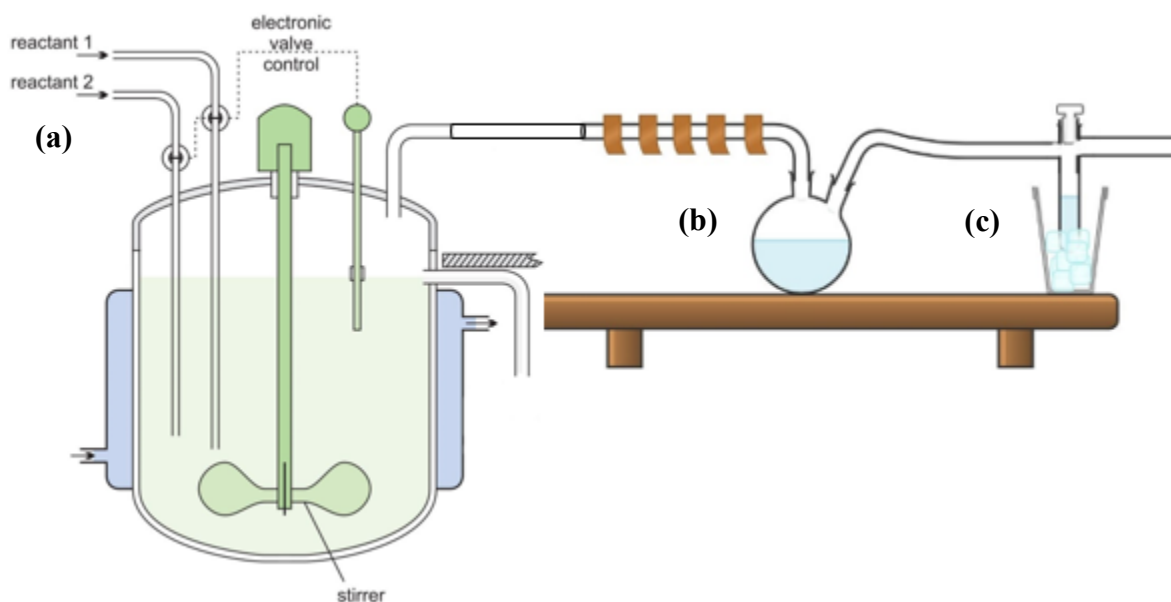


Figure 4-4. Schematic diagram of PLA thermodepolymerization in a (a) batch reactor. The PLA sample (reactant 1) and catalyst $\text{Sn}[\text{Oct}]_2$ (reactant 2) are added to the reactor. Over a period of time, the lactide sample is vacuum pumped to the (b) lactide collector. Any residual lactide is captured by the (c) vapor trap to vacuum

4.2.3 Life Cycle Assessment of PLA – Composting vs Thermal Recycling

4.2.3.1 Introduction

A life-cycle assessment (LCA) study has been carried out hereto to compare and contrast the environmental impacts of PLA in two scenarios: end-of-life composting and end-of-life recycling. Both scenarios involve synthesizing polylactide from corn, as starch is needed to produce the monomers for PLA. This is a cradle-to gate analysis including corn cultivation, starch refining, dextrose production via hydrolysis, fermentation of lactic acid, conversion to lactide and PLA via ring-opening polymerization, and finally composting or recycling. A life-cycle inventory was

carried out to analyze the gross input of raw materials and resources as well as gross output such as emissions and solid waste. Impact categories that have been assessed include land usage, eutrophication, global warming potential, and resource depletion. As a result, an educated decision will be made to conclude which scenario is more environmentally and economically feasible.

4.2.3.2 Product & Process Description

A cradle-to-grave analysis has been performed for two systems regarding PLA production: end-of-life composting and end-of-life recycling. After corn is cultivated, the kernel undergoes a wet milling process and is separated into three parts: (1) the bran/hull; (2) the germ; and (3) the endosperm (gluten and starch). In order to condition the corn grain for further milling and recovery, steeping occurs, softening the kernel while breaking down the protein holding the starch. After steeping, corn and water are discharged, and about 40% protein are separated from corn and recovered as feed supplements [161]. The steeped corn is then milled to tear the kernel, in order to separate the germ and about half the starch and gluten. The starch slurry passes through a series of washing, grinding, and screening to separate the starch and gluten from the rest of the corn grain. In order to obtain dry starch, the slurry is dried with vacuum filters then further flash dried [161]. Conversion to C6 sugars such as dextrose is performed via enzyme hydrolysis, where the hydrolyzed liquor is refined and cooled to crystallize the sugar [41]. Glycolysis is the energy-yielding process in metabolism of dextrose, converting the sugar into two molecules of pyruvate, along with two molecules of ATP and two of NADH. In an anaerobic environment, pyruvate may reduce to lactate or convert to ethanol and reduce to acetaldehyde. Fermentation of dextrose occurs in either of these processes, producing lactic acid as a result [43]. However, lactic acid only produces low molecular weight PLA, which does not have commercial application. This is because PLA polymerization is a moisture sensitive reaction, and much of the moisture within lactic acid

cannot be removed. Instead, one must dimerize lactic acid by first polymerizing it to low molecular weight oligomer via heating. The pre-polymer is then "broken" or depolymerized in the presence of a tin catalyst to produce lactide, which is then purified via recrystallization. Ring-opening polymerization at temperatures above the melting point of lactide will then produce high molecular weight PLA [19]. **Figure 4-5** explains the system for the primary scenario – composting PLA, whereas **Figure 4-6** explains the system for the secondary scenario – recycling PLA; we are assuming 20% PLA is recycled in this case. This life cycle assessment will compare the environmental impacts of both systems based on each of the steps described, and we can then make a decision on which system is more environmentally sustainable.

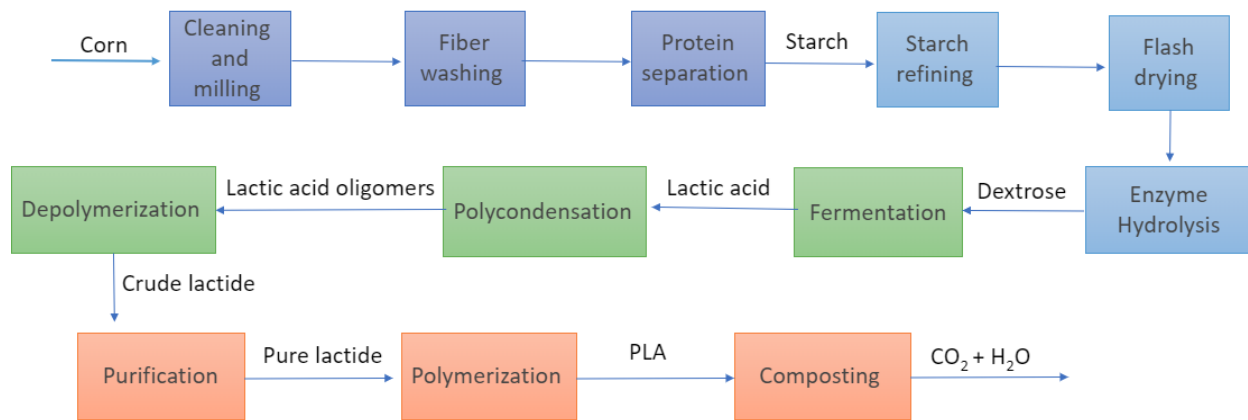


Figure 4-5. Primary scenario of PLA production from corn cultivation to composting

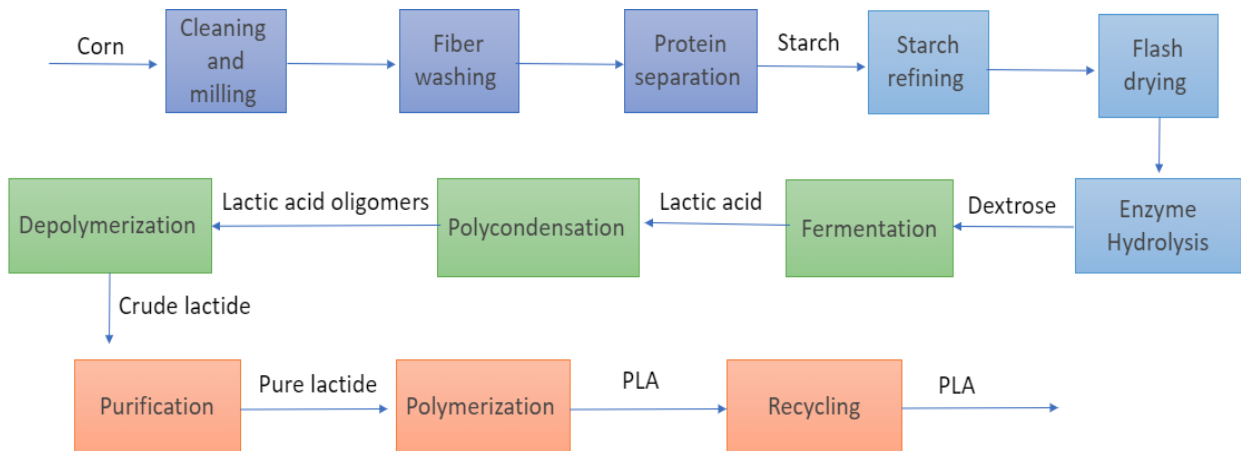


Figure 4-6. Primary scenario of PLA production from corn cultivation to recycling

4.2.3.3 *Goal and Scope*

The goal of this assessment is to compare and contrast the environmental impacts, including global warming, land usage, water use, and resource depletion, of composting PLA versus incorporated a recycling process via thermo-depolymerization. This study assesses the effect of recycling PLA on corn cultivation, starch conversion via wet milling, dextrose production via enzyme hydrolysis, lactic acid fermentation, lactide dimerization, PLA production via melt polymerization, and finally composting/recycling. Geographical specificity was based in Nebraska, US, as that is where most of the corn for PLA production is cultivated. The primary supplier of PLA, NatureWorks, is also headquartered there, and most of the results assessed originate from them. The functional unit used was 150 kilotons of PLA, as that is the current PLA production capacity that NatureWorks' plant has reported; reference flow was 1 kg of PLA. The temporal horizon was chosen to be 20 years, since that is a reasonable timeframe to analyze the effect of impact categories such as global warming potential and resource depletion. It would also reduce the overall impact of the assessment from major events such as startup or carbon sequestration in land. No allocation was implemented, as there were no co-products to consider in the PLA production process.

Even though biobased polymers have the ability to sequester carbon dioxide, that may not necessarily correlate to a significant reduction in GHG emissions, due to PLA's biodegradable behavior. As a result, global warming potential for both composting and recycling is important for this LCA. Water use is another important impact category to be considered, as one must consider the water intake for processes such as corn irrigation, dextrose production, and lactic acid conversion. Understanding how much energy from non-renewable resources goes into the PLA cradle-to-grave process is also imperative to assessing the environmental impact of PLA as opposed to thermoplastics. The land use of crops such as corn and sugarcane to produce PLA is

controversial, as there is a claim that bioplastics derived from resources such as corn and switchgrass would indirectly affect food production by competing for land with food crops. This topic would be important to explore in order to conclude how much feedstock we would need if we switched all plastics to PLA.

LCI often contains a mixture of measured, estimated, and calculated data. The quality of results depends on the quality of data used. Hence, many qualitative and semi-quantitative methods are used in LCA for data quality analysis. The Wiedema method (**Table 4-1**) was used in this study for assessing the data quality. It uses 5 data quality indicators in a matrix approach using 1-5 scoring system for each indicator, with 1 being the best score. Reliability considers whether the data used were measured using a specified and standardized method. Representativeness considers if the data were taken from a large number of sites over an adequate time to even out any normal fluctuations. Temporal correlation looks at how recently the data were measured or published. Geographical correlation considers whether the data were measured from the same area as the current study or a completely different part of the world. Lastly, technological correlation looks at the similarities in technologies used for the data and the technologies used in this LCA study [162].

Table 4-1. Wiedema method used to evaluate LCA data

Indicator Score	1	2	3	4	5
Reliability	Measured data	Calculated data based on measurements	Calculated data partly based on assumptions	Qualified estimate (by expert)	Nonqualified estimate
Representativeness	Representative data from sufficient samples of sites over an adequate period to even out normal fluctuation	Representative data from smaller number of sites but for adequate periods	Representative data from smaller number of sites, but from shorter periods	Data from adequate number of sites but shorter periods	Representativeness unknown or incomplete data from smaller number of sites and/or from shorter periods
Temporal Correlation	Less than 3 years	Less than 5 years	Less than 10 years	Less than 20 years	Age unknown or more than 20 years
Geographical correlation	Data from area under study	Average data from larger area in which the area under study is included	Data from area with similar production conditions	Data from area with slightly similar production conditions	Data from unknown area or area with very different production conditions
Technological correlation	Data from enterprises, processes, and materials under study	Data from processes data from processes and materials under study but from different enterprises	Data on related and materials under study but from different technology	Data on related processes or materials but same technology	Data on related processes or materials but different technology

4.3. Results and Discussion

4.3.1 Lab-Scale Thermal Recycling of PLA in a Reaction Vessel

4.3.1.1 Purity Determination and Stereoisomeric Composition

DSC was performed to verify neat lactide and analyze its chemical purity. The purity was analyzed for PLLA that was collected after a 60-minute reaction time at 200°C, 220°C, and 240°C. **Figure 4-7** displays one melting peak at ~95-100°C for all reaction temperatures, confirming L-lactide.

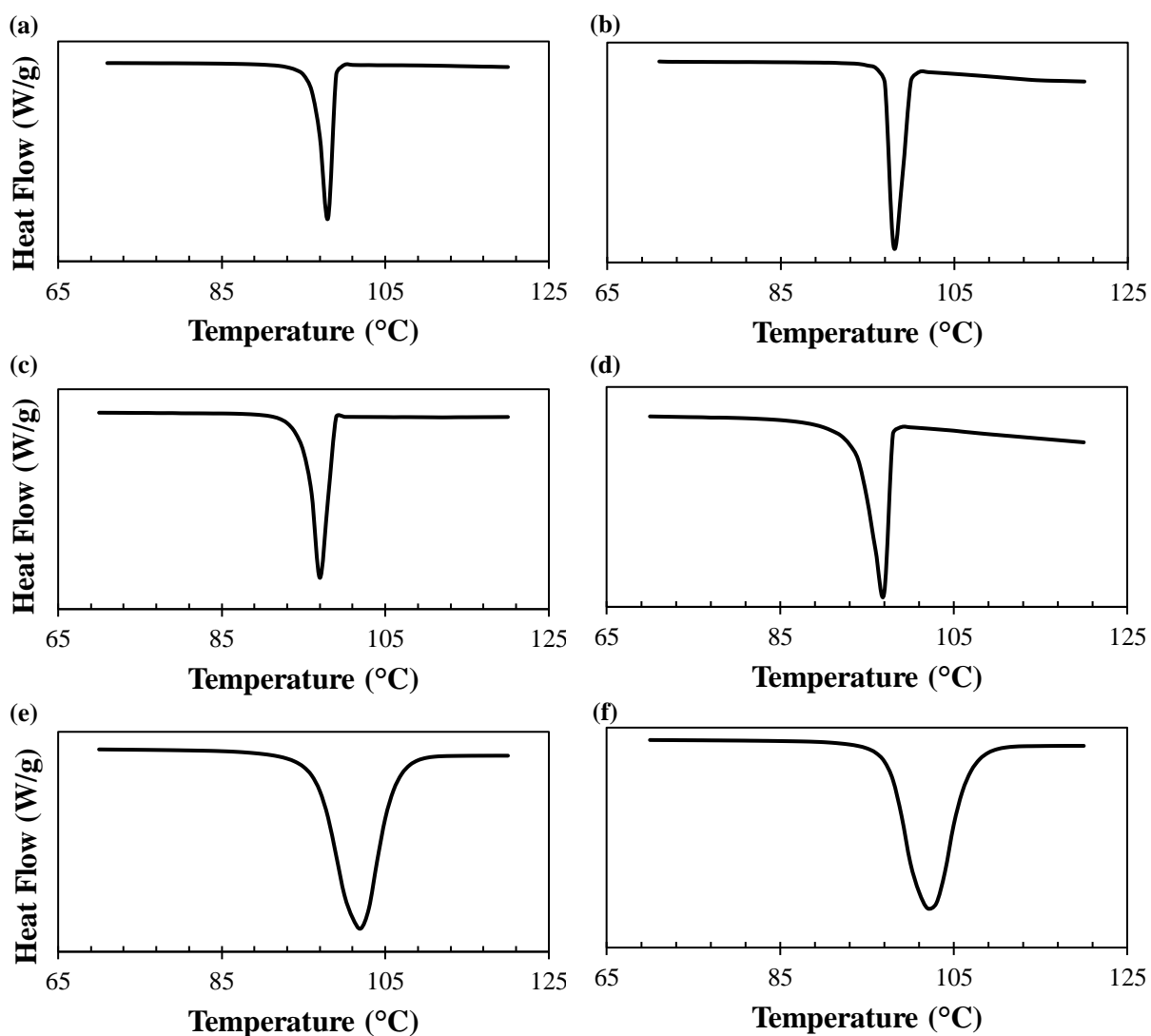


Figure 4-7. DSC purity determination of PLA samples for (a) PLLA at 200°C (b) RePLA at 200°C (c) PLLA at 220°C (d) RePLA at 220°C (e) PLLA at 240°C (f) RePLA at 240°C

The chemical purity (c.p.) of lactide product collected from PLLA depolymerization was analyzed to be ~99.2% at 200°C (**Figure 4-7a**), ~98.3% at 220°C (**Figure 4-7c**), and ~96.0% at 240°C (**Figure 4-7e**). The chemical purity of lactide product collected from RePLA depolymerization was analyzed to be ~99.3% at 200°C (**Figure 4-7b**), ~98.0% at 220°C (**Figure 4-7d**), and ~95.7% at 240°C (**Figure 4-7f**). As the reaction temperature increases, the purity of the lactide product decreases. This is due to racemization, forming meso-lactide as a byproduct at higher temperatures. It has been proposed in previous studies that the racemization mechanism should follow the S_N(II) reaction mechanism on the asymmetrical methine carbon (**Figure 4-8**). This means that the carboxylate anion in an end group attacks the asymmetrical carbon atom in the penultimate unit; this is followed by scission of the bond between ester oxygen and methine carbon. This results in the inversion of the stereoconfiguration and thus the formation of meso-lactide [163].

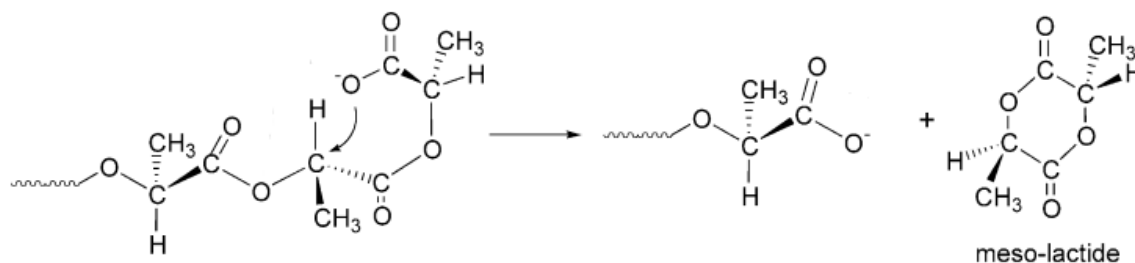


Figure 4-8. Racemization mechanism of PLA depolymerization based on S_N(II) reaction on asymmetrical methine carbon

The optical purity (o.p.) and percent D-content were analyzed based on optical rotation analysis for all samples. The optical purity of lactide product collected from PLLA depolymerization was calculated to be ~95.3% at 200°C, ~93.5% at 220°C, and ~89.6% at 240°C; the percent D-content was ~2.3% at 200°C, ~3.2% at 220°C, and ~5.2% at 240°C. The optical purity of lactide product collected from RePLA depolymerization was calculated to be ~95.0% at 200°C, ~92.8% at 220°C, and ~88.9% at 240°C; the percent D-content was ~2.5% at 200°C, ~3.6% at 220°C, and ~5.5% at

240°C. The stereoisomeric composition was also analyzed using a combination of polarimetry and gas chromatography. Our studies report that lactide products comprise L-lactide and meso-lactide, with <1% D-lactide. **Table 4-2** summarizes these results on lactide chemical purity, observed optical rotation, optical purity, percent D-content, and stereoisomeric composition.

Table 4-2. Summary of purity and isomeric composition results of lactide products from PLA depolymerization at various temperatures

Lactide Sample	c.p. (%)	α_{obs}^{25} (°)	o.p. (%)	D-content (%)	meso-lactide (%)	L-lactide (%)
PLLA (200°C)	99.2	257.3	95.3	2.3	4.7	95.2
PLLA (220°C)	98.3	252.4	93.5	3.2	3.5	96.4
PLLA (240°C)	96.0	241.9	89.6	5.2	5.6	94.3
RePLA (200°C)	99.3	256.5	95.0	2.5	5.1	94.8
RePLA (220°C)	98.0	250.6	92.8	3.6	5.3	94.6
RePLA (240°C)	95.7	240.0	88.9	5.5	11.0	88.9

It is clear that higher temperature reactions lead to lower purity (chemical & optical) results of the lactide products. A suggestion for scaleup to minimize racemization would involve distillation of the lactide monomer before collection. This would separate the meso-lactide from L-lactide.

4.3.1.2 Thermodepolymerization Kinetics

The yield of lactide was measured as a function of the mass of lactide collected over the mass of the PLA sample. The monomer equilibrium concentration (M_e) was then measured, and the depolymerization kinetics of PLA were thus analyzed. The rate of PLA polymerization and depolymerization have been extensively discussed in previous studies [70], [164]. The depolymerization reaction follows zero-order rate kinetics, in which the depolymerization rate only depends on the catalyst concentration. The rate of depolymerization can be expressed as

$$R_d = Ck_d$$

where R_d is the rate of depolymerization, C is the catalyst concentration, and k_d is the rate constant for depolymerization.

The rate of polymerization can be expressed as:

$$R_p = MCk_p$$

where M is the concentration of lactide monomer and k_p is the rate constant for polymerization.

Based on the Arrhenius equation, k_p can be calculated with the below formula,

$$k_p = A_{448} \exp \left(-\frac{E_a}{R} \left(\frac{1}{T} - \frac{1}{448} \right) \right)$$

where A_{448} is the pre-exponential constant, E_a is the activation energy, and T is the reaction temperature. Previous studies have reported the pre-exponential constant and activation energy for PLA reversible kinetics to be $86 \text{ h}^{-1} \text{ cat mol\%}^{-1}$ and 70.9 kJmol^{-1} , respectively [164].

In order to calculate for k_d , the monomer equilibrium concentration M_e must be considered using the equilibrium state assumption:

$$R_p = R_d \text{ at equilibrium}$$

Based on the previous equations discussed, the monomer equilibrium concentration would then become,

$$M_e = \frac{R_d}{R_p}$$

Rearranging this equation results in calculation for the depolymerization rate constant,

$$k_d = M_e k_p$$

The equilibrium concentration was obtained at various temperatures based on lactide yield results. **Figure 4-9** depicts the yield of lactide obtained from PLA thermodepolymerization at a catalyst concentration of 0.6wt% and temperatures of 200°C, 220°C, and 240°C. At increased temperatures, the time to equilibrium decreased, and the monomer equilibrium concentration increased. The yield of lactide was low, as PLA thermodepolymerization represents a zero-order reaction.

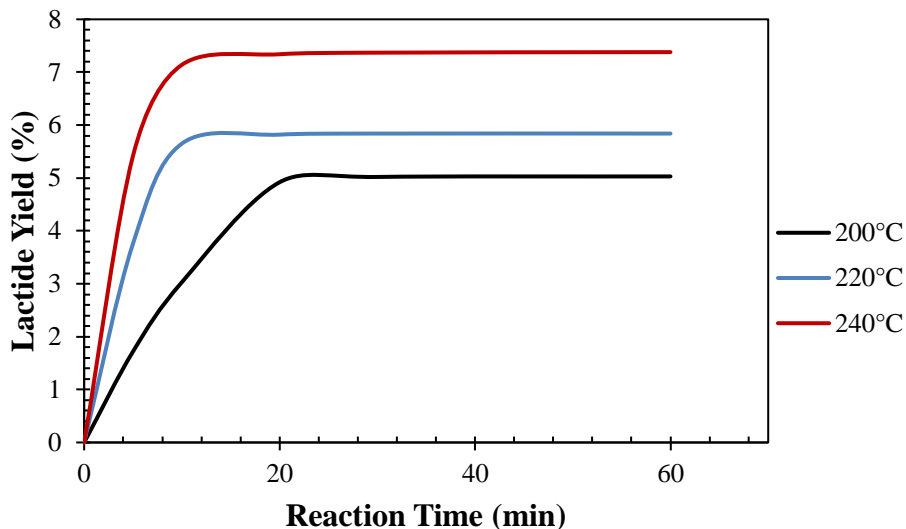


Figure 4-9. Lactide yield of PLA depolymerization at different temperatures

Using the rate constants for polymerization and the equilibrium monomer concentration deduced from **Figure 4-9**, the rate constants for depolymerization were calculated. **Table 4-3** summarizes the results. Results show that the rate of depolymerization proceeds very slowly, and that increasing temperature does not make a significant difference. Running this reaction at higher catalyst concentrations also did not significantly affect the equilibrium monomer concentration; only the time to equilibrium was shortened as C increased.

Table 4-3. Equilibrium monomer concentration and corresponding rate constants at various temperatures

T ($^{\circ}\text{C}$)	M_e (%)	k_p ($\text{h}^{-1} \text{ cat mol}\%^{-1}$)	k_d ($\text{h}^{-1} \text{ cat mol}\%^{-1}$)
180	3.10	106.11	3.28
200	5.02	235.19	11.81
220	5.84	488.69	28.54
240	7.38	959.17	70.79

Using the calculated depolymerization rate constants, an Arrhenius plot was graphed. From the linear regression of the plot in **Figure 4-10**, the activation energy for PLA thermodepolymerization was determined to be $E_a = 97.8$ kJ/mol.

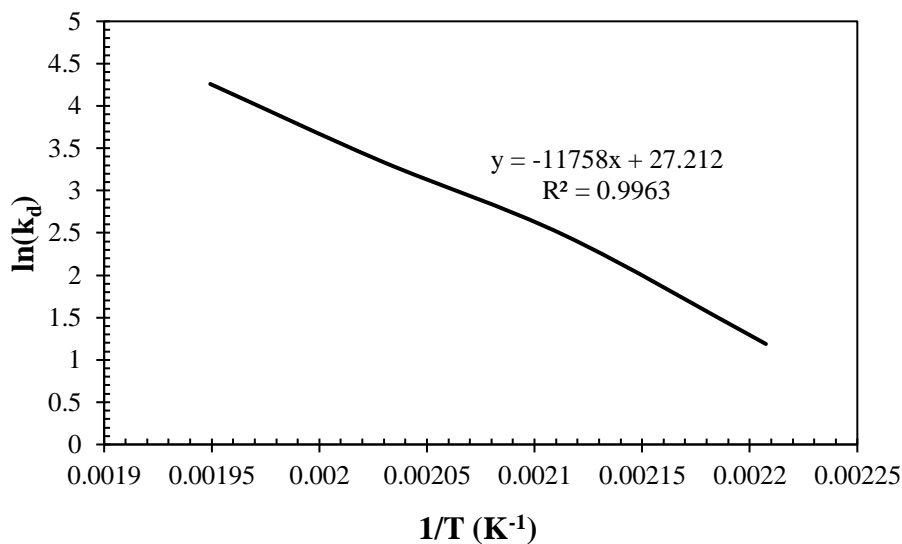


Figure 4-10. Arrhenius model on temperature dependence of the depolymerization rate constant of L-lactide with stannous octoate catalyst

4.3.2 Pilot-Scale Thermal Recycling of PLA in a Batch Reactor

4.3.2.1 Purity and Yield of Lactide

An assessment on the scaleup of PLA thermodepolymerization was studied in a batch reactor. The chemical purity, optical purity and yield of the lactide product were analyzed. **Table 4-4** summarizes these results for lactide products of PLLA thermodepolymerization. Results were similar to the lab-scale process in that the purity (c.p. & o.p.) decreased as the reaction temperature was increased; the meso-lactide formation increased. The yield of lactide was very low, similar to the lab-scale reaction, due to the reaction representing a zero-order rate. In order to increase yield, we suggest a different catalyst and use of an initiator.

Table 4-4. Summary of purity and isomeric composition results of lactide products from PLA depolymerization at various temperatures

Lactide Sample	c.p. (%)	α_{obs}^{25} (°)	o.p. (%)	D-content (%)	meso-lactide (%)	L-lactide (%)
PLLA (200°C)	99.0	258.9	95.9	2.3	4.7	95.2
PLLA (220°C)	98.0	247.0	91.5	3.2	3.5	96.4
PLLA (240°C)	95.5	238.4	88.3	5.2	5.6	94.3

4.3.3 Life Cycle Inventory

A cradle-to-grave approach was used for the final product. The LCI data was mainly obtained from Life Cycle Inventory and Impact Assessment Data for 2014 Ingeo^M Polylactide Production reports published by NatureWorks [41], [165]–[167]. Composting data for PLA was input from literature results by Andrade et. al. [168].

4.3.3.1 Carbon Efficiency of Systems

The Carbon (C) content of corn is 37.9%. From the material energy calculations, it was found that 2.67 kg corn is required for making 1 kg PLA for the primary scenario and the corn requirement reduces to 2.16 kg/kg PLA for the secondary scenario with recycling. Using these quantities, the carbon efficiency for both the systems was calculated as shown in **Table 4-5**. It was found that the carbon efficiency increases for the recycling system as the corn requirement per kg PLA reduces.

Table 4-5. Carbon efficiency for primary and secondary scenario

Component	% C	Amount (kg)	mol C	% C efficiency
PLA	50	1	41.67	
Corn (process 1)	37.9	2.67	84.33	49.41
Corn (process 2)	37.9	2.16	68.22	61.08

4.3.3.2 PLA Composting (System 1) LCI

This section includes the life cycle inventory data for PLA's current adopted system, which involves corn cultivation, corn wet milling to produce starch, dextrose conversion via enzyme hydrolysis, lactic acid production via fermentation, lactide production via dimerization, PLA production by melt polymerization, and finally PLA composting. The following LCI data consider all material inputs and outputs involved with PLA production and composting. Air and water emissions were considered as gross outputs and are discussed in the appendix. In the following tables, A, B, C, D, and E stand for reliability, representativeness, temporal correlation, geographical correlation, and technological correlation, respectively.

Corn Cultivation- Data for corn cultivation, shown in **Table 4-6**, were based on 1 kg production of PLA in the U.S. and was mainly collected from 2004-2007. These results were taken from NatureWorks’ production facility in Nebraska, US. Energy inputs, such as electricity, were required for farm tractors and water irrigation. Material inputs include agrochemicals and water, which was the major input for irrigation. The main product gained from this process is the corn kernel, which will be used in the next step (wet milling) to produce corn starch. Data for water output were not found.

Table 4-6. Corn Cultivation Material and Energy Inputs and Outputs

<i>Inputs/Outputs</i>	<i>Component</i>	<i>Amount</i>	<i>Units</i>	<i>Source</i>	<i>A</i>	<i>B</i>	<i>C</i>	<i>D</i>	<i>E</i>
Energy Input	Electricity	2.30	MJ/kg	NatureWorks	1	1	3	1	1
	Diesel	1.50	MJ/kg	NatureWorks	1	1	3	1	1
	Natural gas								
Material Input	Agrochemicals	0.92	kg	NatureWorks	1	1	3	1	1
	Water irrigation	20.90	kg	NatureWorks	1	1	3	1	1
Product	Corn kernel	2.67	kg	NatureWorks	1	1	3	1	1

Corn Wet Milling- Data for corn wet milling, as shown in **Table 4-7**, was based on 1 kg production of PLA in the U.S. and was mainly collected from 2004-2007. These data were taken from NatureWorks’ production facility in Nebraska, US. Energy input was for transportation purposes from the farmland to the wet milling facility. The major material inputs include water, air, and of course the corn kernel. The wet milling process tears the kernel to separate it from the starch slurry as well as other co-products such as gluten and germ, which are the major material outputs in this process. While 99% of the air input is output, about 64% of the water input is contained in the starch slurry (60% water by composition).

Table 4-7. Corn Wet Milling Material and Energy Inputs and Outputs

<i>Inputs/Outputs</i>	<i>Component</i>	<i>Amount</i>	<i>Units</i>	<i>Source</i>	<i>A</i>	<i>B</i>	<i>C</i>	<i>D</i>	<i>E</i>
Energy input	Diesel	0.02	MJ/kg	NatureWorks	1	1	3	1	1
Material Input	Corn kernel	2.67	kg	NatureWorks	1	1	3	1	1
	Air	3.11	kg	NatureWorks	1	1	3	1	1
	Sulfur	0.35	g	NatureWorks	1	1	3	1	1
	Sulfuric acid	1.23	g	NatureWorks	1	1	3	1	1
	Water	3.39	kg	NatureWorks	1	1	3	1	1
	Enzymes	0.30	g	NatureWorks	1	1	3	1	1
Product	Starch Slurry (60% water)	3.64	kg	NatureWorks	1	1	3	1	1
Co-products	Gluten meal	0.16	kg	NatureWorks	1	1	3	1	1
	Gluten feed	0.46	kg	NatureWorks	1	1	3	1	1
	Debris	0.06	kg	NatureWorks	1	1	3	1	1
	Sulfurous acid	0.93	g	NatureWorks	1	1	3	1	1
	Water	1.57	kg	NatureWorks	1	1	3	1	1
	Air	3.11	kg	NatureWorks	1	1	3	1	1
	Dry germ	0.18	kg	NatureWorks	1	1	3	1	1

Dextrose Production via Enzyme Hydrolysis- As shown in **Table 4-8**, data for dextrose production from starch were based on 1 kg production of PLA in the U.S. and was mainly collected from 2004-2007. Data were taken from NatureWorks' production facility in Nebraska, US. Conversion to dextrose is performed via enzyme hydrolysis, where the hydrolyzed liquor is refined and cooled to crystallize the sugar. Energy and wastewater are expended in this process, as the starch slurry is converted to dextrose. Wastewater is discharged back to the river, accounting for the water input and water in slurry. The difference between the material input and outputs is due to the water imbalance, as some water is evaporated in the process or remains with the product within the production facility.

Table 4-8. Dextrose Production Material and Energy Inputs and Outputs

<i>Inputs/Outputs</i>	<i>Component</i>	<i>Amount</i>	<i>Units</i>	<i>Source</i>	<i>A</i>	<i>B</i>	<i>C</i>	<i>D</i>	<i>E</i>
Energy input	Electricity	4.90	MJ/kg	NatureWorks	1	1	3	1	1
	Gasoline			NatureWorks	1	1	3	1	1
	Diesel			NatureWorks	1	1	3	1	1
	Natural gas			NatureWorks	1	1	3	1	1
Material Input	Starch Slurry (60% water)	3.64	kg	NatureWorks	1	1	3	1	1
	Enzymes	0.73	g	NatureWorks	1	1	3	1	1
	Ca(OH) ₂	0.40	g	NatureWorks	1	1	3	1	1
	Water	12.76	kg	NatureWorks	1	1	3	1	1
Product	Dextrose	1.55	kg	NatureWorks	1	1	3	1	1
Co-products	Wastewater	7.75	kg	NatureWorks	1	1	3	1	1

Lactic Acid Fermentation- **Table 4-9** displays the data for lactic acid production from fermentation of dextrose, which was based on 1 kg production of PLA in the U.S. and was mainly collected from 2004-2007. Results were taken from NatureWorks’ production facility in Nebraska, US. Glycolysis is the energy-yielding process in metabolism of dextrose, converting the sugar into two molecules of pyruvate, along with two molecules of ATP and two of NADH. In an anaerobic environment, pyruvate may reduce to lactate or convert to ethanol and reduce to acetaldehyde. Fermentation of dextrose occurs in either of these processes, producing lactic acid as a result. The difference between the material input and outputs is due to the water imbalance, as some water is evaporated in the process or remains with the product within the production facility.

Table 4-9. Lactic Acid Production Material and Energy Inputs and Outputs

<i>Inputs/Outputs</i>	<i>Component</i>	<i>Amount</i>	<i>Units</i>	<i>Source</i>	<i>A</i>	<i>B</i>	<i>C</i>	<i>D</i>	<i>E</i>
Energy input	Electricity	18.00	MJ/kg	NatureWorks	1	1	3	1	1
	Gasoline								
	Diesel			NatureWorks	1	1	3	1	1
	Natural gas								
Material Input	Dextrose	1.55	kg	NatureWorks	1	1	3	1	1
	Microbial Inoculum Media	1.01	kg	NatureWorks	1	1	3	1	1
	Water	32.98	kg	NatureWorks	1	1	3	1	1
Product	Lactic Acid	1.43	kg	NatureWorks	1	1	3	1	1
Co-product	Wastewater	29.51	kg	NatureWorks	1	1	3	1	1

Dimerization of Lactic Acid to Lactide- Material/energy inputs and outputs data for conversion of lactic acid to lactide are displayed in **Table 4-10**. Lactic acid is dimerized by first polymerizing it to low molecular weight oligomer via heating. The pre-polymer is then "broken" or depolymerized in the presence of a tin catalyst to produce lactide. The water used is either water content in lactic acid or water expended in processing the material. Similar to the previous two steps, the difference between the material input and outputs is due to the water imbalance, as some water is evaporated in the process or remains with the product within the production facility.

Table 4-10. Lactide Production Material and Energy Inputs and Outputs

<i>Inputs/Outputs</i>	<i>Component</i>	<i>Amount</i>	<i>Units</i>	<i>Source</i>	<i>A</i>	<i>B</i>	<i>C</i>	<i>D</i>	<i>E</i>
Energy input	Electricity	8.70	MJ/kg	NatureWorks	1	1	3	1	1
	Gasoline								
	Diesel								
	Natural gas								
Material Input	Lactic Acid	1.43	kg	NatureWorks	1	1	3	1	1
	Water	8.85	kg	NatureWorks	1	1	3	1	1
Product	Lactide	1.03	kg	NatureWorks	1	1	3	1	1
Co-product	Wastewater	6.25	kg	NatureWorks	1	1	3	1	1

PLA Production & Processing- **Table 4-11** displays the material and energy inputs and outputs for PLA production by polymerization of lactide. Once the lactide is vacuum dried in an oven, it is then polymerized in a large-scale extruder at temperatures above its melting point. Much of the energy input goes into this step, as electricity and gas is needed to run the machines for polymerizing lactide. Average monomer conversion to PLA is 97%, based on NatureWorks' data on PLA polymerization.

Table 4-11. PLA Polymerization Material and Energy Inputs and Outputs

<i>Inputs/Outputs</i>	<i>Component</i>	<i>Amount</i>	<i>Units</i>	<i>Source</i>	<i>A</i>	<i>B</i>	<i>C</i>	<i>D</i>	<i>E</i>
Energy input	Electricity	3.10	MJ/kg	NatureWorks	1	1	3	1	1
	Gasoline								
	Diesel								
	Natural gas								
Material Input	Lactide	1.03	kg	NatureWorks	1	1	3	1	1
	Water	9.56	kg	NatureWorks	1	1	3	1	1
Product	Poly(lactide)	1.00	kg	NatureWorks	1	1	3	1	1
Co-product	Wastewater	8.48	kg	NatureWorks	1	1	3	1	1

PLA Composting- After PLA is used for commercial application, its end-of-life process involves composting the bioplastic by undergoing a 2-step degradation process: disintegration and biodegradation. **Table 4-12** displays the material and energy inputs and outputs for PLA composting. Data were taken from Andrade et. al., and calculated for 1 kg of PLA [168]. The polymer chains are broken down by moisture and heat in the compost, producing lactic acid. The microorganisms in the compost then consume and metabolize the broken-down polymer fragments and lactic acid as nutrients. The main products from the process are carbon dioxide, water and humus (biomass).

Table 4-12. PLA Composting Material and Energy Inputs and Outputs

<i>Inputs/Outputs</i>	<i>Component</i>	<i>Amount</i>	<i>Units</i>	<i>A</i>	<i>B</i>	<i>C</i>	<i>D</i>	<i>E</i>
Energy Input	Electricity	0.02	MJ/kg	1	4	3	3	2
Material Input	Compost	0.33	kg	1	4	3	3	2
	Land	0.12	m ²	1	4	3	3	2
	PLA	1.00	kg	1	4	3	3	2
Product	CO ₂	1.53	kg	1	4	3	3	2
	Water	0.05	kg	1	4	3	3	2
	Humus	0.33	kg	1	4	3	3	2

4.3.3.3 PLA Recycling (System 2) LCI

This section includes the life cycle inventory data for our proposed system of PLA, which involves recycling PLA via thermodepolymerization. The PLA waste would first undergo depolymerization in a reactor by heating it at temperatures above its melting point in the presence of tin catalyst. Then, the recovered lactide would be directly pumped from the reactor to the extruder for polymerization to pure PLA. We are assuming that 20% of the PLA used in the US will be recycled, and this assumption will account for our calculated data in the following tables. The following LCI data considers all material inputs and outputs involved with PLA production and composting. Aside from the recycling step, all other steps in the PLA cradle-to-grave process consider 80% of the material/energy input and output from the original system, because 20% of PLA would be reused. In the following tables, A, B, C, D, and E stand for reliability, representativeness, temporal correlation, geographical correlation, and technological correlation, respectively.

Corn Cultivation- Data for corn cultivation, shown in **Table 4-13**, were based on 1 kg production of PLA in the U.S. and was calculated based on the assumption that 20% PLA would be recycled. The original data were taken from NatureWorks but modified from our assumption. Energy inputs, such as electricity, were required for farm tractors and water irrigation. Material inputs include

agrochemicals and water, which was the major input for irrigation. The main product gained from this process is the corn kernel, which will be used in the next step (wet milling) to produce corn starch. Data for water output were not found.

Table 4-13. Corn Cultivation Material and Energy Inputs and Outputs

<i>Inputs/Outputs</i>	<i>Component</i>	<i>Amount</i>	<i>Units</i>	<i>A</i>	<i>B</i>	<i>C</i>	<i>D</i>	<i>E</i>
Energy Input	Electricity	1.84	MJ/kg	3	1	3	1	1
	Diesel	0.08	MJ/kg	3	1	3	1	1
	Natural gas			3	1	3	1	1
Material Input	Agrochemicals	0.75	kg	3	1	3	1	1
	Water irrigation	16.74	kg	3	1	3	1	1
Product	Corn kernel	2.16	kg	3	1	3	1	1

Corn Wet Milling- Data for corn wet milling, as shown in **Table 4-14**, were based on 1 kg production of PLA in the U.S. and was calculated based on the assumption that 20% PLA would be recycled. The original data were taken from NatureWorks but modified from our assumption. Energy input was for transportation purposes from the farmland to the wet milling facility. The major material inputs include water, air, and of course the corn kernel. The wet milling process tears the kernel to separate it from the starch slurry as well as other co-products such as gluten and germ, which are the major material outputs in this process. While 99% of the air input is output, about 64% of the water input is contained in the starch slurry (60% water by composition).

Table 4-14. Corn Wet Milling Material and Energy Inputs and Outputs

<i>Inputs/Outputs</i>	<i>Component</i>	<i>Amount</i>	<i>Units</i>	<i>Source</i>	<i>A</i>	<i>B</i>	<i>C</i>	<i>D</i>	<i>E</i>
Energy input	Diesel	0.02	MJ/kg	NatureWorks	3	1	3	1	1
Material Input	Corn kernel	2.16	kg	NatureWorks	3	1	3	1	1
	Air	2.51	kg	NatureWorks	3	1	3	1	1
	Sulfur	0.29	g	NatureWorks	3	1	3	1	1
	Sulfuric acid	1.00	g	NatureWorks	3	1	3	1	1
	Water	2.74	kg	NatureWorks	3	1	3	1	1
	Enzymes	0.24	g	NatureWorks	3	1	3	1	1
Product	Starch Slurry (60% water)	2.94	kg	NatureWorks	3	1	3	1	1
Co-products	Gluten meal	0.13	kg	NatureWorks	3	1	3	1	1
	Gluten feed	0.37	kg	NatureWorks	3	1	3	1	1
	Debris	0.05	kg	NatureWorks	3	1	3	1	1
	Sulfurous acid	0.75	g	NatureWorks	3	1	3	1	1
	Wastewater	1.26	kg	NatureWorks	3	1	3	1	1
	Air	2.50	kg	NatureWorks	3	1	3	1	1
	Dry germ	0.15	kg	NatureWorks	3	1	3	1	1

Dextrose Production via Enzyme Hydrolysis- As shown in **Table 4-15**, data for dextrose production from starch were based on 1 kg production of PLA in the U.S. and was calculated based on the assumption that 20% PLA would be recycled. The original data were taken from NatureWorks but modified from our assumption. Conversion to dextrose is performed via enzyme hydrolysis, where the hydrolyzed liquor is refined and cooled to crystallize the sugar. Energy and wastewater are expended in this process, as the starch slurry is converted to dextrose. Wastewater is discharged back to the river, accounting for the water input and water in slurry. The difference between the material input and outputs is due to the water imbalance, as some water is evaporated in the process or remains with the product within the production facility.

Table 4-15. Dextrose Production Material and Energy Inputs and Outputs

<i>Inputs/Outputs</i>	<i>Component</i>	<i>Amount</i>	<i>Units</i>	<i>Source</i>	<i>A</i>	<i>B</i>	<i>C</i>	<i>D</i>	<i>E</i>
Energy input	Electricity	3.92	MJ/kg	NatureWorks	3	1	3	1	1
	Gasoline			NatureWorks	3	1	3	1	1
	Diesel			NatureWorks	3	1	3	1	1
	Natural gas			NatureWorks	3	1	3	1	1
Material Input	Starch Slurry (60% water)	2.94	kg	NatureWorks	3	1	3	1	1
	Enzymes	0.59	g	NatureWorks	3	1	3	1	1
	Ca(OH) ₂	0.32	g	NatureWorks	3	1	3	1	1
	Water	10.21	kg	NatureWorks	3	1	3	1	1
Product	Dextrose	1.25	kg	NatureWorks	3	1	3	1	1
Co-products	Wastewater	1.01	kg	NatureWorks	3	1	3	1	1

Lactic Acid Fermentation- **Table 4-16** displays the data for lactic acid production from fermentation of dextrose, which was based on 1 kg production of PLA in the U.S. and was calculated based on the assumption that 20% PLA would be recycled. The original data were taken from NatureWorks but modified from our assumption. Glycolysis is the energy-yielding process in metabolism of dextrose, converting the sugar into two molecules of pyruvate, along with two molecules of ATP and two of NADH. In an anaerobic environment, pyruvate may reduce to lactate or convert to ethanol and reduce to acetaldehyde. Fermentation of dextrose occurs in either of these processes, producing lactic acid as a result. The difference between the material input and outputs is due to the water imbalance, as some water is evaporated in the process or remains with the product within the production facility.

Table 4-16. Lactic Acid Production Material and Energy Inputs and Outputs

<i>Inputs/Outputs</i>	<i>Component</i>	<i>Amount</i>	<i>Units</i>	<i>Source</i>	<i>A</i>	<i>B</i>	<i>C</i>	<i>D</i>	<i>E</i>
Energy Input	Electricity	14.40	MJ/kg	NatureWorks	3	1	3	1	1
	Gasoline								
	Diesel								
	Natural gas								
Material Input	Dextrose	1.25	kg	NatureWorks	3	1	3	1	1
	Microbial Inoculum Media	0.82	kg	NatureWorks	3	1	3	1	1
	Water	26.38	kg	NatureWorks	3	1	3	1	1
Product	Lactic Acid	1.16	kg	NatureWorks	3	1	3	1	1
Co-product	Wastewater	23.61	kg	NatureWorks	3	1	3	1	1

Dimerization of Lactic Acid to Lactide- Material/energy inputs and outputs data for conversion of lactic acid to lactide are displayed in **Table 4-17**. We are again accounting for 20% of PLA recycled and modifying NatureWorks' data as required. Lactic acid is dimerized by first polymerizing it to low molecular weight oligomer via heating. The pre-polymer is then "broken" or depolymerized in the presence of a tin catalyst to produce lactide. The water used is either water content in lactic acid or water expended in processing the material. Similar to the previous two steps, the difference between the material input and outputs is due to the water imbalance, as some water is evaporated in the process or remains with the product within the production facility.

Table 4-17. Lactide Production Material and Energy Inputs and Outputs

<i>Inputs/Outputs</i>	<i>Component</i>	<i>Amount</i>	<i>Units</i>	<i>Source</i>	<i>A</i>	<i>B</i>	<i>C</i>	<i>D</i>	<i>E</i>
Energy Input	Electricity	6.96	MJ/kg	NatureWorks	3	1	3	1	1
	Gasoline								
	Diesel								
	Natural gas								
Material Input	Lactic Acid	1.16	kg	NatureWorks	3	1	3	1	1
	Water	7.08	kg	NatureWorks	3	1	3	1	1
Product	Lactide	0.82	kg	NatureWorks	3	1	3	1	1
Co-product	Wastewater	5.00	kg	NatureWorks	3	1	3	1	1

PLA Production & Processing- **Table 4-18** displays the material and energy inputs and outputs for PLA production by polymerization of lactide. Data account for 20% of PLA waste recycled and is modified accordingly. Once the lactide is vacuum dried in an oven, it is then polymerized in a large-scale extruder at temperatures above its melting point. Since we are incorporating a PLA recycling process via thermodepolymerization, the recycled lactide is also considered in this process. As a result, the amount of lactide input and PLA produced stays the same. Much of the energy input goes into this step, as electricity and gas is needed to run the machines for polymerizing lactide. Average monomer conversion to PLA is 97%, based on NatureWorks' data on PLA polymerization.

Table 4-18. PLA Polymerization Material and Energy Inputs and Outputs

<i>Inputs/Outputs</i>	<i>Component</i>	<i>Amount</i>	<i>Units</i>	<i>A</i>	<i>B</i>	<i>C</i>	<i>D</i>	<i>E</i>
Energy Input	Electricity	3.10	MJ/kg	3	1	3	1	1
	Gasoline							
	Diesel							
	Natural gas							
Material Input	Lactide + Recycled Lactide	1.03	kg	3	1	3	1	1
	Tin Catalyst	1.03	g	3	1	3	1	1
	Water	9.56	kg	3	1	3	1	1
Product	Poly(lactide)	1.00	kg	3	1	3	1	1
Co-product	Wastewater	8.48	kg	3	1	3	1	1

PLA Recycling- While a reduction in energy and material input/output due to recycling is seen for most of the steps in the life cycle of PLA, the recycling process does consume energy. Electricity must be generated for the depolymerization and polymerization reactions, as these reactions occur in large scale machinery such as batch reactors and extruders. The data are displayed in **Table 4-19**, accounting for the lactide recovered.

Table 4-19. PLA Recycling Material and Energy Inputs and Outputs

<i>Inputs/Outputs</i>	<i>Component</i>	<i>Amount</i>	<i>Units</i>	<i>A</i>	<i>B</i>	<i>C</i>	<i>D</i>	<i>E</i>
Energy Input	Electricity	2.24	MJ/kg	3	1	3	1	1
Material Input	PLA Waste	0.80	kg	3	1	3	1	1
	Catalyst	0.20	g	3	1	3	1	1
Product	Lactide	0.19	kg	3	1	3	1	1

PLA Composting- Since we are assuming that 20% of PLA waste is recycled, that means we are assuming that 80% of it will be composted. Based on this assumption, we obtained the data displayed in **Table 4-20** for the material and energy inputs and outputs for PLA composting. The original data were taken from Andrade et. al., and it was modified according to our assumptions.

Table 4-20. PLA Composting Material and Energy Inputs and Outputs

<i>Inputs/Outputs</i>	<i>Component</i>	<i>Amount</i>	<i>Units</i>	<i>A</i>	<i>B</i>	<i>C</i>	<i>D</i>	<i>E</i>
Energy Input	Electricity	31.76	kJ/kg	1	4	3	3	2
Material Input	Compost	0.26	kg	1	4	3	3	2
	Land	0.09	m ²	1	4	3	3	2
	PLA	0.80	kg	1	4	3	3	2
Product	CO ₂	1.53	kg	1	4	3	3	2
	Water	0.05	kg	1	4	3	3	2
	Humus	0.33	kg	1	4	3	3	2

The Life Cycle Inventory (LCI) data of PLA composting vs PLA recycling has been discussed. The LCI data for the original system (without a recycling step) were taken from NatureWorks. The LCI data for the recycling system involve a major assumption that 20% of PLA would be recycled. Thus, the data from NatureWorks were modified accordingly. One will notice that there is a reduction in the material and energy inputs for most of the processes involved in PLA's life cycle, except for its production. This is because 20% of PLA is recycled, leading to energy and material savings in corn cultivation, wet milling, dextrose production, lactic acid conversion, and lactide production. However, the recycling step does expend energy in electricity due to the machinery required to depolymerize PLA back to lactide. This data will be assessed further in the next section, the life cycle impact assessment.

4.3.4 Life Cycle Impact Assessment

The purpose of this analysis was to determine the impact of all emissions from each process on the environmental factors like global warming, eutrophication etc. Various emissions were converted to their equivalence factors for fair comparison between 2 scenarios. Calculations for the conversion for each impact category were done using TRACI 2002 model.

4.3.4.1 Global Warming Impact Category

The major emissions considered for calculating global warming impact were CO₂ sequestration, CO₂ emissions, methane and nitrous oxide emissions. The gross contributions of CO₂ from each process can be seen in **Figure 4-11** and **Table 4-21** for both primary and secondary scenario. CO₂ sequestration was a process involved in corn cultivation. Plants absorb CO₂ from atmosphere during photosynthesis and store it in the plant as biomass. Also, some of the CO₂ is stored in the soil from the roots of the plants. This value is about 0.22 tons/acre/year for soil sequestration (0.12 kg CO₂ eq/ kg PLA) and 1.8 kg CO₂ eq/ kg PLA for the CO₂ stored as biomass. The fixing of atmospheric CO₂ as biomass is considered negative on global warming potential scale and hence reduces the net global warming potential (GWP) for biobased polymers as compared to petroleum-based polymers. Also, the composting step was found to have a major impact on GWP as it produces about 1.5 kg CO₂ eq/ kg PLA. This impact was reduced for secondary scenario with recycling reducing the net GWP from 3 to 2.62 kg CO₂ eq/ kg PLA.

Table 4-21. Contribution analysis of global warming potential

	Primary scenario		Secondary scenario	
	CO₂ eq kg/ kg PLA	% of total contribution	CO₂ eq kg/ kg PLA	% of total contribution
CO₂ sequestration by corn and soil	-1.95	-65.00	-1.66	-63.19
Corn production	0.25	8.33	0.20	7.63
Transport	0.98	32.67	0.96	36.63
Dextrose production	0.29	9.67	0.23	8.85
Lactic acid production	1.16	38.67	0.93	35.41
Lactide production	0.54	18.00	0.43	16.48
PLA production	0.2	6.67	0.16	6.11
Composting	1.53	51.00	1.22	46.71
Recycling	0	0.00	0.14	5.37
Net	3	100	2.62	100

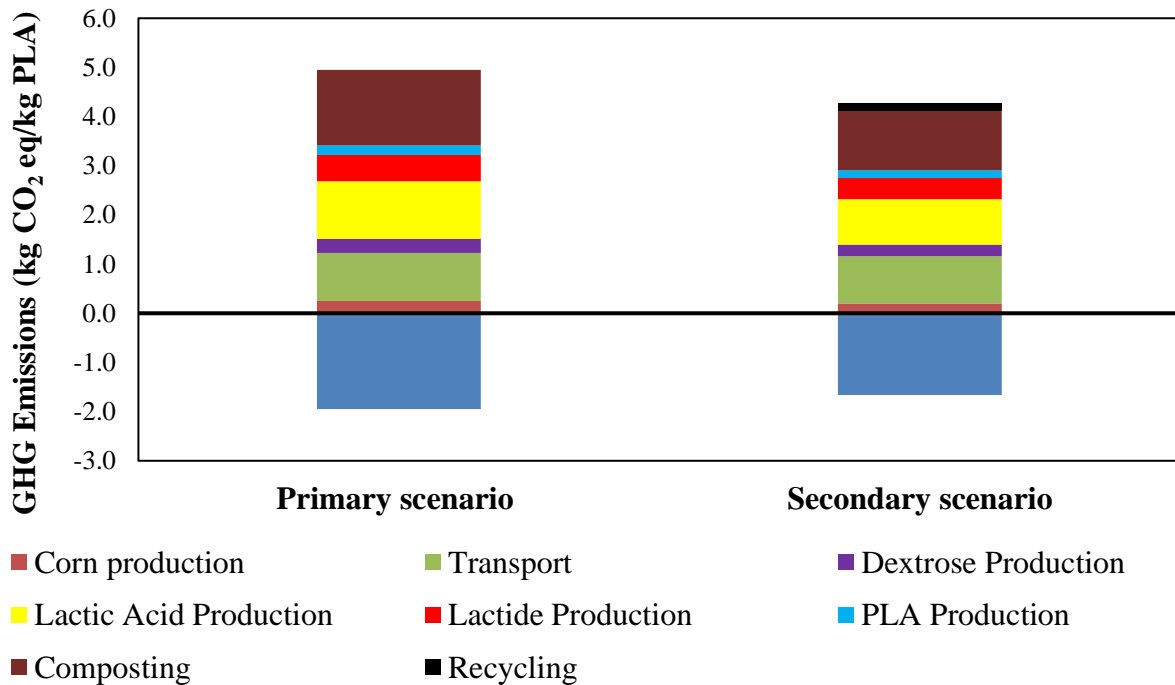


Figure 4-11. Global warming potential of PLA recycling vs composting

4.3.4.2 Land Use Impact Category

In this impact category, the land required for cultivation of corn for primary and secondary scenario was compared. The assumption made was 20% of the produced PLA was recycled into the process for making lactide in the secondary scenario. The average corn production in Nebraska was found to be 185 bu/acre where, 1 bu= 25 kg. Using that and the total PLA requirement according to the reference flow, the total corn requirement was calculated and accordingly the land required for cultivation of the corn was determined. It was found that for making 150,000,000 kg of PLA/year, about 86500 acres of land was required in the primary scenario whereas the requirement reduced to 56000 acres in the secondary scenario with 20% recycling (**Figure 4-12**). The calculations can be found in **Table 4-22**.

Table 4-22. Contribution analysis for land use

	Primary scenario	Secondary scenario	
Corn production in Nebraska	185.0	185.0	bu/acre
1 bu= 25 kg corn			
Corn required of 1 kg PLA	2.7	2.2	kg
PLA required	150000000.0	120000000.0	kg
Corn required	400500000.0	259200000.0	kg
Acres required	86594.6	56043.2	acre

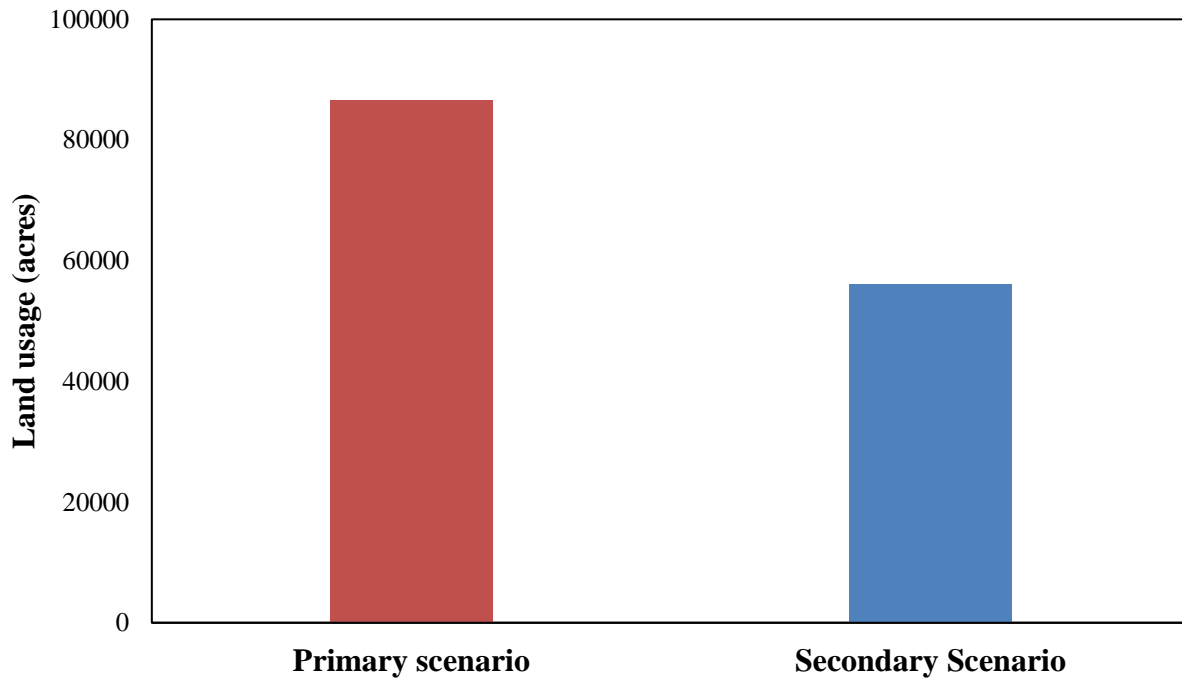


Figure 4-12. Land usage of PLA recycling vs composting

4.3.4.3 Water Use Impact Category

PLA production process involves use of water during all the steps in various forms like irrigation water, process water, steam, heating and cooling water etc. The main step involving highest use of water was corn irrigation. It accounts for 60 % of the total water used in PLA production. The details of water usage for individual steps can be found in **Table 4-23**. Since the corn requirement reduced for the secondary scenario, the water requirement for irrigation was also found to decrease making it more water efficient. (**Figure 4-13**).

Table 4-23. Contribution analysis for water use

	Primary scenario		Secondary scenario	
	kg/kg PLA	% of total contribution	kg/kg PLA	% of total contribution
Corn irrigation	20.92	59.70	16.74	58.18
Corn production	0.48	1.37	0.38	1.33
Dextrose production	6.44	18.38	5.15	17.91
Lactic Acid production	3.47	9.90	2.78	9.65
Lactide production	2.6	7.42	2.08	7.23
PLA production	1.08	3.08	0.86	3.00
Composting	0.05	0.14	0.04	0.14
Recycling	0	0.00	0.74	2.56
Net	35.04	100.00	28.768	100

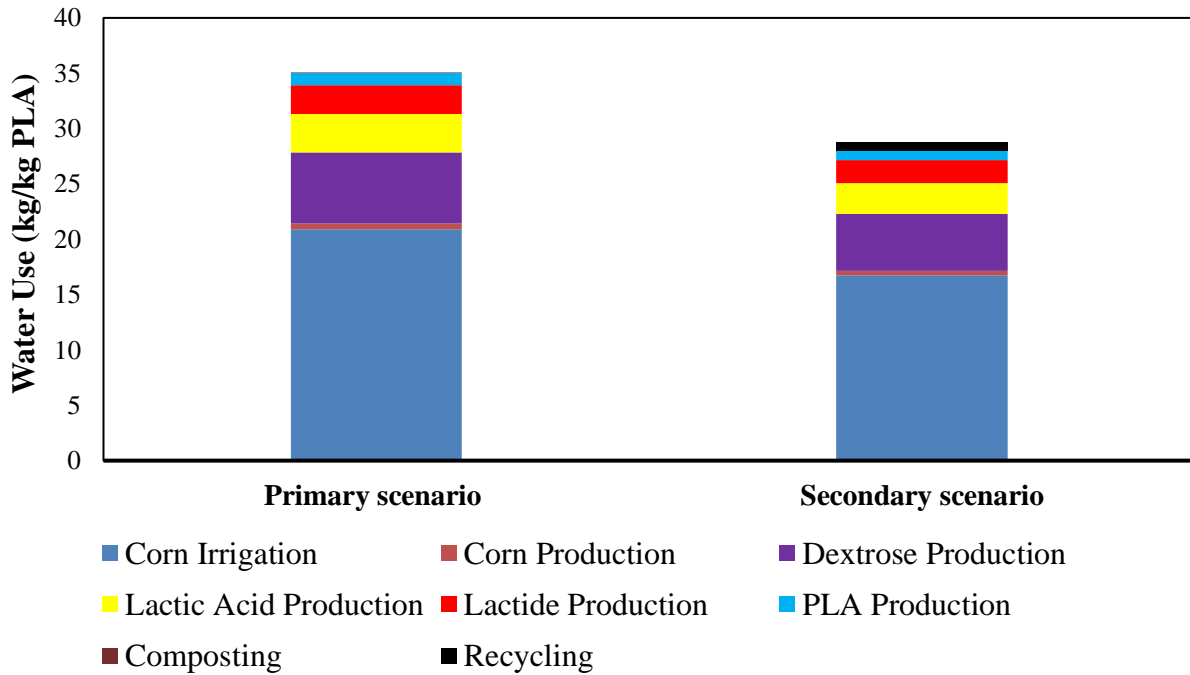


Figure 4-13. Water usage of PLA recycling vs composting

4.3.4.4 Resource Depletion

Table 4-24 shows the cumulative energy consumption and their contribution to total energy consumption in each step of PLA production. The data include all the non-renewable forms of energies used in the process including fossil fuels, gas, diesel, oil, coal and electricity. The major renewable energy involved in the process is sunlight which is 25-28 MJ/kg of PLA and was not considered in the analysis. Lactic acid production step was found to be the most energy intensive process in PLA production accounting for 47% of total energy consumption. For secondary scenario, PLA was converted directly to lactide thus elimination the energy intensive lactic acid production step. Hence, the energy required in this step for secondary scenario was reduced. Although one extra step of energy consumption was added due to the recycling step, it was found to be much less than the lactic acid production step. (**Figure 4-14**)

Table 4-24. Contribution analysis for resource depletion

	Primary scenario		Secondary scenario	
	MJ/kg PLA	% of total contribution	MJ/kg PLA	% of total contribution
Corn production	2.3	6.08	1.84	5.53
Transport	0.8	2.12	0.78	2.35
Dextrose production	4.9	12.96	3.92	11.79
Lactic acid production	18	47.59	14.4	43.30
Lactide production	8.7	23.00	6.96	20.93
PLA production	3.1	8.20	3.1	9.32
Composting	0.02	0.05	0.016	0.05
Recycling	0	0.00	2.242	6.74
Net	37.82	100	33.258	100

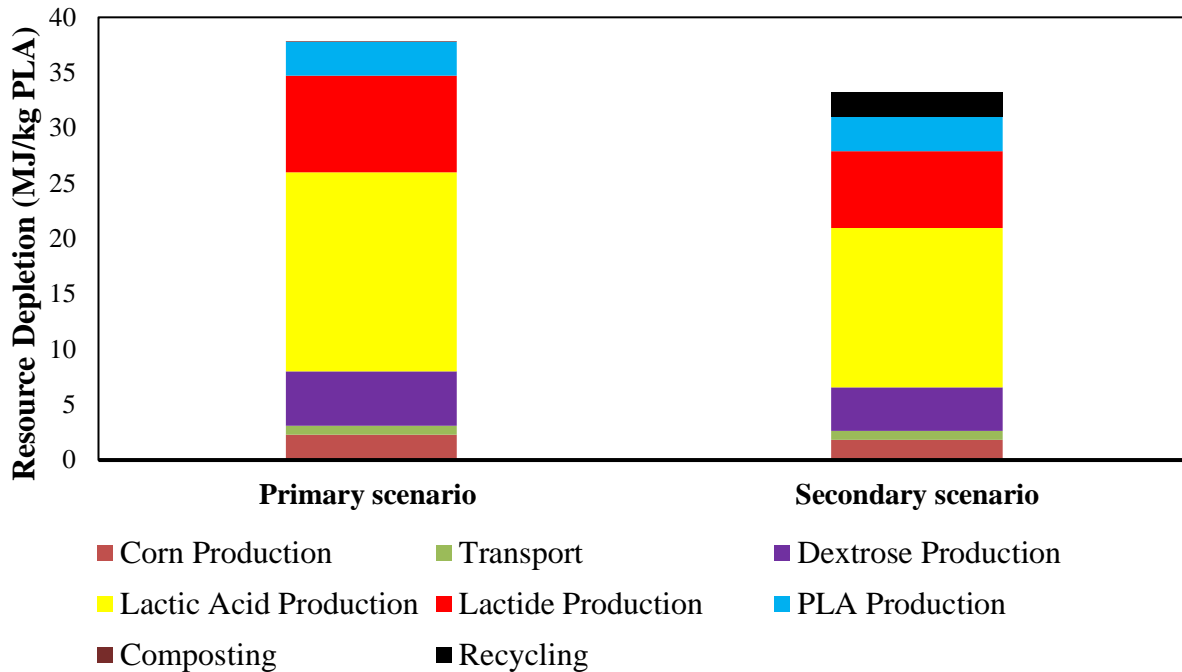


Figure 4-14. Resource depletion for PLA recycling vs composting

4.3.5 Sensitivity Analysis

A sensitivity analysis was done to determine the robustness of the system with respect to the change in the parameters involved. There were two main assumptions made. The first assumption was the percentage of the recycled PLA used. The second assumption was the yield of the corn. By altering the quantities of these variables, the effect of these parameters on the impact categories can be assessed. It can also help us to narrow down the effect of these parameters on specific processes involved in the system. It can also help us to selectively optimize the processes involved in the manufacturing of the PLA

4.3.5.1 Corn Production

The LCI data for production of corn grains were taken from NREL. The corn production data were averaged from the total corn production in the USA. The number of bushels of corn per acre of land grown varies depending on the geography of the area, weather conditions and the

agricultural practices used. Changing the number of bushels of corn grown per acre will reduce the land used for chemical materials production.

4.3.5.2 Percentage of PLA Recycled

The percentage of PLA recycled is an important parameter that will determine all the major design parameters. The first hurdle in determining the exact amount of recycle percentage is the segregation of waste PLA after the use. Waste PLA needs to be collected separately from any other plastic. Presence of other types of plastics can contaminate the PLA in the recycle stage and no longer will it be recyclable. Also, in order to ease the processability of PLA is blended with some other chemicals which in turn causes less amount of PLA recycled at the end of life of PLA. The next issue with PLA recycling is the collection and transport of waste PLA. The recycle plant is located at the manufacturing site. The PLA needs to be collected from various locations around the world and needs to be transported to the manufacturing site. This will cause additional usage of fuels and will impact various categories studied.

4.3.5.3 Sensitivity Analysis for Land Usage

Figure 4-15 shows the effect of recycle percentage and the effect of variation of number of corn bushels grown per acre on the land usage. The number of bushels varied from the best-case scenario of 185 bu/acre to the national average of 179 bu/acre to the worst-case scenario in the past 10 years of 139 bu/acre. As, expected the land usage went down as the number of bushels increased. Also, the effect of recycled PLA on land usage was studied. As the amount of PLA recycled increased, the land usage went down. This is because the amount of corn required for manufacturing new lactide is reduced as the lactide is supplemented from the recycled PLA. The variation of recycled PLA was from 0% to 40%. The amount of PLA recycled cannot be increased

further than 40% due to the difficulties in collecting and transporting PLA. The economic cost of the operation makes the project not viable.

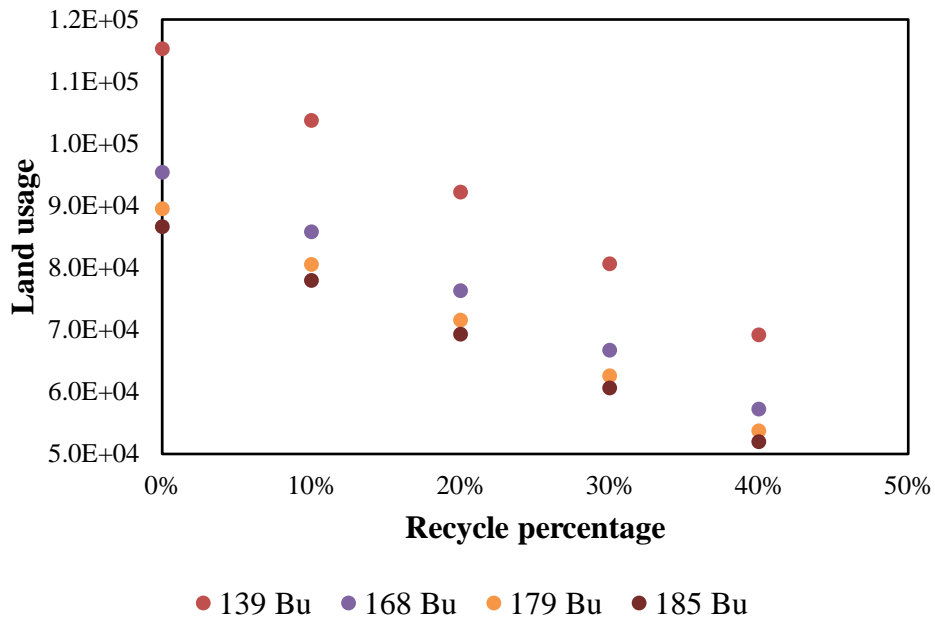


Figure 4-15. Effect of variation in corn production and recycling on land usage

4.3.5.4 Sensitivity Analysis for Water Usage

Figure 4-16 shows the effect of recycle percentage on water usage. As seen from the figure 10 the largest amount of water is used for corn cultivation. This is amount decreases as the amount of corn required for PLA production decreases. This is a major factor in reducing the amount of water required for the whole PLA manufacturing process. The second major component is the dextrose production process. The water usage for that process has been optimized and hence the water requirement for PLA production depends only on amount of corn required for PLA production.

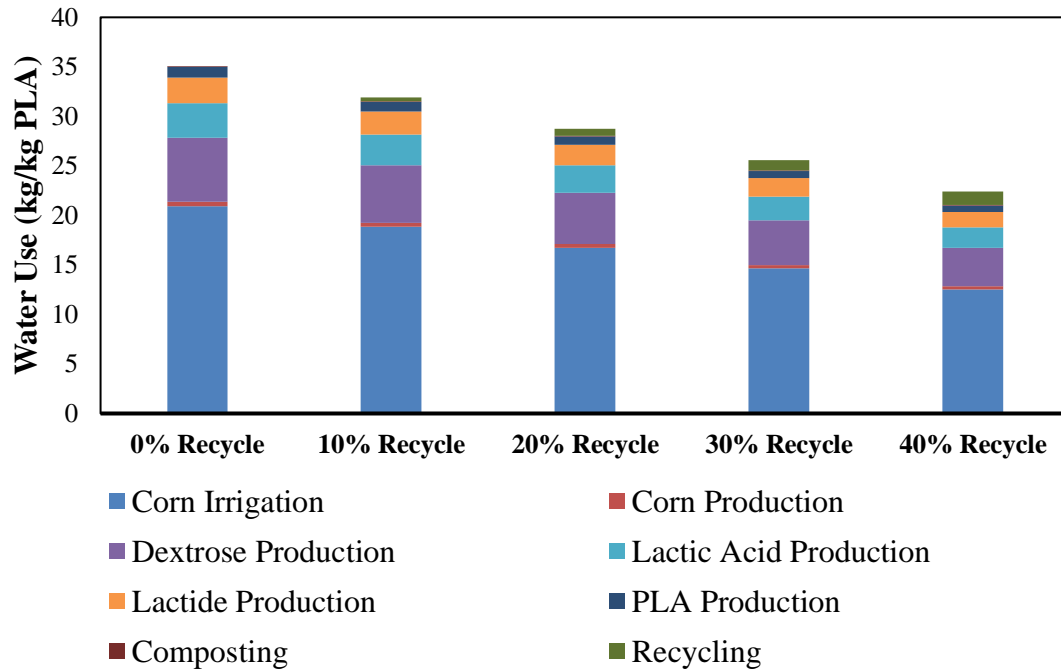


Figure 4-16. Effect of variation in recycling on water usage

4.3.5.5 Sensitivity Analysis for Resource Depletion

Figure 4-17 shows the effect of recycle percentage on resource depletion. The largest amount of resources is used for lactic acid production. The huge amount required is due to the fermentation process required for PLA lactic acid synthesis. The second major step is the lactide production. The drying step involved requires a lot of resources in the form of steam. Lactide needs to be completely dry in order to be used for the next step. This amount decreases as the amount of lactide required for PLA production decreases. This is a major factor in reducing the resources required for the whole PLA manufacturing process. Hence, the resources requirement for PLA production depends only on the initial amount of PLA required for manufacturing process.

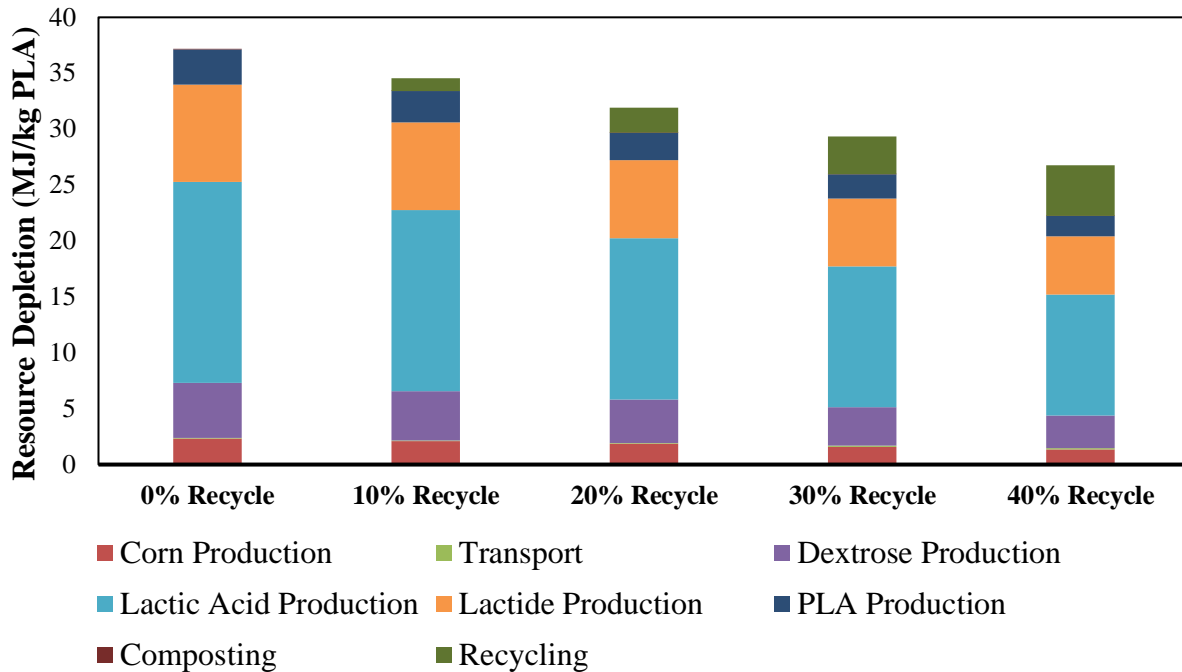


Figure 4-17. Effect of variation in recycling on water usage

4.3.5.6 Sensitivity Analysis for Global Warming Potential

Figure 4-18 shows the effect of recycle percentage on global warming potential. The CO₂ sequestration is a negative amount as it is the amount of carbon dioxide fixed from the atmosphere by corn grains. It also includes the amount that the corn stalk fixes after it has been buried into the ground at the end of life of corn plant. The largest amount of GHG emissions is due to composting and the fuels used for transporting the corn to plant and also for transporting the waste PLA to the recycle plant. As the amount of recycled PLA increases, the corn production goes down and hence the CO₂ sequestered by the corn plants, but it also helps to reduce the CO₂ production in the composting step. As seen from figure 12, the overall GHG emissions decrease as the amount of recycled PLA increases.

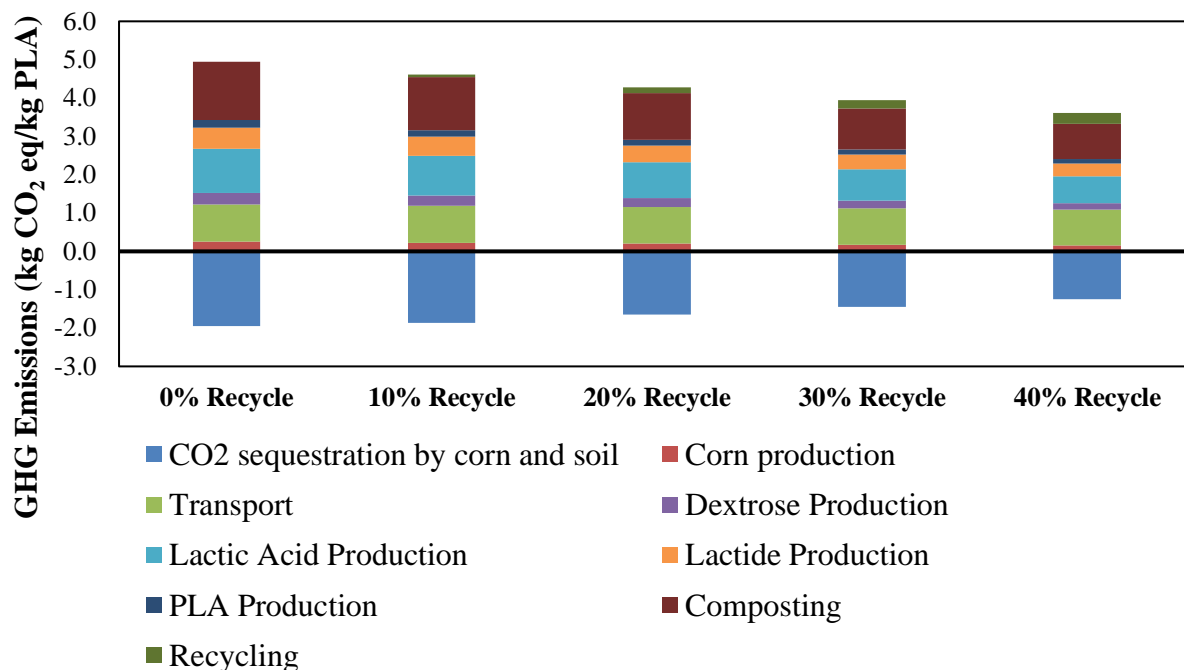


Figure 4-18. Effect of variation in recycling on global warming potential

4.4. Conclusion & Next Steps

A recycling method for PLA via thermodepolymerization has been developed and tested for feasibility. A lab-scale technique was first tested for PLA depolymerization in a reaction vessel. The reaction was then scaled up in a batch reactor to test the scalability of the recycling process. Lactide was first verified using DSC based on the melting peak temperature at ~95-100°C. It was found that the chemical purity and optical purity of the lactide product decreased as a function of temperature; this was due to racemization of PLA depolymerization based on Sn (II) reaction on asymmetrical methine carbon. The yield of lactide was very low, as the reaction was concluded to be of zero-order; the monomer equilibrium concentration reached was less than 10%. The catalyst concentration, particularly of stannous octoate, only speeds up the time to equilibrium, but has no effect on the lactide yield. Suggestions for future work include the use of a co-catalyst such as

triphenylphosphine and initiator such as octanol. Use of these reagents may further increase the monomer equilibrium concentration, or lactide yield, at higher temperatures.

A life-cycle assessment (LCA) study was carried out to assess the environmental impacts of PLA with a cradle-to-gate ending at composting versus recycling. The processes assessed in the life cycle of PLA included corn cultivation, starch refining, dextrose production via hydrolysis, fermentation of lactic acid, conversion to lactide and PLA via ring-opening polymerization, and finally composting or recycling. Life-cycle inventory (LCI) data were taken for both systems with composting and recycling, and it was concluded that material and energy input and output would reduce if recycling PLA was incorporated. In addition, a life-cycle impact assessment was implemented. Assuming 20% of PLA is recycled via thermodepolymerization, key results showed that there was a reduction in land usage, water use, resource depletion, and global warming. A sensitivity analysis was also performed based on the yield of corn and amount of PLA recycled. The sensitivity analyses on all four impact categories reiterated the reduction in environmental impacts that recycling PLA would have. All in all, it has been concluded that recycling PLA is more environmentally sustainable compared to only composting PLA.

Once the PLA recycling efficiency is improved and lactide yield is significantly increased, the next step of this project will involve developing a two-step thermodepolymerization-polymerization procedure (**Figure 4-19**) to recycle PLA in an extruder. The PLA waste would first be heated above melting temperature and depolymerized in an industrial scale batch reactor; this reaction would be in the presence of stannous octoate catalyst and other reagents. The lactide would then be directly pumped into the extruder, which would produce pure PLA via melt polymerization. Based on the results, there may be potential for a scalable infrastructure to recycle PLA for further applications.

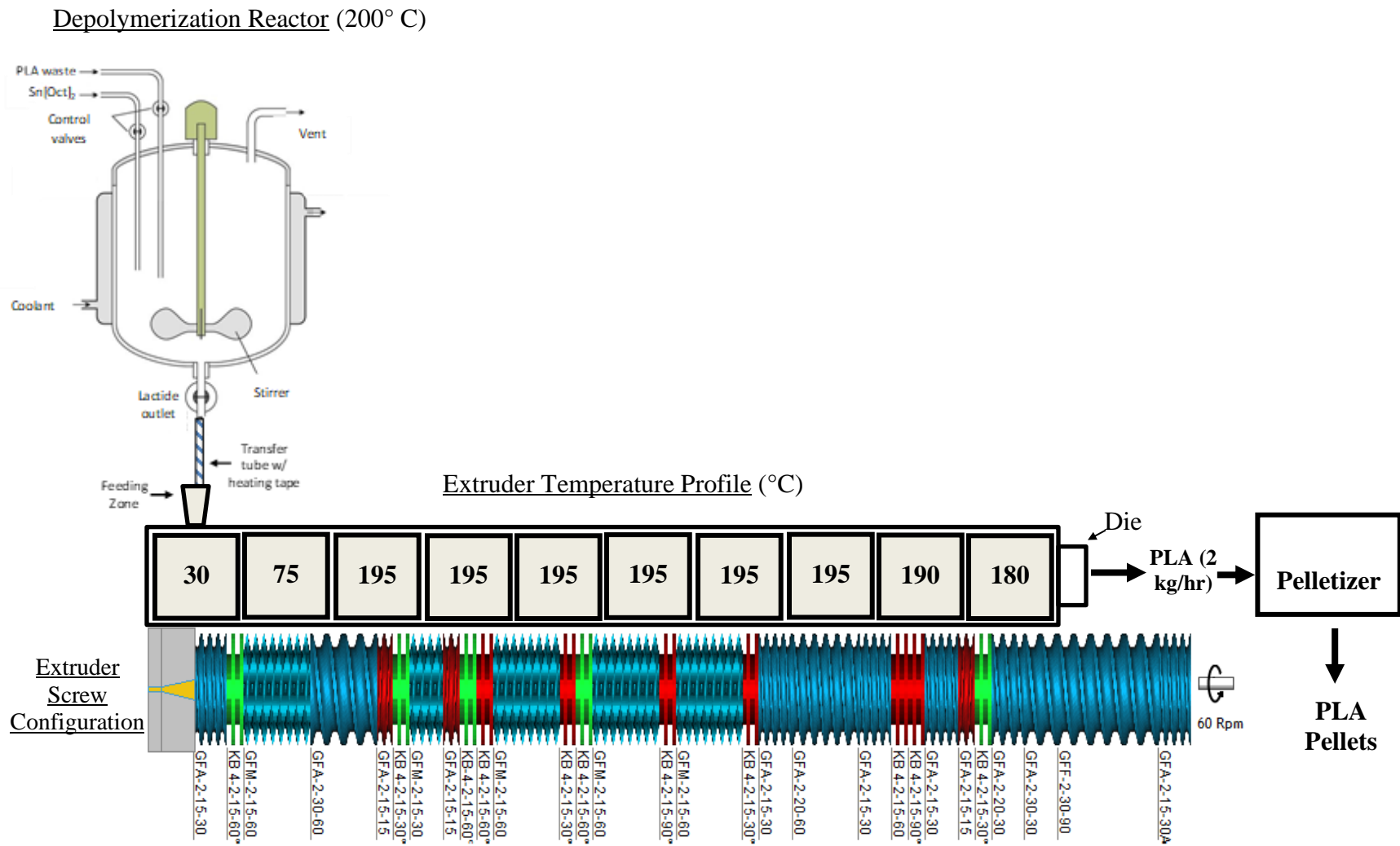


Figure 4-19. Two-step PLA recycling process via thermodepolymerization in a batch reactor, followed by polymerization in a co-rotating twin screw extruder. Diagram includes the temperature profile and screw configuration required to produce high molecular weight PLA from lactide.

5. SUMMARY AND FUTURE WORK

The research conducted behind this thesis has been solely driven by the need for the development of value-added products to expand the commercial application of polylactide (PLA). Understanding the fundamental stereochemistry of PLA and its implication on performance properties is imperative in this discussion. It has been proven in this thesis that modifying the stereochemistry of PLA in turn modifies its crystallinity and thus the material properties of the polymer, determining its product application. Studies on PLA stereochemistry were broken down into three sections – analyzing the effect of PLA stereoisomeric composition on material properties, reactive extrusion of stereocomplex PLA for the development of molecular composites, and thermal recycling of PLA to obtain lactide stereoisomer product.

Chapter 2 focused on characterizing the stereochemistry of PLA and its implication on material performance. We hypothesized that manufacture of lactide monomer yields L-lactide and meso-lactide, with <1% D-lactide, based on statistical analysis. This would typically produce the copolymer poly(L-co-meso-lactide) as opposed to the homopolymers poly(L-lactide) or poly(D-lactide). Using optical rotation analysis and ^1H NMR, we proved our hypothesis in that manufacture of PLA predominantly comprises L-lactide and meso-lactide, with less than 1% D-lactide. The stereochemistry was further explored in its role in tacticity and crystallinity of PLA. Theoretically, poly(meso-lactide) should comprise a syndiotactic structure with *RS* alternating sequences. ^1H NMR disproved this theory and showed that poly(meso-lactide) is predominantly atactic. This is due to random insertion of the meso-lactide chain into the *R* and *S* stereocarbons during ring-opening polymerization via coordination insertion with stannous octoate. ^1H NMR and DSC studies also showed that PLA transitions from a predominantly isotactic, semi-crystalline structure to a predominantly atactic, amorphous structure at 10-20% meso-lactide content. Finally

tensile testing results conclude that an increase in meso-lactide content leads to a 65% increase in the elastic modulus, a 48% decrease in the modulus of resilience and toughness, and a slight decrease (<10%) in the yield strength and ultimate tensile strength. This chapter provides readers a comprehensive understanding of the role PLA stereochemistry can play in the material properties, determining the final application of the product (i.e.: packaging, sutures, utensils, bags, etc.).

Chapter 3 continued studies in PLA stereochemistry with a focus on PLA stereocomplexation. A pilot-scale continuous manufacturing setup was first developed to produce stereocomplex PLA via reactive extrusion of high molecular weight PLLA and PDLA. The characteristics of stereocomplex formation were characterized to optimize the processing conditions for high formation of stereocomplex PLA. More specifically, the effect of temperature and time on PLA stereocomplexation was characterized via DSC. It was concluded that stereocomplexation is a temperature-driven process, and that time does not play a role; it is thermodynamically driven and thermally unstable above its melting peak temperature ($\sim 230^{\circ}\text{C}$). Up to 95% stereocomplex formation was achieved, with a total crystallinity ranging from $X_c = 56\text{-}63\%$ and peak melting temperature of $T_{\text{pm}} = 240^{\circ}\text{C}$.

Stereocomplex PLA was then characterized as a potential reinforcing filler and nucleating agent for PLLA homopolymer. Molecular composites comprising stereocomplex PLA particles in a thermoplastic PLA matrix were developed at different compositions. A 25-35% increase was observed in the yield strength, ultimate tensile strength, and elastic modulus for semi-crystalline PLA and amorphous PLA comprising 30% stereocomplex PLA particles. A 30% increase and 40% increase in the modulus of resilience was observed for semi-crystalline PLA and amorphous PLA, respectively. This is due to the excellent adhesion between the particles and the matrix, as well as

good distribution of the particles in the matrix. The isothermal crystallization kinetics were finally studied on neat semi-crystalline PLA versus semi-crystalline PLA comprising 5% stereocomplex PLA particles. Without a nucleating agent, it takes up to 14.4 minutes minimum to achieve half-time to crystallization of PLA. Using stereocomplex PLA, a half-time to crystallization as low as 1.06 minutes was achieved; two-dimensional crystal growth was observed. Compared to talc, the commercial nucleating agent used in PLA, stereocomplex PLA is an organic, biobased, biodegradable additive that can be used. In addition, it reinforces the mechanical properties of PLA, whereas talc reduces tensile properties such as the ultimate tensile strength and resilience. We see potential application of stereocomplex PLA as melt-spun fibers for textiles or coffee cups due to their high melting point.

Chapter 4 concludes this thesis with the development of a pilot-scale setup to thermally recycle PLA in a batch reactor using stannous octoate. The depolymerization kinetics were first characterized, and results showed that the lactide yield was very low (5-7%) no matter the temperature, time, or catalyst concentration. The reaction was determined to be of zero-order rate, proceeding very slowly. The chemical purity and optical purity of the lactide product were also determined, and it was concluded that the purities decrease as reaction temperature increases. This is due to racemization from formation of meso-lactide, as characterized by gas chromatography-polarimetry. A life-cycle assessment study was also carried out to assess the environmental impacts of PLA with a cradle-to-gate ending at composting versus recycling. Assuming 20% of PLA is recycled via thermo-depolymerization, key results showed that there was a reduction in land usage, water use, resource depletion, and global warming. Sensitivity analyses reiterated our results. We concluded that recycling PLA is more environmentally sustainable compared to only composting PLA.

Future work should further explore PLA stereochemistry on the subjects discussed. As opposed to only copolymerizing L-lactide and D-lactide, or meso-lactide, future studies should focus on copolymerization of all three stereoisomers at various compositions. The tacticity, crystallinity, thermal properties, and mechanical properties of these synthesized copolymers should be characterized. This will give researchers a better understanding on how to fine-tune the material properties of PLA by modifying its stereoisomeric composition. For example, if one wanted to achieve a more elastic polymer with high resilience for application in utensils or bags, one would want to develop PLA of high crystallinity by minimizing the amount of meso-lactide in PLLA. However, if one wanted to form a sealant layer for biaxially oriented PLA film, amorphous PLA can be coextruded with other PLA resin to achieve this. The applications are wide-ranged.

In terms of stereocomplex PLA, future work should focus on modifying the continuous manufacturing setup of stereocomplex PLA to produce melt-spun fibers of stereocomplex PLA. More particularly, the die head of the extruder can be changed from a strand die to a fiber die for stereocomplex PLA fiber productions. The fibers will be used to manufacture molecular composites comprising several compositions of stereocomplex PLA filler in PLA matrix. The material properties and crystallization kinetics should be analyzed and compared with talc filler. Thermal recycling of PLA needs to be optimized further to obtain a higher lactide yield. A cost-effective, reactive catalyst must be proposed to accelerate the depolymerization process of PLA and obtain a high lactide yield. Once this is achieved, a two-step depolymerization-polymerization process will be proposed to thermally recycle PLA waste back to neat PLA. The waste would be heated in a batch reactor, which would pump the lactide product into the extruder for polymerization to pure PLA. In conclusion, there is much to be further explored and studied in the field of PLA stereochemistry.

BIBLIOGRAPHY

BIBLIOGRAPHY

- [1] D. K. A. Barnes and P. Milner, “Drifting plastic and its consequences for sessile organism dispersal in the Atlantic Ocean,” *Mar. Biol.*, vol. 146, no. 4, pp. 815–825, 2005, doi: 10.1007/s00227-004-1474-8.
- [2] J. Hopewell, R. Dvorak, and E. Kosior, “Plastics recycling: challenges and opportunities,” *Philos. Trans. R. Soc. B Biol. Sci.*, vol. 364, no. 1526, pp. 2115–2126, Jul. 2009, doi: 10.1098/rstb.2008.0311.
- [3] J. G. . Derraik, “The pollution of the marine environment by plastic debris: a review,” *Mar. Pollut. Bull.*, vol. 44, no. 9, pp. 842–852, Sep. 2002, doi: 10.1016/S0025-326X(02)00220-5.
- [4] “Marine Debris is Everyone’s Problem,” 2021. <https://marinedebris.noaa.gov/poster/marine-debris-everyones-problem>.
- [5] S. Rathi, “Alternative approaches for better municipal solid waste management in Mumbai, India,” *Waste Manag.*, vol. 26, no. 10, pp. 1192–1200, Jan. 2006, doi: 10.1016/j.wasman.2005.09.006.
- [6] R. Verma, K. S. Vinoda, M. Papireddy, and A. N. S. Gowda, “Toxic Pollutants from Plastic Waste- A Review,” *Procedia Environ. Sci.*, vol. 35, pp. 701–708, 2016, doi: 10.1016/j.proenv.2016.07.069.
- [7] G. S. A. N. Miguel, U. Rey, and J. Carlos, “European trends in the feedstock recycling of plastic wastes,” *Glob. NEST J.*, vol. 9, no. 1, pp. 12–19, 2018, doi: 10.30955/gnj.000432.
- [8] S. Mudgal, L. Lyons, and J. Bain, “Plastic Waste in the Environment – Revised Final Report for European Commission DG Environment. BioIntelligence Service,” 2011. [Online]. Available: <http://www.ec.europa.eu/environment/waste/studies/pdf/plastics.pdf>.
- [9] L. A. Hamilton *et al.*, “Plastics and climate: The hidden costs of a plastic planet,” 2019.
- [10] United Nations, “Transforming Our World: The 2030 Agenda for Sustainable Development,” *A New Era in Global Health*, 2018.
- [11] “PlasticsEurope Plastics—The Facts,” 2020. <https://plasticseurope.org/knowledge-hub/plastics-the-facts-2021/>.
- [12] G. Roland, J. J. R., and L. K. Lavender, “Production, use, and fate of all plastics ever made,” *Sci. Adv.*, vol. 3, no. 7, p. e1700782, Nov. 2021, doi: 10.1126/sciadv.1700782.
- [13] “UNEP Environment Programme - Beat Plastic Pollution,” *UNEP*.

<https://www.unep.org/interactives/beat-plastic-pollution/>.

- [14] F. Gallo *et al.*, “Marine litter plastics and microplastics and their toxic chemicals components: the need for urgent preventive measures,” *Environ. Sci. Eur.*, vol. 30, no. 1, p. 13, 2018, doi: 10.1186/s12302-018-0139-z.
- [15] “Drowning in Plastics – Marine Litter and Plastic Waste Vital Graphics,” 2021. [Online]. Available: <https://www.unep.org/resources/report/drowning-plastics-marine-litter-and-plastic-waste-vital-graphics>.
- [16] R. Narayan, “Carbon footprint of bioplastics using biocarbon content analysis and life-cycle assessment,” *MRS Bull.*, vol. 36, no. 9, pp. 716–721, Sep. 2011, doi: 10.1557/mrs.2011.210.
- [17] R. Narayan, “Biobased and Biodegradable Polymer Materials: Rationale, Drivers, and Technology Exemplars,” in *Degradable Polymers and Materials*, vol. 939, American Chemical Society, 2006, pp. 282–306.
- [18] R. Narayan, “Biobased & Biodegradable Plastics: Rationale, Drivers, and Technology Exemplars,” in *Degradable Polymers and Materials: Principles and Practice (2nd Edition)*, vol. 1114, American Chemical Society, 2012, pp. 2–13.
- [19] M. Jamshidian, E. A. Tehrani, M. Imran, M. Jacquot, and S. Desobry, “Poly-Lactic Acid: Production, Applications, Nanocomposites, and Release Studies,” *Compr. Rev. Food Sci. Food Saf.*, vol. 9, no. 5, pp. 552–571, Aug. 2010, doi: 10.1111/j.1541-4337.2010.00126.x.
- [20] K. W. Meereboer, M. Misra, and A. K. Mohanty, “Review of recent advances in the biodegradability of polyhydroxyalkanoate (PHA) bioplastics and their composites,” *Green Chem.*, vol. 22, no. 17, pp. 5519–5558, 2020, doi: 10.1039/D0GC01647K.
- [21] S. A. Rafiqah *et al.*, “A Review on Properties and Application of Bio-Based Poly(Butylene Succinate),” *Polymers*, vol. 13, no. 9. 2021, doi: 10.3390/polym13091436.
- [22] R. Jumaidin, S. N. Mohd Zainel, and S. M. Sapuan, “Chapter 2 - Processing of Thermoplastic Starch,” in *Advanced Processing, Properties, and Applications of Starch and Other Bio-Based Polymers*, F. M. Al-Oqla and S. M. B. T.-A. P. Sapuan Properties, and Applications of Starch and Other Bio-Based Polymers, Eds. Elsevier, 2020, pp. 11–19.
- [23] M. Winnacker and B. Rieger, “Biobased Polyamides: Recent Advances in Basic and Applied Research,” *Macromol. Rapid Commun.*, vol. 37, no. 17, pp. 1391–1413, Sep. 2016, doi: 10.1002/marc.201600181.
- [24] V. Siracusa and I. Blanco, “Bio-polyethylene (Bio-PE), Bio-polypropylene (Bio-PP) and Bio-poly(ethylene terephthalate) (Bio-PET): Recent developments in bio-based polymers analogous to petroleum-derived ones for packaging and engineering applications,”

- Polymers (Basel)*., vol. 12, no. 8, 2020, doi: 10.3390/APP10155029.
- [25] L. Jiang and J. Zhang, “Biodegradable and Biobased Polymers,” in *Applied Plastics Engineering Handbook*, M. B. T.-A. P. E. H. (Second E. Kutz, Ed. Elsevier, 2017, pp. 127–143.
- [26] M. Labet and W. Thielemans, “Synthesis of polycaprolactone: a review.,” *Chem. Soc. Rev.*, vol. 38, no. 12, pp. 3484–3504, Dec. 2009, doi: 10.1039/b820162p.
- [27] F. V Ferreira, L. S. Cividanes, R. F. Gouveia, and L. M. F. Lona, “An overview on properties and applications of poly(butylene adipate- co -terephthalate)-PBAT based composites,” *Polym. Eng. Sci.*, vol. 59, no. s2, pp. E7–E15, Mar. 2019, doi: 10.1002/pen.24770.
- [28] M. Aslam, M. A. Kalyar, and Z. A. Raza, “Polyvinyl alcohol: A review of research status and use of polyvinyl alcohol based nanocomposites,” *Polym. Eng. Sci.*, vol. 58, no. 12, pp. 2119–2132, Dec. 2018, doi: 10.1002/pen.24855.
- [29] European Bioplastics E.V., “Bioplastics,” 2018. <https://www.european-bioplastics.org/>.
- [30] A. Di Bartolo, G. Infurna, and N. T. Dintcheva, “A review of bioplastics and their adoption in the circular economy,” *Polymers (Basel)*., vol. 13, no. 8, 2021, doi: 10.3390/polym13081229.
- [31] “D6866-22 - Standard Test Methods for Determining the Biobased Content of Solid, Liquid, and Gaseous Samples Using Radiocarbon Analysis.” ASTM, pp. 1–19, 2022, doi: 10.1520/D6400-19.
- [32] S. A. Ashter, “Overview of Biodegradable Polymers,” in *Introduction to Bioplastics Engineering*, S. A. B. T.-I. to B. E. Ashter, Ed. Oxford: Elsevier, 2016, pp. 19–30.
- [33] R. Narayan, “The Promise of Bioplastics - Bio-Based and Biodegradable-Compostable Plastics,” in *Bio-Based Plastics*, Chichester, UK: John Wiley & Sons Ltd, 2013, pp. 347–357.
- [34] “EN 13432- Certified Bioplastics Performance in Industrial Composting.” European Standards, pp. 1–5, 2015.
- [35] “EN 14995 - Plastics - Evaluation of compostability - Test scheme and specifications.” European Standards, pp. 1–24, 2006.
- [36] “ISO 17088:2021- Plastics — Organic recycling — Specifications for compostable plastics.” ISO, pp. 1–21, 2021.
- [37] “D6400-04- Standard Specification for Compostable Plastics.” ASTM International, pp. 1–3, 2004.

- [38] R. Narayan, "Biodegradability... Sorting through Facts and Claims," *Bioplastics Mag.*, vol. 4, 2009, [Online]. Available: [http://www.bpiworld.org/resources/Documents/Narayan Bioplastics Article 2009.pdf](http://www.bpiworld.org/resources/Documents/Narayan%20Bioplastics%20Article%202009.pdf).
- [39] A. P. Gupta and V. Kumar, "New emerging trends in synthetic biodegradable polymers – Polylactide: A critique," *Eur. Polym. J.*, vol. 43, no. 10, pp. 4053–4074, Oct. 2007, doi: 10.1016/j.eurpolymj.2007.06.045.
- [40] D. R. Witzke, R. Narayan, and J. J. Kolstad, "Reversible kinetics and thermodynamics of the homopolymerization of L-lactide with 2-ethylhexanoic acid Tin(II) salt," *Macromolecules*, vol. 30, no. 23, pp. 7075–7085, 1997, doi: 10.1021/ma970631m.
- [41] E. T. H. Vink, K. R. Rábago, D. A. Glassner, and P. R. Gruber, "Applications of life cycle assessment to NatureWorks™ polylactide (PLA) production," *Polym. Degrad. Stab.*, vol. 80, no. 3, pp. 403–419, Jan. 2003, doi: 10.1016/S0141-3910(02)00372-5.
- [42] W. J. Groot and T. Borén, "Life cycle assessment of the manufacture of lactide and PLA biopolymers from sugarcane in Thailand," *Int. J. Life Cycle Assess.*, vol. 15, no. 9, pp. 970–984, Nov. 2010, doi: 10.1007/s11367-010-0225-y.
- [43] G. Liu, J. Sun, J. Zhang, Y. Tu, and J. Bao, "High titer l-lactic acid production from corn stover with minimum wastewater generation and techno-economic evaluation based on Aspen plus modeling," *Bioresour. Technol.*, vol. 198, pp. 803–810, 2015, doi: 10.1016/j.biortech.2015.09.098.
- [44] L. T. Sin, *Polylactic Acid - A Practical Guide for the Processing, Manufacturing, and Applications of PLA (2nd Edition)*, 2nd ed. Elsevier, 2019.
- [45] L. Feng *et al.*, "Determination of D-lactide content in lactide stereoisomeric mixture using gas chromatography-polarimetry," *Talanta*, vol. 164, no. August 2016, pp. 268–274, Mar. 2017, doi: 10.1016/j.talanta.2016.11.038.
- [46] K. A. M. Thakur, R. T. Kean, E. S. Hall, M. A. Doscotch, and E. J. Munson, "A Quantitative Method for Determination of Lactide Composition in Poly(lactide) Using ¹H NMR," *Anal. Chem.*, vol. 69, no. 21, pp. 4303–4309, Nov. 1997, doi: 10.1021/ac970792o.
- [47] L. E. Chile, P. Mehrkhodavandi, and S. G. Hatzikiriakos, "A Comparison of the Rheological and Mechanical Properties of Isotactic, Syndiotactic, and Heterotactic Poly(lactide)," *Macromolecules*, vol. 49, no. 3, pp. 909–919, 2016, doi: 10.1021/acs.macromol.5b02568.
- [48] F. E. Kohn, J. W. A. Van Den Berg, G. Van De Ridder, and J. Feijen, "The ring-opening polymerization of D,L-lactide in the melt initiated with tetraphenyltin," *J. Appl. Polym. Sci.*, vol. 29, no. 12, pp. 4265–4277, 1984, doi: 10.1002/app.1984.070291255.

- [49] T. Tsukegi, T. Motoyama, Y. Shirai, H. Nishida, and T. Endo, “Racemization behavior of l,l-lactide during heating,” *Polym. Degrad. Stab.*, vol. 92, no. 4, pp. 552–559, Apr. 2007, doi: 10.1016/j.polymdegradstab.2007.01.009.
- [50] Natureworks, “High-Performance Ingeo Grades,” 2017. [Online]. Available: https://www.natureworkslc.com/~media/Files/NatureWorks/Technical-Documents/One-Pagers/natureworks_high-performance-ingeo_nonwovens_pdf.pdf.
- [51] T. P. Haider, C. Völker, J. Kramm, K. Landfester, and F. R. Wurm, “Plastics of the Future? The Impact of Biodegradable Polymers on the Environment and on Society,” *Angew. Chemie Int. Ed.*, vol. 58, no. 1, pp. 50–62, Jan. 2019, doi: 10.1002/anie.201805766.
- [52] M. Karamanlioglu, A. Houlden, and G. D. Robson, “Isolation and characterisation of fungal communities associated with degradation and growth on the surface of poly(lactic) acid (PLA) in soil and compost,” *Int. Biodeterior. Biodegradation*, vol. 95, pp. 301–310, Nov. 2014, doi: 10.1016/j.ibiod.2014.09.006.
- [53] M. Karamanlioglu and G. D. Robson, “The influence of biotic and abiotic factors on the rate of degradation of poly(lactic) acid (PLA) coupons buried in compost and soil,” *Polym. Degrad. Stab.*, vol. 98, no. 10, pp. 2063–2071, Oct. 2013, doi: 10.1016/j.polymdegradstab.2013.07.004.
- [54] H. Y. Sintim *et al.*, “In situ degradation of biodegradable plastic mulch films in compost and agricultural soils,” *Sci. Total Environ.*, vol. 727, p. 138668, Jul. 2020, doi: 10.1016/j.scitotenv.2020.138668.
- [55] E. Castro-Aguirre, F. Iñiguez-Franco, H. Samsudin, X. Fang, and R. Auras, “Poly(lactic acid)—Mass production, processing, industrial applications, and end of life,” *Adv. Drug Deliv. Rev.*, vol. 107, pp. 333–366, 2016, doi: 10.1016/j.addr.2016.03.010.
- [56] N. Kawashima, T. Yagi, and K. Kojima, “Pilot-Scale Composting Test of Polylactic Acid for Social Implementation,” *Sustainability*, vol. 13, no. 4, p. 1654, 2021, doi: 10.3390/su13041654.
- [57] F. Dadaser-Celik, S. T. Azgin, and Y. S. Yildiz, “Optimization of solid content, carbon/nitrogen ratio and food/inoculum ratio for biogas production from food waste,” *Waste Manag. Res.*, vol. 34, no. 12, pp. 1241–1248, 2016, doi: 10.1177/0734242X16659922.
- [58] X. Quecholac-Piña, M. D. C. Hernández-Berriel, M. D. C. Mañón-Salas, R. M. Espinosa-Valdemar, and A. Vázquez-Morillas, “Degradation of plastics under anaerobic conditions: A short review,” *Polymers (Basel)*, vol. 12, no. 1, pp. 1–18, 2020, doi: 10.3390/polym12010109.
- [59] A. Shrestha, M. C. A. A. van-Eerten Jansen, and B. Acharya, “Biodegradation of

- bioplastic using anaerobic digestion at retention time as per industrial biogas plant and international norms,” *Sustain.*, vol. 12, no. 10, 2020, doi: 10.3390/su12104231.
- [60] M. Nazareth, M. R. C. Marques, M. C. A. Leite, and Í. B. Castro, “Commercial plastics claiming biodegradable status: Is this also accurate for marine environments?,” *J. Hazard. Mater.*, vol. 366, pp. 714–722, Mar. 2019, doi: 10.1016/j.jhazmat.2018.12.052.
- [61] A. R. Bagheri, C. Laforsch, A. Greiner, and S. Agarwal, “Fate of So-Called Biodegradable Polymers in Seawater and Freshwater,” *Glob. Challenges*, vol. 1, no. 4, p. 1700048, Jul. 2017, doi: 10.1002/gch2.201700048.
- [62] M. Hong and E. Y.-X. Chen, “Chemically recyclable polymers: a circular economy approach to sustainability,” *Green Chem.*, vol. 19, no. 16, pp. 3692–3706, 2017, doi: 10.1039/C7GC01496A.
- [63] P. McKeown and M. D. Jones, “The Chemical Recycling of PLA: A Review,” *Sustain. Chem.*, vol. 1, no. 1, pp. 1–22, 2020, doi: 10.3390/suschem1010001.
- [64] T. Casalini, F. Rossi, A. Castrovinci, and G. Perale, “A Perspective on Polylactic Acid-Based Polymers Use for Nanoparticles Synthesis and Applications,” *Front. Bioeng. Biotechnol.*, vol. 7, no. October, pp. 1–16, 2019, doi: 10.3389/fbioe.2019.00259.
- [65] N. F. Zaaba and M. Jaafar, “A review on degradation mechanisms of polylactic acid: Hydrolytic, photodegradative, microbial, and enzymatic degradation,” *Polym. Eng. Sci.*, vol. 60, no. 9, pp. 2061–2075, 2020, doi: 10.1002/pen.25511.
- [66] A. Kalendova, J. Smotek, P. Stloukal, M. Kracalik, M. Slouf, and S. Laske, “Transport Properties of Poly(lactic acid)/Clay Nanocomposites,” *Polym. Eng. Sci.*, vol. 59, no. 12, pp. 2498–2501, Dec. 2019, doi: 10.1002/pen.25251.
- [67] F. M. I. Franco, “Hydrolytic degradation of Neat and Modified Poly(lactic acid) with Nanoparticles and Chain Extenders by Water-Ethanol Solutions,” Michigan State University, 2018.
- [68] M. A. Elsayy, K.-H. Kim, J.-W. Park, and A. Deep, “Hydrolytic degradation of polylactic acid (PLA) and its composites,” *Renew. Sustain. Energy Rev.*, vol. 79, pp. 1346–1352, Nov. 2017, doi: 10.1016/j.rser.2017.05.143.
- [69] P. C. Mayekar, E. Castro-Aguirre, R. Auras, S. Selke, and R. Narayan, “Effect of nano-clay and surfactant on the biodegradation of poly(lactic acid) films,” *Polymers (Basel)*, vol. 12, no. 2, pp. 1–16, 2020, doi: 10.3390/polym12020311.
- [70] X. Shi, “Design and engineering of biobased materials – Process engineering and thermal recycling of poly(lactic acid), and studies in functional silane and siloxane,” Michigan State University, 2014.

- [71] L. Feng, S. Feng, X. Bian, G. Li, and X. Chen, “Pyrolysis mechanism of Poly(lactic acid) for giving lactide under the catalysis of tin,” *Polym. Degrad. Stab.*, vol. 157, pp. 212–223, 2018, doi: 10.1016/j.polymdegradstab.2018.10.008.
- [72] K. J. Jem and B. Tan, “The development and challenges of poly (lactic acid) and poly (glycolic acid),” *Adv. Ind. Eng. Polym. Res.*, vol. 3, no. 2, pp. 60–70, Apr. 2020, doi: 10.1016/j.aiepr.2020.01.002.
- [73] V. DeStefano, S. Khan, and A. Tabada, “Applications of PLA in modern medicine,” *Eng. Regen.*, vol. 1, pp. 76–87, 2020, doi: 10.1016/j.engreg.2020.08.002.
- [74] A. Gregor *et al.*, “Designing of PLA scaffolds for bone tissue replacement fabricated by ordinary commercial 3D printer,” *J. Biol. Eng.*, vol. 11, no. 1, p. 31, Dec. 2017, doi: 10.1186/s13036-017-0074-3.
- [75] V. Nagarajan, A. K. Mohanty, and M. Misra, “Perspective on Polylactic Acid (PLA) based Sustainable Materials for Durable Applications: Focus on Toughness and Heat Resistance,” *ACS Sustain. Chem. Eng.*, vol. 4, no. 6, pp. 2899–2916, Jun. 2016, doi: 10.1021/acssuschemeng.6b00321.
- [76] M. Z. Mulla, M. R. Rahman, B. Marcos, B. Tiwari, and S. Pathania, “Poly Lactic Acid (PLA) Nanocomposites: Effect of Inorganic Nanoparticles Reinforcement on Its Performance and Food Packaging Applications,” *Molecules*, vol. 26, no. 7, 2021, doi: 10.3390/molecules26071967.
- [77] B. M. Chamberlain, M. Cheng, D. R. Moore, T. M. Ovitt, E. B. Lobkovsky, and G. W. Coates, “Polymerization of lactide with zinc and magnesium β -diiminato complexes: Stereocontrol and mechanism,” *J. Am. Chem. Soc.*, vol. 123, no. 14, pp. 3229–3238, 2001, doi: 10.1021/ja003851f.
- [78] J. Lunt, “Large-scale production, properties and commercial applications of polylactic acid polymers,” *Polym. Degrad. Stab.*, vol. 59, no. 1–3, pp. 145–152, Jan. 1998, doi: 10.1016/S0141-3910(97)00148-1.
- [79] J. Ahmed and S. K. Varshney, “Polylactides—Chemistry, Properties and Green Packaging Technology: A Review,” *Int. J. Food Prop.*, vol. 14, no. 1, pp. 37–58, Jan. 2011, doi: 10.1080/10942910903125284.
- [80] C. M. B. Goncalves, J. A. P. Coutinho, and I. M. Marrucho, *Poly(Lactic Acid): Optical Properties*. Hoboken, NJ, USA: John Wiley & Sons, Inc., 2010.
- [81] H. Tsuji and Y. Ikada, “Stereocomplex formation between enantiomeric poly(lactic acid)s. X. Binary blends from poly(D-lactide-CO-glycolide) and poly(L-lactide-CO-glycolide),” *J. Appl. Polym. Sci.*, vol. 53, no. 8, pp. 1061–1071, Aug. 1994, doi: 10.1002/app.1994.070530808.

- [82] H. Tsuji and Y. Ikada, "Crystallization from the melt of poly(lactide)s with different optical purities and their blends," *Macromol. Chem. Phys.*, vol. 197, no. 10, pp. 3483–3499, Oct. 1996, doi: 10.1002/macp.1996.021971033.
- [83] D.-K. Yoo and D. Kim, "Production of optically pure poly(lactic acid) from lactic acid," *Polym. Bull.*, vol. 63, no. 5, pp. 637–651, Nov. 2009, doi: 10.1007/s00289-009-0115-2.
- [84] M. Wisniewski, A. Le Borgne, and N. Spassky, "Synthesis and properties of (D)- and (L)-lactide stereocopolymers using the system achiral Schiff's base/aluminium methoxide as initiator," *Macromol. Chem. Phys.*, vol. 198, no. 4, pp. 1227–1238, Apr. 1997, doi: 10.1002/macp.1997.021980424.
- [85] L.-E. Chile, P. Mehrkhodavandi, and S. G. Hatzikiriakos, "A Comparison of the Rheological and Mechanical Properties of Isotactic, Syndiotactic, and Heterotactic Poly(lactide)," *Macromolecules*, vol. 49, no. 3, pp. 909–919, Feb. 2016, doi: 10.1021/acs.macromol.5b02568.
- [86] F. E. Kohn, J. W. A. Van Den Berg, G. Van De Ridder, and J. Feijen, "The ring-opening polymerization of D,L-lactide in the melt initiated with tetraphenyltin," *J. Appl. Polym. Sci.*, vol. 29, no. 12, pp. 4265–4277, Dec. 1984, doi: 10.1002/app.1984.070291255.
- [87] G. Gorrasi and R. Pantani, "Effect of PLA grades and morphologies on hydrolytic degradation at composting temperature: Assessment of structural modification and kinetic parameters," *Polym. Degrad. Stab.*, vol. 98, no. 5, pp. 1006–1014, May 2013, doi: 10.1016/j.polymdegradstab.2013.02.005.
- [88] T. Standau, C. Zhao, S. Murillo Castellón, C. Bonten, and V. Altstädt, "Chemical Modification and Foam Processing of Polylactide (PLA)," *Polymers (Basel)*, vol. 11, no. 2, p. 306, Feb. 2019, doi: 10.3390/polym11020306.
- [89] M. Cristea, D. Ionita, and M. M. Iftime, "Dynamic Mechanical Analysis Investigations of PLA-Based Renewable Materials: How Are They Useful?," *Materials (Basel)*, vol. 13, no. 22, p. 5302, Nov. 2020, doi: 10.3390/ma13225302.
- [90] K. Cink, J. Smith, J. Nangeroni, and J. R. Randall, "Extruded Polylactide Foams Blown with Carbon Dioxide. Patent EP1735373 B1," 2006.
- [91] Á. Kmetty and K. Litauszki, "Development of Poly (Lactide Acid) Foams with Thermally Expandable Microspheres," *Polymers (Basel)*, vol. 12, no. 2, p. 463, Feb. 2020, doi: 10.3390/polym12020463.
- [92] S. Hajba and T. Tábi, "Cross Effect of Natural Rubber and Annealing on the Properties of Poly(Lactic Acid)," *Period. Polytech. Mech. Eng.*, vol. 63, no. 4, pp. 270–277, Aug. 2019, doi: 10.3311/PPme.12825.
- [93] E. W. Fischer, H. J. Sterzel, and G. Wegner, "Investigation of the structure of solution

- grown crystals of lactide copolymers by means of chemical reactions,” *Kolloid-Zeitschrift und Zeitschrift für Polym.*, vol. 251, no. 11, pp. 980–990, Nov. 1973, doi: 10.1007/BF01498927.
- [94] M. Ryner, K. Stridsberg, A.-C. Albertsson, H. von Schenck, and M. Svensson, “Mechanism of Ring-Opening Polymerization of 1,5-Dioxepan-2-one and L-Lactide with Stannous 2-Ethylhexanoate. A Theoretical Study,” *Macromolecules*, vol. 34, no. 12, pp. 3877–3881, Jun. 2001, doi: 10.1021/ma002096n.
- [95] D. Pholharn, Y. Srithep, and J. Morris, “Effect of initiators on synthesis of poly(L-lactide) by ring opening polymerization,” *IOP Conf. Ser. Mater. Sci. Eng.*, vol. 213, no. 1, p. 012022, Jun. 2017, doi: 10.1088/1757-899X/213/1/012022.
- [96] J. L. Robert and K. B. Aubrecht, “Ring-Opening Polymerization of Lactide To Form a Biodegradable Polymer,” *J. Chem. Educ.*, vol. 85, no. 2, p. 258, Feb. 2008, doi: 10.1021/ed085p258.
- [97] J. G. Kirkwood and R. H. Cole, *Dielectrics, intermolecular forces, optical rotation*. New York: Gordon and Breach, 1965.
- [98] “D3418-21- Standard Test Method for Transition Temperatures and Enthalpies of Fusion and Crystallization of Polymers by Differential Scanning,” *ASTM Standard*. ASTM International, pp. 1–7, 2021, doi: 10.1520/D3418-21.
- [99] “ISO 11357-3:2018- Plastics — Differential scanning calorimetry (DSC) — Part 3: Determination of temperature and enthalpy of melting and crystallization.” ISO, pp. 1–6, 2018.
- [100] R. L. Blaine, “Determination of Polymer Crystallinity by DSC,” 2002. [Online]. Available: http://www.tainstruments.com/pdf/literature/TA123new.pdf?fbclid=IwAR3SmI9_boX-6EEedOaulhKfI2goyspND2rPJ6uBCMxhFwAM2ITHWYVXWXEQ.
- [101] E. W. Fischer, H. J. Sterzel, and G. Wegner, “Investigation of the structure of solution grown crystals of lactide copolymers by means of chemical reactions,” *Kolloid-Zeitschrift Zeitschrift für Polym.*, vol. 251, no. 11, pp. 980–990, 1973, doi: 10.1007/BF01498927.
- [102] “D882-18- Standard Test Method for Tensile Properties of Thin Plastic Sheeting,” *ASTM Standard*. ASTM International, pp. 1–12, 2018, doi: 10.1520/D0882-18.
- [103] K. Athanasiou, “Sterilization, toxicity, biocompatibility and clinical applications of polylactic acid/ polyglycolic acid copolymers,” *Biomaterials*, vol. 17, no. 2, pp. 93–102, Jan. 1996, doi: 10.1016/0142-9612(96)85754-1.
- [104] A. A. Ignatius and L. E. Claes, “In vitro biocompatibility of bioresorbable polymers: poly(L, DL-lactide) and poly(L-lactide-co-glycolide),” *Biomaterials*, vol. 17, no. 8, pp.

- 831–839, Jan. 1996, doi: 10.1016/0142-9612(96)81421-9.
- [105] S. R. Andersson, M. Hakkarainen, S. Inkinen, A. Södergård, and A. C. Albertsson, “Polylactide Stereocomplexation Leads to Higher Hydrolytic Stability but More Acidic Hydrolysis Product Pattern,” *Biomacromolecules*, vol. 11, no. 4, pp. 1067–1073, 2010, doi: 10.1021/bm100029t.
- [106] D. J. Mooney, D. F. Baldwin, N. P. Suh, J. P. Vacanti, and R. Langer, “Novel approach to fabricate porous sponges of poly(d,l-lactic-co-glycolic acid) without the use of organic solvents,” *Biomaterials*, vol. 17, no. 14, pp. 1417–1422, Jul. 1996, doi: 10.1016/0142-9612(96)87284-X.
- [107] M. Scimeca, S. Bischetti, H. K. Lamsira, R. Bonfiglio, and E. Bonanno, “Energy Dispersive X-ray (EDX) microanalysis: A powerful tool in biomedical research and diagnosis,” *Eur. J. Histochem.*, vol. 62, no. 1 SE-Reviews, Mar. 2018, doi: 10.4081/ejh.2018.2841.
- [108] E. Spotti, E. Berni, and C. Cacchioli, “Characteristics and Applications of Molds: PLA,” in *Meat Biotechnology*, New York, NY, France: Springer New York, 2016, pp. 181–195.
- [109] S. Inkinen, M. Hakkarainen, A.-C. Albertsson, and A. Södergård, “From Lactic Acid to Poly(lactic acid) (PLA): Characterization and Analysis of PLA and Its Precursors,” *Biomacromolecules*, vol. 12, no. 3, pp. 523–532, Mar. 2011, doi: 10.1021/bm101302t.
- [110] J. E. Kasperczyk, “HETCOR NMR study of poly(rac-lactide) and poly(meso-lactide),” *Polymer (Guildf.)*, vol. 40, no. 19, pp. 5455–5458, 1999, doi: 10.1016/S0032-3861(99)00128-7.
- [111] T. M. Ovitt and G. W. Coates, “Stereochemistry of lactide polymerization with chiral catalysts: New opportunities for stereocontrol using polymer exchange mechanisms,” *J. Am. Chem. Soc.*, vol. 124, no. 7, pp. 1316–1326, 2002, doi: 10.1021/ja012052+.
- [112] D. W. Grijpma and A. J. Pennings, “(Co)polymers of L-lactide, 1. Synthesis, thermal properties and hydrolytic degradation,” *Macromol. Chem. Phys.*, vol. 195, no. 5, pp. 1633–1647, May 1994, doi: 10.1002/macp.1994.021950515.
- [113] L. Feng, B. Zhang, X. Bian, G. Li, Z. Chen, and X. Chen, “Thermal Properties of Polylactides with Different Stereoisomers of Lactides Used as Comonomers,” *Macromolecules*, vol. 50, no. 16, pp. 6064–6073, Aug. 2017, doi: 10.1021/acs.macromol.7b00818.
- [114] D. W. Grijpma and A. J. Pennings, “(Co)polymers of L-lactide 2: Mechanical Properties,” *Macromol. Chem. Phys.*, vol. 195, no. C, pp. 1649–1663, 1994, doi: 10.1016/B978-0-444-99523-0.50007-6.
- [115] Materion Brush Performance Alloys, “Yield Strength and Other Near-Elastic Properties,”

2012.

- [116] “Mechanical Properties of Materials,” *Mechanicalc, Inc.*
<https://mechanicalc.com/reference/mechanical-properties-of-materials>.
- [117] P. J. Davis and P. Rabinowitz, “Approximate Integration over a Finite Interval,” in *Methods of Numerical Integration*, P. J. Davis and P. B. T.-M. of N. I. (Second E. Rabinowitz, Eds. Elsevier, 1984, pp. 51–198.
- [118] F. C. Campbell, *Elements of Metallurgy and Engineering Alloys*. ASM International, 2008.
- [119] M. Nofar, R. Salehiyan, and S. Sinha Ray, “Rheology of poly (lactic acid)-based systems,” *Polym. Rev.*, vol. 59, no. 3, pp. 465–509, 2019, doi: 10.1080/15583724.2019.1572185.
- [120] K. S. Bonifer *et al.*, “*Bacillus pumilus* B12 Degrades Polylactic Acid and Degradation Is Affected by Changing Nutrient Conditions,” *Front. Microbiol.*, vol. 10, no. November, pp. 1–13, Nov. 2019, doi: 10.3389/fmicb.2019.02548.
- [121] H. Tsuji, “Poly(lactide) stereocomplexes: Formation, structure, properties, degradation, and applications,” *Macromol. Biosci.*, vol. 5, no. 7, pp. 569–597, 2005, doi: 10.1002/mabi.200500062.
- [122] H. Tsuji and Y. Ikada, “Stereocomplex formation between enantiomeric poly(lactic acid)s. XI. Mechanical properties and morphology of solution-cast films,” *Polymer (Guildf)*, vol. 40, no. 24, pp. 6699–6708, 1999, doi: 10.1016/S0032-3861(99)00004-X.
- [123] H. Tsuji and Y. Ikada, “Stereocomplex Formation between Enantiomeric Poly(lactic acid)s. 6. Binary Blends from Copolymers,” *Macromolecules*, vol. 25, no. 21, pp. 5719–5723, 1992, doi: 10.1021/ma00047a024.
- [124] Y. Ikada, K. Jamshidi, H. Tsuji, and S. H. Hyon, “Stereocomplex Formation between Enantiomeric Poly(lactides),” *Macromolecules*, vol. 20, no. 4, pp. 904–906, 1987, doi: 10.1021/ma00170a034.
- [125] D. Brizzolara, H. J. Cantow, K. Diederichs, E. Keller, and A. J. Domb, “Mechanism of the stereocomplex formation between enantiomeric poly(lactide)s,” *Macromolecules*, vol. 29, no. 1, pp. 191–197, 1996, doi: 10.1021/ma951144e.
- [126] J. Zhang, H. Sato, H. Tsuji, I. Noda, and Y. Ozaki, “Infrared spectroscopic study of CH₃···O=C interaction during poly(L-lactide)/Poly(D-lactide) stereocomplex formation,” *Macromolecules*, vol. 38, no. 5, pp. 1822–1828, 2005, doi: 10.1021/ma047872w.
- [127] A. Gupta, A. K. Pal, E. M. Woo, and V. Katiyar, “Effects of Amphiphilic Chitosan on Stereocomplexation and Properties of Poly(lactic acid) Nano-biocomposite,” *Sci. Rep.*,

- vol. 8, no. 1, pp. 1–13, 2018, doi: 10.1038/s41598-018-22281-1.
- [128] J. Jeong, M. Ayyoob, J. H. Kim, S. W. Nam, and Y. J. Kim, “In situ formation of PLA-grafted alkoxy silanes for toughening a biodegradable PLA stereocomplex thin film,” *RSC Adv.*, vol. 9, no. 38, pp. 21748–21759, 2019, doi: 10.1039/c9ra03299a.
- [129] X. Su, L. Feng, and D. Yu, “Formation of stereocomplex crystal and its effect on the morphology and property of PDLA/PLLA blends,” *Polymers (Basel)*, vol. 12, no. 11, pp. 1–14, 2020, doi: 10.3390/polym12112515.
- [130] Y. Srithep, D. Pholharn, and T. Akkaprasa, “Effect of molecular weight of poly(L-lactic acid) on the stereocomplex formation between enantiomeric poly(lactic acid)s blendings,” *IOP Conf. Ser. Mater. Sci. Eng.*, vol. 526, no. 1, 2019, doi: 10.1088/1757-899X/526/1/012024.
- [131] E. Tarkhanov, A. Lehmann, and A. Menrath, “Halfway to Technical Stereocomplex PLA Products—An Arduous Path to a Breakthrough,” *Macromol. Mater. Eng.*, vol. 2000417, pp. 1–6, 2020, doi: 10.1002/mame.202000417.
- [132] Y. Li *et al.*, “Evaluation of thermal resistance and mechanical properties of injected molded stereocomplex of poly(l-lactic acid) and poly(d-lactic acid) with various molecular weights,” *Adv. Polym. Technol.*, vol. 37, no. 6, pp. 1674–1681, 2018, doi: 10.1002/adv.21824.
- [133] X. R. Gao *et al.*, “Rapid preparation and continuous processing of polylactide stereocomplex crystallite below its melting point,” *Polym. Bull.*, vol. 76, no. 7, pp. 3371–3385, 2019, doi: 10.1007/s00289-018-2544-2.
- [134] J. R. Sarasua, A. L. Arraiza, P. Balerdi, and I. Maiza, “Crystallinity and mechanical properties of optically pure polylactides and their blends,” *Polym. Eng. Sci.*, vol. 45, no. 5, pp. 745–753, May 2005, doi: 10.1002/pen.20331.
- [135] T. Biela and M. Studies, *Encyclopedia of Polymeric Nanomaterials*. Berlin, Heidelberg: Springer Berlin Heidelberg, 2020.
- [136] B. H. Toby and R. B. Von Dreele, “GSAS-II: the genesis of a modern open-source all purpose crystallography software package,” *J. Appl. Crystallogr.*, vol. 46, no. 2, pp. 544–549, Apr. 2013, doi: 10.1107/S0021889813003531.
- [137] H. Tsuji and I. Fukui, “Enhanced thermal stability of poly(lactide)s in the melt by enantiomeric polymer blending,” *Polymer (Guildf)*, vol. 44, no. 10, pp. 2891–2896, 2003, doi: 10.1016/S0032-3861(03)00175-7.
- [138] Q. Xie, L. Han, G. Shan, Y. Bao, and P. Pan, “Polymorphic Crystalline Structure and Crystal Morphology of Enantiomeric Poly(lactic acid) Blends Tailored by a Self-Assemblable Aryl Amide Nucleator,” *ACS Sustain. Chem. Eng.*, vol. 4, no. 5, pp. 2680–

- 2688, 2016, doi: 10.1021/acssuschemeng.6b00191.
- [139] H. Urayama, T. Kanamori, K. Fukushima, and Y. Kimura, “Controlled crystal nucleation in the melt-crystallization of poly(L-lactide) and poly(L-lactide)/poly(D-lactide) stereocomplex,” *Polymer (Guildf)*, vol. 44, no. 19, pp. 5635–5641, 2003, doi: 10.1016/S0032-3861(03)00583-4.
- [140] S. Körber, K. Moser, and J. Diemert, “Development of High Temperature Resistant Stereocomplex PLA for Injection Moulding,” *Polymers (Basel)*, vol. 14, no. 3, 2022, doi: 10.3390/polym14030384.
- [141] A. Gupta, N. Mulchandani, M. Shah, S. Kumar, and V. Katiyar, “Functionalized chitosan mediated stereocomplexation of poly(lactic acid): Influence on crystallization, oxygen permeability, wettability and biocompatibility behavior,” *Polymer (Guildf)*, vol. 142, pp. 196–208, 2018, doi: 10.1016/j.polymer.2017.12.064.
- [142] J. Zhang, H. Sato, H. Tsuji, I. Noda, and Y. Ozaki, “Differences in the CH₃···O=C interactions among poly(L-lactide), poly(L-lactide)/poly(D-lactide) stereocomplex, and poly(3-hydroxybutyrate) studied by infrared spectroscopy,” *J. Mol. Struct.*, vol. 735–736, no. SPEC. ISS., pp. 249–257, 2005, doi: 10.1016/j.molstruc.2004.11.033.
- [143] C. Alemán, B. Lotz, and J. Puiggali, “Crystal Structure of the α -Form of Poly(l-lactide),” *Macromolecules*, vol. 34, no. 14, pp. 4795–4801, Jul. 2001, doi: 10.1021/ma001630o.
- [144] W. Hoogsteen, A. R. Postema, A. J. Pennings, G. Ten Brinke, and P. Zugenmaier, “Crystal structure, conformation and morphology of solution-spun poly(L-lactide) fibers,” *Macromolecules*, vol. 23, no. 2, pp. 634–642, Jan. 1990, doi: 10.1021/ma00204a041.
- [145] P. De Santis and A. J. Kovacs, “Molecular conformation of poly(S-lactic acid),” *Biopolymers*, vol. 6, no. 3, pp. 299–306, Mar. 1968, doi: 10.1002/bip.1968.360060305.
- [146] J. Kobayashi *et al.*, “Structural and optical properties of poly lactic acids,” *J. Appl. Phys.*, vol. 77, no. 7, pp. 2957–2973, Apr. 1995, doi: 10.1063/1.358712.
- [147] T. Okihara *et al.*, “Crystal structure of stereocomplex of poly(L-lactide) and poly(D-lactide),” *J. Macromol. Sci. Part B Phys.*, vol. 30, no. 1–2, pp. 119–140, Mar. 1991, doi: 10.1080/00222349108245788.
- [148] H. Tsuji, “Poly(lactic acid) stereocomplexes: A decade of progress,” *Adv. Drug Deliv. Rev.*, vol. 107, pp. 97–135, 2016, doi: 10.1016/j.addr.2016.04.017.
- [149] N. López-Rodríguez, I. Martínez de Arenaza, E. Meaurio, and J. R. Sarasua, “Improvement of toughness by stereocomplex crystal formation in optically pure polylactides of high molecular weight,” *J. Mech. Behav. Biomed. Mater.*, vol. 37, pp. 219–225, 2014, doi: 10.1016/j.jmbbm.2014.05.022.

- [150] F. C. Campbell, *Structural Composite Materials*. Materials Park, Ohio: ASM International, 2010.
- [151] D. Hull and T. W. Clyne, *An Introduction to Composite Materials*, 2nd ed. Cambridge: Cambridge University Press, 1996.
- [152] S. C. Schmidt and M. A. Hillmyer, "Polylactide stereocomplex crystallites as nucleating agents for isotactic polylactide," *J. Polym. Sci. Part B Polym. Phys.*, vol. 39, no. 3, pp. 300–313, Feb. 2001, doi: 10.1002/1099-0488(20010201)39:3<300::AID-POLB1002>3.0.CO;2-M.
- [153] K. Harnisch and H. Muschik, "Determination of the Avrami exponent of partially crystallized polymers by DSC- (DTA-) analyses," *Colloid Polym. Sci.*, vol. 261, no. 11, pp. 908–913, 1983, doi: 10.1007/BF01451668.
- [154] M. Nofar, W. Zhu, C. B. Park, and J. Randall, "Crystallization Kinetics of Linear and Long-Chain-Branched Polylactide," *Ind. Eng. Chem. Res.*, vol. 50, no. 24, pp. 13789–13798, Dec. 2011, doi: 10.1021/ie2011966.
- [155] A. M. Harris and E. C. Lee, "Improving mechanical performance of injection molded PLA by controlling crystallinity," *J. Appl. Polym. Sci.*, vol. 107, no. 4, pp. 2246–2255, Feb. 2008, doi: 10.1002/app.27261.
- [156] G. Kale, R. Auras, S. P. Singh, and R. Narayan, "Biodegradability of polylactide bottles in real and simulated composting conditions," *Polym. Test.*, vol. 26, no. 8, pp. 1049–1061, 2007, doi: 10.1016/j.polymertesting.2007.07.006.
- [157] R. G. Sinclair, "The Case for Polylactic Acid as a Commodity Packaging Plastic," *J. Macromol. Sci. Part A*, vol. 33, no. 5, pp. 585–597, May 1996, doi: 10.1080/10601329608010880.
- [158] Y. Fan, H. Nishida, Y. Shirai, and T. Endo, "Control of racemization for feedstock recycling of PLLA," *Green Chem.*, vol. 5, no. 5, pp. 575–579, 2003, doi: 10.1039/b304792j.
- [159] F. D. Kopinke, M. Remmler, and K. Mackenzie, "Thermal decomposition of biodegradable polyesters - I: Poly(β -hydroxybutyric acid)," *Polym. Degrad. Stab.*, vol. 52, no. 1, pp. 25–38, 1996, doi: 10.1016/0141-3910(95)00221-9.
- [160] R. B. Cassel, "Purity Determination and DSC Tzero Technology," *Therm. Anal. Rheol.*, pp. 1–8.
- [161] EPA, "Corn Wet Milling," *Compil. Air Pollut. Emiss. Factors*, pp. 1–9, 1995.
- [162] M. A. Curran, *Life Cycle Assessment Student Handbook*. John Wiley & Sons, Ltd, 2015.

- [163] Y. Fan, H. Nishida, Y. Shirai, and T. Endo, "Racemization on thermal degradation of poly(L-lactide) with calcium salt end structure," *Polym. Degrad. Stab.*, vol. 80, no. 3, pp. 503–511, 2003, doi: 10.1016/S0141-3910(03)00033-8.
- [164] D. R. Witzke, "Introduction to Properties, Engineering, and Prospects of Polylactide Polymers," Michigan State University, 1997.
- [165] E. T. H. Vink and S. Davies, "Life Cycle Inventory and Impact Assessment Data for 2014 Ingeo® Polylactide Production," *Ind. Biotechnol.*, vol. 11, no. 3, pp. 167–180, 2015, doi: 10.1089/ind.2015.0003.
- [166] E. T. H. Vink, S. Davies, and J. J. Kolstad, "The eco-profile for current Ingeo® polylactide production," *Ind. Biotechnol.*, vol. 6, no. 4, pp. 212–224, 2010, doi: 10.1089/ind.2010.6.212.
- [167] E. T. H. Vink, D. A. Glassner, J. J. Kolstad, R. J. Wooley, and R. P. O'Connor, "The eco-profiles for current and near-future NatureWorks® polylactide (PLA) production," *Ind. Biotechnol.*, vol. 3, no. 1, pp. 58–81, 2007, doi: 10.1089/ind.2007.3.058.
- [168] M. F. Cosate de Andrade, P. M. S. Souza, O. Cavalett, and A. R. Morales, "Life Cycle Assessment of Poly(Lactic Acid) (PLA): Comparison Between Chemical Recycling, Mechanical Recycling and Composting," *J. Polym. Environ.*, vol. 24, no. 4, pp. 372–384, 2016, doi: 10.1007/s10924-016-0787-2.